Reversible solid oxide cells for bidirectional energy conversion in spot electricity and fuel markets

Diego Villarreal Singer

Submitted in partial fulfillment of the
requirements for the degree of
Doctor of Philosophy
in the Graduate School of Arts and Sciences

COLUMBIA UNIVERSITY

2017

ABSTRACT

Reversible solid oxide cells for bidirectional energy conversion in spot electricity and fuel markets

Diego Villarreal Singer

The decarbonization of the energy system is one of the most complex and consequential challenges of the 21st century. Meeting this challenge will require the deployment of existing low carbon technologies at unprecedented scales and rates and will necessitate the development of new technologies that have the ability to transform variable renewable energy into high energy density products. Reversible Solid Oxide Cells (RSOCs) are electrochemical devices that can function both as fuel cells or electrolyzers: in fuel cell mode, RSOCs consume a chemical fuel (H_2, CO, CH_4, etc.) to produce electrical power, while in electrolysis mode they consume electric power and chemical inputs (H_2O, CO_2) to produce a chemical fuel (H_2, CO, CH_4, etc.). As such, RSOC systems can be thought of as flexible energy hubs that have unique potential to bridge the low power density renewable infrastructure with that of high energy density fuels in an efficient, dynamic, and bidirectional fashion. This dissertation explores the different operational sensitivities and design trade-offs of a methane based RSOC system, investigates the optimum operating strategies for a system that adapts to variations in the hourly spot electricity and fuel prices in Western Denmark, and provides an economic analysis of the system under a wide variety of design assumptions, operational strategies, and fuel and electricity market structures.

In order to perform such comprehensive analyses, a 0-D computational model of a methane based RSOC system was developed in Python. In fuel cell mode, the system generates power by consuming natural gas, while in electrolysis mode the system generates synthetic natural gas (SNG) by electrolyzing steam and catalytically hydrogenating recycled CO_2 into CH_4 downstream of the RSOC. The model's flexibility

enables the simulation of part-load operation, allowing the user to assess the changes in output, efficiency, and operating cost as the system is operated across multiple points. The model has the ability to evaluate the impact that changes in design choices and operating parameters (Area Specific Resistance, temperatures, current density, etc.) have on the system as it interfaces with time varying exogenous factors such as fuel and electricity prices. As such, one of the main contributions of this model is the ability to run simulations in which the operating strategy of the RSOC system responds and adapts to varying market signals.

The computational model is used to develop a series of hourly optimizations for finding the optimal operating strategy for an RSOC system that can buy or sell electricity and gas in the spot electricity and natural gas markets in Western Denmark. After receiving an electricity and gas price signal, the optimization determines the operating mode (fuel cell, electrolysis or idle) and operating point (e.g., current density) that maximize the operating profits every hour for the given electricity and gas price pair. In order to avoid the speculation associated with traditional energy storage simulations, the system is opened at both ends, allowing it to instantaneously buy and sell any electricity or gas that is generated. Thus, the system never stores any of the products and it buys and sells them at the instantaneously available market price. By assuming that market prices reflect all existing information, this design choice removes the necessity of having to speculate about the future in order to determine the optimum operating strategy. This approach is one of the innovations presented in this work.

The optimizations aim at maximizing the operating profits at each hour of the year, and decisions of operating mode and point are based on marginal operating costs for each electricity and natural gas price pair. The full economic analysis, however, requires the understanding of how design choices (e.g. operating limits, heat management, gas recycling systems, etc.) affect the investment costs, and therefore

a Total Plant Cost (TPC) model is developed. For each design choice, the TPC model is used to compute a cost of the system per m^2 of active electrode area or kW of output. This value, assumed to be a sunk cost that does not affect the operating decision, together with the operating profits resulting from the optimization is used to assess the overall profitability of the system. For a system with $100\,m^2$ of active electrode area, conventional costing metrics suggest that the balance of plant (BoP) components for managing the system's heat (Heat exchangers, evaporators, condensers) are the main cost drivers and represent roughly 50% of the TPC. The cost of the electrochemical RSOC stack, assembly, power inverter and piping represent 35% of the cost, with the other 15% coming from pumps, compressors and the methanation system.

Twenty different optimization scenarios are developed in order to quantify the effect that system design choices, operating limits, and market prices have on the operating profile and on the overall economics of the system. The first 12 case studies are based on real hourly spot electricity and natural gas prices for the years 2009-2014 in Western Denmark. For the last 8 scenarios, a forecasted hourly time-series for electricity in the Danish grid for the year 2050 and two fixed SNG prices (high and a low) are used. The 2050 prices, which assume a fossil fuel free system, are used to understand the role and value that RSOC systems can offer in deeply decarbonized energy systems. For each optimization, different parameters such as the initial ASR and the operating limits (maximum current densities for each mode of operation) are varied in order to find the impact that these changes have on the system's design (balance of plant components), hourly operating mode, investment costs, hourly operating profits, and overall plant profits.

For the 2009-2014 optimizations, it is found that the sale of electricity (fuel cell mode) and fuel (electrolysis mode) is not large enough to cover the fixed costs associated with the plant. Fuel cell mode dominates the operation (61% of the time) with

electrolysis representing only $\sim 4\%$ of the operating hours. ASR is found to have an important impact on the system's economics, due to the fact that a lowering of the ASR leads to a reduction in the size of the heat management system, which in turn reduces the Total Plant Cost.

For the 2050 dataset, it is found that under the high gas price scenario electrolysis mode dominates (50% of the time), and fuel cell operation represents 15% of the hours in the year. For the low SNG price, electrolysis still dominates (48% of the time), and fuel cell operation increases to 30% of the operating hours. Furthermore, for the high SNG scenario, the sale of fuel and electricity are large enough to cover the system's fixed cost, making the system attractive from an investment perspective. For the low SNG price, the system also becomes profitable when using ASR values of 0.4 Ωcm^2 or below.

Contents

List of Figures **vi**

List of Tables **xii**

1 Introduction and Motivation **1**

1.1 Motivation 4

1.2 The vision 6

1.2.1 Fulfilling the vision 7

1.3 Carbon based fuels in a carbon constrained world 9

1.4 Fuels from air, water, and renewable energy 10

1.4.1 Sources of H_2 11

1.4.2 Sources of CO_2 12

1.4.2.1 CO_2 from biomass 13

1.4.2.2 Direct Air Capture 14

1.5 Tying chemistry to renewable electricity: the long-term goal 15

1.5.1 The need for variable operation 15

2 Background **17**

2.1 Reversible Solid Oxide Technology 17

2.1.1 Modes of operation 18

2.1.2 Thermodynamics 23

2.1.3 Thermoneutral voltage 26

2.2 Literature review 28
2.2.1 Solid oxide cells for fuel synthesis 30
2.2.1.1 SOEC - atmospheric operation 31
2.2.1.2 Pressurized operation 33
2.2.1.3 "Off-design" operation 34
2.2.2 Reversible solid oxide cells for energy storage 35
2.3 Methanation chemistry and technology 37
2.3.1 Methanation chemistry 38
2.3.1.1 Syngas methanation 38
2.3.1.2 CO_2 methanation 40
2.3.2 Catalysts and reactors 42

3 Computational model of RSOC system 45

3.1 Model description 46
3.2 System configurations 47
3.2.1 RSOC with internal reforming and external catalytic methanation 48
3.2.1.1 Fuel cell mode 48
3.2.1.2 Electrolysis mode 51
3.3 Stack Model 54
3.3.1 Fuel Cell mode 56
3.3.1.1 Electrochemical model 56
3.3.1.2 Mass Balances 57
3.3.1.3 Energy Balance 63
3.3.2 Electrolysis mode 63
3.3.2.1 Electrochemical model 64
3.3.2.2 Mass balance 64
3.3.2.3 Energy balance 68
3.3.3 Degradation 68

3.4 Balance of Plant components . . . 69
3.4.1 Pre-heaters . . . 70
3.4.1.1 Sizing pre–heaters . . . 71
3.4.2 Electric heaters . . . 71
3.4.3 Evaporator . . . 72
3.4.4 Turbomachinery . . . 73
3.4.4.1 Blowers and pumps . . . 73
3.4.4.2 Compressors . . . 74
3.4.5 Catalytic combustor . . . 74
3.4.6 Reactors . . . 76
3.4.6.1 Mass of the catalyst and required reactor volume . . . 80
3.4.7 Water separator . . . 81
3.4.8 Pressure drops . . . 82
3.5 Part-load operation . . . 83
3.5.1 Pre-heaters . . . 84
3.5.2 Blowers . . . 86
3.6 System cost model . . . 87
3.6.1 SOC stack costs . . . 87
3.6.2 BoP component costs . . . 90
3.6.3 Annualized costs . . . 98

4 System Sensitivity to operating variables 100

4.1 Process variables . . . 100
4.1.1 Fuel Utilization . . . 101
4.1.2 Control strategies . . . 102
4.2 Fuel Cell mode sensitivities . . . 103
4.2.1 Base-case profile . . . 104
4.2.1.1 Sensitivity to STCR . . . 111

4.2.1.2 Sensitivity to Fuel Utilization . . . 115
4.2.2 Sensitivity to ASR . . . 117
4.3 Electrolysis mode sensitivities . . . 119
4.3.1 Base-case profile . . . 119
4.3.2 Sensitivity to ASR . . . 130
4.4 Part-load operation . . . 133
4.4.1 Net system efficiency . . . 134
4.4.2 BoP over-design . . . 135

5 Optimization of RSOC operating strategy with market price time-series: the Danish case 139

5.1 The Danish energy system . . . 140
5.1.1 Overview of the Danish Power system and its market structure 144
5.1.1.1 The West Denmark electricity market . . . 145
5.1.1.2 The importance of wind in the Danish power system 150
5.2 Optimum operating strategy of a RSOC in the Danish system . . . 156
5.2.1 Data . . . 159
5.2.2 Problem formulation . . . 159
5.3 Optimization results . . . 164
5.3.1 Base case (Rev-BC): system profile results . . . 166
5.3.2 Base case (Rev-BC): yearly analysis . . . 172
5.3.2.1 The contribution of negative prices . . . 177
5.3.2.2 Full plant cost analysis: base-case (Rev-BC) . . . 177
5.3.3 Fuel cell only operation . . . 185
5.3.4 Sensitivity to ASR (Rev-ASR) . . . 188
5.3.4.1 Full plant cost analysis (Rev-ASR) . . . 190
5.3.4.2 Variations on operational limits . . . 194
5.3.4.3 TPC required for breaking even . . . 199

5.3.5 Impact of degradation rate: (Rev-Deg) 200
5.3.6 Simpler chemistries to lower CAPEX 205
5.3.7 Value of reversibility 207
5.3.8 2050 scenario 208
5.3.8.1 Sensitivity to ASR in low SNG scenario 214
5.3.8.2 Sensitivity to operating limits in low SNG scenario . 216

6 Future Work **220**
6.1 Variations on system design 220
6.1.1 Co-electrolyis and pressurized systems 221
6.2 Heat integration 222
6.3 Economic optimization and stack degradation 222
6.4 Scaling down BoP components 224
6.5 Ancillary services and other markets 224

7 Conclusion **226**

Bibliography **233**

List of Figures

2.1 SOC in fuel cell mode 21

2.2 SOC in electrolysis mode 23

2.3 Polarization curve for a planar SOC operating at at 850 °C 26

2.4 Enthalpy and Gibbs free energy for H_2O and CO_2 electrolysis 27

2.5 Solid Oxide Cells for fuel synthesis 30

2.6 Methanation equilibrium composition for a 3:1 H_2/CO mixture. 39

2.7 CH_4 yield at equilibrium for direct CO methanation 40

2.8 Methanation equilibrium composition for a 4:1 H_2/CO_2 mixture. 41

2.9 CH_4 yield at equilibrium for a direct CO_2 methanation 42

3.1 Generic "Open-ended" RSOC system 48

3.2 Fuel cell mode RSOC with internal CH_4 reforming 49

3.3 Electrolysis mode with catalytic CO_2 methanation 52

3.4 SOFC control volume with Anode Gas Recycling 58

3.5 Generic counterflow heat exchanger 70

3.6 Methanation on catalytic heat exchanger 78

3.7 Comparison of Gibbs minimization routines for methanator reactor . . . 79

3.8 Vapor-liquid equilibrium for methanator exit gas separation. 82

3.9 Pre-heater with bypass valve 85

3.10 Stack costs per kW as a function of production volume. 89

3.11 Stack costs per m^2 as a function of production volume. 90

4.1 Fuel cell mode RSOC with internal CH_4 reforming. Power, voltage and stack efficiency. 106
4.2 FC mode base-case scenario: Gross system efficiency. 106
4.3 FC mode base-case scenario: Heat generation and Air ratios required. . . 107
4.4 FC mode base-case scenario: Power consumed by air blowers and percentage of total stack power used by air blowers. 109
4.5 FC mode base-case scenario: parasitics power consumption. 110
4.6 FC mode base-case scenario: Stack gross power and system net power. . 110
4.7 FC mode base- case scenario: Stack and Net System Efficiency. 112
4.8 FC mode base-case scenario: OCV and stack gross power as a function of STCR. 113
4.9 FC mode base-case scenario: Stack efficiency as a function of STCR. . . 113
4.10 FC mode base-case scenario: Power output for different STCR. 114
4.11 FC mode base-case scenario: Gross and Net System Power at different STCR. 114
4.12 FC mode base-case scenario: Cell voltage and power for different in-cell fuel utilizations 115
4.13 FC mode base-case scenario: stack efficiency for different in-cell fuel utilization rates. 116
4.14 FC mode base-case scenario: gross power for different ASR values. 118
4.15 FC mode base-case scenario: stack efficiency for different ASR values. . . 118
4.16 Electrolysis: stack load and voltage 121
4.17 Electrolysis: H_2 generation 122
4.18 Electrolysis: stack efficiency 123
4.19 Electrolysis: stack heat requirements 124
4.20 Methanator sensitivity to reaction temperature 125
4.21 CH_4 yield as a function of reaction temperature 125

4.22 Electrolysis: Net system efficiency based on LHV 127
4.23 Electrolysis mode parasitics 128
4.24 Electrolysis heating requirements breakdown 129
4.25 Electrolysis mode: parasitics vs. stack electricity load 130
4.26 Electrolysis mode: voltage current relationship for different ASR's 131
4.27 Electrolysis mode: stack efficiency at different ASR values. 132
4.28 Electrolysis mode: system efficiency at different ASR values. 132
4.29 Electrolysis mode: Total system load for different ASR values. 133
4.30 Part-Load FC operation: Net system efficiency fuel cell mode. 135
4.31 Part-Load electrolysis operation: Net system efficiency. 136
4.32 Part-Load fuel cell pre-heater oversizing. 137
4.33 Part-load: electrolysis pre-heater oversizing. 138

5.1 Gross Energy Consumption for Denmark 1990-2014. 141
5.2 Gross Energy Consumption, GDP growth, Energy intensity and CO_2 emissions for Denmark 1990-2014. 141
5.3 Evolution of power grid in Denmark. 143
5.4 Electricity mix Denmark for selected years. 143
5.5 Renewable power production mix Denmark for selected years. 144
5.6 Danish grid interconnections. 146
5.7 Wind power generation Western Denmark (2009-2014) 151
5.8 Western Denmark day-ahead spot prices (2009-2014) 152
5.9 Western Denmark day-ahead spot prices with spikes filtered out (2009-2014) 153
5.10 Western Denmark average daily logarithmic volatility for natural gas and electricity 154
5.11 Day-ahead hourly spot market price vs. wind fraction of total demand for the year 2009-2014. 155
5.12 Yearly frequency of negative prices in Western Denmark 156

5.13 Negative price distribution vs. wind percentage of total demand for the year 2009-2014. 157
5.14 Negative price frequency in DK1 for each day of the week. 158
5.15 Western Denmark electricity and natural gas prices for each week of the year 2014 160
5.16 Western Denmark electricity and natural gas prices for each week of the year 2014 161
5.17 System profile Jan 1st - Jan 7th 2009. 168
5.18 System profile Sep 8th - 14th 2011. 169
5.19 System profile April 23-29 2013. 171
5.20 System profile Dec 18-24 2014 172
5.21 Mode of operation per year 173
5.22 2009-2014 base-case optimization yearly profits. 174
5.23 Percent contribution of each year to 6 year cumulative profits 175
5.24 Yearly capacity factors for the Rev-Base simulation 176
5.25 Contribution of each mode of operation to yearly profits 176
5.26 Contribution of positive and negative electricity prices to total electrolysis profits 178
5.27 Break-down of TPC for base-case simulation. 182
5.28 Yearly operating profits, annualized CAPEX and plant profits for Rev-BC simulation. 183
5.29 Fuel cell only optimization: yearly profits and aggregate profits at different operating points. 186
5.30 Break-down of TPC for fuel cell only optimization. 187
5.31 Yearly operating profits, annualized CAPEX and plant profits for fuel cell only optimization. 188

5.32 ASR sensitivity: yearly operational profits for different initial ASR assumptions 189
5.33 ASR sensitivity: Cumulative yearly operational profits for different initial ASR values 190
5.34 ASR sensitivity: Operating profits, annuities and plant profits for different initial ASR. 192
5.35 Net power out and operational profits for first week of January 2009 for different initial ASR. 193
5.36 Cumulative total plant profits for different initial ASR values. 194
5.37 Comparison of operating profits for changes in operating limits for different ASR values 197
5.38 Comparison of total plant profits for changes in operating limits for different ASR values 198
5.39 Yearly operating profits for no degradation, degradation with BoP oversize, and degradation wit no oversize 202
5.40 Cumulative operating profits for no degradation, degradation with BoP oversize, and degradation wit no oversize 203
5.41 Cumulative total plant profits for no degradation, degradation with no oversize, and degradation with BoP oversize 204
5.42 Electricity and SNG prices for 2050 scenario. 209
5.43 Operation by mode for 2050 scenario at low and high SNG prices 210
5.44 2050 operational profits for Low and High SNG cases; % profit contribution of each mode for low and high SNG cases 211
5.45 2050 operational profits for Low and High SNG cases; % profit contribution of each mode for low and high SNG cases 212
5.46 2050 low SNG price scenario sensitivity to ASR 215

5.47 Operating profits, annuity and total plant profits for 2050 low SNG price case at different ASR and operating current density limits 217

List of Tables

2.1 Operating voltage and thermoneutral relationships. 28

3.1 Equilibrium constant coefficients 61
3.2 System component pressure drops 83
3.3 BoP cost component scaling table 97
3.4 Cost factors for BoP equipment 98

4.1 Model parameters and operating variables 101
4.2 FC mode base-case assumptions and results 104
4.3 Electrolysis input and output summary 120

5.1 Model assumptions for optimization runs 165
5.2 Cases for optimum operating strategy 166
5.3 Component costs and TPC for base-case scenario. 180
5.4 Contribution of each equipment category and TPC at different ASR . . . 191
5.5 Fuel cell and electrolysis operational bounds for different ASR 195
5.6 Annualized TPC comparison:base operating limits & new operating limits 196
5.7 TPC Breakeven requirements 199
5.8 Area of air pre-heaters, air flow rates and annualized TPC for different degradation strategies. 203
5.9 Return on Investment of base and new operating limits for the 2050 low SNG cases. 218

Acknowledgements

First and foremost, I would like to thank Professor Klaus Lackner for guiding me throughout this process and for allowing me to freely pursue my interests and ideas. Professor Lackner's unparalleled intellectual capabilities are a true source of inspiration, and his unique approach to solving complex problems have forever shaped the way I think. Learning from him has been one of the most rewarding and gratifying experiences of my life, and I will always be proud to call myself a Lackner alumn.

I would also like to thank my co-adviser Chris Graves for opening the doors of his lab in Denmark, and for trusting me from day one. Chris's guidance and profound knowledge of solid oxide cells and electrochemistry were crucial for the development of this dissertation. I am indebted to him for being such a patient and dedicated mentor.

My time at Columbia wouldn't have been the same without my friends and colleagues at the Lenfest Center. In particular, I would like to thank my friends Josh Browne and Zara L'Heureux. Josh has been my oldest friend at Columbia and he always provided invaluable technical and non-technical guidance. Zara was a wonderful resource for discussing all things related to thermodynamics, heat transfer, and Python.

I would also like to thank other friends and colleagues from whom I learned invaluable lessons: Juan Carlos de Obeso, a great friend and running companion that showed me that thoughtful and systematic analysis yields the best results; Andrés Lajous for teaching me how to think about public policy and politics; and José

Ahumada for being my family from day one.

I really want to thank my mother Silvia and my father Javier for their unconditional support and for reminding me that there is always light at the end of the tunnel. And a huge thank you to my brother Sebastián, who has always believed in my projects and has been an irreplaceable source of knowledge, kindness and thoughtful advice.

And above all, I would like to thank my wife Diana. Diana took a leap of faith 6 years ago and decided to support my dreams, even if doing so meant sacrificing some of her own. This work belongs to her as much as anyone else, and its completion would've been impossible without her everyday support. Muchas gracias.

Financial support from the Department of Earth & Environmental Engineering at Columbia University and from the Consejo Nacional de Ciencia y Tecnología (CONACYT) is gratefully acknowledged.

Para Diana, Martín y Tomás.

Chapter 1

Introduction

In a world constrained by the total allowable carbon emissions, the development of infrastructure that is capable of storing, processing, and transforming variable renewable power into cheap and reliable energy products and services is one of the most important and critical challenges.

Reversible solid oxide cell technology (RSOC) has been suggested as a technology that can help integrate renewable power into the grid, while also providing an avenue for synthesizing high energy density carbon neutral fuels. RSOC are electrochemical devices that can be operated in two independent and mutually exclusive modes: one which produces fuel using chemical inputs and electricity (electrolysis); and one in which it produces power by consuming fuels (fuel cell mode). In this thesis, the use of RSOC's coupled to catalytic chemical reactors to produce methane (using recycled CO_2) in electrolysis mode (effectively power-to-gas), and low carbon power when operating in fuel cell mode (gas-to-power) are investigated. The inherent flexibility of RSOC systems allow for multiple system configurations, which result in different efficiencies, power densities, and potential lifetimes.

In the work presented herein, system configurations that are open at both ends, and thus have the ability to buy electricity and sell fuels (electrolysis mode) or buy fuels and sell electric power (fuel cell mode) at any point in time are investigated. These open systems can be thought of as "modular energy hubs", where the same infrastructure can provide both fuels or efficient energy conversions (e.g. delivering electric power from specific fuels). The purpose of this thesis is then to investigate how these

systems react to different operating variables (temperature, steam-to-carbon ratio, fuel and electricity prices, etc.) and design parameters (Area Specific Resistance, degradation rates, etc.), and to investigate the optimum strategies for integrating these systems into spot electricity and fuel markets where the price signals are changing every hour. To achieve this, a computational model of a RSOC that consumes methane in fuel cell mode and produces methane by hydrogenating CO_2 in electrolysis mode is developed from scratch. The model is tested against many operational variables and parameters, and is then used to develop operating strategies in which the system's mode (fuel cell, electrolysis or idle) and output varies on an hourly basis in response to spot electricity and fuel prices in Western Denmark for the years 2009-2014. A detailed economic analysis is performed for each optimization and the impact of different assumptions and design parameters (e.g. ASR, CO_2 price, etc.) are investigated. Lastly, a forecast of prices for electricity and fuel for Denmark in the year 2050 is used to assess the value that the proposed systems can offer in grids that are dominated by renewable energy.

This dissertation is broken down into four general sections:

- Part One (Chapters 1-2) —The first part of the thesis is an overall discussion of the current state of solid oxide cell technology, energy storage technologies, and the merits of converting intermittent renewable power into carbon based fuels. A brief discussion on the different ways in which carbon can be recycled from concentrated sources or the atmosphere is presented. Part one also includes an in depth discussion of the physics and chemistry behind the RSOC technology and catalytic fuel synthesis.

- Part Two (Chapter 3-4) —In part two of the thesis a computational model for simulating an end-to-end RSOC "energy hub" is developed and presented. The merits and shortcomings of the model are discussed, as well as an in-depth

discussion of the main unit operations within the system. A discussion of the behavior of the system under different assumptions, operating strategies, and off-design operation, is presented. Lastly a discussion and a framework for estimating the total plant cost (TPC) is offered.

- Part Three (Chapter 5) —In part three, the computational model of the RSOC system described in the previous chapters is used to run a series of temporal optimizations for finding the optimal operating strategy for an RSOC that can buy/sell electricity/fuel in the Danish wholesale markets for electricity and gas. Historical electricity prices from the Danish grid and from the Scandinavian gas markets are used as inputs to the simulation. Sensitivity to underlying assumptions (initial ASR, operating limits, degradation, etc) are investigated, and the profitability of each system and simulation is presented. These results are then used to gain insight as to how RSOC fit in the current electricity and gas markets; what value can be derived from reversible operation; and the value that reversibility can offer in electricity systems in which the share of variable renewable power is considerable. Lastly, an optimization is performed for a case in which the 2050 spot electricity prices for Western Denmark are projected.

- Part Four (Chapter 6-7) —Lastly, a series of concluding remarks are presented, alongside future research avenues that can be derived from the work discussed throughout this. A series of simulations and questions that were not explored in this thesis but that could yield important results are emphasized and briefly discussed.

In order to set the stage for the questions explored in this dissertation, the following sections in this chapter will introduce the reader to the overarching themes of the thesis and will lay out the motivations behind this work.

1.1 Motivation

One of the key drivers of development and the subsequent increase in the quality of life that was experienced around the globe during the 20th century has been access to cheap and abundant energy. The corresponding growth in energy consumption has largely been met by the consumption of fossil fuels, which resulted in a rapid increase in the concentration of CO_2 in the atmosphere. This, in turn, has lead to ever increasing risks of irreversible climate change. With more than 1.2 billion people still lacking access to electricity and 2.6 billion without clean cooking facilities [68], the 21st century is likely to see important growth in per-capita energy consumption. This brings up a crucial question: how can the world provide for our future energy needs while limiting the amount of fossil carbon it mobilizes into the atmosphere?

Although the modern economy depends on a cheap and uninterrupted access to energy products and services, the system that was built to satisfy these needs exists as two different sub-systems that hardly overlap: in one sub-system, primary energy is transformed in large-scale centralized facilities into electricity which is then carried in transmission lines and distributed to end users. This subsystem, which has been dominated by fossil fuels, has grown dramatically in size and has seen some important shifts in the past decades. In 1973 there was a total of 6,131 TWh of electricity generated around the world, out of which 75.2% was generated using fossil fuels (38.3% coal, 24.8% oil, 12.1% natural gas). By 2013, the total amount of electricity generated had increased to 23,322 TWh (almost a 4x increase) and the share of fossil fuels had dropped to 67.4% (41.3% coal, 21.7% gas, 4.4% oil) [67]. The drop in the contribution of fossil fuels is largely due to the penetration of nuclear energy during the 70's and 80's, and the slow but increasingly important contribution of renewables (solar, wind, geothermal, biomass). At the same time, the oil crisis of the 1970's and the oil price increase of the 90's and 2000's, as well as tighter environmental regulations in the developed economies, contributed to the incredible drop in fuel

oil's share of the electricity generation mix.

At the same time, another large-scale and centralized sub-system was created in order to extract and refine crude oil into liquid fuels used, primarily, to power the transport sector. The high energy density of hydrocarbon fuels coupled with the difficulty of storing electricity, made liquid hydrocarbons the fuel of choice for all major prime movers [112]. Indeed, it has been the high energy density of these liquid fuels that has allowed for the globalized and interconnected world of today. Oil has dominated the transport sector, and has lost little to no market share to other fuels even though energy consumption for transport has increased from 1,081 Mtoe to 2,563 Mtoe between 1973 and 2013. In 1973 oil represented 94.4% of the total final consumption of the transport sector. In 2013 this number stood at 93.5% [67]. The remarkable dependence of the transportation sector on liquid fuels underscores the difficulty of decarbonizing the transport sector, making this one of the most pressing challenges for a sustainable future.

Recent technological advances and the dramatic decrease in the cost of renewable conversion technologies (particularly solar power), have put forth the idea that diffuse energy resources can be harvested in decentralized locations which can then be interconnected via small grids and clever software. The so called "Distributed generation" (DG) has many virtues: it reduces the inefficiencies associated with transmission and distribution of electric power, it increases system resilience, and it allows for the consumer to control the generation process. It is no surprise then that DG is becoming an increasingly important feature of the energy system. DG has largely been confined to the production of electricity for consumption at the point of generation (e.g. rooftop solar, small-scale CHP), and up to very recently the production of fuels in a distributed fashion had not been considered. The risks associated with rising CO_2 concentrations puts pressure on carbon based fuels, as net carbon emissions need to essentially drop to zero by the end of the 21st century in order to avoid the

most dire climatic impacts. Thus, it is increasingly important to develop strategies and technologies that can catalyze the decarbonization of all sectors of the economy. Transport poses a particularly tough challenge, as high energy density fuels will be required for most aviation, marine, and heavy duty vehicles and applications. Figuring out how marry the DG infrastructure that is beginning to develop with the production of carbon neutral fuels is therefore one of the most important and pressing challenges.

1.2 The vision

Using renewable energy sources such as wind to meet the energy requirements of an increasingly affluent and populated world requires solving (at least) two general challenges. The first challenge is matching intermittent supply with large aggregate demand. This will require the development of affordable large-scale energy storage systems, and the ability to smartly operate them such that the system never experiences shortfalls or blackouts . The second challenge is that applications like aviation, marine transport and heavy-duty vehicles will require high density energy carriers, making the electrification of an important part of the transport sector virtually impossible. Thus, the production of renewable fuels will be a key ingredient of future low carbon infrastructure. Historically, these two pieces (energy storage and sustainable fuels) have been thought of as mutually exclusive: one pertaining to the world of electric infrastructure and the other to large-scale petrochemical facilities. We posit that this is no longer the case.

Carbon based fuels are fantastic energy carriers and thus it is not surprising that we have used them for transport applications, where high energy density is required. To illustrate the superiority of hydrocarbon fuels in holding energy, consider the fact that gasoline has an energy density of ~ 45 MJ/kg, while lithium ion batteries have $<$ 1 MJ/kg. Furthermore because most carbonaceous fuels exist in a thermodynamically

favorable state at STP, they can be extremely stable over long periods of time. This translates into ease of storage and transportation. From this perspective, hydrocarbon fuels make ideal energy storage vectors. For example, if one were to make synthetic natural gas (SNG) from variable renewable electricity, water and CO_2, the SNG could be stored for months or even years within existing natural gas storage facilities, allowing for the seasonal storage of renewable electricity. Nonetheless, fuels have by and large been ignored for distributed renewable energy storage applications for two fundamental reasons: first, their production has historically been tied to large-scale centralized infrastructure, thereby complicating the possibility of using diffuse distributed resources (e.g. solar) as inputs into the system. Secondly, sourcing non-fossil carbon and hydrogen (the fundamental building blocks of hydrocarbons) has always been a challenging and expensive endeavor. Recent advancements in material science, solid oxide cell technology, automation, point source and direct capture of CO_2 may allow for the production of carbon neutral fuels in a distributed and non-continuous manner, creating the possibility of closing the carbon cycle with liquid or gaseous fuels, as well as using them to store intermittent energy sources.

1.2.1 Fulfilling the vision

Whatever the future energy infrastructure may look like, it will have to have (at least) the following general attributes: it must be cheap, it should operate seamlessly and at phenomenally large total scales (tens or hundreds of TW), and must have low carbon emissions. Recent work by Dahlgren [20] suggests that a new paradigm for building energy infrastructure is upon us, where the operation of many small mass-produced units can replace single large units, all while achieving the same levels of overall capacity (scale) and while providing better opportunities for long-term cost reductions and design improvements. In order to achieve this, we must be able to design a system that is intrinsically small, that has the ability to scale by operating

many units in parallel, while achieving low overall costs. If such a system could be designed, marrying the two major energy sub-systems (electricity and fuels) could be achieved in both a centralized and distributed fashion. This, in turn, would allow for the transformation of intermittent electricity into carbon neutral hydrocarbon fuels, and vice-versa. Recent advancements in reversible solid oxide cells, catalytic chemistry, and automation, point towards a potential path for fulfilling this vision.

Reversible solid oxide cells (RSOCs) are a special category of electrochemical systems, where the same device can either convert fuels into electricity or use electricity to make fuels depending on the mode of operation. When running as a fuel cell, RSOCs consume a fuel (H_2, CH_4, CO) to generate power via an electrochemical reaction. When operating as an electrolyzer, the RSOC uses a supplied current to perform a thermodynamically unfavorable reaction such as the splitting of H_2O into H_2 and O_2 or the reduction of CO_2 into CO and O_2. The products of electrolysis (H_2 and CO) can then be combined in catalytic reactors or reacted inside the cell channels to form a wide range of hydrocarbon fuels, thereby storing the initial electrical energy supplied to the cell in the C–H bonds of the hydrocarbon fuels. Because of this, the system's energy and power density are decoupled from one another, as the energy is stored in the carbon/hydrogen atoms of the catalytically derived fuel . This makes scaling the total storage capacity cheap, as it is a function of the total volume of the fuel/oxides reservoirs and not the electrode surface area (as is the case with conventional batteries) or the volume of the electrolyte (as is the case with conventional flow batteries). As long as chemical inputs or fuels are supplied, RSOC will operate. This feature cannot be overstated, and it is one of the defining attributes of the technology. This allows for existing infrastructure, such as the natural gas grid, to effectively serve as a cheap large-scale storage reservoir. Furthermore, because RSOCs are intrinsically small, they can be scaled from kWs to GWs by operating many devices in parallel. In contrast with traditional energy conversion devices, there

is no physical upper limit to the scale of a RSOC system as many stacks (composed of a number of individual cells) can be operated in parallel to achieve any desired output. If anything, the lower or upper limits to the size of RSOC systems is set by the ancillary operations (such as gas heating, compression, water condensation, etc.) that are part of the balance of systems.

1.3 Carbon based fuels in a carbon constrained world

In its most recent assessment report, the IPCC states that in order to avoid the most sever consequences associated with a warming planet, it is imperative to limit the concentration of atmospheric CO_2 below 450 ppm [4]. Given that today the concentration is around 400 ppm, this leaves a total allowable carbon budget of roughly 50 ppm ($\sim$ 200 Gt of carbon) , implying that in a not too distant future net global CO_2 emissions must converge to zero. This harsh reality suggests that unless carbon can be recycled directly from the atmosphere, the use of carbon based fuels as energy storage vectors and/or its use in the transport sector are severely limited. Therefore, if the future energy system is to have any carbon based fuels it will require infrastructure capable of combining renewable power with recycled CO_2 to generate sustainable carbon based fuels. Such an infrastructure would need to have, at the very least, the following attributes:

1. Efficient and affordable conversion technologies that can convert electricity into chemical energy, and chemical energy into electricity.

2. Infrastructure and technologies to recycle CO_2 from the atmosphere at an affordable price.

3. Cheap and abundant renewable power that can be directed into both the power-

to-fuels infrastructure and the atmospheric capturing of CO_2.

4. The ability to ramp up and down in order to respond and adapt to changes in resource availability and fluctuating prices in competitive electricity markets.

5. Distributed small-scale and mass-produced systems which are seamlessly strung together via automation and software.

RSOC coupled with catalytic reactors poses many of the attributes listed above, and thus they are a promising candidate for enabling the development of this type of infrastructure. The uniqueness that RSOC provide is that they present an interesting way of tying well understood chemical synthesis processes with electricity in a bi-directional way at relatively high efficiencies. Nonetheless, the sustainability of synthetic fuels, and ROSC in general, is ultimately a function of where its inputs (H_2, CO_2, electricity) come from. Therefore it is important to understand where and how these resources can be sourced in order to build a net zero carbon system. In the next sections, a quick survey of the different ways in which carbon neutral fuels can be synthesized is provided, as well as a brief discussion of the different ways in which CO_2 can be sourced and recycled.

1.4 Fuels from air, water, and renewable energy

Hydrocarbons are fungible molecules that can be synthesized via well understood chemical processes as long as one has a source of H_2, C and energy. Fortunately, the Earth's biosphere, hydrosphere and atmosphere provide very large reservoirs for sourcing these molecules. Generally speaking, one can think of two different routes for making carbon neutral fuels using air, water and renewable energy as the main inputs: (1) a biological route (natural or artificial), where plants or microorganisms are used to convert sunlight, water and carbon dioxide into stored chemical energy (carbohydrates, lipids) which are then transformed into fuels via other biological pro-

cesses (e.g. fermentation); (2) an industrial synthetic fuel route, where renewable energy (solar, wind, etc.) is used for separating H_2 from H_2O, and CO_2 is sourced directly from the atmosphere via some industrial direct air capture mechanism (DAC). Of course, these two routes can overlap, and in some cases plant biomass or microorganisms (e.g. algae) may be gasified and/or pyrolyzed to generate H_2, CO_2 or syngas ($CO + H_2$) which can then be transformed into a wide variety of fuels (e.g. methane, methanol, diesel, gasoline, etc.) via some industrial catalytic reaction. Similarly, CO_2 captured via DAC can be fed into greenhouses and/or bio-reactors to enhance the efficiency of the biological conversion.

Although these general routes differ in their complexity, scope and technological readiness, they all share the common denominator of using a renewable source of energy to extract H_2 from H_2O and combine it with CO_2 (sourced from the air), to produce a wide variety of carbon based fuels. The difference between these options is the machinery behind the conversion steps (biological vs. abiogenic), the chemical pathways, and the efficiencies with which they operate. The topic of "sustainable fuels" has been widely studied in the literature [**Ganesh2014c**, 52, 55, 99, 100, 110], and there are many different strategies that one can employ to achieve this goal. Because this dissertation focuses on the link between renewable electricity and chemical fuels, a discussion of all the possible routes for making renewable synfuels falls outside the scope of this work. However, because H_2 and CO_2 are the main building blocks used in the catalytic fuel synthesis modeled in this thesis, a brief discussion of the different ways in which these molecules can be sourced from the environment is presented below.

1.4.1 Sources of H_2

Hydrogen is one of the key building blocks for making carbon based fuel, and therefore if one is interested in making sustainable carbon based synfuels, H_2 must come

from a biogenic source or from the dissociation of H_2O. In the former case, the hydrogen tends be attached to some carbon molecules (as in the case of biomass and bio-methane) and must be separated through some chemical transformation such as gasification or pyrolysis. Once the H_2 is separated, it must be purified before it can be used as a feedstock for sustainable fuel production. In the case of dissociating H_2 from H_2O, this can be achieved through thermolysis (splitting by direct use of heat), thermochemical reactions, high and low temperature electrolysis (dissociation using electricity and heat), and photoelectrolysis (dissociation using photochemical cells). Graves et al. [55] provides a thorough review of the merits and challenges of each one of these approaches. Independently of which dissociation strategy is chosen, for fuels to be renewable the process must be powered by renewable (solar, wind, hydro, nuclear, geothermal) or nuclear energy. Because of the fact that renewable resources can be easily converted into electricity via mechanical, photovoltaic or thermal processes, electrolysis is a natural technological choice for sourcing H_2 from H_2O.

In Chapter 2 we provide a thorough discussion of the merits of high temperature solid oxide cells as the technology of choice for the electrolysis step, but generally speaking they offer an advantage over other technologies as they require less electrical energy per mol of H_2 (as they operates at high temperatures and the resistive heating of the cell supplies part of the required dissociation energy) and they have the ability to co-electrolyze H_2O and CO_2 into H_2 and CO, making them ideal candidates for producing syngas for fuel synthesis.

1.4.2 Sources of CO_2

In order to produce non-fossil carbon fuels, CO_2 must be efficiently captured from natural or anthropogenic sources. Generally speaking one can think of four main sources for recycled CO_2:

- CO_2 from fossil fuel burning power plants

- CO_2 from industrial processes (e.g. cement and aluminum production)
- CO_2 from biomass
- CO_2 from the air

Although fossil fuel burning plants and/or industrial processes likely provide some of the cheapest sources of pure CO_2, they do not offer a long-term route for carbon neutral fuels, as their use still implies the mobilization and accumulation of fossil carbon into the atmosphere. All else being equal, they potentially displace carbon from fossil fuel consumption, but their initial source was still a fossil and therefore carbon ends up accumulating in the atmosphere. Therefore, for fuels to be carbon neutral, the CO_2 contained within the fuel must be recycled directly from the atmosphere. Currently, there are two paths to achieve this: using biomass or a DAC technology.

1.4.2.1 CO_2 from biomass

Biomass provides a way of capturing and recycling CO_2 from the atmosphere, as plants convert atmospheric CO_2 into biomass via photosynthetic processes. Indeed photosynthesis provides a cheap method for converting solar energy, H_2O and atmospheric CO_2 into carbohydrates which can then be gasified or pyrolyzed to generate H_2 and CO. The chemical energy stored in the biomass may also be harnessed via combustion and the resulting CO_2 may be captured and separated form the flue stack or exhaust stream. Using biomass as a source of carbon offers the advantage of relying on natural biological process for capturing atmospheric CO_2, however the low power densities associated with biomass (< 1 W/m^2) imply that extremely large areas are required to produce substantial amounts of bio-energy and/or CO_2. At very large scales, this may pose societal problems as land for energy crops would compete with plots dedicated for food production. The amount of resources (e.g. water, fertilizer,

etc) required for growing and harvesting the biomass, as well as they type of crop (edible vs not edible) will ultimately determine how sustainable the fuel is.

1.4.2.2 Direct Air Capture

The other strategy for sourcing CO_2 from the atmosphere is to separate it from the air using DAC technologies. Direct air capture refers to a technology that is capable of directly removing CO_2 from the atmosphere and delivering a stream of pure CO_2 for permanent disposal or to be used for industrial applications. Removing CO_2 from the air is not new, it has been successfully implemented in submarines and spaceships for many decades. Because the free energy of mixing is a logarithmic function with respect to the partial pressure of the gas, removing CO_2 from a gas mixture becomes more costly (from an energetic point of view) at lower concentrations. Lackner [82] estimates that his passive DAC systems would have an energy consumption somewhere in the order of 50 kJ per mol of air captured CO_2. Considering the fact that the ΔH for water electrolysis at 850 °C is roughly 250 kJ/mol, it can be seen that the capture of CO_2 from the air is a fraction of the energy required to dissociate H_2 from H_2O. Thus, it is hard to envision an RSOC system in which air capture drives the energetic costs for the system. Thus, the challenges of developing large-scale infrastructure capable of removing CO_2 from the air lie in the scales, efficiencies, and relatively low costs at which this infrastructure would have to operate in order to supply enough CO_2 for a global synfuel industry.

There are many approaches for removing carbon dioxide from the atmosphere, most of them relying on the chemical absorption or adsorption of CO_2. Goeppert et al. [48] provide a comprehensive review of the existing technologies, as well as the underlying physics and thermodynamics of each. Although the existing technologies vary in the way in which the CO_2 is separated from the air, all of them undergo a process that can be broken down into three separate stages: first, contacting the

active surface with air; second, absorption or adsorption of the CO_2 onto a sorbent; and third, recovery of the sorbent and release of the captured CO_2 [83]. The process can be performed in a continuous fashion or in batches.

1.5 Tying chemistry to renewable electricity: the long-term goal

As stated throughout this chapter, renewable carbon based fuels possess certain attributes that could allow them to become a key enabling technology of the low carbon infrastructure of the future. To achieve this vision, cheap renewable energy must be available in order to separate H_2 from water and CO_2 from the air, and these processes must be combined in an efficient way in order to transform the H_2 and CO_2 into high density energy carriers. If the fuel is being used for energy storage applications, the reverse process (going from fuel to electricity) is also required. Put differently, if carbon neutral fuels are to be used for energy storage and/or transport applications, infrastructure that is able seamlessly link renewable electricity sources to chemical transformations processes (in both directions) must be developed. Indeed, it is this particular link that is the overarching theme of this dissertation.

1.5.1 The need for variable operation

Solar and wind electricity are intermittent in nature, therefore at large scales and penetrations it is important for the infrastructure around it to operate in a flexible fashion, ramping its output up and down in order to react to changes in the underlying resource availability. Even if the a particular system is not designed for load balancing applications, competitive electricity markets that base their clearing price on marginal costs can exhibit dramatic swings in the price of electricity as variable renewable resources become more/less available throughout the day (see Chapter 5

for a discussion of the impact of wind on the Danish electricity markets). Furthermore, as distributed generation becomes a bigger part of the energy systems, load shifting, peak shaving and time-of-use tariffs are expected to play a crucial role in guaranteeing stability within the system. With this regard, variable operation and reversibility of RSOC could prove to be a unique and valuable characteristic, as the RSOC systems could switch modes and reduce/increase its output as a function of exogenous signals sent by a central Independent System Operator (ISO) or other DG devices. That is, it is important to design cheap and reliable RSOC systems that have the ability to optimize the link between variable electricity and chemistry in a bi-directional fashion at different time increments. Doing this will allow a particular system to operate with higher capacity factors, and could enable carbon neutral fuels to participate in energy storage applications operating at hourly, daily, and seasonal timescales.

As with all novel ideas and technologies, it is hard to pinpoint exactly how/why they will succeed in the future. Nonetheless, RSOC's possess many attributes that make them a unique candidate for bridging electricity and fuel production. Historically, the electric sector has seen very little overlap with the infrastructure built to produce high energy density fuels. This, however, could very well change in a not too distant future. The development of RSOC systems capable of operating at different scales in both a centralized and distributed paradigm seems poised for disrupting the old paradigms and for bridging two critical sectors that have seen virtually no overlap. This great potential is the main driver of the work presented in this dissertation, which aims at contributing and informing the discussion and knowledge of RSOC in the context of energy storage, carbon neutral fuel production and their integration into spot electricity markets.

Chapter 2

Background

The main purpose of this dissertation is to model reversible solid oxide cell (RSOC) systems coupled with catalytic reactors in order to gain insight into the different strategies that can be used to operate these systems under a wide variety of technical and economic assumptions, as well as to elucidate the role that they can play in the decarbonization of the energy system. Before delving into the details of the RSOC system model developed for this dissertation, it is important to briefly discuss the fundamental chemistry and thermodynamics behind solid oxide cells. Thus, this chapter will provide the reader with the necessary background to understand the basic principles behind RSOC as well as the existing technologies that can be employed for the synthesis of methane from CO_2 and H_2. The first part of the chapter will focus on the thermodynamics and chemistry of RSOC and will discuss the existing "state-of-the-art" technology. A brief discussion of RSOC system level modeling will also presented. The second part of the chapter discusses the current technologies that are used at large scales for methanation, and will briefly touch on the key aspects of the catalytic reaction that could enable small-scale methanation operations.

2.1 Reversible Solid Oxide Technology

Solid oxide cells are electrochemical devices that operate at high temperatures (650-900 °C) originally designed for the production of electric power (fuel cell mode) via the oxidation of a chemical fuel. As their name suggests, solid oxide cells are composed of solid state materials (metals and ceramics) with three main components: a fuel

electrode, an oxygen electrode, and a ceramic electrolyte used for the transport of oxygen ions. Each electrode is a good electronic conductor and is porous in nature in order to allow for the diffusion of gases towards the inner electrolyte [1]. The electrolyte, a thin ceramic (typically Yttria-stabilized zirconia YSZ), is a good O^{2-} conductor but needs to be a material that does not exhibit electronic conduction. Typically, SOC's are manufactured with planar or tubular geometries. For the purpose of the work presented in this thesis, all discussions and modeling will pertain to planar cell geometries. In planar designs, the main cell components are configured as thin flat planes with the electrolyte sandwiched between the two porous electrodes. The interconnection is ribbed on both sides and provides channels for the gases to flow through [31, 111]. Stacks are formed by piling cells on top of each other with electrical interconnect plates between each adjacent electrode. Generally speaking, planar cells exhibit lower manufacturing costs, while tubular cells have faster start-up/cool and are less prone to gas leakages[107]. .

2.1.1 Modes of operation

SOC have the ability to be operated as fuel cells, generating power from a chemical fuel, or as electrolyzers, which use a current to drive a thermodynamically unfavorable chemical reaction (e.g., splitting H_2O into H_2 and O_2). Although these two modes of operation (fuel cell and electrolysis) have traditionally been thought of as two separate processes requiring separate dedicated units, in the case of solid oxide cells reversing the direction of the current allows for the same device to switch between operating as fuel cell and operating as an electrolyzer [93]. The ability for a SOC to become

[1] By mixing the electrode material with a good ionic conductor (typically the electrolyte material), electrodes can be composite materials that also exhibit ionic conductivity. This is desirable as it helps the overall performance of the of SOC by extending the reaction zone from the immediate vicinity of the electrolyte into the electrode bulk [81, 130]

"reversible"[2], meaning it can flip back and forth between both modes of operation, is determined solely by the ability of the system and cell to deliver all reactants in both modes to the electrode reaction sites. There is nothing intrinsic in the electrochemistry that would make it impossible for a fuel cell to operate in a reversible manner. However, some implementations lend themselves to nearly reversible operation, while others by design have difficulties in operating in both directions. As pointed out by Graves [52], there are certain cell designs that won't allow reversible operation, such as simple aqueous electrolytic cells where electrodes are immersed in the aqueous electrolyte and therefore it is impossible to supply H_2 gas to the electrodes if fuel cell mode operation was desired.

Solid oxide cells transport oxygen ions and thus they are capable of oxidizing (in fuel cell mode) or reducing (in electrolysis mode) CO/CO_2 mixtures in addition to H_2/H_2O. This capability is a key difference between SOC and proton exchange membrane (PEM) and alkaline cells, which are based on the conduction of protons (H^+) and hydroxide ions (OH^-), respectively [52]. Thus, RSOCs can use a variety of fuels in fuel cell mode to produce power and have the ability to electrolyze both steam and CO_2 into a gas mixture rich in H_2 and CO [9, 31, 32, 53]. This mixture, in turn, can be used to synthesize a wide variety of high energy density carbon based fuels, effectively storing the electric energy in the high-energy carbon-hydrogen bonds.

The chemistry involved in RSOCs includes steam reforming of a fuel (typically methane), the shifting of CO via the water-gas shift reaction, and an electrochemical oxidation/reduction:

$$CH_4 + H_2O \longleftrightarrow CO + 3\,H_2 \qquad \text{(R2.1)}$$

[2]When referring to SOC's, the term reversible refers to the ability of the cell to switch back and forth between fuel cell and electrolysis mode by reversing the polarization. The term should not be confused with use of the word in classic thermodynamic discussions, where reversibility is a term used to describe a process in which entropy does not increase and in which a particular outcome of a thermodynamic cycle can be reversed by traversing the cycle back. Indeed, the cell can cycle between the two states, but there is an entropy penalty that is paid during each switch.

$$CO + H_2O \longleftrightarrow CO_2 + H_2 \tag{R2.2}$$

$$H_2 + \frac{1}{2}O_2 \longrightarrow H_2O \tag{R2.3}$$

When RSOC's are operated in fuel cell mode (see Fig. 2.1), fuel is supplied to the anode while an oxidant (typically air) is supplied to the cathode side of the cell. On the fuel side electrode (anode), fuel diffuses through the porous electrode and at the electrode/electrolyte boundary oxygen ions are extracted from the electrolyte and the following electrochemical reactions take place:

$$H_2 + O^{2-} \longrightarrow H_2O + 2\,e^- \tag{R2.4}$$

In addition to reaction R2.4, electrochemical oxidation of CO, CH_4 and other species does occur (as depicted in Fig. 2.1) . This, however, tends to be ignored for modeling purposes due to the fact that the kinetics of H_2 oxidation are much faster than the electrochemical oxidation of CO or CH_4 [89].

On the cathode side, air diffuses through the porous electrode and at the boundary between the electrode and the electrolyte O_2 is electrochemically reduced:

$$\frac{1}{2}O_2 + 2\,e^- \longrightarrow O^{2-} \tag{R2.5}$$

As mentioned before, if electrodes are mixed with good ionic conductors, or made from mixed ionic/electronic conduction materials, they can exhibit good ionic conductivity which in turn extends the triple phase boundary (the reaction zone) from the electrode/electrolyte interface into the electrode bulk. Oxygen ions are transported via solid state diffusion through the electrolyte from the air electrode side to the electrolyte/anode interface.

The free movement of oxygen ions in the electrolyte generates a concentration difference across its two sides, and the diffusion of oxygen will establish an electrochemical potential. Absent an external potential, if the anode is connected to the cathode via an external circuit, electrons will flow (generating a current) as long as

gases on both sides are supplied. Therefore, without an external potential the SOC will act as a fuel cell, and the net reaction becomes:

$$H_2 + \frac{1}{2} O_2 \longrightarrow H_2O \tag{R2.6}$$

Due to the high temperatures of operation and because the cell's anode support

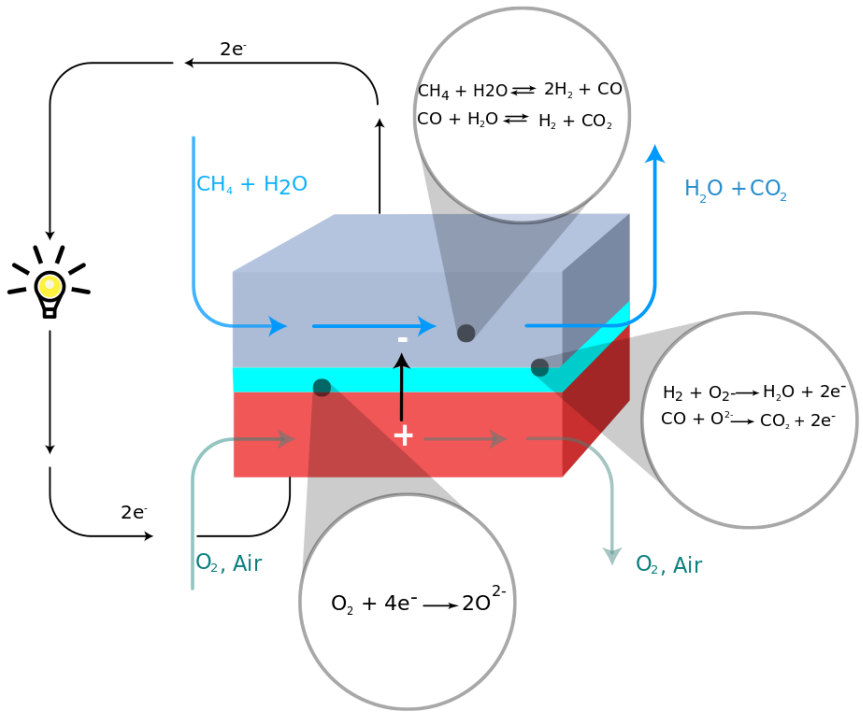

Figure 2.1: SOC in fuel cell mode

layer is made out of Ni (a good reforming catalyst), RSOC's operating in fuel cell mode have the ability to internally reform (and electrochemically oxidize) some hydrocarbons (e.g., methane, methanol) into hydrogen and carbon monoxide [85] which are then electrochemically consumed at the triple-phase boundary to produce power Reactions R2.4 to R2.6). As shown on Fig. 3.2, as the carbonaceous fuel diffuses through the porous electrode towards the electrolyte, it gets reformed into a mixture of hydrogen and carbon monoxide. It has been shown that the electrochemical oxidation of H_2 exhibits much faster kinetics than that of CO [89]. For this reason, it is

generally assumed that only H_2 is involved in the electrochemical reaction in the fuel cell, even though the SOC is capable of electrochemically oxidizing CO. The temperature at which the SOC operates and the presence of steam in the mixture, favors the shifting of CO (via the water gas shift reaction) which increases the concentration of H_2 in the bulk gas which is then is electrochemically oxidized. Direct electrochemical oxidation of methane is possible in SOC's [51, 65, 122], although carbon formation is an existing challenge for these types of cells[61, 63, 64]. The ability to internally reform fuels is an attractive feature of RSOCs as it eliminates the need for external reformers, simplifying the overall design and reducing investment costs. Another advantage of internally reforming the fuel is that some of the heat produced by the stack can be used by the highly endothermic reforming reaction, helping reduce the amount of cooling air required to maintain a stable thermal gradient across the cell.

In electrolysis mode, RSOCs are capable of generating hydrogen or syngas from a H_2O or H_2O and CO_2 mixture. In electrolysis mode, steam or CO_2 (or a mixture of both) flows on one of the electrodes and a voltage is applied to the cell. This potential drives the electrochemical reduction of the gases, resulting in an ion being transported through the electrolyte:

$$H_2O + 2\,e^- \longrightarrow H_2 + O^{2-} \tag{R2.7}$$

$$CO_2 + 2\,e^- \longrightarrow CO + O^{2-} \tag{R2.8}$$

Ions recombine to produce pure O_2 on the other electrode:

$$2\,O^{2-} \longrightarrow O_2 + 4\,e^- \tag{R2.9}$$

Thus, the net reaction when performing co-electrolysis of H_2O and CO_2 becomes:

$$H_2O + CO_2 \longrightarrow CO + H_2 + O_2 \tag{R2.10}$$

Just as in the case of fuel cell operation, if a mixture of H_2O and CO_2 is being electrolyzed, some equilibrium reactions will occur (mainly water-gas shifting) as

the gases flow through the electrode towards and the electrode/electrolyte interface. Electrolysis will be sustained as long as electricity and feedstock gases are provided.

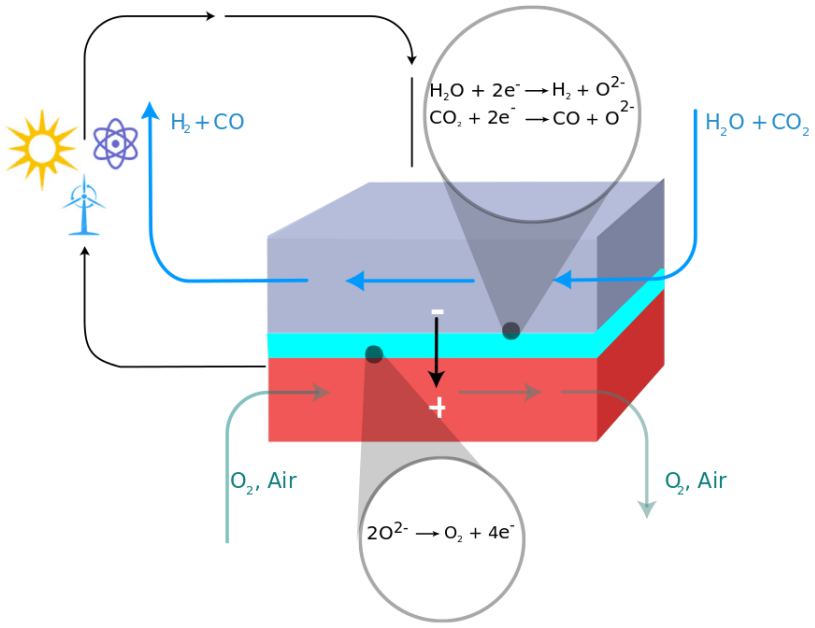

Figure 2.2: SOC in electrolysis mode

2.1.2 Thermodynamics

From a thermodynamic point of view, the maximum work output generated by the stack (fuel cell mode) or the minimum electric input required (electrolysis mode) is determined by the free energy of the electrochemical reaction, which is related to the cell's reversible potential via the following relationship:

$$\Delta G = -nFU_{rev} \tag{2.1}$$

where n is the number of electrons transfered during the reaction, F is Faraday's constant and U_{rev} is the reversible potential. U_{rev} is typically the voltage measured

at open circuit (OCV) and it is defined by the Nernst equation.

$$U_{rev} = \frac{-\Delta G_{rxn}(T_{op})}{2F} - \frac{RT_{op}}{2F} \ln \left(\frac{y_{\text{eq}}^{H2O}}{y_{\text{eq}}^{H2} \left(y_{\text{eq}}^{O2} \frac{P}{P^o} \right)^{\frac{1}{2}}} \right) \tag{2.2}$$

where $\Delta G_{rxn}(T_{op})$ is the Gibbs free energy of the H_2 oxidation reaction at the operating temperature of the cell, $y_{\text{H}_2}, y_{\text{H}_2\text{O}}, y_{\text{O}_2}$ are the equilibrium mole fractions of H_2, H_2O and O_2 at the electrode/electrolyte interfaces [3] (prior to the electrochemical reaction), P is the operating pressure of the cell and P^o is the reference pressure. From basic principles we know that:

$$\Delta G = \Delta H - T\Delta S \tag{2.3}$$

thus if the maximum/minimum electric work generated/required (fuel cell/electrolysis) is defined by ΔG, then there must be an amount of energy equal to $T\Delta S$ that manifests itself in the form of heat. In cases where the entropy change is negative, the cell will generate heat, while those with positive entropy changes will consume heat from the surroundings. It follows, then, that for a RSOC operating isothermally the ideal efficiencies for each mode are:

$$\eta_{FC} = \frac{\Delta G}{\Delta H} \tag{2.4}$$

$$\eta_{EL} = \frac{\Delta H}{\Delta G} \tag{2.5}$$

The OCV is the voltage measured when no current is being drawn from the system. However, when the system is operating and a current is being drawn or supplied, the operating voltage varies from the OCV due to three main irreversible losses: Ohmic losses, activation and concentration overpotentials[4]. Thus, the operating voltage is

[3] For a discussion of how these mole fractions are calculated see Section 3.3.1.2

[4] It is important to mention that the OCV is not necessarily the reversible voltage, as other losses such as leakage can occur which will make the OCV deviate from the reversible voltage.

simply the difference between the OCV and the cell's overpotentials:

$$U_{op} = U_{rev} - \eta_{ohmic} - \eta_{act} - \eta_{conc} \tag{2.6}$$

Activation overpotentials pertain to the irreversibilities associated with charge transfer limitations at the triple phase boundary [58]. Due to the high operating temperatures, activation overpotentials are very low in SOC even without the use of a special catalyst, making this an attractive advantage of SOC's. Concentration overpotentials are related to transport limitations within the porous electrode. Lastly, Ohmic losses mainly result from the ionic resistivity of the electrolyte ceramic. The Ohmic overpotential is linearly dependent upon the current density and decreases with increasing temperature[70]. In electrolyte supported cells, activation and concentration overpotentials tend to be small relative to the ohmic losses, thus the latter overpotentials dominate over a range of currents. This, in turn, results in the typical current-voltage curve for SOC's exhibiting a linear relationship over a wide range of currents . As seen in Fig. 2.3, the relationship between current and voltage tends to be linear except at the extremes, where the reaction becomes mass-transfer limited and the concentration overpotential dominates [108]. Modeling the activation and concentration overpotentials is a non-trivial matter, therefore one approach for simplifying the problem is to bundle the various resistances into a single area specific resistance (ASR), which is simply defined as the slope of the i-V curve. Thus, (2.6) can be written as:

$$U_{op} = U_{rev} - iASR \tag{2.7}$$

Beyond the decrease in ionic resistivity, in electrolysis mode there are thermodynamic advantages for operating the RSOC at high temperatures [55] . As shown in Fig. 2.4, as temperature increases the electrical energy required for the electrolysis decreases (ΔG) and the Joule heating that is generated due to the internal resistance of the cell can be applied towards the TdS heat demand for splitting H_2O and/or CO_2. This

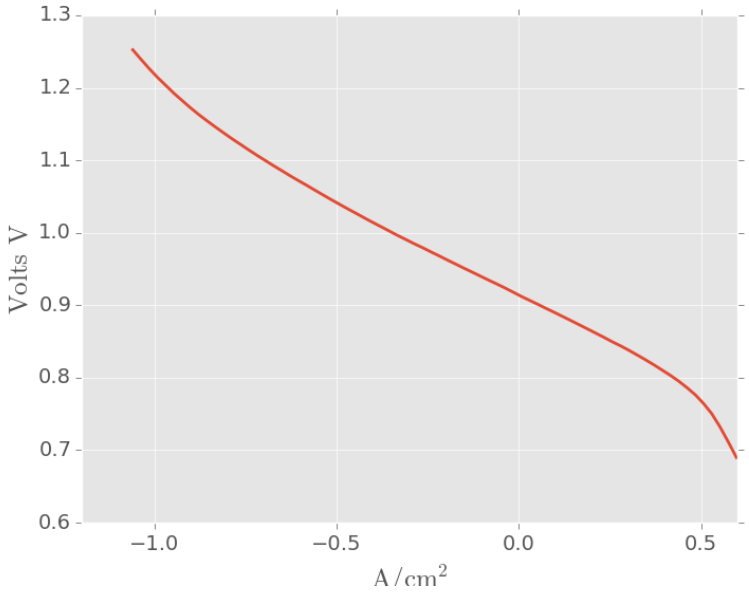

Figure 2.3: Polarization curve for a planar SOC operating at 850 °C for a 50% H_2O-25% H_2-25% Ar mixture at 1 atm. Adapted from [32]

allows for operation near the thermoneutral voltage, which implies an electrical-to-chemical efficiency of close to 100%. The following section (Section 2.1.3) gives an in-depth discussion of the thermoneutral voltage and its implications.

2.1.3 Thermoneutral voltage

Strictly speaking, the thermoneutral voltage is equal to the voltage where the cell's power is equal to the heat generated by all reactions (chemical and electrochemical) occurring inside the cell. The thermoneutral voltage is typically defined as the change in enthalpy per unit of charge transferred:

$$U_{TN} = \frac{\Delta H}{nF} \tag{2.8}$$

Thus, U_{TN} can be used to assess the heat removal or addition requirements for a particular operating mode (fuel cell or electrolysis) and for a given operating point (e.g. current/voltage). For a typical cell operating with H_2:H_2O redox chemistry, the

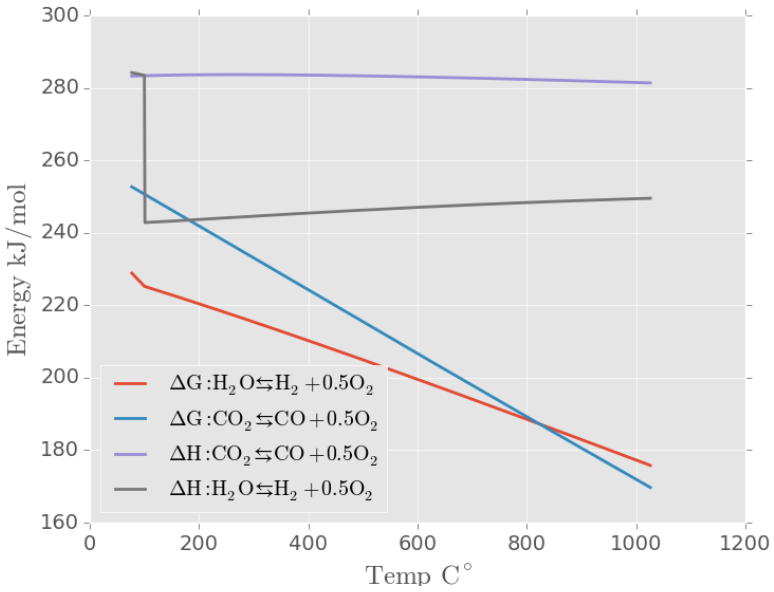

Figure 2.4: Enthalpy and Gibbs free energy for H_2O and CO_2 electrolysis

thermoneutral voltage in fuel cell mode is always above the operating voltage, as the electric power generated by the stack is always smaller than the net heat generated due to the negative entropy associated with the electrochemical reaction ($U_{op} < U_{TN}$). Thus, in fuel cell mode the cell is always exothermic and requires active cooling. In electrolysis mode, however, it is possible to have operating voltages that are below U_{TN}, which imply that the cell operates endothermically, extracting heat from the environment. Absent a high temperature heat source, operating the cell below U_{TN} implies that the cell cools as it operates. If one wishes to operate exothermically, such that the cell produces more heat than it consumes, the operating voltage must be above the thermoneutral voltage. Table 2.1 summarizes these relationships.

For cells that operate with pure H_2 as a fuel, the calculation of the thermoneutral voltage is straightforward, as the only reaction occurring is the electrochemical oxidation/reduction of hydrogen. In the case of SOCs that operate with internal reforming, the calculation of U_{th} is a more difficult task as the steam reforming of

Voltage	Operating Mode	Result
$U_{op} > U_{TN}$	*Fuel Cell*	$Q_{net} > 0$. Cooling Required.
$U_{op} < U_{TN}$	*Electrolysis*	$Q_{net} < 0$. Heating Required.
$U_{op} > U_{TN}$	*Electrolysis*	$Q_{net} > 0$. Cooling Required.
$U_{op} = U_{TN}$	*Electrolysis*	$Q_{net} = 0$. Isothermal operation.

Table 2.1: Operating voltage and thermoneutral relationships.

methane, water-gas shift and electrochemical oxidation all occur simultaneously. In order to correctly compute U_{th} for setups with internal reforming, we use an approach based on the method suggested by [126] where the net heat output of the stack (including all reforming, shifting and electrochemical reactions) is set to zero the resulting relationship is used to solve for the stack's voltage. This heat balance will be discussed in detail later and is summarized in equation (3.22). The resulting U_{th} can therefore be defined as :

$$\begin{aligned} U_{th} = &- \left(\frac{\xi_{SRM} \cdot \Delta H_{rxn,SRM}}{i} + \frac{\xi_{WGS} \cdot \Delta H_{rxn,WGS}}{i} + \frac{\xi_{redox} \cdot \Delta H_{rxn,redox}}{i} \right) \\ &+ \sum \dot{n}_f^i \cdot h^i(T_{out}) - \sum \dot{n}_o^i \cdot h^i(T_{in}) \end{aligned} \tag{2.9}$$

where $\dot{n}_f^i$ is the molar flow of species i coming out of the stack, $\dot{n}_o^i$ is the molar flow of species i coming into the stack, h^i is the species enthalpy at the specified temperature, and $\xi_{SRM}, \xi_{WGS}, \xi_{redox}, \Delta H_{rxn,SRM}, \Delta H_{rxn,WGS}$ and $\Delta H_{rxn,redox}$ are the molar extents and heat of reactions for reactions R2.1 to R2.3

2.2 Literature review

The use of solid oxide fuel cells for power generation has attracted the interest of researchers, governments, and companies for more than 30 years and has been heavily studied and documented in the literature. The main drivers that generated interest to develop and roll-out SOFC technology were its fuel flexibility, its high fuel-to-electricity efficiency, its use of common materials (no precious metals required), and its relatively pure exhaust products (almost pure CO_2 once the H_2O is condensed)

which translates to low emission rates of particulates, CO and VOC's, implying little pollution beyond the carbon dioxide generated during its operation [115]. Due to the fact that SOCs in fuel cell mode have been an active area of research for many decades, this section will only focus on briefly reviewing the existing literature on SOCs for energy storage applications and synthetic fuel production. If the reader wishes to delve into the literature of SOFC, the following reviews provide a good starting point: for a general review of SOFC technology and applications see Choudhury et. al. [17]; for a general review of SOFC models see Wang et. al. [120]; for a review of mathematical modeling of SOFC see Haijmolana et. al. [57]; for a review of different SOFC based systems and their integration with other technologies (bottoming cycles, gas turbines, CHP, etc.) see Zhang et. al. [134].

In recent years, the constraint on carbon emissions and the increasing penetration of variable renewable energy technologies has created an interest in developing systems that can store intermittent electricity at large scales in an efficient and cheap manner. Because of their ability to operate both as fuel cells and electrolyzers, SOCs that operate reversibly have gained interest as devices that can be used for storing/delivering power at large scales and with relatively high round trip efficiencies [73, 93, 125, 127]. SOCs have also been proposed as a key enabling technology for the production of high energy density carbon neutral fuels [10, 31, 55, 116]. In a way, the concept of the "energy hub" presented in this thesis can be thought of as a hybrid of the storage systems, whose main objective is to store and deliver power in a highly efficient manner, and the electrolysis designs whose main objective is to make synthetic fuels at a constant, cheap, and reliable manner. In the following sections, a brief review the use of RSOC for closed storage applications, as well as the use of SOCs for synthetic fuel production is presented. The main objective of this section is to provide the reader with some background on the existing technologies and designs, as well as on their inherent limitations and challenges.

2.2.1 Solid oxide cells for fuel synthesis

As previously mentioned, the use of solid oxide electrolyzers in synthetic fuel production has gained a lot of attention in recent years. Hydrocarbons are fungible molecules, therefore if one starts with the right reactants and conditions it is possible to make many types of carbonaceous fuels such as methane, methanol, gasoline, jet-fuel, etc. Generally speaking, as long as one has access to pure H_2, CO_2, CO and/or a mixture of these (e.g. syngas), it is possible to make high energy density fuels by combining these molecules under the right operating conditions and with the right catalysts. Historically, syngas ($CO+H_2$) has been produced by reforming natural gas [6] or by gasifying coal. This, however, implies the use of fossil carbon which is problematic if one is to design a low carbon energy system. Thus, it is desirable to find a source of these elements that does not originate from a fossil carbon. Solid oxide cells

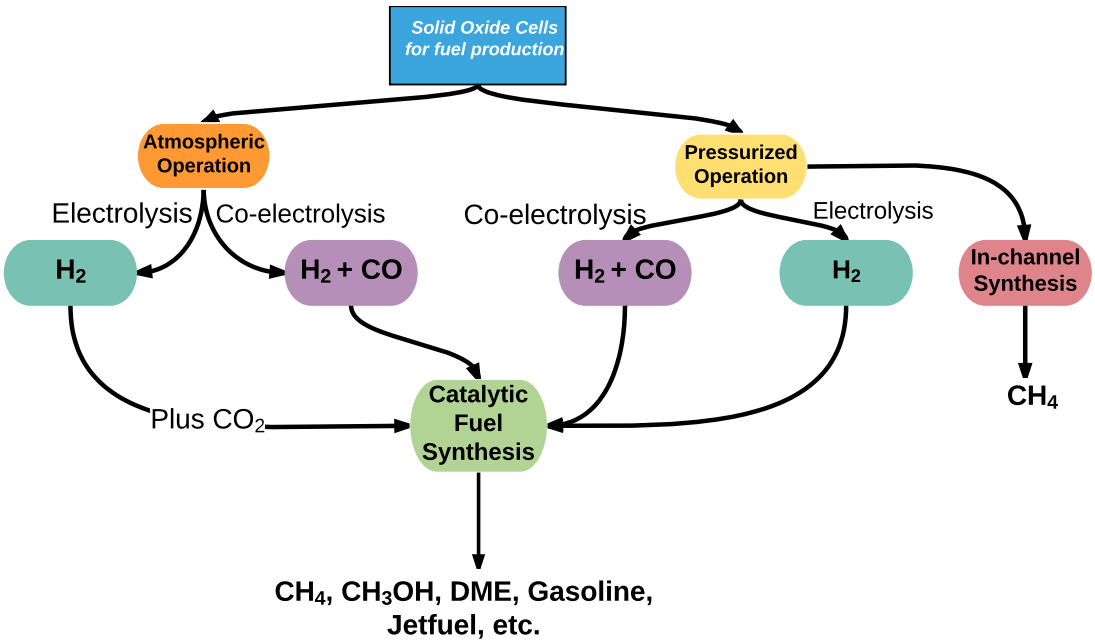

Figure 2.5: Solid Oxide Cells for fuel synthesis

offer a promising way to achieve this, as they can operate at very high efficiencies [32] and have the ability to simultaneously split CO_2 and H_2O into a mixture of pure CO

and H_2 using electricity and heat. Thus, if a renewable source of power and a stream of recycled CO_2 is available, a sustainable carbon neutral fuel can be produced [55, 59, 93]. Fig. 2.5 shows the different ways in which SOCs can be operated for the purpose of making synthetic fuels, which can be broken down into two general categories: the first are stacks operating at atmospheric pressure which electrolyze pure H_2O or perform co-electrolysis of H_2O and CO_2; under the second category, SOCs are pressurized which can lead to simpler Balance of Plant (BoP) arrangements and higher efficiencies [74, 116]. Recent studies have reported that pressurizing the cells can also lead to in-channel fuel synthesis, which greatly increases the overall efficiency of the system and can lead to very high round trip efficiencies if operated reversibly [73, 127].

2.2.1.1 SOEC - atmospheric operation

In recent years, there has been a number of studies that use solid oxide electrolyzers operated at atmospheric pressure for fuel synthesis. Generally speaking, the studies either focus on the the stack and the influence that operating parameters (temperature, fuel utilization, S/C ratio, etc.) might have on the H_2 and/or syngas composition or focus on full process modeling in which the produced H_2 and/or syngas is converted into synthetic natural gas (SNG) via "power-to-gas" technologies, or into liquid fuels such as methanol, gasoline, or DME. Because the main goal of this thesis is to provide an end-to-end model, this section will only focus on system studies. For reference on stack level studies, see [16, 31, 32, 52, 53, 76, 78]. In the category of SNG De Saint Jean et. al. have done some of the most relevant work. In a recent study, they performed a parametric study of synthetic natural gas synthesis using a solid oxide electrolyzer operated at atmospheric pressure [25, 26]. The parameters for the SOC are obtained experimentally. In this work, natural gas is synthesized in an external methanator and a process efficiency of 75.8% is reported. CAPEX cost

estimates and final cost per Nm^3 of SNG are also provided. Similarly, Barelli et. al. [5] report a system model for the production of "hydromethane", a mixture of CH_4 and H_2, using a solid oxide electrolyzer operated at atmospheric pressure. Their study includes both steam electrolysis and co-electrolysis sensitivity studies, and they report a maximum system efficiency of 60% with a H_2 molar fraction of 26%.

Most of the studies found in the literature that deal with the synthesis of liquid fuels using solid oxide electrolyzers are operated at high pressures. This is due to the fact that reactors for liquid fuel synthesis (methanol, DME, gasoline, FT products) need to operate at high pressures and it is energetically cheaper to compress H_2O and/or CO_2 than it is to compress syngas. Thus, most of these studies make use of pressurized stacks in order to boost the overall system efficiency. Pressurized stacks, however, are only in the lab/pilot scale and have not been commercialized yet. There are, however, a few reports that study atmospheric high temperature electrolysis for liquid fuel synthesis. Botta et al. [10] report a process for synthesizing DME using atmospheric (and pressurized) co-electrolysis in which they are able to achieve power-to-fuel efficiencies in the order of 64%. Similarly, Gregoire et al. [86] provide a design for a power-to-methanol system in which atmospheric co-electrolysis is used upstream of a methanol synthesis train. After clever heat integration, this study reports a power-to-fuel efficiency of 53% (LHV). In its review of syngas production technologies, Graves et al. [55] suggest that SOCs are a promising technology for FT liquids and provide a rough estimate of the energy and cost associated with making gasoline using a high temperature electrolyzer operating at atmospheric pressure.The authors report that for an optimistic scenario of high capacity factors and low CAPEX, synthetic gasoline could be made for 2-6 $/gal depending on the cost of electricity.

2.2.1.2 Pressurized operation

As mentioned before, operating the SOCs at high pressures can be beneficial when the reduced products (H_2 and CO) are intended for fuel synthesis. As such, most studies that focus on the production of fuels via high temperature electrolysis use pressurized stacks. In a paper published in 2012, Sun et al. [116] performed a thermodynamic analysis of pressurized solid oxide cells for the production of synthetic dimethyl ether and methane. The study discusses the optimal operating conditions that yield the H_2:CO ratios required both for SNG and DME synthesis, and reports that if the stack is operated at relatively low temperatures (e.g. 650 °C) and high pressures (35 atm), the syngas resulting from the co-electrolysis operation may contain a large fraction (∼25%) of *in-situ* generated methane. This finding, that low temperature and high pressure can lead to *in-situ* methane formation has been exploited by other groups to propose storage mechanisms with high roundtrip efficiency. This topic is further discussed in the section below.

In a two part study, Giglio et al. provide an in depth analysis of an SNG plant coupled to a solid oxide electrolyzer operated at 33 bars [46, 47]. In these papers, the authors report electricity-to-fuel efficiencies of around 81% (LHV). The authors also provide and in-depth analysis of the CAPEX requirements and report the production cost of SNG for a wide variety of electricity, CO_2 and CAPEX costs.

Similarly, Hansen et al. [59] provide a system level model for studying the production of synthetic natural gas and methanol using a pressurized stack. In this study, the authors report high overall system efficiencies of 76-86% for the SNG process, and 75-88% for the methanol process.

Rivera-Tinoco et al. [106] present a techno-economic study of a power-to-methanol system where two different designs, one that uses a PEM electrolyzer and one that uses a SOEC, are compared [106]. In this study, the authors find that the system that uses solid oxide electrolyzers has a much higher CAPEX than the one that relies on

a PEM electrolyzer. Using somewhat conservative assumptions with respect to cost, the authors find that methanol synthesized in the SOEC based system is roughly 15 times more expensive than market priced methanol. For the case of the PEM system, the authors report that the synthetic methanol is 2.5 times more expensive.

On the synthesis of liquid fuels, Becker et al. [8] provide a systems level thermochemical process for making FT liquids by coupling a SOC operated at 5 bar with a catalytic reactor. The authors also provide economic analysis of the system. The authors report an electricity-to-fuels efficiency of 54 % and claim that the liquids can be made for 4-15$/gal depending on the price of electricity. Similarly, Fu et al. [40] provide a study of syngas production using pressurized SOEC for FT liquid synthesis, and they report system efficiencies of ∼74%.

2.2.1.3 "Off-design" operation

As discussed in subsequent chapters, one of the main focus of this thesis is studying the advantages that arise when a RSOC system is operated across many different currents and flows. As such, it is worth doing a quick survey of the literature with respect to "off-design" and dynamic operation, which pertains to the system level implications of ramping the system up and down across a wide range of flows/currents/voltages. As is the case with most of the SOC literature, most of the existing literature on off-design analysis has focused on systems operating in fuel cell mode. After a survey of the literature, no published studies on the off-design operation of RSOC were found, thus this one of the central contributions of this thesis.

Kupecki et al. [80] published a paper on the off-design operation of a DME fed SOFC. The paper provides some clear guidelines as to how to approach off-design modeling for the SOC and the BoP. It also highlights the interaction between system components across different operating points.

Milewski et al. [91] also published a mathematical model for off-design operation

of a SOFC coupled with a gas turbine. The author provide performance maps for the components and the system, and find that the efficiency is higher when operated at flows lower than the design point[5].

Lastly, for some background on the impacts and implications of dynamic operation, as well as startup and shutdown strategies the reader can consult the following studies: [2, 3, 19, 87, 94, 95].

In recent years, there have been a few studies that deal with the off-design operation of solid oxide electrolysis systems. Sanz-Bermejo et al. [108] performed a parametric study of a SOEC system, with H_2 as its main product, at part load operation. It reports system efficiencies for a wide range of assumptions on the ramp-up rate, the operating temperature, and the operating strategy (e.g. constant current vs. constant voltage). The study also provides some useful heuristics for modeling BoP components at part-load, but offers no economic analysis.

Peptitas et al. [103] provides a study of a H_2 based SOEC at various loads, although their results do not really reflect a truly "off-design" scenario, as the system is designed for different loads (e.g. exothermic vs endothermic) rather than choosing one particular design and operating it above and below the design point.

2.2.2 Reversible solid oxide cells for energy storage

The study of RSOC for energy storage applications is a novel topic in the literature. Because the technology is in its infancy, most of the system level studies rely on computational models rather than experimental setups. There are a few studies that rely on experimental work, although most are limited to cell or stack level analysis. Thus, the literature on RSOC can be broken down into two general categories: studies that draw the boundary at the cell/stack level; and studies that are less concerned about the intricacies of the cell, and focus on the system analysis. Given that the

[5]This is a very important finding and is discussed in depth in Chapter 4

main topic of this thesis is a systems level analysis, the literature reviewed in this section will focus on the latter category. If the reader is interested in recent advances of RSOC at the cell level, the following references provide a good starting point: for robustness of SOC to current switching see [75] for implications of reversibility on cell degradation see [49, 54]; for impact of current switching on electrode durability see [129].

Ren et al. provide a system model of a RSOC storage system with high temperature heat storage. The RSOC is operated at high pressure and they report a storage efficiency (full cycle) of 42-64% depending on the operating point, which does not include BoP parasitics.

In a recent study, Wendel et al. [126] describe a method for choosing the operating conditions which result in high round trip efficiencies ($\sim$ 85%) for a closed RSOC storage system. The system is based on storing all exhaust gases and oxides, and assumes high pressures ($\sim$ 10 bar) and low temperatures ($\sim$650 °C) for the stack. The authors put forth the thesis that the thermoneutral voltage is a key parameter that should be used to inform the system design. No analysis on the BoP parasitics and/or the system integration implications are discussed.

Jensen et al. [73] present a study of a CH_4 based large-scale energy storage RSOC system. The novel element of this study is twofold: it uses underground caverns to store the CH_4 and CO_2; and by using some of the heuristics suggested by [126, 127], mainly high pressure and low operating temperature, it is able to synthesize the CH_4 in the cell channel thereby decreasing the complexity of the BoP and decreasing the thermal losses. This, the authors claim, can boost the round-trip efficiency to $\sim$ 70%. The study also provides a detailed economic analysis of the plant, that results in a storage cost of about \$0.03/kWh.

Er-rib et al. [38] study a RSOC system in which CO_2 and H_2O are co-electrolyzed to produce syngas (electrolysis mode), which is then converted into SNG in a catalytic

reactor. On the reverse fuel cell cycle, the SNG is consumed on the SOC to produce power. The SNG is injected or retrieved from the natural gas network, thus the proposed design can be thought of as an "open system" as the system can consume more energy than it stores or vice-versa. The main focus of the paper is to study the catalytic methanation reactors, and this is done in ASPEN plus. The setup proposed in this paper is very similar to the one that we use for the work in this thesis, the main difference being that the one presented in later chapters of this thesis has more nuanced BoP modeling, is based on steam electrolysis rather than co-electrolysis, and is constructed in such a way that it allows for the modeling and characterization of off-design operation.

Al-musleh, et al. [1] present an RSOC model for electricity storage based on hydrocarbons and liquid CO_2. Results are presented for several cycles: liquid methane, gaseous methane, methanol and methanol-water mixture. The authors report round-trip efficiencies ranging from 55-59%.

2.3 Methanation chemistry and technology

Methanation, a process that has been widely studied and has been around for more than 70 years [7, 69, 92], can be thought of as the hydrogenation of carbon oxides (CO and CO_2) to form CH_4 via a catalytic reaction. The study and development of methanation technology has had two main drivers: first, it has been used as a cheap and efficient way to remove CO and CO_2 impurities in catalytic processes that are extremely sensitive to their presence (such as the synthesis of NH_3) [7], and second as a way to produce synthetic natural gas (SNG) from existing coal resources [79, 92, 132]. In recent years, however, the formation of SNG has gained renewed interest as it has been proposed as a pathway to store intermittent renewable electricity in the form of chemical energy. The gasification and methanation of biomass has also been proposed as a route to develop carbon neutral natural gas. In the context of the

work presented in this thesis, methanation is a critical piece of the RSOC energy hub concept. In this section the main chemistry and industrial setups for methanation processes are reviewed and discussed to provide the reader with some background on this technology.

2.3.1 Methanation chemistry

As stated before, under the right conditions and with the aid of a metal catalyst carbon oxides can be efficiently converted into methane. Methanation is possible for both syngas or pure CO_2, although the methanation of syngas has historically been the de facto technology for making SNG.

2.3.1.1 Syngas methanation

Generally speaking, methanation is usually carried out in a heterogeneous catalytic process in which syngas is converted into methane:

$$3\,H_2 + CO \rightleftharpoons CH_4 + H_2O \qquad \Delta H = -206.0\,\text{kJ} \tag{R2.11}$$

As water is formed, the water gas shift reaction can change the H2:CO ratio within the reactor:

$$CO + H_2O \rightleftharpoons H_2 + CO_2 \qquad \Delta H = -41.0\,\text{kJ} \tag{R2.12}$$

The water-gas shift in combination with reaction R2.11 can lead to another pathway to form CH_4 [92]:

$$2\,H_2 + 2\,CO \rightleftharpoons CH_4 + CO_2 \qquad \Delta H = -247\,\text{kJ} \tag{R2.13}$$

At high pressures and low temperatures, the formation of soot can occur via the Boudouard reaction:

$$2\,CO \rightleftharpoons C + CO_2 \qquad \Delta H = -173\,\text{kJ} \tag{R2.14}$$

The Boudouard reaction is of particular relevance, as soot is an important poison to the catalysts used in the methanation reaction. Therefore, reaction conditions must be controlled to avoid the formation and deposition of carbon on the catalyst surface. From a thermodynamic perspective, the methanation of syngas is favored at

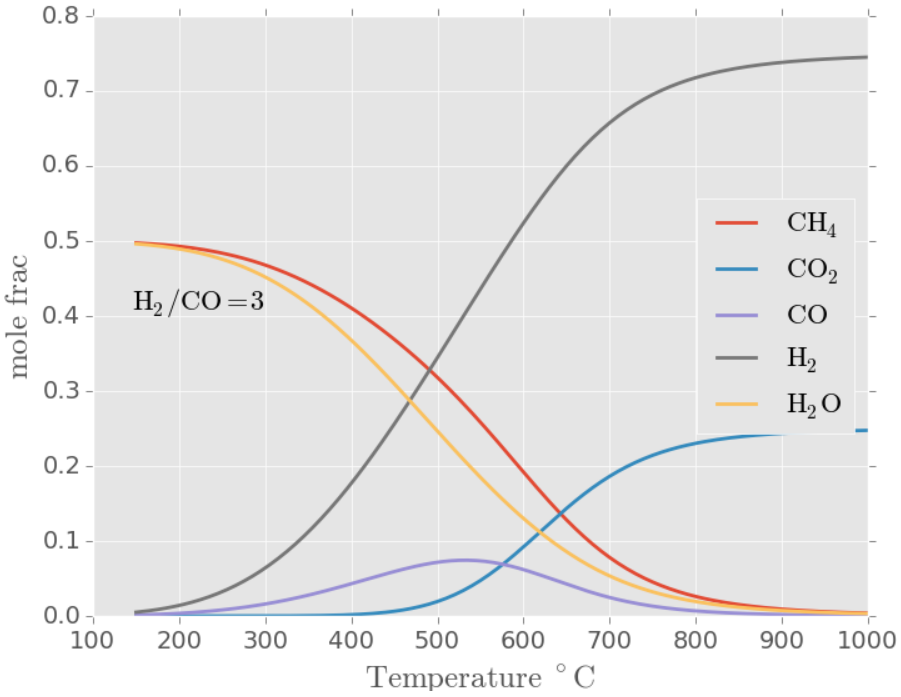

Figure 2.6: Methanation equilibrium composition for a 3:1 H_2/CO mixture.

low temperatures and high pressures. This is a direct consequence of the reduction in volume and exothermic nature of the reaction. Figure 2.6 shows the equilibrium composition for a 3:1 H_2/CO mixture at 1 atm calculated via a Gibbs minimization routine[6]. As suggested by the figure, at lower temperatures the equilibrium mole fraction of CH_4 is the greatest and as temperature rises, the equilibrium becomes less favorable and the amount of unreacted CO and H_2 increases. The influence of pressure on the conversion of reactants into the desired CH_4 product can be quite significant. Figure 2.7 shows the CH_4 yield as a function of temperature for a 3:1

[6]All gases are assumed to be ideal and no carbon formation is considered.

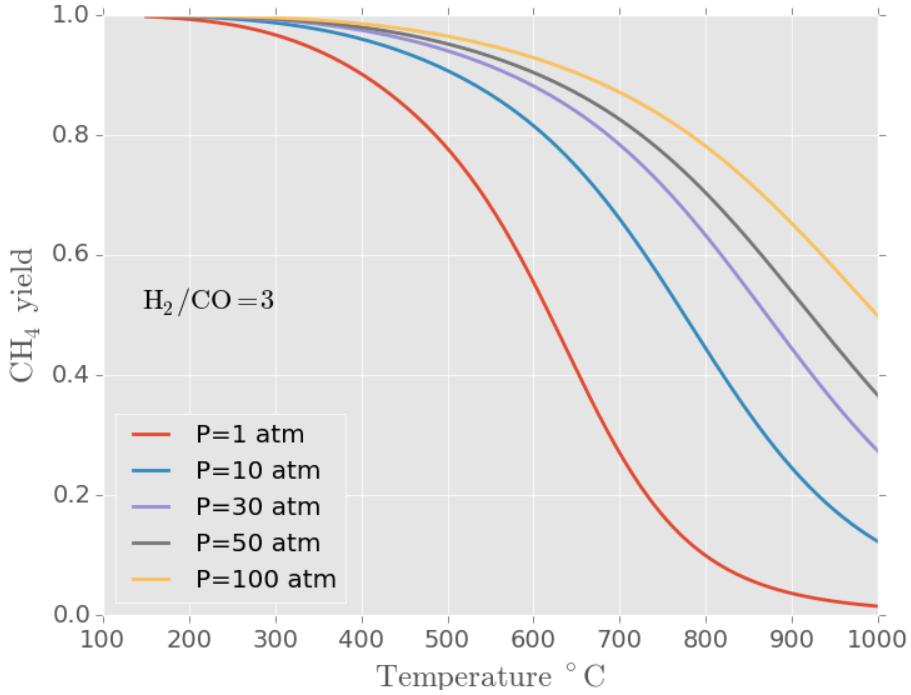

Figure 2.7: CH_4 yield at equilibrium for direct CO methanation

H_2/CO mixture at pressures of 1, 30, 50 and 100 atmospheres. As suggested by the plot, high pressures promotes the conversion of CO into CH_4. The figure also suggests that the impact becomes less important for pressures greater than 50 atm.

2.3.1.2 CO_2 methanation

Apart form the pathways defined in (Reactions R2.11 to R2.13), methane can also be formed by the direct hydrogenation of CO_2 via the following reaction:

$$4\,H_2 + CO_2 \rightleftharpoons CH_4 + 2\,H_2O \qquad \Delta H = -165\,\text{kJ} \tag{R2.15}$$

As discussed earlier, the direct methanation of CO_2 is of particular interest as it has the ability to open the door for carbon neutral SNG production which can serve as a an effective energy storage vector for variable renewable energy. As suggested by reaction R2.15, direct CO_2 hydrogenation requires a stoichiometry of 4:1 H_2 to CO_2.

Just as in the case of syngas methanation, the reduction in molar volume and its

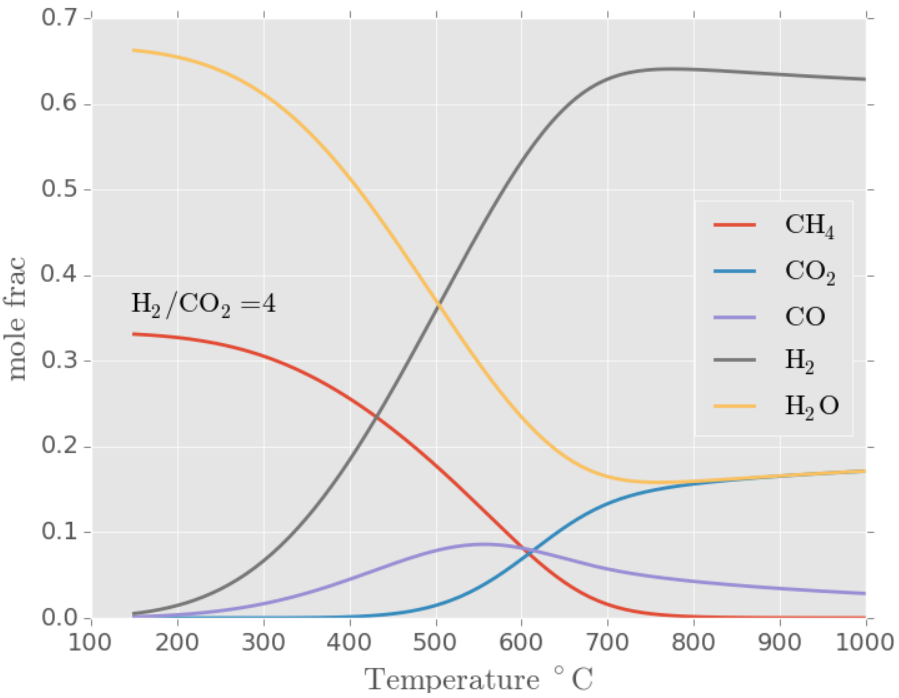

Figure 2.8: Methanation equilibrium composition for a 4:1 H_2/CO_2 mixture.

exothermic nature suggests that reaction R2.15 is favored at low temperatures and high pressures. Figure 2.8 shows the equilibrium mole fractions for a 4:1 H_2/CO_2 mixture at 1 atm at different temperatures. As expected, the mole fraction of CH_4 is greatest at lower temperatures and starts to decrease considerably beyond 400 °C. At temperatures above 450 °C the concentration of CO increases due to the reverse water gas shift reaction (which is the reverse of reaction R2.12) and due to steam reforming which is the reverse of (reaction R2.11). Direct methanation of CO_2 is less prone to carbon deposition, as the presence of steam dilutes the reactants and inhibits reaction R2.14 [41]. As expected, increasing the pressure of the reaction helps to increase the CH_4 yield as shown in Fig. 2.9. It is important to notice that at sufficiently low temperatures the CH_4 yield can be maintained at 90+ % at atmospheric pressure, however kinetics tend to become the rate limiting factor.

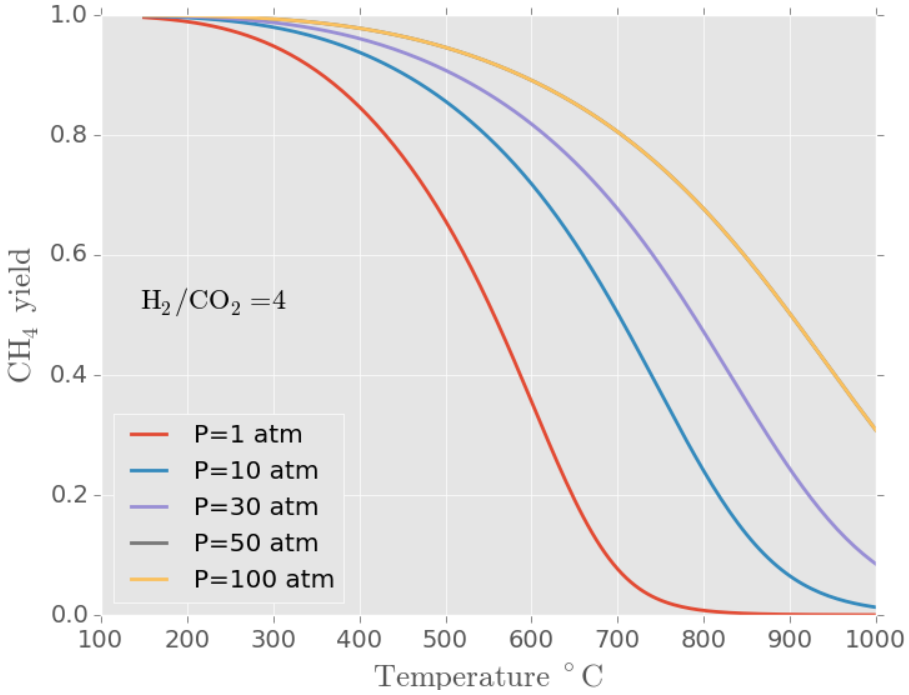

Figure 2.9: CH_4 yield at equilibrium for a direct CO_2 methanation

However, with a sufficiently active catalyst the direct hydrogenation of CO_2 can be performed at atmospheric pressure [71] with high conversion rates. This is attractive, as it can lead to lower capital cost requirements, operating costs (compression cost avoidance) and is ideal for small-scale distributed setups.

2.3.2 Catalysts and reactors

Reactions R2.11 to R2.15 all have highly negative free-energy values, but due to their exothermic nature they must be carried out within low temperature regimes in which the reactions are kinetically limited [41]. In order to achieve yields for commercial applications, a metal based catalyst is employed employed. In large industrial processes, Ni is the most common catalyst used but other metals such as Ru, Rh, Pt, Fe and Co can also be used [79]. A good review on the recent advance in methanation catalysts was recently performed by Gao et. al [42]. In this work, Gao et. al find that Ni is

still the most widely used catalyst for methanation and Fischer-Tropsch synthesis. The activity and selectivity of this catalyst is highly dependent on the metal loading, the dispersion of the Ni particles and the composition of the support. Typically the Ni catalyst deposited on a Al_2O_3 support. The use of Ni as a methanation catalyst still has some challenges, mainly sensitivity to carbon deposition, sintering, $Ni(CO)_4$ formation and sulfur poisoning[42]. High temperatures can lead to catalyst deactivation, and due to the fact that the methanation reactions are quite exothermic, heat management is very important for the catalyst's lifetime and stability. Recently, Ru has gained attention as a catalyst for methanation reactions, particularly its use in the direct methanation of CO_2 at atmospheric pressures [42, 71]. Because of its very high activity, Ru catalysts can be employed for methanation reactions at low temperatures which is attractive for operating at near ambient pressures, as yields tend to be very high under these conditions (see Fig. 2.7 and Fig. 2.9). Ru based catalysts are also sensitive to sintering and carbon deposition, so heat management is of the utmost importance.

In large-scale industrial processes, hydrogenation of CO and/or CO_2 tends to be carried out in catalytic fixed bed reactors [72, 79, 121]. Because methanation reactions are highly exothermic, these reactors can exhibit large temperature gradients as the reactants get converted into products, which causes problems for the durability of the catalyst and the efficiency of the plant [30, 72]. One way in which this is solved is by employing large recycle loops that add CH_4 to the syngas/CO_2 feed, diluting the inlet reactants which helps manage the increase in temperature. This, however, means that the conversion per pass is lowered and that the total flowrates are high relative to the stoichiometric requirements. As such, a typical methanation train is composed of several reactors connected in series with intermediate gas cooling and product recycling. The use of fluidized bed reactors has also been explored as an option, as they tend to be well suited for large-scale exothermic processes [79].

The particular details of the methanation plant will vary across designs in order to meet the particular heat, efficiency, and/or feedstock requirements. For example, the TREMP process developed by Haldor Topsoe employs several reactors in parallel with inter-cooling. In each reactor down the train, the operating temperature decrease and the process tries to minimize recylcing costs by managing heat as high-pressure superheated steam [72]. In contrast, the RMP process (developed by Ralph M. Parsons Company) is also a setup of several fixed-bed reactors in series with intermediate gas cooling but it does not employ any gas recycling. A detailed discussion of the pros and cons of each of the existing technologies is outside the scope of this work, but Kopyscinski et. al.[79] provides a comprehensive review of the existing methanation technologies which should be consulted for further details on this topic.

One of the main challenges of operating methanation reactors at low temperatures is that the conventional Ni catalysts exhibit low activity at temperatures below 300 °C, and for high CO content there is an affinity to form $Ni(CO)_4$, which leads to deactivation. Thus, in order to operate at lower temperatures, it is necessary to use non Ni catalysts. Because of its high activity, Ru catalysts can lead to lower operating temperatures and offer a way to help manage the heat of the reaction by being washcoated into the surface of a heat exchanger as suggested by Janke et. al. [71]. That is, rather than employing fixed-bed and/or fluidized bed reactors, the methanation reaction occurs a at the surface of the heat exchanger which in turn leads to cheap and efficient thermal management of the reaction. This is particularly interesting as it leads to new and cheaper reactor designs that are nicely suited for a wide small-scale distributed applications. This design idea is the basis for the methanation reactor modeled in this thesis, and a detailed discussion of this type of design is provided in Section 3.4.6.

Chapter 3

Computational model of RSOC system

The purpose of this chapter is to introduce the computational model that was developed for simulating a range of end-to-end RSOCs systems. As stated in previous chapters, the main goal of this thesis is to perform system level analysis to assess the different operational strategies that can be employed for RSOC systems under a wide variety of market signals (fuel and electricity prices), degradation rates, and expected lifetimes. Although there exists a wide array of software and tools for modeling SOC at the cell and system levels, none of them could be employed to capture a dynamic system interfacing with fluctuating electricity and fuel markets (see Section 2.2.2 for a discussion on RSOC modeling). For this reason, a model was developed from scratch in order to accurately represent a dynamic RSOC system that could respond and adapt to exogenous market factors. The computational model that was built had to have enough nuance and complexity to capture the trade-offs associated with operating under different parameters (e.g. cell temperature, voltage, fuel utilization), while maintaining a sufficiently simple and computationally lean framework that could be used to perform temporal optimizations over hourly and daily resolutions. The model and all of its supporting libraries were built using Python 2.7 and the scientific computing library SciPy. In the first sections of this chapter, a brief description of the model and the main RSOC system configurations used throughout this thesis are presented. Subsequently a detailed discussion of the electrochemical model used for simulating the RSOC is offered. Lastly, BoP components and the equations used for solving energy and material balances are described in detail.

3.1 Model description

The main purpose for developing a system level model from scratch was to have complete control over the different components and processes that exist in an end-to-end RSOC system. One of the main contributions of this model is the ability to run simulations in which the operating strategy of the system responds and adapts to fluctuating market signals such as hourly fuel and electricity prices. Thus, this model can be used to run temporal optimizations at different resolutions to investigate what are the optimum operating strategies for a dynamic RSOC system that operates in a particular market. The results of this type of optimization are discussed in Chapter 5.

The computational model is built around 4 main libraries:

1. A stack library that contains the modules that simulates the RSOC stack (see Section 3.3).

2. A BoP library that contains all modules for simulating BoP components (heaters, pumps, compressors, etc. see Section 3.4).

3. A thermodynamic library that contains all relevant thermodynamic data (based on the NIST Chemistry Workbook[88]) as well as routines developed for running chemical equilibrium calculations.

4. An economic library that contains all modules used in costing and contains all relevant economic variables.

The four libraries can be easily strung together to form end-to-end systems (like the ones described in Section 3.2.1) that are used to investigate behavior at the system level, or can be run individually to investigate one particular component. Because all libraries are built from scratch in Python, once an end-to-end system is developed it is easy to write optimization wrappers that leverage SciPy's powerful optimization tools to perform system level optimizations that can, for example, respond to exogenous variables such as fluctuating electricity and fuel prices.

3.2 System configurations

All of the end-to-end systems presented throughout this thesis can be described as having three main sections: in the upstream section inlet gases and/or liquids are pre-treated (heated, evaporated, etc.) in order to meet a specific set of conditions required by the electrochemical stack (T, P, composition) ; in the midstream, the gases enter the RSOC stack where they undergo either electrochemical oxidation (fuel cell mode) or electrochemical reduction (electrolysis mode); and in the downstream the exhaust gases are pre-treated and vented (fuel cell mode) or sent to catalytic reactors for further transformation into carbon-based fuels (e.g. CH_4 or CH_3OH). Fig. 3.1 depicts this generic system.

Because the system's modes of operation are mutually exclusive, it is desired to develop setups that favor the use of ancillary components (e.g. heaters, blowers, compressors) in both modes of operation thereby reducing system complexity and capital cost. From looking at Fig. 3.1, it is easy to see that the addition of tanks for the exhaust gases and products would result in a "closed" system similar to the one described by [9, 73]. The RSOC system configurations (the "energy hubs") studied in this thesis are presented as "open" systems that are connected to fuel and/or electricity grids when operating as fuel cells or electrolyzers. That is, none of the chemical inputs and/or outputs need to be stored for use at a later time. These "open-ended" systems can be thought of as RSOC storage devices with infinite storage reservoirs, as the natural gas grid from a single device's perspective is effectively infinite. These configurations can easily be modified and "closed" at any end in order to study conventional storage approaches similar to the ones offered by [9, 73].

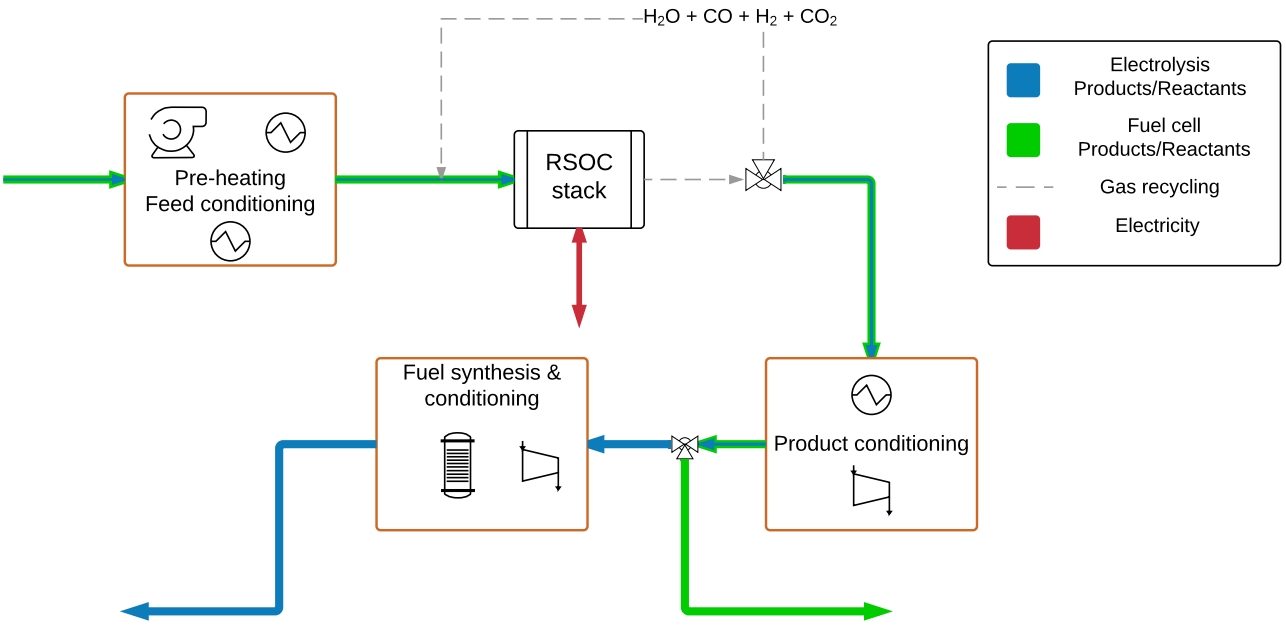

Figure 3.1: Generic "Open-ended" RSOC system

3.2.1 RSOC with internal reforming and external catalytic methanation

The first "base" configuration is based on a RSOC system operating at atmospheric pressure that uses CH_4 as a feedstock when operated in fuel cell mode and produces CH_4 by electrolyzing water and hydrogenating CO_2 in an external catalytic methanator when operated in electrolysis mode. It is connected to the natural gas infrastructure for injecting (electrolysis) or retrieving (fuel cell) CH_4 for its operation. All CO_2 used during the electrolysis step is assumed to be available form a concentrated source (e.g. power plant or industrial process), or to be sourced via direct air capture [30].

3.2.1.1 Fuel cell mode

Fig. 3.2 shows the system when operated in fuel cell mode. The main features of the design include: heat-exchangers to recuperate the thermal energy from the oxidated

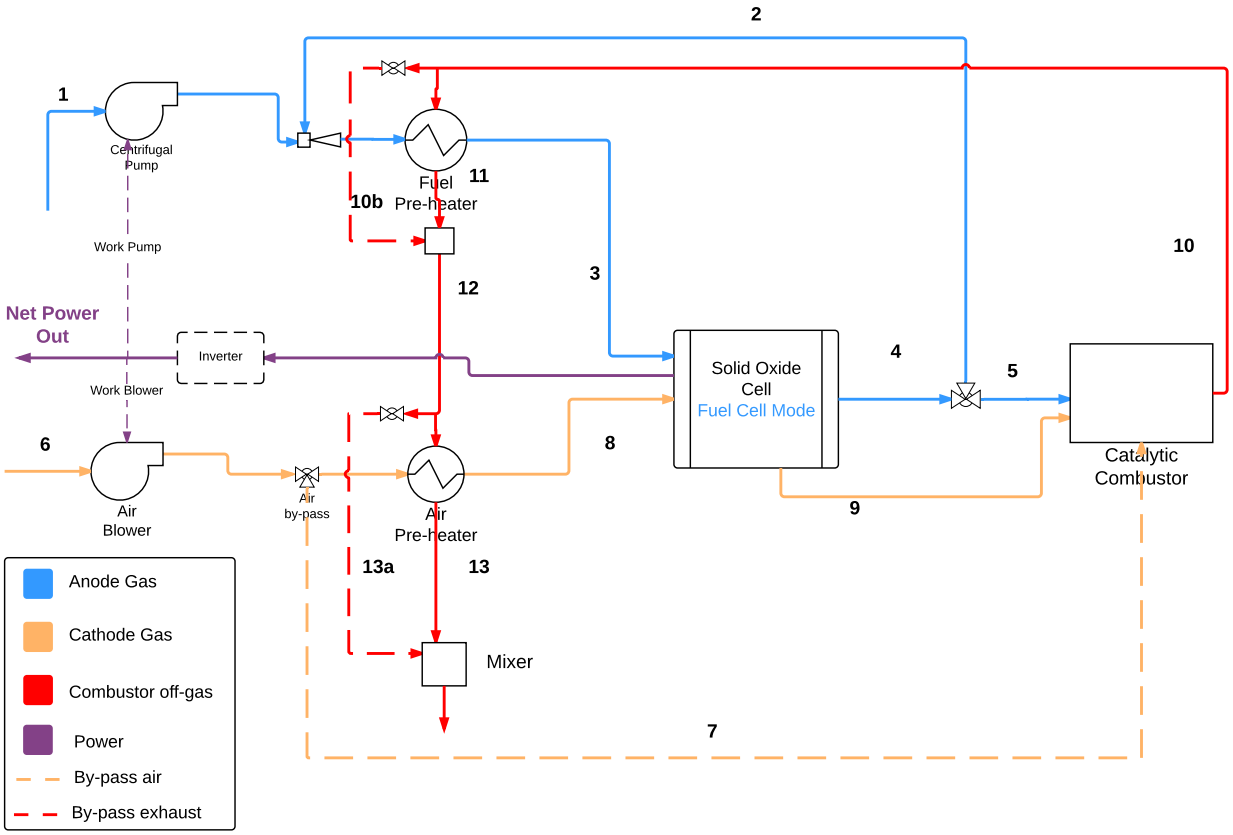

Figure 3.2: Fuel cell mode RSOC with internal CH_4 reforming

exhaust streams (#10) for pre-heating the fuel and air streams; internal reforming of the fuel without the need for an external pre-reformer thereby reducing capital costs and system complexity; product stream recycling on the fuel electrode side (stream # 2) used to increase overall fuel utilization rate and to provide all necessary steam to the inlet of the stack to reduce coke formation; the use of a catalytic combustor for oxidizing the unreacted anode gases (see Section 3.4.5 for details); and incorporation of an air by-pass stream (stream # 7) to provide cold air for maintaining the temperature of the combustor within the allowed ranges (#7). Each one of these features has specific operating parameters and ranges, and can impact the overall efficiency and operating cost of the system in different ways. These implications and trade-offs are discussed in a parametric study presented in Chapter 4.

The main challenge of operating this design in fuel cell mode is maintaining the temperature of the stack and of the catalytic reactor within the "safe-zones" of operation. At all voltages, the electrochemical oxidation of H_2 results in the production of heat which needs to be actively managed in order to avoid damaging the structural integrity of the SOC. As discussed in Section 3.3.1.2, the heat produced by the stack is managed by sweeping extra air through the oxygen electrode channel which effectively absorbs the heat produced by the irreversibilities of the stack. The power consumed by the air blowers is proportional to the volumetric flow rate of the air, thus the optimum operating point of the fuel cell becomes a trade-off between the increase in power per unit area that is achieved by increasing the current density (lowering the voltage) and the increasingly large loads that are required for moving the required air masses that are used to maintain the predefined nominal temperature of the cell. When operating outside the design point, this trade-off becomes more important as the parasitic power consumption of the blowers increases to the power of 2.5[1]

Due to the high temperatures at which the gases exit the stack and the fact that the combustion of unreacted species is highly exothermic, managing the thermal load of the catalytic combustor is also an important task. At temperatures above 850 °C the oxidating catalyst is deactivated, thus it is necessary to operate below these temperatures. A similar strategy as the one described above is used, except that in this case a stream of air at ambient temperature is injected directly into the combustor to absorb the extra thermal energy. Just as in the case of the stack, keeping the parasitics loads associated with flowing air into the combustor is an important design consideration. Chapter 4 has a detailed discussion of heat management strategies for fixed operating points and for part-load operation.

[1]This power law is a consequence of combining as equations (3.42) and (3.62), which suggest that the work required by the blower is a product of the volumetric flowrate and the pressure drop of the gas across the system.

3.2.1.2 Electrolysis mode

In electrolysis mode, steam is electrolyzed to form H_2 which is catalytically reacted with CO_2 to generate CH_4 which is subsequently cooled, compressed and injected into the natural gas infrastructure. When operating in electrolysis mode, the system requires more ancillary equipment, particularly heat exchangers and blowers, making the overall process more complicated than the fuel cell operation. Fig. 3.3 depicts the system. The main reasons for the increase in complexity are the following: first, the catalytic reaction (methane synthesis) that occurs downstream of the stack operates at a low temperature relative to the stack's exhaust, thus extra cooling for the inlet reactants as well the use of a cold air stream for managing the highly exothermic methanation reaction is required. Second, CH_4 needs to be delivered at a specific temperature and pressure and with a specific purity. This in turn requires the use of inter-staged compression and product purification via steam condensation. Third, because the electrolyzer can operate endothermically ($U_{op} < U_{th}$) or exothermically ($U_{op} > U_{th}$) extra equipment is required for managing either the cases in which extra-heat is to be supplied to the reactant streams and stack (endothermic mode), or the cases for which active cooling is required which will be achieved via air sweep just like in the FC case.

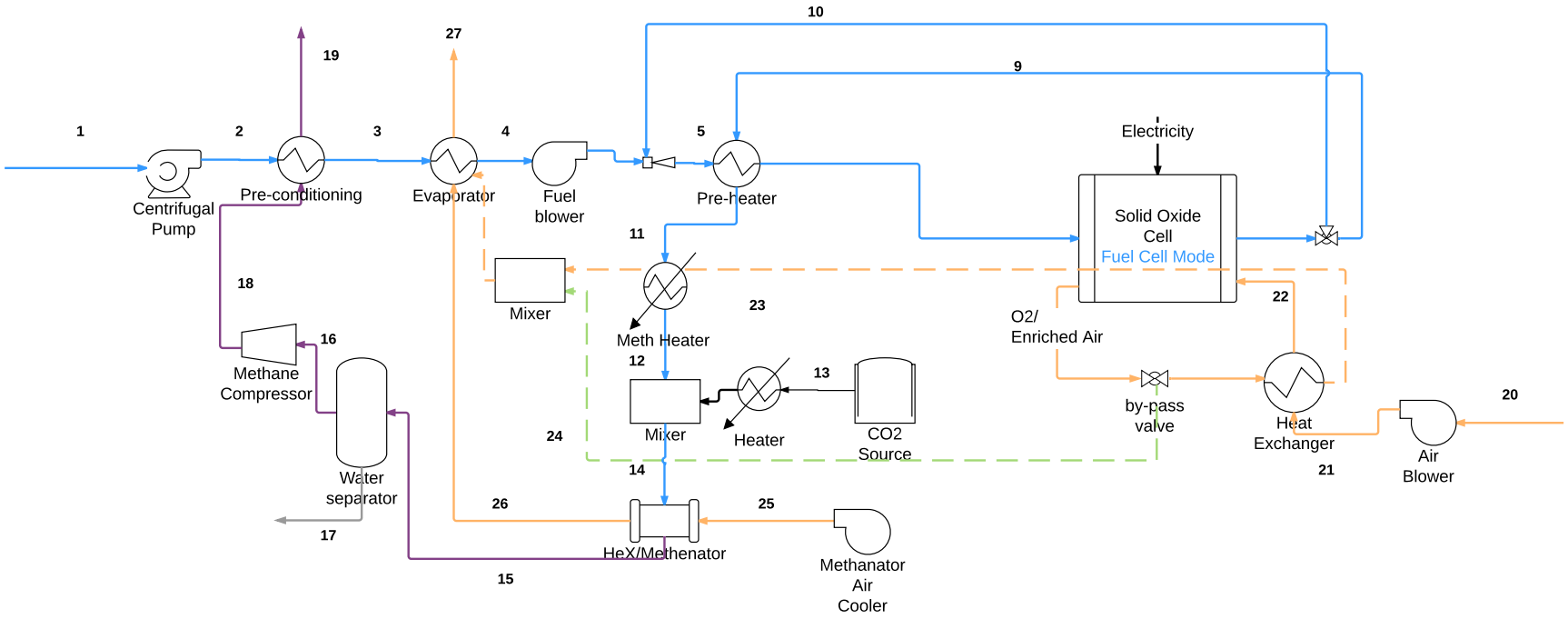

Figure 3.3: Electrolysis mode with catalytic CO_2 methanation

In electrolysis mode, the main features of the system include: heat-exchangers to recuperate thermal energy from hot exhaust gases for pre-heating inlet gases (streams #5, 11, 12, etc); product stream recycling on the H_2O electrode to provide a small fraction of H_2 to the inlet of the stack in order to avoid oxidation of the Ni electrode; evaporators for making steam (stream #3); catalytic heat exchanger where the methanation reaction takes place (see Section 3.4.6 for more details); fuel compressor with inter-stage cooling for compressing CH_4 prior to grid injection; air blowers to provide ambient air for managing exothermic heat loads for the RSOC and/or the methanator; water separator for condensing out liquid water for CH_4 purification;bypass valves and streams (#7, 23, 24) to provide heat to the evaporator when available (e.g. exothermic operation); electric heaters to provide thermal loads when no process heat is available.

One of the main challenges when operating in electrolysis mode is the ability to manage and integrate process heat in order to increase the overall system efficiency. There are three main points in the process that require careful consideration with respect to heat management and integration: the solid oxide stack, the methanation reactor, and the water evaporator. When operating in endothermic mode, there is not enough heat available for supplying all the load required for the evaporator.

Heat management: stack In electrolysis mode, the stack may be operating exothermically or endothermically, depending on the voltage of operation. When operating in exothermic mode, meaning that the stack experiences net heat production, the heat in the stack is managed via the introduction of sweep air on the oxygen electrode side. The amount of air required is a function of the operating point of the stack, and its introduction will lower the Nernst potential by decreasing the partial pressure of oxygen in the gas. Increasing the operating voltage results in more hydrogen produced per unit area, but after $U_{op} > U_{th}$, heat production will increase in

a non-linear fashion requiring more air for cooling. Thus, just as is the case for when operating in fuel cell mode, there is a trade-off between the parasitic power consumption of the air blowers required for cooling the stack and the hydrogen production gains seen by increasing the voltage. The heat from the stack is recycled within the system and used to provide the energy required by the water evaporator upstream of the stack. In endothermic mode the stack has net heat consumption, requiring heat addition in order to keep the operating temperature within the design parameters. Heat is added to the stack via electric heaters, and their electric load is a considerable part of the parasitics at low operating voltages[2].

Heat management: methanation CO_2 hydrogenation is a highly exothermic reaction that requires constant heat removal in order to maintain a favorable equilibrium. In the proposed systems, a heat exchanger is coated with a highly active Ru catalyst so that the reaction occurs on the surface of the heat exchanger (see Section 3.4.6 for more details). This simplifies the heat removal process which allows operation within a narrow temperature range. The heat removed during the reaction is reused by integrating it into the water evaporator.

3.3 Stack Model

A zero dimensional model is developed to capture the electrochemical and thermodynamic processes occurring at the solid oxide cell. Balance of plant components are modeled using a black-box approach that performs mass and energy balances around each unit of operation. In order to capture the behavior of the system when operating intermittently and in response to varying price signals (see Chapter 5), a framework for part-load operation is developed and explained in Section 3.5. The cells in the RSOC stack are modeled as planar Ni/YSZ supported solid oxide cells consisting of

[2]This, of course, is a particular design decision and different setups might allow for more efficient ways of addressing this need.

three main parts: a Ni-yttria-stabilized zirconia (Ni-YSZ) fuel electrode, a porous strontium doped lanthanum manganite composite oxygen electrode (Sr-LSM) and a thin YSZ electrolyte used for transporting oxide ions (O^{2-}). These cells are based on the ones described in [53].

The main purpose of the zero dimensional RSOC stack module is to solve for the power, voltage, chemical compositions and mass flows of all species involved in electrolysis and fuel cell modes. In FC mode, the cell level chemistry involves steam reforming of methane, water-gas shift reaction, and electrochemical oxidation of H_2. In electrolysis mode, the cell can model both the electrochemical reduction of steam or the co-electrolysis of steam and CO_2. At the cell level, the following general assumptions are employed:

- All reactions are assumed to be at equilibrium and changes in reaction rates across the length of the cell are neglected.
- Mixture at the fuel channel exit is at equilibrium.
- Single cell performance used to represent whole SOC stack.
- Temperature of the cell (T_{op}) is assumed to be the average between inlet (T_{in}) and outlet temperature (T_{out}) of the reacting gases.
- Difference between the inlet and outlet temperature of the cell must satisfy a given temperature change (ΔT_{cell}) that is pre-defined before each simulation.
- There is no heat exchange between the stack and the outside environment.
- The stack is assumed to operate adiabatically.
- The pressure drop ΔP across the cell is neglected for cell-level calculations (see Section 3.4.8 for the inclusion of pressure drop across the stack for BoP performance calculations).

- RSOC stack employs an anode gas-recycling loop (AGR) in both FC and EL modes.

3.3.1 Fuel Cell mode

Reversible solid oxide cells operated in fuel cell mode (RSOC-FC) generate electric power via the electrochemical oxidation of the supplied fuel. Due to the high operating temperatures and because the cells anode support layer is made out of Ni (a good reforming catalyst), RSOC-FC has the ability to internally reform hydrocarbons (i.e. methane, methanol) into hydrogen and carbon monoxide [85] and the H_2 is then electrochemically consumed at the triple-phase boundary to produce power. The ability to internally reform fuels is an attractive feature of RSOCs, as it lowers the cooling demand for the stack, it eliminates the need for external reformers, and can simplify the overall design potentially resulting in lower capital costs. For the purpose of this model, we consider that the RSOC-FC internally reforms all supplied fuels into a mixture of H_2, CO, CO_2 and H_2O. Although CO can be electrochemically oxidized into CO_2, this reaction has been shown to occur at rates that are 1-3 times slower than the oxidation of H_2 and much slower than the water-gas shift reaction [89]. Thus, all CO is expected to be shifted making the electrochemical oxidation of H_2 the only source of power generation.

3.3.1.1 Electrochemical model

The electricity generated by the stack can be easily calculated by means of an electrochemical relationship. The operating voltage of the cell is defined as:

$$U_{op,FC} = U_{N,FC}(T_{op}, p_j) - i_{op} ASR(T_{op}) \tag{3.1}$$

Where U_N is the Nernst potential which is a function of the equilibrium partial pressure of gas species j in the bulk (see Section 2.1.2), i_{op} is the operating current

density and ASR is the Area specific resistance which represents the cell's overall resistance.

Finally, the DC power generated by the stack is calculated by:

$$P_{op} = U_{op,FC} \cdot I_{cell} \tag{3.2}$$

where I_{cell}, the total current flowing through the cell, is related to the current density i_{op} by:

$$I_{cell} = i_{op} \cdot A_{cell} \tag{3.3}$$

where A_{cell} is the total active surface area of the stack.

3.3.1.2 Mass Balances

Fuel electrode balances As previously mentioned, in fuel cell mode the RSOC internally reforms CH_4 in the presence of H_2O in order to provide the required H_2 for the electrochemical reaction. The use of an anode gas recycling stream (AGR) is employed in order to provide the required steam for the methanation reaction, as well as to avoid the deposition of solid carbon on the electrode surface. The recycle rate is usually chosen to meet a minimum steam-to-carbon (S/C) ratio that will inhibit carbon deposition. For high temperature SOC's, S/C ratios of 2–3 have been shown to represent a "safe–zone" of operation [123]. It is important to mention that the recycle rate will have an impact on the efficiency of the cell, as the addition of steam at the inlet of the cell will change the equilibrium gas composition, decreasing the hydrogen yield and cell voltage [12]. Thus choosing a S/C ratio is a trade–off between carbon formation and cell voltage. For an in–depth discussion about the impacts of AGR on system performance, see Chapter 4.

The model assumes very fast equilibrium at the inlet of the anode and subsequent electrochemical oxidation of H_2. Thus in order to compute the gas compositions at the exit of the stack, we assume that steam reforming of methane (SMR) reaction R2.1, water-gas shift (WGS) reaction R2.2 and electrochemical oxidation of

H_2 reaction R2.3occur simultaneously: Fig. 3.4 shows a control volume around the

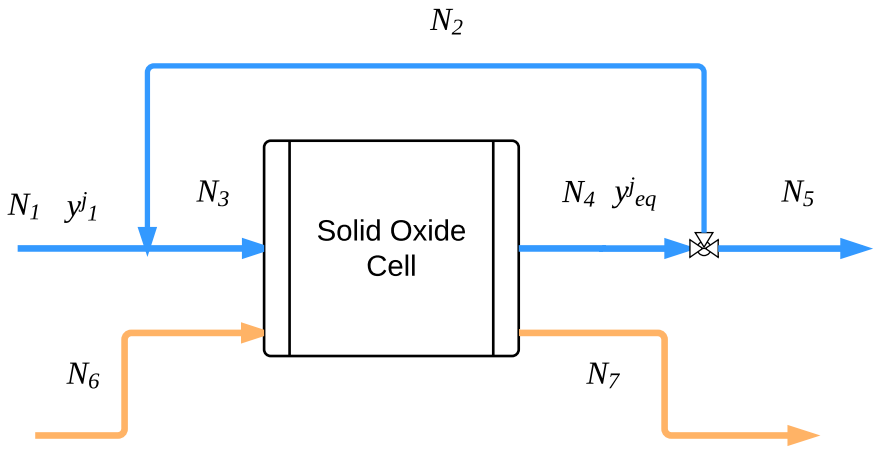

Figure 3.4: SOFC control volume with Anode Gas Recycling

RSOC, with five different molar flow rates at the anode side ($\dot{N}_1, \dot{N}_2, \dot{N}_3, \dot{N}_4$, and $\dot{N}_5$), two molar flow rates at the cathode side ($\dot{N}_6, \dot{N}_7$), and the equilibrium molar fraction of species j at the outlet of the stack y^j_{eq}. The equilibrium mole fraction y^j_{eq} sets y^j_4, y^j_5, and y^j_2. It follows then that for any given stream i:

$$\dot{N}_i = \sum y^j_i \cdot \dot{N}^j_i \tag{3.4}$$

By definition, then, the molar flow rate of species j at the outlet of the stack is:

$$\dot{N_4}^j = y^j_{eq} \cdot \dot{N}_4 \tag{3.5}$$

Assuming that r represents the fraction of the outlet gas recycled to the inlet of the stack, the molar flow rate for species j at the entrance of the stack can be written as:

$$\dot{N_3}^j = \dot{N_1}^j + y^j_{eq} \cdot (r \cdot \dot{N}_4) \tag{3.6}$$

Using the method suggested by [18], the equilibrium compositions y^j_{eq} and molar flow rates at the outlet of stack ($\dot{N}_4$) are computed. Let ξ_{SMR}, ξ_{WGS} and ξ_{redox}

represent the molar extent of reactions for equations reaction R2.1, reaction R2.2 and reaction R2.3. By definition, then:

$$y_{eq}^{\mathrm{CH_4}} = \frac{y_1^{\mathrm{CH_4}}\dot{N}_1 - \xi_{SMR}}{\dot{N}_1 + 2\xi_{SMR}} \tag{3.7a}$$

$$y_{eq}^{\mathrm{H_2O}} = \frac{y_1^{\mathrm{H_2O}}\dot{N}_1 - \xi_{SMR} - \xi_{WGS} + \xi_{redox}}{\dot{N}_1 + 2\xi_{SMR}} \tag{3.7b}$$

$$y_{eq}^{\mathrm{H_2}} = \frac{y_1^{\mathrm{H_2}}\dot{N}_1 + 3\xi_{SMR} + \xi_{WGS} - \xi_{redox}}{\dot{N}_1 + 2\xi_{SMR}} \tag{3.7c}$$

$$y_{eq}^{\mathrm{CO_2}} = \frac{y_1^{\mathrm{CO_2}}\dot{N}_1 + \xi_{WGS}}{\dot{N}_1 + 2\xi_{SMR}} \tag{3.7d}$$

$$y_{eq}^{\mathrm{CO}} = \frac{y_1^{\mathrm{CO}}\dot{N}_1 + \xi_{SMR} - \xi_{WGS}}{\dot{N}_1 + 2\xi_{SMR}} \tag{3.7e}$$

The molar flow rate of the H_2 utilized can be written in terms of the fuel utilization rate U_f, thus $\xi 3$ can be re-defined as:

$$\xi_{redox} = \left(\dot{N}_3^{\mathrm{H_2}} + 3\xi_{SMR} + \xi_{WGS}\right) \cdot U_f \tag{3.8}$$

After some algebraic manipulation[3], ξ_{redox} can be written in terms of the molar flow rate of the feed ($\dot{N}_1$).

$$\xi_{redox} = \frac{\left(y_1^{\mathrm{H_2}}\dot{N}_1 + 3\xi_{SMR} + \xi_{WGS}\right)}{1 - r + r \cdot U_f} \tag{3.9}$$

Substituting (3.9) into (3.7) and simplifying, the equilibrium mole fractions can be

[3]see [18] for more details

written in terms of three unknowns: ξ_{SMR}, ξ_{WGS} and $\dot{N}_1$:

$$y_{eq}^{\mathrm{CH_4}} = \frac{y_1^{\mathrm{CH_4}}\dot{N}_1 - \xi_{SMR}}{\dot{N}_1 + 2\xi_{SMR}} \tag{3.10a}$$

$$y_{eq}^{\mathrm{H_2O}} = \frac{y_1^{\mathrm{H_2O}}\dot{N}_1 - \xi_{SMR} - \xi_{WGS} + \dfrac{\left(y_1^{\mathrm{H_2}}\dot{N}_1 + 3\xi_{SMR} + \xi_{WGS}\right)\cdot U_f}{1 - r + r\cdot U_f}}{\dot{N}_1 + 2\xi_{SMR}} \tag{3.10b}$$

$$y_{eq}^{\mathrm{H_2}} = \frac{y_1^{\mathrm{H_2}}\dot{N}_1 + 3\xi_{SMR} + \xi_{WGS}}{\dot{N}_1 + 2\xi_{SMR}} \cdot \left(\frac{(1-r)(1-U_f)}{1 - r + r\cdot U_f}\right) \tag{3.10c}$$

$$y_{eq}^{\mathrm{CO_2}} = \frac{y_1^{\mathrm{CO_2}}\dot{N}_1 + \xi_{WGS}}{\dot{N}_1 + 2\xi_{SMR}} \tag{3.10d}$$

$$y_{eq}^{\mathrm{CO}} = \frac{y_1^{\mathrm{CO}}\dot{N}_1 + \xi_{SMR} - \xi_{WGS}}{\dot{N}_1 + 2\xi_{SMR}} \tag{3.10e}$$

Thus, if one knows the composition and flowrate of the fuel prior to the recycle stream mixing (y_1^i & $\dot{N}_3$) for a given fuel utilization (U_f) and pre–defined recycle rate (r) the equilibrium compositions at the outlet of the stack can be computed by solving an algebraic system of three independent equations with three unknowns. Using the chemical equilibrium equations for reactions reaction R2.1 and reaction R2.2 together with Faraday's law, a set of three independent equations is used to solve for ξ_{SMR}, ξ_{WGS} and $\dot{N}_1$:

$$K_{SMR}(T) = \frac{y_{eq}^{\mathrm{CO}} \cdot \left(y_{eq}^{\mathrm{H_2}}\right)^3}{y_{eq}^{\mathrm{H_2O}}\, y_{eq}^{\mathrm{CH_4}}} \cdot \left(\frac{P}{P^o}\right) \tag{3.11}$$

$$K_{WGS}(T) = \frac{y_{eq}^{\mathrm{H_2}} \cdot y_{eq}^{\mathrm{CO_2}}}{y_{eq}^{\mathrm{H_2O}}\, y_{eq}^{\mathrm{CO}}} \tag{3.12}$$

$$I_{cell} = 2 \cdot F \cdot \xi_{redox} = \frac{\left(y_1^{\mathrm{H_2}}\dot{N}_1 + 3\xi_{SMR} + \xi_{WGS}\right)}{1 - r + r\cdot U_f} \tag{3.13}$$

Where K_{SMR} and K_{WGS} are the equilibrium constants for the steam reforming and water-gas shift reactions. The equilibrium constants are a function of temperature and they are computed using a polynomial equation:

$$\log K_p = AT^4 + BT^3 + CT^2 + DT + E \tag{3.14}$$

	Reforming (SMR)	**Shift (WGS)**
A	$2.631\,21 \times 10^{-11}$	$5.473\,01 \times 10^{-12}$
B	$1.240\,65 \times 10^{-7}$	$-2.574\,79 \times 10^{-8}$
C	$-2.252\,32 \times 10^{-4}$	$4.637\,42 \times 10^{-5}$
D	$1.950\,28 \times 10^{-1}$	$-3.915\,00 \times 10^{-2}$
E	$-6.613\,95 \times 10^{1}$	$1.320\,97 \times 10^{-1}$

Table 3.1: Equilibrium constant coefficients

Values for the constants A-E are taken from [15] and tabulated in Table 3.1 By substituting equations (3.10) into (3.11) to (3.13), the stack module solves the equilibrium molar fractions using the *fsolve* function available through Python's SciPy open source library. Once the equilibrium mole fractions have been determined, computing the molar flow rates and compositions of the remaining streams is straightforward using equations (3.5), (3.6) and the following relationships:

$$\dot{N}_2 = \dot{N}_3 - \dot{N}_1 \tag{3.15}$$

$$\dot{N}_5 = \dot{N}_4 - \dot{N}_2 \tag{3.16}$$

Lastly, once the mass balance has been solved it is straight forward to calculate the equilibrium mole fractions prior to the electrochemical reaction that are used for computing the stack's OCV (see equation (2.2)). To do this, the method outlined above is used with two important differences:

1. The inlet molar compositions are set to equal the ones resulting from $\dot{N}_3$.

2. The fuel utilization rate (U_f) is set to zero

It can easily be seen that under these conditions, ξ_{redox} becomes zero and the routine computes the equilibrium compositions by simultaneously solving equations (3.11) and (3.12), which in turn would emulate the equilibrium compositions right before the electrochemical reaction takes place.

Oxygen electrode balance As stated in the assumption section above, the stack model assumes that the RSOC operates at a predefined nominal temperature T_{op}. In fuel cell mode, the RSOC's operate exothermically which requires heat to be actively removed from the stack in order to maintain the thermal stress under control to avoid damaging the cell. Therefore, thermal management is of the utmost importance for proper cell operation.

One common strategy for managing the heat in the cell is to sweep the cell with excess air on the cathode side. The extra air is used to absorb the heat that is being generated by the cell. The computational model developed in this thesis assumes that excess air is added on the cathode side in order to maintain the difference between the temperature of the inlet and outlet gases within the bounds of a predefined ΔT_{cell}. The calculation of the molar flow rate of air entering the cathode $\dot{N}_6$ is broken down into two separate components:

$$\dot{N}_6 = \dot{N}^{Air}_{stoich} + \dot{N}^{Air}_{sweep} \tag{3.17}$$

Where $\dot{N}^{Air}_{stoich}$ is the stoichiometric amount of air required for the electrochemical reaction at a given current density i_{op} and $\dot{N}^{Air}_{sweep}$ is the amount of excess air required to maintain the thermal gradient of the cell below ΔT_{cell}.

The stoichiometric flow rate of air is easily calculated using the molar extent of hydrogen consumption ξ_{redox} and assuming that air contains 79% N_2 and 21% O_2:

$$\dot{N}^{Air}_{stoich} = \frac{\xi_{redox}}{2} + \frac{\xi_{redox}}{2} \cdot \frac{79}{21} \tag{3.18}$$

The sweep air required $\dot{N}^{Air}_{sweep}$ will be a function of the heat being produced by the stack, as well as the inlet and outlet temperature of the gases.

$$\dot{N}^{Air}_{sweep} = \frac{Q_{stack}}{h_7(T_{out}) - h_6(T_{out})} \tag{3.19}$$

Where Q_{stack} is the net heat generated by the stack and $h_7(T_{out})$ and $h_6(T_{in})$ are the specific molar enthalpies of air at the stack exit and inlet temperatures. The model

assumes that $\dot{N}_{sweep}^{Air}$ cannot be negative, and in cases in which no sweep air is required it is set to zero.

3.3.1.3 Energy Balance

The energy balance of the RSOC-FC can easily be computed once all the molar flow rates and operating temperatures are know. For the purpose of the computational model, the RSOC is assumed to be a perfectly well insulated body operating at an average temperature T_{op} with a maximum thermal gradient of ΔT_{cell}. Thus, by specifying these two parameters the inlet and outlet temperatures of the gases (in both the anode and the cathode) are set:

$$T_{in} = \frac{2T_{op} - \Delta T_{cell}}{2.0} \tag{3.20}$$

$$T_{out} = \Delta T_{cell} + T_{in} \tag{3.21}$$

Once the inlet and outlet temperatures are known, the heat produced by the stack (to be removed by the sweep gas) is calculated by performing an energy balance around the control volume shown in Fig. 3.4 enclosing the junction of streams 3 and 4:

$$\begin{aligned} Q_{stack} = &\sum \dot{N}_4^j \cdot h_4^j(T_{out}) - \sum \dot{N}_3^j \cdot h_3^j(T_{in}) \\ &+ P_{op} + \xi_{SRM} \cdot \Delta H_{rxn,SRM} + \xi_{WGS} \cdot \Delta H_{rxn,WGS} \\ &+ \xi_{redox} \cdot \Delta H_{rxn,redox} \end{aligned} \tag{3.22}$$

3.3.2 Electrolysis mode

When operated in electrolysis mode (RSOC-EL), RSOC's take an electrical input and use it to drive a thermodynamically unfavorable reaction. As discussed in Chapter 2, electrolysis can be thought of as the reverse operation of the electrochemical oxidation that drives the fuel cell operation. RSOC have the ability to co-electrolyze H_2O and CO_2 into H_2 and CO [53], making them an attractive technology for syngas production from non-fossil based feedstocks. Due to the fact that the catalytic processes used

for fuel production that are investigated in this thesis operating solely on a mixture of H_2 and CO_2, co-electrolysis is not considered in this model. Thus when the cell operates in electrolysis mode it only performs the electrochemical reduction of H_2O, and CO_2 is added downstream during the catalytic fuel synthesis.

3.3.2.1 Electrochemical model

Because electrolysis is the reverse of fuel cell operation, the electrochemical model established in section Section 3.3.1.1 can be directly applied for electrolysis operation. Thus for a negative operating current density i_{op} equations (3.1) and (2.2) can be rewritten for electrolysis operation as:

$$U_{N,EL} = -U_{N,FC} \tag{3.23}$$

$$U_{op,FC} = -U_{op,FC} \tag{3.24}$$

3.3.2.2 Mass balance

Steam electrode balances Due to the fact that the splitting of H_2O is the only reaction considered when operating in electrolysis mode, the mass and energy balances are greatly simplified[4]. Although electrolysis cells can be operated with pure H_2O on the fuel electrode side, some H_2 is usually added to the inlet gas in order to avoid the oxidation of the Ni/YSZ electrode [32], [31]. In order to provide the incoming steam with some H_2, a fraction of the gas exiting the cell (r_{EL}) is recycled back and mixed with the inlet steam before entering the cell. The value of r_{EL} will have an impact on the overall performance of the cell, as the addition of H_2 will increase the cell voltage, increasing the electrical load requirements. For the purpose of this model, the r_{EL} is fixed at a given value such that the H_2O/H_2 ratio at the inlet of the cell meets

[4]When considering co-electrolysis, because Ni is a good catalyst it is necessary to consider the equilibrium compositions that arise from the reverse water–gas shift reaction when performing the mass and energy balance. A procedure similar to the one described by[116] can be employed

a pre–defined value. For an in–depth discussion of the impact of r_{EL} on the overall performance of the system see Chapter 4.

The electrochemical reduction of H_2O is simply written as:

$$H_2O \longrightarrow H_2 + \frac{1}{2}O_2 \tag{R3.16}$$

Because there is no need to perform equilibrium calculations, solving for the molar flow rates and stream compositions is straightforward and does not require the use of non–linear equation solvers. Using the control volume depicted in Fig. 3.4, and re–defining the component molar fraction of stream 4 as y_4^j, all streams and components can be written in terms of the molar flow rate of the feed ($\dot{N}_1$), the molar extent of reaction of reaction R3.16 ξ_{EL}, the steam conversion ratio (λ_{SC}), and the recycle rate r_{EL}. The following are the simplified expressions for each stream resulting from some algebraic manipulation:

Stream 1

$$\dot{N}_1 = \left(\frac{(1-r_{EL})\cdot\xi_{EL}}{\lambda_{SC}} + \lambda_{SC}\cdot r_{EL}\right)\left(\frac{1}{y_1^{H_2O}}\right) \tag{3.25a}$$

Stream 3

$$\dot{N}_3 = \frac{\dot{N}_1}{1-r_{EL}} \tag{3.25b}$$

$$y_3^{H_2O} = \frac{y_1^{H_2O}\dot{N}_1 - r_{EL}\xi_{EL}}{\dot{N}_1} \tag{3.25c}$$

$$y_3^{H_2} = \frac{y_1^{H_2}\dot{N}_1 + r_{EL}\xi_{EL}}{\dot{N}_1} \tag{3.25d}$$

Stream 4

$$\dot{N}_4 = \frac{\dot{N}_1}{1-r_{EL}} \tag{3.25e}$$

$$y_4^{H_2O} = \frac{y_1^{H_2O}\dot{N}_1 - \xi_{EL}}{\dot{N}_1} \tag{3.25f}$$

$$y_4^{H_2} = \frac{y_1^{H_2}\dot{N}_1 + \xi_{EL}}{\dot{N}_1} \tag{3.25g}$$

Stream 2

$$\dot{N}_2 = \frac{\dot{N}_1 r_{EL}}{1 - r_{EL}} \tag{3.25h}$$

$$y_2^j = y_4^j \tag{3.25i}$$

Stream 5

$$\dot{N}_5 = \dot{N}_4 - \dot{N}_2 \tag{3.25j}$$

$$y_5^j = y_4^j \tag{3.25k}$$

If the operating current density i_{op} is known, then ξ_{EL} can be computed using Faraday's law, where:

$$\xi_{EL} = \frac{i_{op}}{2F} \cdot A_{cell} \tag{3.26}$$

Once ξ_{EL} is known, for a given λ_{SC} equations (3.25) can be solved by substitution and the mass balance for the control volume is completed.

Oxygen electrode balances When operating in electrolysis mode, the cell does not require O_2 as a reactant and therefore blowing air into the oxygen electrode is not required. However, because the RSOC's can be operated exothermically, endothermically, or under a thermoneutral profiles (depending on the operating point that is chosen), flowing air through the oxygen electrode is often employed as a strategy to maintain a constant average operating temperature T_{op} when the cell is operating exothermically. For this reason, the mass balance in the oxygen electrode when operating exothermically is different than when the cell is operated endothermically or at the thermoneutral point.

Endothermic & thermoneutral operation

As mentioned before, when the stack is operated at the thermoneutral point there is no need for any heat management as all the heat that is generated by the stack perfectly balanced by the heat consumed during the reaction. When operated in

endothermic mode, the additional heat required to maintain a constant average cell temperature is provided by an external electric heater. Thus, under these two cases the flow of air at the inlet of the stack is not required and thus the mass balance on the oxygen electrode is defined by the stoichiometric O_2 generated during electrolysis:

$$\dot{N}_6 = 0 \tag{3.27}$$

$$\dot{N}_7 = \frac{\xi_{EL}}{2} \tag{3.28}$$

Because there is no air flowing through the cell, $y_7^{N_2} = 0$ and $y_7^{O_2} = 1$, making the molar composition of $\dot{N}_7$ pure O_2.

Exothermic operation

In electrolysis mode, exothermic operation will occur in cases where the operating current density is high enough such that the cell voltage is higher than the thermoneutral voltage $U_{op} > U_{th}$. In these cases, the cell generates extra heat during its operation which must be removed in order to maintain the thermal stress under control. As in fuel cell mode, in electrolysis mode the oxygen electrode channel can be swept with air in order to maintain the temperature gradient of the cell within the allowable ΔT_{cell}. The molar flow rate through the oxygen electrode $(\dot{N}_6, \dot{N}_7)$ is again broken down into two components:

$$\dot{N}_{\{6,7\}} = \dot{N}_i^{O_2} + \dot{N}_{sweep}^{Air} \tag{3.29}$$

At the inlet of the cell $\dot{N}_6^{O_2} = 0$, and thus:

$$\dot{N}_6 = \dot{N}_{sweep}^{Air} \tag{3.30}$$

$\dot{N}_{sweep}^{Air}$ is found using equation (3.19) (for information on how to calculate Q_{stack} see Section 3.3.2.3). At the outlet of the cell, $\dot{N}_7^{O_2}$ is found using equation (3.28) and $\dot{N}_{sweep}^{Air}$ is again computed using equation (3.19).

3.3.2.3 Energy balance

Computing the energy balance of the stack control volume is straight forward once all streams in the fuel electrode side have been calculated. The same process as the one described in Section 3.3.1.3 is used where the heat produced or generated by the stack is calculated by performing an energy balance around the junction of streams 3 and 4. Because the only reaction involved is the electrochemical reduction of steam, (3.22) is re–written as:

$$Q_{stack} = \sum \dot{N}_4^j \cdot h_4^j(T_{out}) - \sum \dot{N}_3^j \cdot h_3^j(T_{in}) - P_{op,EL} - \xi_{EL} \cdot \Delta H_{rxn,H_2ox} \qquad (3.31)$$

Where $\Delta H_{rxn,H_2ox}$ is the heat of reaction for the oxidation of H_2 and $P_{op,EL}$ is the power required by the electrolysis stack which can be calculated using equation (3.2). The way in which equation (3.31) is written suggests that when the cell is operated exothermically $Q_{stack} < 0$, endothermically $Q_{stack} > 0$ and in thermoneutral operation $Q_{stack} = 0$.

3.3.3 Degradation

The SOC's degradation is a key parameter in the model, as it affects the lifetime of the system, as well as its operational output. Modeling degradation at the cell level is extremely hard, thus in order to simplify the problem degradation at the RSOC stack is modeled as an increase in area specific resistance (ASR). This increase will have a negative impact on the operating voltage of the cell, lowering the voltage at a given current in fuel cell operation, or increasing it in electrolysis mode as the cell ages. This, in turn, will have an impact on the system's output, heat to power ratio, and therefore can have great impact on the system economics (see Section 5.3.5 for economic impact of degradation). Because degradation is modeled as an increase in ASR, the evolution of the stack's ASR can easily be captured by the following general

expression:

$$\mathrm{ASR}(t) = \mathrm{ASR}_0 f(t) \tag{3.32}$$

where $f(t)$ is a function that describes how the system degrades with time. For example, if we assume the cell degrades linearly with time at a fixed rate, then $\mathrm{ASR}(t)$ can be expressed as:

$$\mathrm{ASR}(t) = \mathrm{ASR}_0 \left(1 + rt\right) \tag{3.33}$$

where r is the rate at which the cell degrades. Thus, if the system degraded at a rate of 1%/1000hrs, then if the system had an initial ASR of $0.5\Omega\mathrm{cm}^2$ and it operated for 2,000 hrs we would expect the system to have degraded 2% from its initial value, and therefore it would have an ASR of $0.51\Omega\mathrm{cm}^2$.

This simple approach to degradation modeling allows for flexibility as the degradation function $f(t)$ can follow any shape or form (e.g. linear, exponential, hyperbolic) and can be extended to be a function not only of a particular point in time but of the device's history and/or particular operating point and mode.

3.4 Balance of Plant components

The balance of plant components for the end–to–end ROSC systems consists of all the units required for heating, compressing, mixing, and reacting gases (outside of the stack) as well as the equipment required for converting DC into AC power (or vice versa). All components are modeled as 0-D black boxes using thermodynamic equations. Reactive processes (e.g. the methanation reactors) are assumed to operate at equilibrium and conversions are calculated using Gibbs free minimization procedures. Turbomachinery components are modeled using fixed isentropic efficiencies.

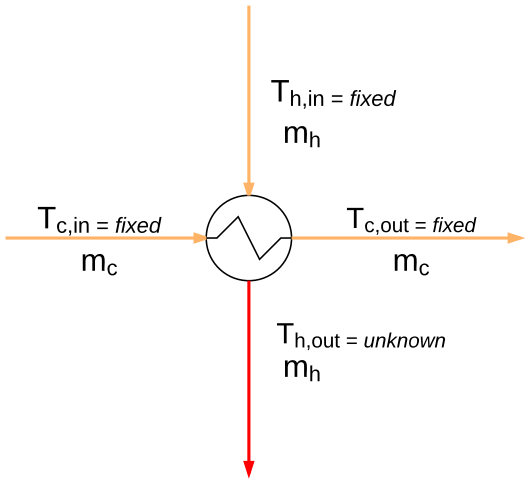

Figure 3.5: Generic counterflow heat exchanger

3.4.1 Pre-heaters

For the purpose of this model, pre-heaters are assumed to be 0-D planar counterflow heat exchangers (see Fig. 3.5). In order to avoid getting into the details of channel geometry and fin efficiencies, the model assumes a constant heat transfer coefficient. When running at constant (nominal) current density, the inlet and outlet temperatures of the cold streams ($T_{c,in}, T_{c,out}$) and the inlet temperature of the hot stream ($T_{h,in}$) are known, as they are either specified a priori (e.g. operating temperature of the cell) or are the calculated outputs of other processes within the system (e.g. temperature after methanation). Under this conditions, the pre–heater module has two main purposes: to compute the outlet temperature of the hot stream ($T_{h,out}$); and to calculate the size of heat exchanger required (if none is specified). The pre–heater module calculates $T_{h,out}$ by performing a heat balance on the heat exchanger following the method suggested by [50]. Using Fig. 3.5, the heat required to increase the temperature of the cold stream to the outlet temperature is defined as:

$$Q_{req} = \dot{n}_c \left(h_{c,out} - h_{c,in}\right) \tag{3.34}$$

where $\dot{n}_c$ is the molar flow rate of the cold stream, $h_{c,out}$ is the molar enthalpy of the cold stream at the outlet temperature and $h_{c,in}$ is the molar enthalpy of the cold stream at the inlet temperature. The exit temperature of the hot stream can then be approximated using the following relationship:

$$T_{h,out} = T_{h,in} - \frac{Q_{req}}{\dot{n}_h C_p} \tag{3.35}$$

where $\dot{n}_h$ is the molar flow rate of the hot stream and C_p is the molar heat capacity at the known $T_{h,in}$.

3.4.1.1 Sizing pre–heaters

In order to size the pre–heaters, the Log Mean Temperature Difference (LMTD) method is employed [109]. The LMTD method provides a straightforward way for relating the Q_{req} to the area of the heat exchanger A_{HeX}:

$$A_{HeX} = \frac{Q_{req}}{U \cdot \text{LMTD}} \tag{3.36}$$

where U is the heat transfer coefficient, and LMTD is:

$$\text{LMTD} = \frac{(T_{h,in} - T_{c,out}) - (T_{h,out} - T_{c,in})}{\ln\left(\frac{T_{h,in} - T_{c,out}}{T_{h,out} - T_{c,in}}\right)} \tag{3.37}$$

In all cases, the performance of the heat exchanger is defined by a constant U of 163 W/m^2–K which is a good approximation for planar devices and low pressure gases [3].

3.4.2 Electric heaters

Electric heaters are employed when operating in electrolysis mode as a way to provide heat to certain processes and/or units for which waste heat is not readily available and/or in cases where heat-integration is non-trivial. Because a detailed heat-integration effort is outside the scope of this model, electric heaters are used as a

simplification in order to satisfy energy balances and to approximate the cost and magnitude of system parasitics. For example, electric heaters are employed as a way to provide the necessary energy when the RSOC operates below U_{th} or to pre-heat incoming CO_2 to the methanator's operating temperature. As such, electric heaters take in an energy requirement and compute a resulting electric load after efficiency losses are taken into account:

$$P_{heater} = \frac{Q_{req}}{\eta_{elec}} \tag{3.38}$$

For all cases, the efficiency of the electric heaters (η_{elec}) is set to 0.95, consistent with assumptions found in other studies [108],[103]. This efficiency is assumed to stay constant when operating at part-load points.

3.4.3 Evaporator

As with other BoP components, the evaporator used in electrolysis mode is modeled thermodynamically as a 0–D black box. The modeling is intended to capture the energetic cost associated with steam formation. The evaporator module assumes that water in the liquid phase is delivered at 100 °C and saturated steam exits at 100 °C. Thus, the energy required for steam formation is simply:

$$Q_{evap} = \dot{n}_{feed} \Delta \mathrm{H}_{evap} \tag{3.39}$$

where $\dot{n}_{feed}$ is the molar flow of the water in the feed and $\Delta \mathrm{H}_{evap}$ is the latent heat of vaporization of water. Because water evaporation is a energetically expensive process ($\Delta \mathrm{H}_{evap} = 40.65$ kJ mol^{-1}) heat integration is important in order to keep the system efficiency within a reasonable range of operation. We assume that all waste heat available from the methanator ($Q_{meth,a}$) and from the RSOC's outlet O_2 electrode side ($Q_{\mathrm{O}_2,a}$) is used for the evaporation process. The available heat from stream i ($Q_{i,a}$) is simply calculated as the enthalpy change between the waste-heat's initial

temperature (T_o) and the temperature of evaporation

$$Q_{i,a} = \dot{n}_i \left(h_o - h_f\right) \tag{3.40}$$

where $\dot{n}_i$ is the molar flowrate of stream i and h_o and h_f are the stream's specific molar enthalpies at T_o and at the temperature of evaporation. In cases for which the total available heat is not enough to meet the heating requirements, an electric heater is used. The final electric load of the evaporator is:

$$P_{evap} = \frac{Q_{evap} - Q_{meth,a} - Q_{\mathrm{O}_2,a}}{\eta_{elec}} \tag{3.41}$$

Lastly, it is assumed that part-load operation does not affect the performance of the evaporator.

3.4.4 Turbomachinery

3.4.4.1 Blowers and pumps

Blowers and pumps are used to move air or liquid water around the system. The main purpose of modeling these ancillary units is to capture the parasitic losses that are associated with their operation. In the case of air blowers, these become particularly important when operating at high current densities (see Chapter 4 for a detailed discussion). Detailed modeling of turbomachinery is a complex task that is well beyond the scope of this thesis, thus for the purpose of this model the pumps and blowers are modeled as constant isentropic efficiency processes. The work required to operate the blowers is determined from:

$$W_{blow} = \frac{\dot{V} \cdot \Delta P_{gas,sys}}{\eta_{s,blow}} \tag{3.42}$$

where $\dot{V}$ is the volumetric flowrate of the air or liquid, $\Delta P_{gas,sys}$ is the required system pressure rise, and $\eta_{s,blow}$ is the isentropic efficiency. The required system pressure rise can be calculated by summing the individual pressure drops across different components of the system.

3.4.4.2 Compressors

In both modes of operation, compression is modeled as isentropic processes with constant efficiency. In fuel cell mode, a compressor is used to increase the pressure of the feed gas so that it may overcome the pressure drops as it flows through the system. In electrolysis mode, the fuel compressor is mainly used for compressing the synthesized CH_4 gas to the required temperature and pressure for injection into the natural gas grid. The particular temperature and pressure at which natural gas must be injected into the grid will vary for suppliers, markets and regions. According to [14], the range of pressure and temperature characteristic for injection into a natural gas grid is 0.1–25 MPa and -20–90 °C. For the purpose of the modeling a pressure of 3 MPa and 50 °C is used.

The compressor is modeled as a multi-stage compressor with inter-stage cooling, a mechanical efficiency (η_{mech}) of 0.80 , and an isentropic efficiency (η_{is}) of 0.75. The work for the compressor is calculated as:

$$W_{comp} = \frac{\gamma}{\gamma - 1} \left(\frac{RT}{M \eta_{mech}} \right) \left(\frac{P_f}{P_o} \right)^{\frac{\gamma - 1}{\gamma}} \tag{3.43}$$

where $\frac{P_f}{P_o}$ is the compression ration at each stage, R is the universal gas constant, T_o is the temperature at the inlet of the compressor, γ is the molar heat capacity ratio ($\frac{C_p}{C_v}$) and M is the molecular weight. Assuming constant isentropic efficiency, the final discharge temperature is defined as:

$$T_f = T_o \left[1 + \frac{\left(\frac{P_f}{P_o} \right)^{\frac{\gamma - 1}{\gamma}} - 1}{\eta_{is}} \right] \tag{3.44}$$

3.4.5 Catalytic combustor

When operating in fuel cell mode, a catalytic combustor is employed in order to oxidize the exiting unreacted anode gases (after the anode recycle split). As a result

of the combustion, the chemical energy in the unreacted H_2 and CO is converted into thermal energy and released into the bulk gas. Based on the work by Yu et. al. [131], the catalytic combustor is modeled as a 0-D ceramic honeycomb monolith with a Pt/Al_2O_3 washcoat. Yu et. al. [131] reports that at temperatures close to 800 °C, there is $\sim$ 100% conversion of the unreacted anode gases. The study also reports a maximum operating temperature of 850 °C after which the catalyst experiences activity loss and irreversible damage. For this reason, the combustor module assumes that a T_{comb} of 850 °C is the upper limit for the temperature of the flue gas exiting the combustor. The oxygen required for the combustion is provided by mixing the outlet stream of the cathode gas which contains excess air that was used for managing the thermal gradient within the cell. Furthermore it is assumed that the monolith is perfectly insulated so the heat transfer between the monolith and the outside environment is assumed to be zero.

Due to the fact that the solid oxide cell is operating very near the maximum T_{comb}, it is assumed that the catalytic combustor operates within a narrow temperature range so that the gas exiting the monolith is never above T_{comb}. In order to achieve the isothermal operation, a stream of air at ambient temperature (that by-passes the pre-heater upstream of the RSOC) is added to the combustor to absorb the thermal energy that is released as a consequence of the catalytic conversion. The combustion reactions are:

$$CH_4 + 2\,O_2 \longrightarrow CO_2 + 2\,H_2O \tag{R3.17}$$

$$CO + \frac{1}{2}\,O_2 \longrightarrow CO_2 \tag{R3.18}$$

$$H_2 + \frac{1}{2}\,O_2 \longrightarrow H_2O \tag{R3.19}$$

Assuming that the extent of reaction for all combustion processes is equal to one, the heat released during the combustion Q_{comb} is:

$$Q_{comb} = \dot{n}_{CH_4,in}\Delta H_{rxn,m} + \dot{n}_{CO,in}\Delta H_{rxn,c} + \dot{n}_{H_2,in}\Delta H_{rxn,h} \tag{3.45}$$

where $\dot{n}_{CH_4,in}, \dot{n}_{CO,in}, \dot{n}_{H_2,in}$ are the molar flow rates of CH_4, CO and H_2 into the combustor and $\Delta H_{rxn,\{m,c,h\}}$ are the heats of reactions corresponding to reactions R3.17 to R3.19. The amount of cold by-passed air that will be required for isothermal operation can easily be computed by:

$$\dot{n}_{by-pass} = \frac{-Q_{comb}}{h_{air,c} - h_{air,o}} \tag{3.46}$$

where $h_{air,c}$ and $h_{air,o}$ are the specific molar enthalpies of air at the combustor temperature T_{comb} and at ambient temperature T_o. Assuming an extent of reaction equal to 1 for reactions R3.17 to R3.19, the outlet composition of the gas is computed using the following relationships:

$$\dot{n}_{CH_4,out} = 0 \tag{3.47}$$

$$\dot{n}_{H_2,out} = 0 \tag{3.48}$$

$$\dot{n}_{CO,out} = 0 \tag{3.49}$$

$$\dot{n}_{CO_2,out} = \dot{n}_{CO_2,in} + \dot{n}_{CH_4,in} + \dot{n}_{CO,in} \tag{3.50}$$

$$\dot{n}_{H_2O,out} = \dot{n}_{H_2O,in} + 2\dot{n}_{CH_4,in} + \dot{n}_{H_2,in} \tag{3.51}$$

$$\dot{n}_{O_2,out} = \dot{n}_{O_2,in} + 0.21\dot{n}_{by-pass} - 2\dot{n}_{CH_4,in} - 0.5\dot{n}_{CO,in} - 0.5\dot{n}_{H_2,in} \tag{3.52}$$

$$\dot{n}_{N_2,out} = \dot{n}_{N_2,in} + 0.79\dot{n}_{by-pass} \tag{3.53}$$

3.4.6 Reactors

As discussed in Section 2.3.2 the synthesis of CH_4 via the selective hydrogenation of CO_2 is a well established technology that is routinely used in industry. Although it is mostly used as a way to remove small traces of CO_2 in processes that might be sensitive to the presence of CO_2 (such as in the catalytic synthesis of NH_3), in recent years the catalytic hydrogenation of CO_2 has gained renewed interest as a path for storing variable renewable energy in the form of synthetic natural gas (SNG) [25, 26, 38]. The hydrogenation of CO_2 requires, at least, a 4:1 ratio of H/C and is a highly

exothermic process:

$$CO_2 + 4\,H_2 \rightleftharpoons CH_4 + 2\,H_2O \qquad \Delta H = -164\,\text{kJ} \tag{R3.20}$$

Because CO_2 hydrogenation is an highly exothermic reaction, it is favored at low temperatures, however if these are too low kinetic rates are unfavorable. Thus, when operating CO_2 methanator reactors heat management is extremely important in order to maintain the temperature of the reactor within acceptable ranges.

As previously discussed, methanation is usually carried out in catalytic fixed bed reactors, however managing strongly exothermic reactions in these types of reactors is a non-trivial task that usually requires operating many reactors in series with cooling between them (see Section 2.3.2). One alternative to using fixed-bed reactors with complex heat management systems is to deposit the hydrogenation catalyst on the surface of a monolith, which has been successfully used for natural gas reforming [39]. This is a particularly attractive approach as it reduces the capital cost of the plant by replacing fixed bed reactors with much cheaper monoliths and simplifies the heat management operation. The use of monoliths as catalytic reactors is well-suited for small-scale and distributed applications where BoP complexity must be reduced as much as possible.

For the purpose of this model, we assume that methanation is carried out in a monolith (see Fig. 3.6) using a highly active Ru/Al_2O_3 catalyst like the one reported by Janke et al. [71]. Janke et al. report that for a mixture of 4:1 H_2/CO_2, a reactor operating at 1 bar with 10% Ru catalyst has high selectivity towards methanation and operates close to equilibrium at $T \sim 280\,°C$ and low space velocities. For modeling purposes, rather than defining a conversion of CO_2 at a given temperature, it is assumed that the reaction is in equilibrium and the resulting mole fractions are calculated via a Gibbs minimization routine that is solved using SciPy's SLSQP constrained optimization function. In order to assess the accuracy of this routine a 4:1 H_2/CO_2 mixture is brought to equilibrium at temperatures ranging from 150-800 °C

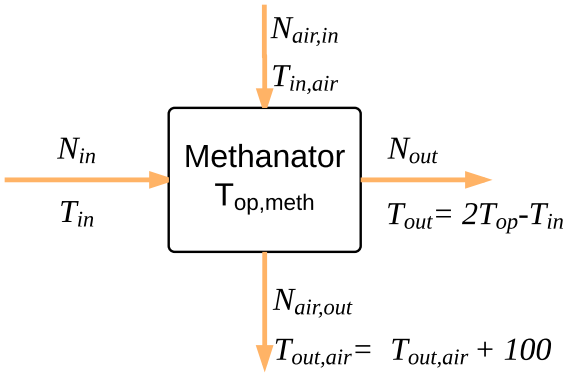

Figure 3.6: Methanation on catalytic heat exchanger

and the results are compared against a Gibbs minimization reactor set up in ASPEN Plus that use the Redlich-Kwong equations of state.

Fig. 3.7 shows the results of this comparison. As it can be seen, there is agreement between the two models at the specified inlet conditions and temperature ranges. This figure suggests that the major disagreement occurs at around 480 °C, where the largest absolute difference is in the fraction of H_2, a difference that peaks at ~ 0.0027. The small differences between the two models suggest that the implemented Gibbs minimization is very robust for modeling purposes and its results are valid over the temperature ranges of interest. As plot(1) in Fig. 3.7 shows, the hydrogenation of CO_2 is very sensitive to increases in the operating temperature of the reaction due to its highly exothermic nature. For this reason, it is very important to design the monoliths such that the operating temperature stays within a narrow range. In order to achieve this, the following assumptions are made:

- The methanation reactor is modeled as a number of monoliths coated with a Ru catalyst arranged in series.
- The highly exothermic reaction is controlled by transferring the heat of reaction to a stream of air.

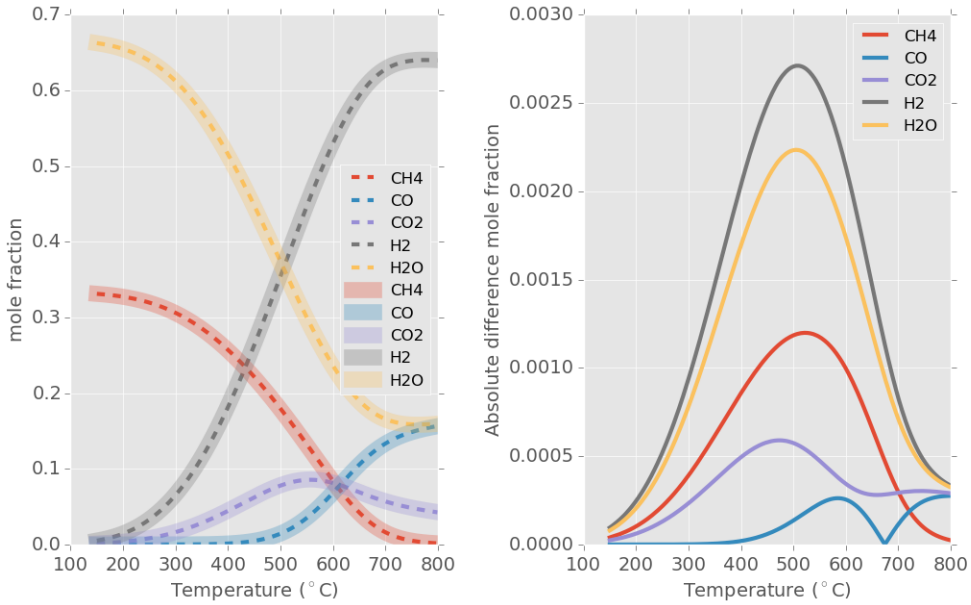

Figure 3.7: Comparison of Gibbs minimization routines. Plot(1): Solid lines - ASPEN; broken lines- python; Plot(2): Absolute difference

- A temperature rise of 100 °C is fixed between the inlet and the outlet of the methanation streams.
- The inlet of the methanation stream is assumed to be at 250 °C.
- The reaction (and equilibrium calculations) occurs at a temperature $T_{op,meth}$ which is equal to the average of the inlet and outlet streams (∼300 °C)(see Fig. 3.6).

The energy balance takes the following form:

$$Q_{meth} = \sum \dot{n}_{i,out} h_{i,out} - \dot{n}_{i,in} h_{i,in} + \xi_{meth} \Delta H_{rxn,meth} \tag{3.54}$$

where $\dot{n}_{i,out}$and$\dot{n}_{i,in}$ are the molar flow of species i at the outlet and inlet of methanation stream, $h_{i,out}$and$h_{i,in}$ are their molar enthalpies at the outlet and inlet temperatures, ξ_{meth} is the molar extent of reaction (which is simply $\dot{n}_{\mathrm{CH_4},out} - \dot{n}_{\mathrm{CH_4},in}$), and $\Delta H_{rxn,meth}$ is the standard heat of reaction for the methanation reaction.

From this, the amount of air needed on the cold side is calculated by:

$$\dot{n}_{air,meth} = \frac{Q_{meth}}{C_{p,air-Top} \cdot \Delta T_{air}} \tag{3.55}$$

where $C_{p,air-Top}$ is the molar heat capacity of air at the average temperature $T_{op,meth}$ and $\Delta T_{air} = T_{air,out} - T_{air,in}$.

3.4.6.1 Mass of the catalyst and required reactor volume

The amount of catalyst required will be dependent on the size of the system, the flow rate of the gases going into the monolith, and the yield of the methanation reaction. For the purpose of this model, the required amount of catalyst to be coated into the monolith is calculated using a variation of the space velocities reported by Janke et. al. [71]. Janke et. al report a very low GHSV of only $101\,\mathrm{h}^{-1}$ at a temperature of 250 °C, however higher space velocities can be assumed due to the fact that the average operating temperature is higher than 250 °C. Duyar et al. [28] report that the activation energy of the methanation reaction with the 10% Ru/Al_2O_3 catalyst is roughly $66\,\mathrm{kJ\,mol}^{-1}$ and provide the following empirical rate equation:

$$R_{\mathrm{CH_4},f} = 35.5 \times \exp(\frac{-66100}{RT}) \times p_{\mathrm{H_2}}^{0.88} \times p_{\mathrm{CO_2}}^{0.34} \times p_{\mathrm{CH_4}}^{-0.11} \times p_{\mathrm{H_2O}}^{-0.23} \tag{3.56}$$

This rate equation suggests two important things: first, that the reaction is almost first order with respect to H_2; secondly for a 100 °C temperature rise, the reaction rate increases by roughly 19x. Because the monoliths are operating on average at 300 °C with a temperature change of 100 °C between inlet and outlet gases, a GHSV of $1000\,\mathrm{h}^{-1}$ is assumed.

With this in mind,for a known feed flow rate the volume of the monolith can be easily calculated using the following relationship:

$$V_{mono} = \frac{V_{feed}}{\mathrm{GHSV}} \tag{3.57}$$

V_{feed} is the volumetric flowrate of the feed gases in L/hr. The ceramic monolith used by Janke et al. is reported as having a catalyst loading of $2\,\mathrm{g/in}^3$, thus the required

mass of the catalyst m_{cat} is simply:

$$m_{cat} = \frac{V_{mono}}{2\,\mathrm{g/in^3}} \tag{3.58}$$

V_{mono} is the total volume of the monolith. As reported by Janke et. al., this particular loading takes into account the fact that the thickness of the washcoat cannot exceed 200 µm.

Finally, the total number of monoliths required can easily be computed by dividing the total volume of the monolith (V_{mono}) by the volume of each individual monolith. Commercial monoliths are usually 150mm × 150mm × 300mm, thus for a $1\,\mathrm{m^3}$ total monolith volume, roughly 150 monoliths would be required. The particular length of the monoliths, however, can be adjusted to fit a particular design.

3.4.7 Water separator

In electrolysis mode, before the natural gas is compressed for injection into the natural gas grid, the un-electrolyzed steam and the water generated during the methanation process needs to be separated. Water is separated from the stream by means of condensation in a flash tank operating at atmospheric pressure. The stream that enters the flash tank is mostly a mixture of H_2O, CH_4 and H_2 and therefore modeling the vapor-liquid equilibrium for this mixture is a non-trivial task. Fig. 3.8 show the vapor-liquid equilibrium for a mixture of 0.686 H_2O, 0.032 H_2, 0.281 CH_4 and 0.000679 CO, a typical composition exiting the methanator[5], that was modeled in the well-known chemical process simulation software ASPEN Plus. At temperatures below 40 °C, there is less than 5% H_2O in the vapor phase. We therefore assume that the flash is a constant temperature process operating at 35 °C. Because the water separator involves a phase-change, the energy balance is broken down into the energy associated with cooling the mixture from the initial temperature (e.g. the exiting

[5](see Chapter 4 for further discussions)

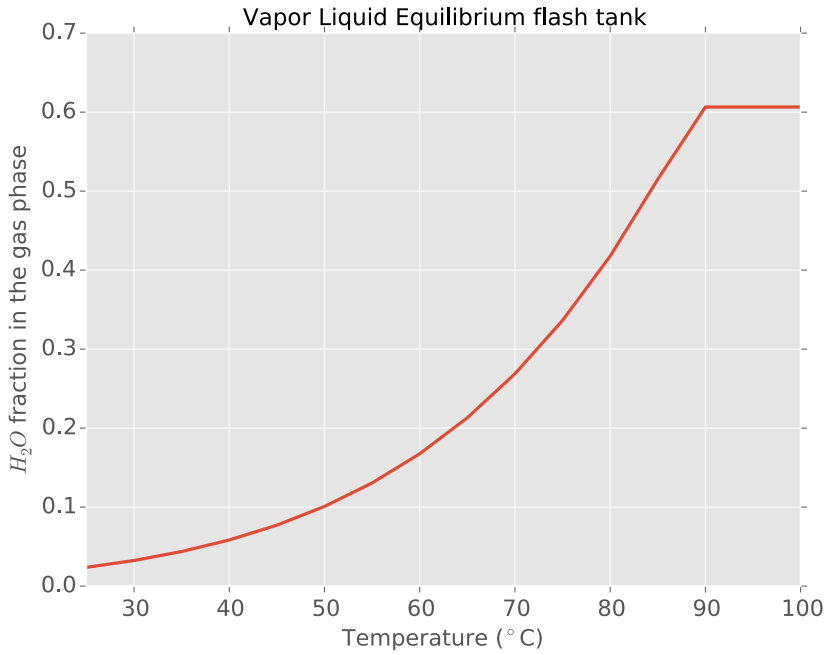

Figure 3.8: Vapor-liquid equilibrium for 0.686 H_2O, 0.032 H_2, 0.281 CH_4, 0.000679 CO mixture

temperature of the methanator) to the operating temperature of the flash (35 °C), and the energy released from the condensation of water.

The energy balance is calculated as follows:

$$\dot{Q}_{flash} = \sum \dot{n}_i \left(h_{i,T_{flash}} - h_{i,T_o} \right) - \dot{n}_{\mathrm{H_2O}} \Delta H_{cond} \tag{3.59}$$

where $\dot{n}_i$ is the molar flow of species i into the flash, $h_{i,T_{flash}}$ is the molar enthalpy of species i at the operating temperature of the separator (35 °C in our case), h_{i,T_o} is the molar enthalpy of species i at the initial temperature, and ΔH_{cond} is the latent heat of condensation of water.

3.4.8 Pressure drops

Calculating the exact pressure drops for system components requires detailed understanding of their particular design and complex modeling tools, which is outside the

Component	Pressure Drop (mbar)	Reference
Pre-heaters	100	[105]
RSOC	30	[11]
Evaporator	10	[12]
Methanation	150	[30]
Combustor	20	[105]

Table 3.2: System component pressure drops

scope of this work. For this reason, the values used in this model are taken from the literature and listed in Table 3.2 below.

3.5 Part-load operation

One of the main objectives of this thesis is to quantify the value that RSOC systems can have when its operating point is optimized as a function of fluctuating electricity and fuel prices (see Chapter 5). As such, the RSOC will have to operate through a wide range of possible operating points (e.g. current densities) so that its output electricity or fuel is the optimum given particular market conditions at each hour of the day. Doing this will require the system to be able to operate at "part-load.

The term "part-load operation" is used to describe the operation of the RSOC system below its "rated" design, which corresponds to the operating point (e.g. current density) used to size the major system components such as heat exchangers, blowers, and the SOC stack. In order to meet the system requirements at the extremes, the rated design is taken to be the highest operating current (and thus gas flow rates) at which the system is expected to operate. One of the main challenges of operating at part-load is to make sure that the temperature requirements of the gases going into the cell and into the catalytic reactor are met at all operating points. Detailed modeling of part-load operation of complex systems can be a very difficult task, as it requires in-depth knowledge of every component in the system. Rather than trying to come up with detailed part-load modeling of every single component,

we reduce the part-load modeling of the BoP components to the two main pieces that have the greatest effect on system efficiency and parasitics, namely pre-heaters and gas blowers. Furthermore, in order to simplify the computational complexity of the model, it is assumed that the rated efficiency of all components is kept constant at part-load operation, and thus the impact of part-load operation on system parasitics is quantified via the changes in temperatures of the gas streams after they go through oversized pre-heaters and changes in system pressure drops (due to the lowering of the flows) which affect the work required by the turbo-machinery.

3.5.1 Pre-heaters

As previously described, when operating in part-load it is assumed that the system components are designed for the highest possible flows and current densities. Given that the areas of the pre-heaters are fixed for the highest possible flow rates, when the system operates below the design point the gases effectively spend more time within the heat exchanger resulting in an increase of the total heat transfer. This, in turn, poses problems for maintaining the inlet temperature of the gases into the RSOC constant when operating below the rated point. In order to avoid this problem, bypass valves that divert part of the gases entering the hot side of the pre-heaters are added to the system design (see Fig. 3.9). The amount of by-passed gases at each heat exchanger is calculated such that the pre-defined temperature requirements for gases entering the stack (the outlet of the cold-stream) at both the air and fuel electrodes are met.

Fig. 3.9 shows a schematic of an air or fuel pre-heater with a bypass valve. Typically, both inlet temperatures are known ($T_{h,in}, T_{C,in}$) and the exiting cold temperature ($T_{C,out}$) is fixed at the stack's inlet temperature requirements. Finally, the total flowrate of the hot stream and cold streams ($\dot{m}_{h,1}, \dot{m}_{c,1}$) are also known. Thus, there are three parameters that need to be solved for: the flowrate of the hot gas through

the pre-heater ($\dot{m}_{h,2}$), the flowrate of the gas through the bypass ($\dot{m}_{h,3}$), and the exiting temperature of the hot gas ($T_{h,out}$). Thus three equations relating the area of the pre-heater, the flowrate of the gases and their temperatures need to be solved simultaneously. Recall from Section 3.4.1.1 that the area of the pre-heater is a function of the heat transfer requirement and the log-mean temperature difference (3.36) and (3.37). Because the area of the pre-heater is fixed at the design point, (3.36) can be rearranged and together with (3.37) it can be used to solve for $T_{h,out}$:

$$\text{LMTD} = A_{HeX} \cdot Q_{req} \cdot U$$

$$\text{LMTD} = \frac{(T_{h,in} - T_{c,out}) - (T_{h,out} - T_{c,in})}{\ln\left(\frac{T_{h,in} - T_{c,out}}{T_{h,out} - T_{c,in}}\right)}$$

Once $T_{h,out}$ has been computed, the flowrate of the gas passing through the pre-heater

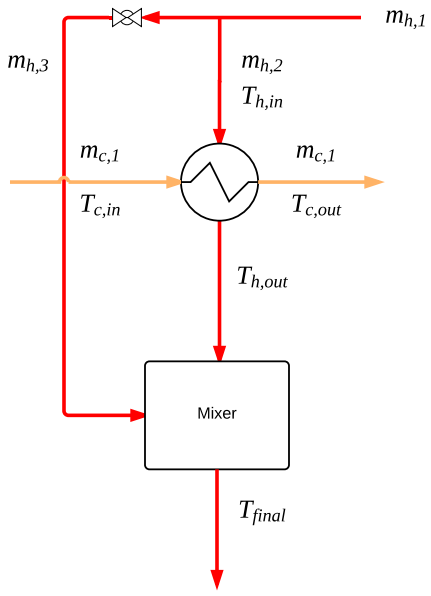

Figure 3.9: Pre-heater with bypass valve

($\dot{m}_{h,2}$) can easily be calculated:

$$\dot{m}_{h,2} = \frac{Q_{req-off}}{C_p \cdot (T_{in} - T_{out})} \tag{3.60}$$

Lastly, a simple material balance around the bypass valve is used to calculate the remaining streams:

$$\dot{m}_{h,3} = \dot{m}_{h,1} - \dot{m}_{h,2} \tag{3.61}$$

Just as in the case of the equilibrium calculations presented in Section 3.3.1.2, SciPy's *fsolve* function is used to find the solution to the equation set described above.

3.5.2 Blowers

As described in previous sections, blowers represent a very important component of the BoP and their parasitic load is modeled as a function of the total volume of gas and the required pressure drop across the system. When operating during part-load conditions, the total system component pressure drop will have to be recomputed and will scale with the ratio of the volumetric flowrate ($\dot{V}$) to the volumetric flowrate at the reference point ($\dot{V}_{design}$). This can be estimated using the relationship suggested by [3]:

$$\Delta P_{sys} = \Delta P_{design} \left(\frac{\dot{V}}{\dot{V}_{design}} \right)^{1.5} \tag{3.62}$$

where ΔP_{design} is the system pressure drop at the reference design point. When operating at lower volumes, one would expect the parasitic load to decrease as the total system pressure drop will decrease in a non-linear fashion. Although counter intuitive at first, as it suggest that oversizing the BoP could lead to higher system efficiencies, it is important to keep in mind that the economic penalty for over designing the BoP is significant and can make a system uneconomic (see Section 5.3.2.2 for a detailed discussion about the economic impact of oversizing the BoP), thus even though there might be some efficiency gains from decreases in system pressure drops, the impact on overall system costs needs to be taken into account when evaluating the impact of part-load operation.

3.6 System cost model

The capital cost associated with novel energy technologies is a key driver for investment decisions and integration at a large scale. In this section we present the system cost model that is employed in order to analyze the total plant cost (TPC) associated with the RSOC system described in Section 3.2. Estimating the costs is a complex task that varies with factors such as component size, design, purchase volumes, contractor services, delays, etc. Thus, this type of analysis should be viewed as an approximation to provide insight and to ascertain whether a particular design or strategy is "feasible". As a matter of fact, in its Power Plant Cost Estimation Methodology NETL suggests that as a first approximation most techno-economic studies have an error of -15 to -30% on the low side and 20 to 50% on the high side[43].

Depending on the particular piece of equipment, the purchase cost will be a function of unit scale, design complexity and/or production volumes. For the purpose of the cost model developed for this thesis, the component costs (C_i) for a particular design size are calculated in one of two ways: by using an empirical correlation that relates cost to some operating parameter ((3.63)) or through a power law that relates scale and cost. The particular strategy employed for each component depends on the availability of data in the peer-reviewed literature, including reference costs and sizes and is discussed in Section 3.6.2. Because balance of plant components tend to be more mature technologies than solid oxide cells, the discussion about costs is divided in two sections: first a section discussing SOC stack cost projections and main cost drivers; and then a section aon the BoP component costs.

3.6.1 SOC stack costs

The cost associated with the RSOC stacks is a key parameter and one of the most difficult to assess, as the technology has not yet been commercialized and most exist-

ing projections depend on a wide variety of assumptions about manufacturing costs and production volumes. Because SOFC's can be operated as electrolyzers [13, 62, 84, 93], using cost data for SOFC's is a reasonable proxy for the stack costs associated with a RSOC system. The US Department of Energy through the Solid State Energy Conversion Alliance (SECA) and FutureGen programs have supported the development of SOFC's and have set a cost target of $225 kWe (US$2011) for an n-th of a kind system manufactured in high volumes [119]. With this in mind, there have been several studies that attempt to estimate the manufacturing costs of producing SOFC's at different scales. The two most widely cited are the study by Thjissen [117] and the one conducted by Weimar et. al the Pacific Northwest Laboratories in the USA[124]. Thijssen finds that production volumes are the dominant factor that can drive the cost of the stack down, and that actual cell and stack scale-up plays only a marginal role in total cost reductions [117]. In this same study, Thjissen also suggests that planar anode-supported SOFC's (like the SOC used for the computational model described in previous sections) have a cost advantage over tubular designs, as the former have lower cell and stack packing costs.

Apart from these two studies, there are multiple techno-economic assessments in the literature that use a wide range of assumptions about production volumes, power densities, and overpotentials to come up with some cost estimate for the SOFC stacks. Figure 3.10 depicts the cost of an SOFC used in different studies throughout the literature in $/kW whereas Fig. 3.11 shows the same costs but as a function of total cell active area ($/m^2). In both cases, the data is presented as a function of manufactured production volumes. All prices are normalized to $2009 USD and when manufacturing volumes are not explicitly stated in the studies a value of 250 MW/yr is assumed, which corresponds to what the D.O.E considers high volume production. As can be seen from Fig. 3.10 and Fig. 3.11 there is a dramatic drop in the cost of the SOC stack as the yearly production volumes increase. These two

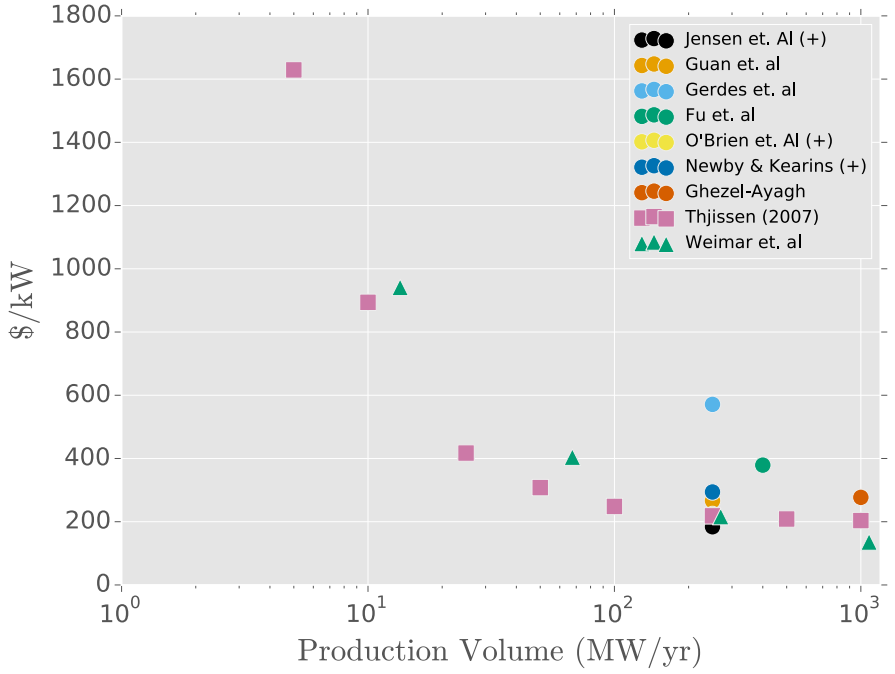

Figure 3.10: stack cost in $2009 USD/kW. (+) denotes cases for which no production data was available. Data from: [40, 44, 45, 56, 73, 96, 98, 117, 124]

plots also include various data points for each of the Thjissen and Weimar et. al. studies. Figure 3.10 shows agreement between the price estimates of Thjissen and Weimar et al. The clustering of many of the data points around the 250 MW/yr mark suggest that many of the techno-economic studies tend to assume SOC costs that correspond to high volume production scenarios. When looking at the SOC costs per m^2 of active area (Fig. 3.11) there is less agreement between the Thjissen and Weimar curves which is due to the difference in power densities in the two studies.

The cost of the SOC used in subsequent chapters will assume a high volume market of 250 MW/yr, which corresponds to a cost of $1,000/$m^2$. This prices include installation costs and therefore can be directly used to calculate total plant costs (TPC).

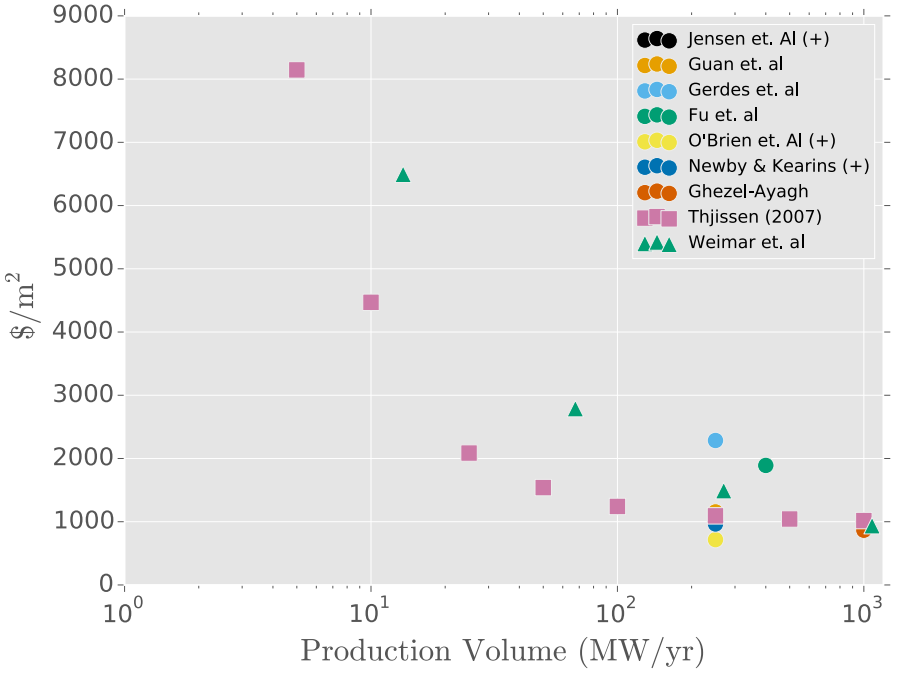

Figure 3.11: stack cost in \$2009 USD/m^2. (+) denotes cases for which no production data was available. Data from: [40, 44, 45, 56, 73, 96, 98, 117, 124]

3.6.2 BoP component costs

As mentioned before, purchase and installation costs for all BoP components will scale according to some design variable (e.g. heat exchange area, volumetric flow rate, total load, etc.) and will be calculated via an empirical relationship or a power law that relates cost and capacity. For well established components such as heat exchangers and pumps, the bare module cost C_p (e.g. cost of equipment not including transportation and installation) are calculated using the following relationship:

$$\log_{10} C_p = K_1 + K_2 \log_{10}(A) + K_3 \left[\log_{10}(A)\right]^2 \tag{3.63}$$

where A is the capacity or size parameter of the equipment and K_1, K_2 & K_3 are constants that depend on each type of equipment. The values for these constants are taken from Turton et. al [118]. Furthermore, these constants assume that the equipment operates at atmospheric pressure and within a specific range of temperatures

and sizes (A). The bare module costs can be corrected for higher pressure, temperatures, material needs, and the cost associated with transportation and installation. Thus, the bare module cost C_p can be converted into bare erect costs (BEC) using the relationship reported by [46]:

$$\text{BEC} = C_p \cdot (B_1 + B_2 \cdot F_M \cdot F_p) \tag{3.64}$$

where B_1 and B_2 are constants unique to each component, F_M is a constant used to correct for different materials, and F_p is a value used for operating pressure deviations. All values of B_1, B_2, F_M and F_p are taken from [46]. For certain equipment types, a "bare module" (F_{BM})factor is provided that bundles all values for B_1, B_2, F_M and F_p into a single factor which can be then be easily applied to calculate the BEC:

$$\text{BEC} = C_p \cdot F_{BM} \tag{3.65}$$

For cases in which the empirical relationship defined in (3.63) does not apply, a power law is used to compute the equipment cost. This power law relates the cost of the equipment for a given size or capacity to a reference cost and size. Thus, the equipment and its cost can easily be scaled:

$$C_i = C_{ref} \left(\frac{S_{new}}{S_{ref}} \right)^{\alpha} \tag{3.66}$$

where C_i is the equipment cost for a given size S_{new}, C_{ref} is the reference cost at capacity S_{ref}, and α is the scaling exponent which traditionally is < 1. As a rule of thumb, costs tend to scale with an $\alpha \sim \frac{2}{3}$, which implies that the cost per unit of output/capacity is halved when the size is increased by a factor 4. Thus, equipment costs can be quite sensitive to the value of α. Although equation (3.66) has traditionally been used to describe the economies of unit scale, the experience of mass-manufacturing suggests that these reductions are also seen when production is scaled in numbers rather than in unit size. As the work of Dahlgren suggests [20, 21],

there is reason to believe that larger cost reductions can be attained via the mass-manufacturing of small-scale components than through traditional economies of unit scale. Although this was traditionally accepted for consumer goods and electronics, the dramatic cost reductions seen recently in the photovoltaic and battery industries suggest that it also applies to the energy sector. This observation, as a matter of fact, is at the heart of the potential cost reductions of SOC's that were discussed in Section 3.6.1.

Table 3.3 lists the empirical constants, reference costs, reference capacities, and scaling exponent for all major components of the base-case RSOC system described in Section 3.2. Table 3.4 lists the values of B_1andB_2 as well as the material factors for the different types of equipment components. Table 3.3 and Table 3.4, in conjunction with equations (3.64) and (3.66) can be used to compute the cost of all major components of the RSOC system at different scales and operating points. Unless otherwise stated, these costs should be taken as installed costs.

RSOC

As discussed in the previous section, the cost of the the RSOC stack depends on a critical assumption that relates the cost of the stack to the size of the market (e.g. total production volume). As a base case, we assume that the RSOC costs \$1,000/m^2 which corresponds to a high production scenario. As discussed in Section 3.6.1, it is expected for RSOC costs to scale linearly with the active area or with the peak power, thus we assume a scaling exponent of 1. This cost includes transportation and installation, thus it is considered to be a TPC value. Refer to Section 3.6.1 for an in-depth discussion about the costs of RSOC stacks.

Balance of stack & stack assembly

The balance of stack and stack assembly costs are based on the work by Jensen et. al. [73], and the peak power in electrolysis mode is used as the scaling unit. It is assumed the cost scales linearly with power and the computed values are assumed to

be TPC costs.

Pre-heaters

For heaters with area $>10\,m^2$, the pre-heaters are modeled as fixed tube heat exchangers. For equipment with area $< 2\,m^2$, the pre-heaters are assumed to be double pipe heat exchanger. The total heat exchange area, calculated using the method described in Section 3.4.1, is used to scale up the equipment. Due to the high operating temperatures associated with the gases coming in/out of the SOC, the pre-heaters are assumed to be made of a Ni-alloy [46]. The material factor (F_M) for these alloys is high, thus the bare erect costs (BEC) associated with the pre-heaters are higher than for low temperature heat exchange operations.

Electric heaters

The cost for the electric heaters that are employed throughout the system are based on the numbers reported by [27]. The heater electric load at the design point is assumed to be the scaling factor and an installation factor of 2.47 is assumed in order to compute the final installed cost.

Compressors

To cost the methane compressor, we assume that the equipment is a rotary compressor and that the scaling parameter is the power consumption of the device at the design point. The power is calculated using the method described in Section 3.4.4.1. The BEC is calculated using a bare module factor of 2.4 [46].

Water pump

A water pump is used upstream of the steam generation to compensate for any pressure drops in the system and to move the water into the steam generating unit. The equipment is assumed to be a centrifugal pump and the shaft power (kW) is used as the scaling attribute. The pump's power consumption is calculated according to the method described in Section 3.4.4.1. A material factor of 1 is assumed [46] and given that the system operates at atmospheric pressure, a pressure factor of 1 is assumed.

The BEC cost for the pump is calculated using the values in listed in Table 3.3.

Air blowers

The BEC for the air blowers is based on the work by Zhang et. al. [133]. A volumetric flow rate is used as the scaling variable and a scaling factor of 0.6 is employed. The values reported by Zhang et. al. are assumed to be TPC values.

Combustor

The catalytic combustor's cost is based on the techno-economic assessment by Zhang et. al [133]. It is computed using a mass flow rate as the scaling parameter and a scaling factor of 0.66. The reported values by Zhang are assumed to be TPC values.

Methanation monoliths

As described in previous sections, for the purposes of this thesis the methanation reaction is assumed to occur at low temperatures and atmospheric pressures on the surface of a Ru coated monolith, rather than a traditional packed-bed reactor. Section 3.4.6.1 describes how to calculate the total volume of monolith required for a given feed flow rate. Because this is a novel concept, the cost of the monoliths is hard to estimate and should be treated as such. For the purpose of costing the monoliths, off-the-shelf ceramic monoliths with dimensions 150 x 150 x 300 mm were quoted on the Alibaba website [104] at \$592/m^3. A bare module factor of 2.5 was assumed and the price scales linearly with the volume (e.g. no reduction associated with unit scale). The catalyst that is coated onto the monoliths is considered as a different cost element (see below).

Catalyst

In Section 3.4.6 the use of a highly active 10% Ru/Al_2O_3 catalyst was proposed as the catalyst for the methanation reaction. The price of this type of catalyst is not readily available, as all the existing prices are for small lab-scale experiments. In order to estimate the cost of the catalyst, a factor of 3 was assumed for the price of pure Ru. Currently, Ru sells for about \$42/troy oz [66] which corresponds to roughly

$1.35/gram. Thus, if we assume that the price of the catalyst will be 3 times the price of pure metal, the price of Ru catalyst is estimated at $4.06/gram. It is important to highlight that only 10% Ru is required, therefore the final cost of the catalyst will be the adjusted price of Ru times 10% of the total catalyst mass calculated. Furthermore, it is assumed that the price of catalyst scales linearly with the mass and does not exhibit any cost reductions via unit scale.

Inverter

The RSOC generates DC in fuel cell mode and consumes DC in electrolysis mode. Because the system is interacting with an outside grid (buying power when operated as an electrolyzer and delivering electricity in fuel cell mode), the power generated or consumed must be rectified. The AC/DC inverter is rated at the peak power in electrolysis mode, as this is larger than the highest power output of the fuel cell, and its cost is based on a NIST SiC inverter technology reported by Newby et. al [96]. The cost is assumed to be linear with the power output and it is reported as a TPC value.

Evaporator

The cost of the evaporator is based on a large-scale (250 MW) RSOC system developed by Jensen et. al. [73]. Scaling down the evaporator is done using the mass flow rate of the steam generator at the design point in electrolysis mode. A scaling exponent of 0.7 is assumed. The cost reported by Jensen et. al. is assumed to be a TPC.

Water condenser

The water condenser/separator is used to knock out the water after the methane synthesis in order for the gas to be compressed and injected into the NG system. The condenser is based on the values reported by Jensen et. al. [73] and is scaled using the mass flow rate at the design point. A scaling exponent of 0.66 is employed and the value is assumed to be a TPC.

Instrumentation & controls

The instrumentation and controls for the RSOC system is calculated based on the values provided by Thjissen [117]. These are scaled using the peak load of the plant in electrolysis mode as the scaling unit and a factor of 0.66 is employed.

Piping & valves

The cost for the pipes and valves in the system is computed based on the data provided by Jensen et. al. [73]. The peak load in electrolysis mode is used as the scaling unit and it is assumed that the costs scale linearly (e.g. scaling exponent of 1).

Component	**Variable**	**Unit**	**Scaling**	$\mathbf{K}_1$	$\mathbf{K}_2$	$\mathbf{K}_3$	S_{ref}	$C_{ref}(\$)$	α	**Ref**
Air/fuel preheater	Hex area	m^2	Empirical	4.3247	-0.303	0.1634	-	-	-	[118]
Fuel pump	Work	kW	Empirical	3.8696	0.3161	0.122	-	-	-	[118]
Compressor	Work	kW	Empirical	5.0355	-1.8002	0.8253	-	-	-	[118]
Monolith housing	Vessel vol	m^3	Empirical	3.5565	0.37776	0.0905	-	-	-	[118]
SOC	Active area	m^2	Power law	-	-	-	1	1,000-5,400	1	[117, 124]
Balance of Stack	Active area	m^2	Power law	-	-	-	1.00	13.2	1	[73]
Stack Assembly	Active area	m^2	Power law	-	-	-	1	34.2	1	[73]
Air blowers	Vol flowrate	$ft^3 min^{-1}$	Power law	-	-	-	7,979	5,351	0.83	[133]
Combustor	Mass flowrate	$kg\,s^{-1}$	Power law	-	-	-	0.327	146	0.66	[133]
Inverter	Peak load	kW	Power law	-	-	-	1	82	1	[96]
Evaporator	Mass flow	ton hr^{-1}	Power law	-	-	-	694	51,500,000	0.7	[73]
Electric heaters	Heater load	kW	Power law	-	-	-	2,200	250,000	0.9	[27]
CH_4 monoliths	Monolith vol	m^3	Power law	-	-	-	1	592.59	1.0	[104]
Catalyst	catalyst mass	gr	Power law	-	-	-	1	4.06	1.0	see above.
Water condenser	Mass flow	ton hr^{-1}	Power law	-	-	-	122	4,700,000	0.66	[73]
Inst. & control	Peak load	kW	Power law	-	-	-	3,100	105,710	0.66	[117]
Piping and valves	Peak load	kW	Power law	-	-	-	1	34	1	[73]

Table 3.3: BoP cost component scaling table

Component	F_M	F_{BM}	B1	B2
Pre-heater (double pipe HeX)	2.68 (Ni-SS)	-	1.74	1.55
Fuel pump	1	-	1.89	1.35
Pre-heater (fixed tube HeX)	2.68 (Ni-SS)	-	1.63	1.65
Methane compressor	-	2.4	-	-
Monoliths	-	2.4	-	-

Table 3.4: Cost factors for BoP equipment

Finally, all costs should be escalated to a chosen base year in order for the correct TPC to be assessed. Normalizing costs to a base year can be easily be done by applying the following relationship:

$$\frac{C_1}{C_2} = \frac{\mathrm{CI}_1}{\mathrm{CI}_2} \tag{3.67}$$

where C_1 and C_2 represent the cost of equipment for the known and calculated base year, and CI_1 and CI_2 are the cost indexes at the known and calculated years, respectively. For the purpose of this thesis, the chemical engineering plant cost index (CEPCI) is used as the index for normalizing costs.

3.6.3 Annualized costs

As discussed in the previous sections, the cost of each component within the RSOC system will scale according to some design variable (e.g. heat exchange area, volumetric flow rate, etc.) and therefore every system design and operating strategy will result in a different total investment cost. Because system components have different lifetimes (e.g. stacks tend to have lifetimes of $\sim$ 5 yrs while most of the BoP components have lifetimes of $\sim$ 20 yrs), it is important to normalize all component costs so that a total plant cost can correctly be assessed. In order to do this, all costs are annualized using an annuity loan expression:

$$C_{yr,i} = C_i \left[\frac{i}{1 - (1+i)^{-n}} \right] \tag{3.68}$$

where C_i is the component cost, i is the discount rate and n is the lifetime of the component. Thus, the total plant cost on an annualized basis is obtained by summing all of the individual annualized costs:

$$\text{TPC}_{yr} = \sum_{n=i}^{k} C_{yr,n} \tag{3.69}$$

Thus, in order for the operation of the RSOC to break-even, a yearly profit that is equal to TPC_{yr} is required. The impact that different assumptions, operating strategies, and market prices have on the total profitability of the system is explored at length in chapter Chapter 5.

Chapter 4

System Sensitivity to operating variables

Before embarking on any system level analysis, it is important to understand how system parameters and operating variables affect the performance, both at the stack and system level, of the RSOC system discussed in Section 3.2. To do this, steady-state parametric analysis is presented throughout this chapter. This type of analysis is very useful for understanding the underlying dynamics of the system, and to have a better feel for the sensitivity that the system has to variations in both design parameters and operating variables. In the first section of the chapter, a discussion of the different parameters and operating variables that the RSOC model takes (such as T, ASR, $STCR$ ratio, etc.) as well as the outputs computed (e.g. $Power, \eta_{sys}$, etc.) is presented. After this, a detailed discussion on the impact that design parameters and operating variables have on the solid oxide stack's performance, in both fuel cell and electrolysis modes, is presented. Lastly, the chapter will finish by offering a discussion on the impact that the previously discussed parameters have on the overall RSOC system.

4.1 Process variables

The system models described in Section 3.2 require the input of a series of parameters and operating variables that will be critical for calculating the behavior of the system. The user-defined inputs can be broken down into two categories: stack-level parameters and operating variables. In this work we define a "*stack-level parameter*" as an input that remains constant over a range of operating points, and cannot be

Parameter	Type of Variable	Description
T_{op}	Stack parameter	Nominal Operating temperature of stack (K)
ΔT_{cell}	Stack parameter	Temperature increase across stack.
ASR	Stack parameter	Area Specific Resistance Ωcm^2
Area	Stack parameter	Active area of RSOC stack (m^2)
r_{deg}	Stack parameter	Degradation rate %ASR/1000 hrs
x^i_{feed}	Operating variable	Molar composition feed gas
STCR	Operating variable	Steam-to-carbon ration (FC only)
U_f	Operating variable	Fuel utilization (FC only)
λ_{SC}	Operating variable	Steam utilization (EL only)
i_{op}	Operating variable	Operating current density (A/cm^2)
T_{feed}	Operating variable	Temperature of feed

Table 4.1: Model parameters and operating variables

directly controlled or modified by an operator. These parameters can be thought of as a set of values that are linked to the physical characteristics and design of the solid oxide cell, such as the ASR, the degradation of the cell and the tolerable temperature increase across the cell (ΔT_{cell}).

On the other hand, "*operating variables*" are variables that can be adjusted and controlled in order to satisfy a particular operating strategy. These operating variables are the "dials" that will be available to our optimization routines when trying to maximize the system's economic value as a function of varying exogenous variables. Examples of these variables are operating current density (i_{op}), steam-to-carbon ratio (STCR), fuel and steam utilization (U_f, λ_{SC}), etc. Table 4.1 below describe the model's parameters and operating variables.

4.1.1 Fuel Utilization

Fuel utilization is a critical variable in SOC modeling. As previously discussed, the use of anode gas recycling (AGR) in fuel cell mode is employed in order to provide the necessary steam for the internal reforming to take place as well as for maintaining a desired steam-to-carbon ration in order to avoid coking at the electrode surface.

Conversely, in electrolysis mode AGR is employed in order to provide a small amount of H_2 at the inlet of the cell to avoid oxidation of the Ni electrode. RSOC's that operate with anode gas recycling loops, the in-cell fuel utilization ($U_{f,cell}$) will differ from the overall system fuel utilization ($U_{f,sys}$), as the gas entering the cell will be a mixture of the fuel fed to the system (pure CH_4 in fuel cell mode and H_2O in electrolysis mode) and mixture of recycled unreacted H_2, CO and H_2O. Thus, the total volume and energy content of the stream entering the cell will be higher than that of the stream at the inlet of the system, lowering the $U_{f,cell}$ relative to the overall $U_{f,sys}$. When operating in fuel cell mode the in-cell fuel utilization can be defined in terms of the stack's total current and the extent of reaction for the steam reforming and water-gas shift reactions by manipulating equation (3.13). We use the definition provided by [102] to define $U_{f,sys}$:

$$U_{f,sys} = \frac{U_{f,cell}}{1 - r\,(1 - U_{f,cell})} \tag{4.1}$$

It can easily be seen that for cases in which the recycle rate is equal to zero, $U_{f,sys}$ and $U_{f,stack}$ are equal to each other.

4.1.2 Control strategies

There are several ways in which the operator of a RSOC system can control the power generated or fuel produced. Traditionally, the maximization of cell efficiency for a given power or fuel production rate has dictated the overall operating strategy of the system. However, as is discussed in detail in Chapter 5, in environments where prices of electricity and fuel are constantly varying, rather than operating at a predetermined point, one could employ a strategy where the operating point is varied in order to maximize the system's profits for a given set of exogenous variables (e.g. fuel and electricity prices). For this reason, it is important to identify the different ways in which the system can be controlled in order to achieve the "optimum" operating point. For a stack operating at fixed inlet and nominal temperatures, the regulation

of power or fuel produced can be achieved by varying the flows of inlet fuel/steam and air. The particular flows required will depend on the type of cell operating strategy that is desired. Two strategies are available:

(1) A constant voltage strategy

(2) A constant fuel utilization U_f strategy

Under a constant voltage operation, the fuel and air flows are manipulated such that the cell operates at the average operating temperature (T_{op}), within the allowed temperature increase for both anode and cathode gases, and at a constant voltage across all possible points. On the other hand, the constant fuel utilization strategy does not require operation at a specific voltage but rather implies a flow of fuel and air such that the temperature constraints are met and that fuel utilization is always the same independent of the particular voltage and current. In this work, we will always assume a constant fuel utilization strategy. Of course, this is a deliberate assumption and it should not be taken as a guarantee that it leads to best possible outcome. More than anything, it is a way to simplify the computational models and to set a baseline for the analysis presented in Chapter 5. Because SOC are electrochemical systems, in order to make interpretation of the results and behavior of the stack easier, the operating current density (i_{op}) is used as the control variable of the system, which is related to the gas flows by Faraday's Law.

4.2 Fuel Cell mode sensitivities

In order to better understand the sensitivities that the system has to different stack-parameters and operating variables, a parametric study is performed. This study is based on the CH_4 "energy hub" that was presented in Section 3.2. As such, all assumptions laid out in this previous section apply unless noted otherwise. In order to construct the different parametric studies, a set of "base-case" assumptions for

Model Inputs	**Value**
Total Active Area	$1\,m^2$
ASR	$0.5\ \Omega \cdot cm^2$
Current density	0.1-1.5 $\frac{A}{cm^2}$
Operating P	1 bar
Recycle rate	0.668
System fuel utilization ($U_{f,sys}$)	0.85
Inlet fuel composition	100 CH_4
Inlet air comp	0.21 O_2, 0.79 N_2
Fuel inlet temp	298 K
Nominal cell operating temperature T_{op}	1023 K
ΔT_{cell} anode channel	100 K
ΔT_{cell} cathode channel	100 K
Model Outputs	**Value**
Fuel feed	mol/sec
Air feed	mol/sec
Inlet fuel T	973
Inlet Air T	973
Output anode T	1073
Output cathode T	1073
Anode outlet composition	CO: 0.035, CO_2: 0.298 H_2: 0.0896,H_2O: 0.577, CH_4: 0

Table 4.2: FC mode base-case assumptions and results

stack parameters and operating variables is constructed and presented in Table 4.2. This table presents all input parameters required for studying cell behavior and also reports the expected outputs. Unless specified otherwise, the values presented in Table 4.2 are held constant for each sensitivity analysis.

4.2.1 Base-case profile

The operating current density (i_{op}) of the stack is an important operating variable that is used throughout this work to control the power generated by the cell. Due to the fact that the stack is operating at fixed system fuel utilization, i_{op} can be controlled by adjusting the flow rate of the feed into the system. Fig. 4.1 shows the

power and operating voltage as a function of current density, and the stack's electrical efficiency as a function of current density. As Fig. 4.1 suggests, the power density has a parabolic shape with respect to the current and under the base-case assumptions it peaks at a power density of $0.48\,\mathrm{W/cm^2}$ at a current density of $1\,\mathrm{A/cm^2}$. As expected, there is an inverse relationship between current density and the stack's efficiency, such that the greatest efficiencies are attained at low currents. Due to this inverse relationship, the operating currents of the RSOC will always be to the left of the peak power density, as nothing is gained from operating at higher currents and an efficiency penalty is incurred. The stack's efficiency is defined as the gross DC power generated by the stack (neglecting BoP energy requirements) divided by the total energy of the gases entering the cell (based on the LHV):

$$\eta_{cell} = \frac{P_{gross}}{\sum \dot{n}_i \cdot LHV} \tag{4.2}$$

Under the assumptions laid out in Table 4.2, the stack's efficiency ranges from 12-48%, with a value of 25% at peak power. It is important to mention that low efficiencies at the cell level reflect two design choices: a fixed fuel utilization and relatively high anode gas recycle rates. As the volume of gas recycled into the cell increases, the energy content of the stream entering the cell goes up but the in-cell fuel utilization is kept constant, thus it lowers the per-pass conversion. At the system level, however, the use of an AGR stream increases the overall gross system efficiency as each H_2 molecule has more than one opportunity to be converted into electricity. The gross system efficiency can therefore be defined as:

$$\eta_{sys} = \frac{P_{gross}}{\dot{N}_{\mathrm{CH_4},in}} \tag{4.3}$$

where P_{gross} is the gross power generated by the stack and $\dot{N}_{\mathrm{CH_4}in}$ is the total molar flow of fuel into the system. Fig. 4.2 depicts the gross system's efficiency at different operating points. Increasing the current of the system implies an increase in heat generation inside the cell. Due to the fact that it is desired to operate at a constant

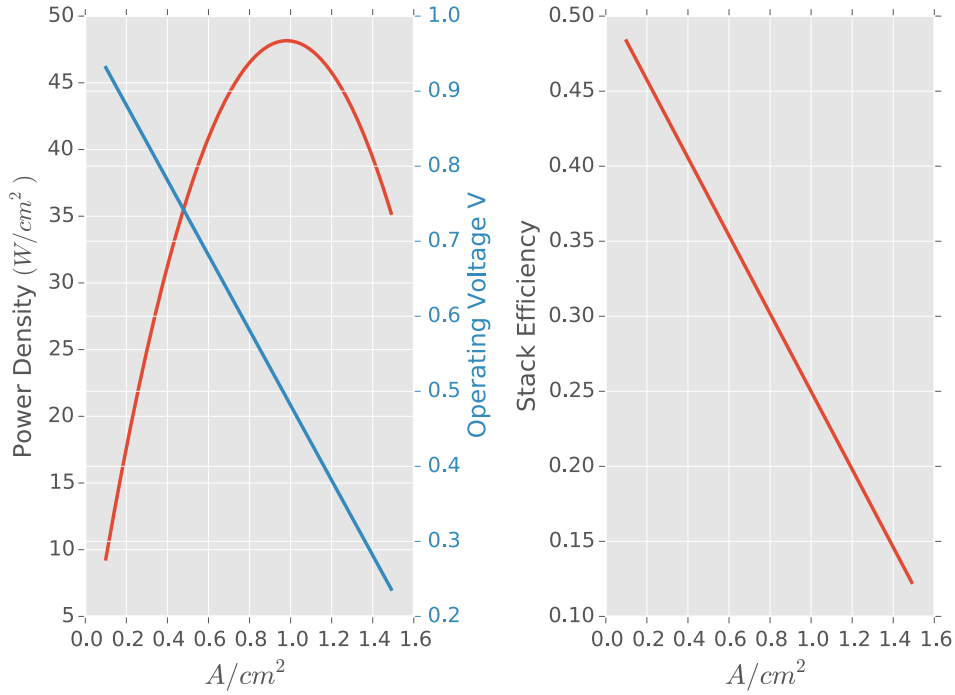

Figure 4.1: Fuel cell mode RSOC with internal CH_4 reforming. Figure (a): Power and voltage vs. current density; (b): stack efficiency

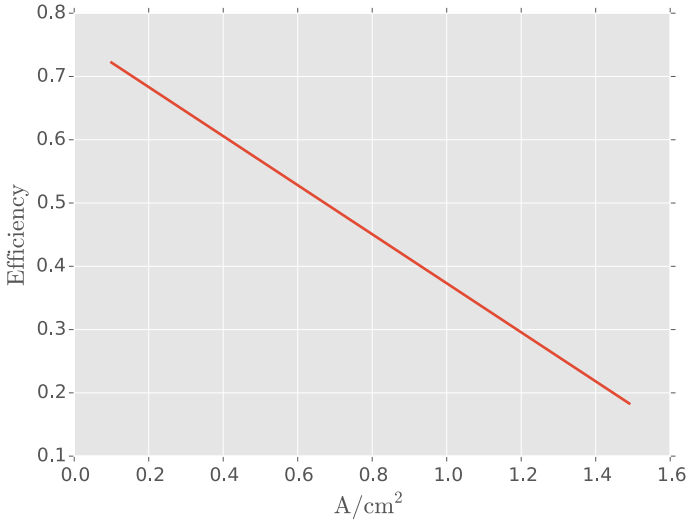

Figure 4.2: FC mode base-case scenario: Gross system efficiency.

average cell temperature and within the allowable thermal gradient across the gas channels (defined as ΔT_{cell}), the increase in heat generation is managed by increasing the amount of air flowing through the cathode such that the above constraints are met. Fig. 4.3 depicts the increase in heat generated by the stack as the current is increased,

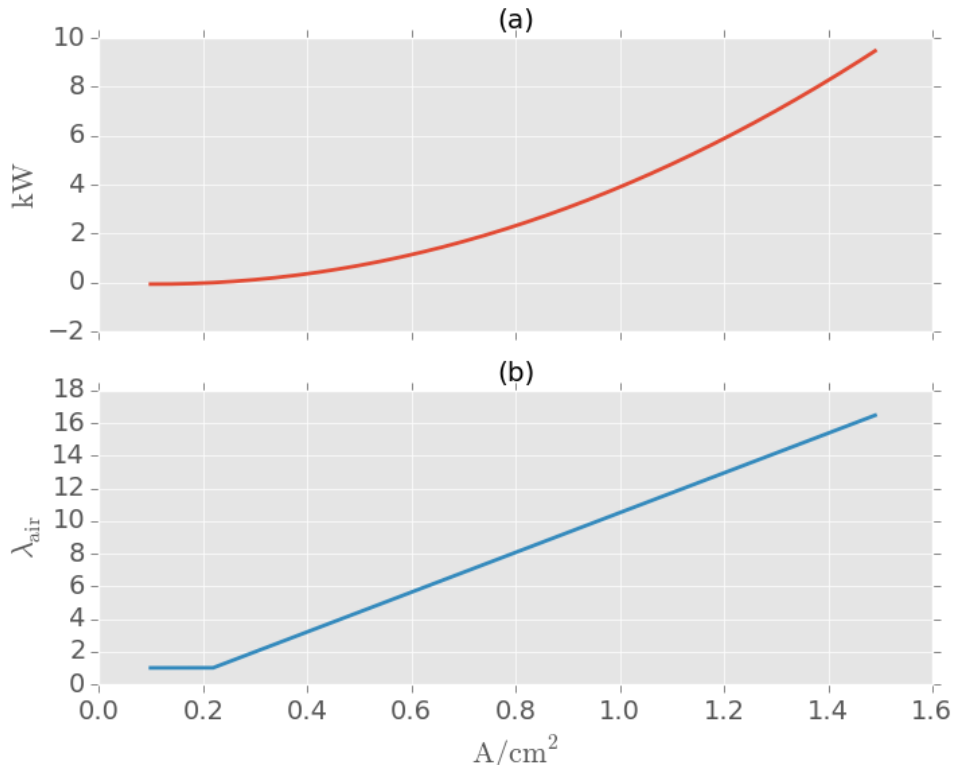

Figure 4.3: FC mode base-case scenario: (a): Heat generation; (b): Air ratios required

as well as the number of air ratios required (λ_{air}), which is the ratio of the total air flowing through the channel to the stoichiometric air required ($\lambda_{air} = \frac{Air}{Air_{stoich}}$). In Fig. 4.3(a) heat generation by the stack increases non-linearly with the current, with a range of roughly 0.01 kW to 9.8 kW. Similarly, the air ratios required (Fig. 4.3(b)) increase from $\sim 1\lambda_{air}$ at 0.1 A/cm^2 to roughly 16.2 λ_{air} at 1.5 A/cm^2. It is worth noting that at very low current densities, not enough heat is generated by the stack to maintain the highly endothermic steam reforming reactions while meeting the 100 degree temperature increase, thus there is no need for extra air to cool the stack.

The non-linear increase in heat production will have an important impact on the overall system efficiency, as the work required to move increasingly larger volumes of air through the cathode channel will result in an increase in parasitic loads. Although the oxidation potential of Ni usually limits the operating voltage of the fuel cell, the parasitic loads associated with the air blowers will put an upper limit to the current at which the cell can operate which will be somewhat lower than the theoretical Ni oxidation potential.

System impacts At the system level, the RSOC in fuel cell mode will be greatly affected by the parasitic power consumption of the BoP and all ancillary equipment associated with the conversion of DC into AC. These parasitics will lower the net power produced by the stack and will have a negative impact on the overall system's efficiency. Following the convention defined in (4.3) the net system efficiency is simply defined as:

$$\eta_{net,sys} = \frac{P_{net}}{\dot{N}_{\mathrm{CH_4},in} \cdot LHV} \tag{4.4}$$

Where the net power P_{net} is the power after all system parasitics have been taken into account:

$$P_{net} = P_{gross} - \sum P_{parasitics} \tag{4.5}$$

Where $\sum P_{parasitics}$ is the sum of all individual parasitic power consumption associated with the operation of the system (air blowers, fuel compressor, heaters and ancillary electrical equipment).

The main parasitics associated with the RSOC in fuel cell mode are the air blowers that are used to sweep extra air through the cathode channel in order to cool the cell. As shown in Fig. 4.3, the heat produced by the cell increases non-linearly with the current, causing the power consumption of the air blowers to increase non-linearly as the current is increased. This effect can be seen in Fig. 4.4, where we see that the power required by the blowers increases non-linearly with increasing

current. The sensitivity of the system to air blower power production can be seen in this figure. At high currents, the parasitics represent the majority of the power generated by the stack and operating at currents greater than $1.5\,\mathrm{A/cm^2}$ becomes impractical as the blowers consume more power than the one generated by the stack. Therefore, the net power produced by the system is, to a large extent, limited by the air that is used to maintain the stack's temperature increase within the allowed ΔT. After the air blowers, the inverter losses represent the second largest parasitic

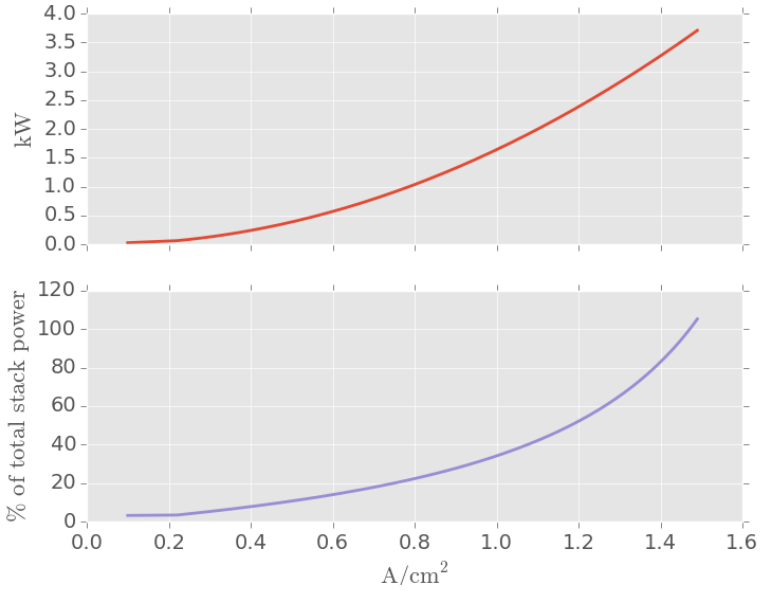

Figure 4.4: FC mode base-case scenario: Top: Power consumed by air blowers; Bottom: percentage of total stack power used by air blowers.

losses in the system as depicted in Fig. 4.5. In this figure we can see that the work associated with the fuel compressor is marginal, and that the air blower and inverter losses account for most of the system parasitics. It is also worth noting that at low current densities, the fraction of losses associated with the inverter is large relative to the air blower. This is mainly due to the fact that the inverter assumes fixed conversion losses of 8% while the air required for cooling at low currents is small. As the current is increased, the electricity required to operate the air blowers becomes

more substantial and dominates the system parasitic losses. As seen in Fig. 4.6, the

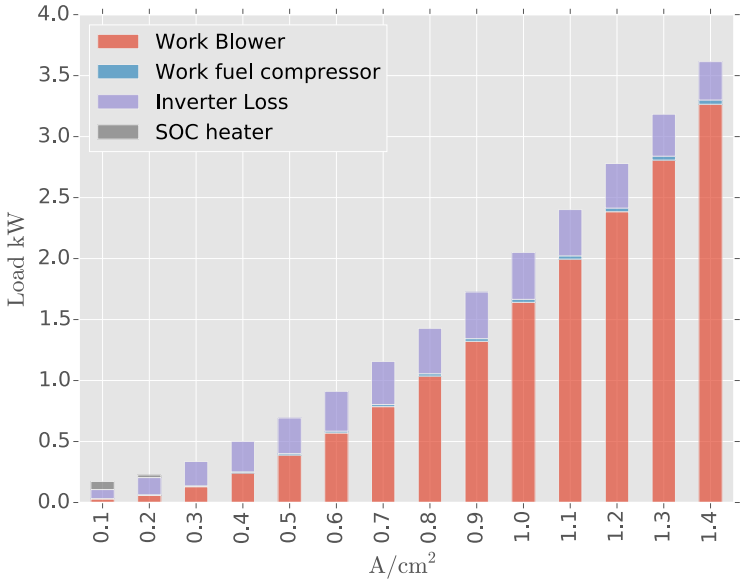

Figure 4.5: FC mode base-case scenario: parasitics power consumption.

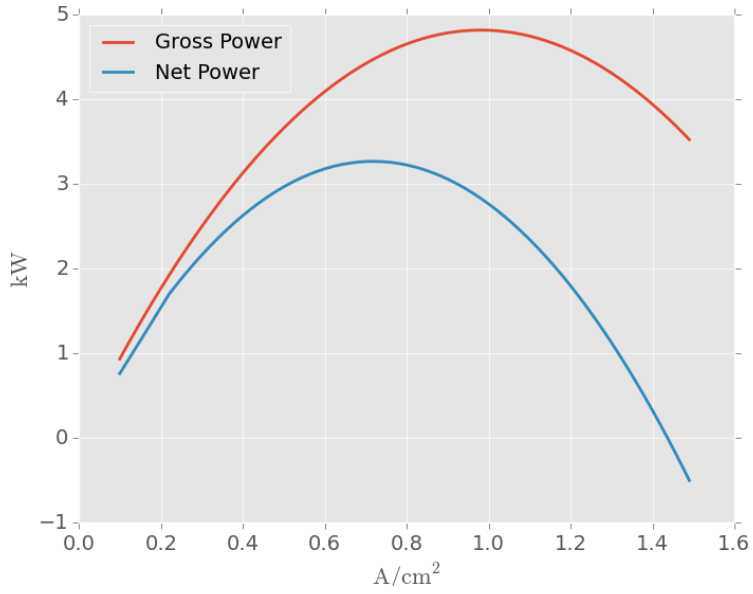

Figure 4.6: FC mode base case-scenario: Stack gross power (top); System Net Power (bottom)

net power produced by the system is substantially lowered once all the parasitics have been taken into account. The reduction in power is seen across all current densities and it becomes more pronounced at high operating currents. It is also worth noting that not only is the net peak power drastically reduced, but it is also shifted to lower operating currents. For example, the gross peak power occurs at a current of roughly $0.98\,\mathrm{A/cm^2}$, whereas it occurs at about $0.72\,\mathrm{A/cm^2}$ for the net system case. Although the total peak power is drastically reduced, the shifting to lower currents implies that at the system level peak power will occur at higher efficiencies. Fig. 4.7 depicts the net system efficiency vs. the stack efficiency across all operating currents. There are two things worth noting about this figure. The first is that there is a region of lower efficiency at very low current densities, which is the opposite of what is seen at the stack level where efficiency always decreases with increasing current. This is due to the fact that at very low currents, there is not enough heat produced by the stack to supply the highly endothermic steam reforming reaction while maintaining the pre-defined $100\,^{\circ}\mathrm{C}$ temperature rise across the anode and cathode channels. Therefore, when the current is very low heat has to be supplied to the stack in order to meet the temperature rise constraint while satisfying the stack's energy balance (see equation (3.22)). The other thing worth noting is that although the net system efficiency is higher for lower currents, its slope is more pronounced when compared to the stack, which implies that the efficiency drops rapidly as the current is increased. As suggested by Fig. 4.4, the system's net efficiency approaches zero at around $1.4\,\mathrm{A/cm^2}$.

4.2.1.1 Sensitivity to STCR

When operated in fuel cell mode, steam-to-carbon ratio (STCR) plays a key role in determining the power density of the cell, as well as the efficiency with which it operates. As discussed earlier, a STCR ratio of at least 2 is required in order to avoid

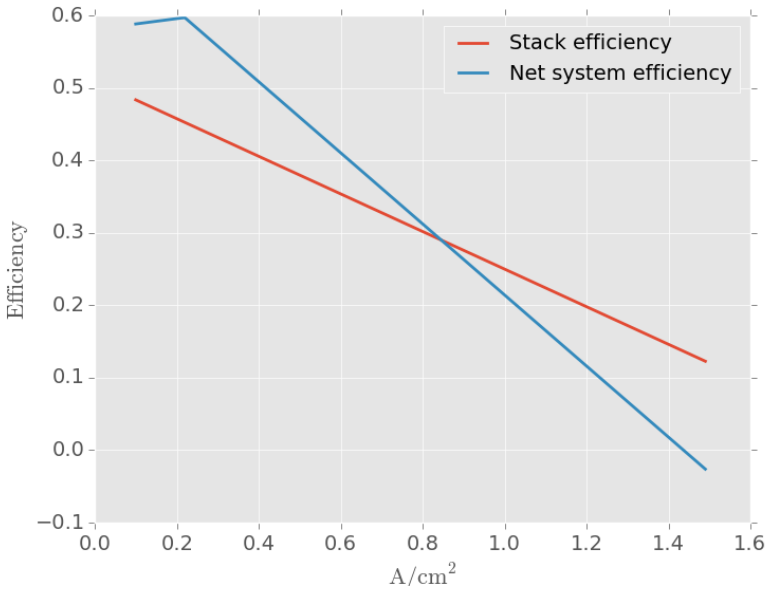

Figure 4.7: FC mode base- case scenario: Stack and Net System Efficiency.

carbon deposition on the surface of the electrodes. To illustrate the impact that STCR ratio has on the cell's behavior, we take the assumptions laid out in Table 4.2 and fix the operating current at $0.5\,\mathrm{A/cm^2}$ while varying the recycle rate such that the STCR ratio goes from 1 to 7. Fig. 4.8 and Fig. 4.9 show the impact that this has on OCV, power generation and stack efficiency. As the STCR ratio is increased, the cell's OCV drops due to the fact that steam dilutes the fuel at the entrance of the cell, leading to a decrease in partial pressures. As a consequence, the gross power generated by the stack at the chosen operating point decreases non-linearly with an increase in STCR ratio. The decrease in gross power as STCR is increased is seen across all operating points, which means that the higher the STCR ratio the lower the peak power that the stack will be able to achieve (see Fig. 4.10). The gross efficiency of the cell is also affected by an increase in STCR ratio. As can be seen from equation (4.2), the decrease in gross power production as well as the increase of available fuel at the stack's entrance will inevitably lower the cell efficiency, as

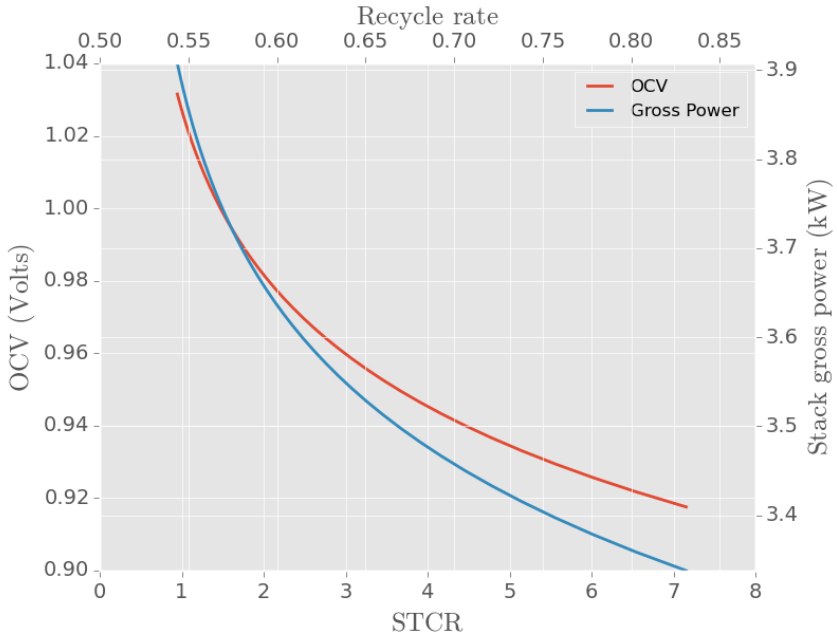

Figure 4.8: FC mode base-case scenario: OCV (left) and stack gross power (right) as a function of STCR.

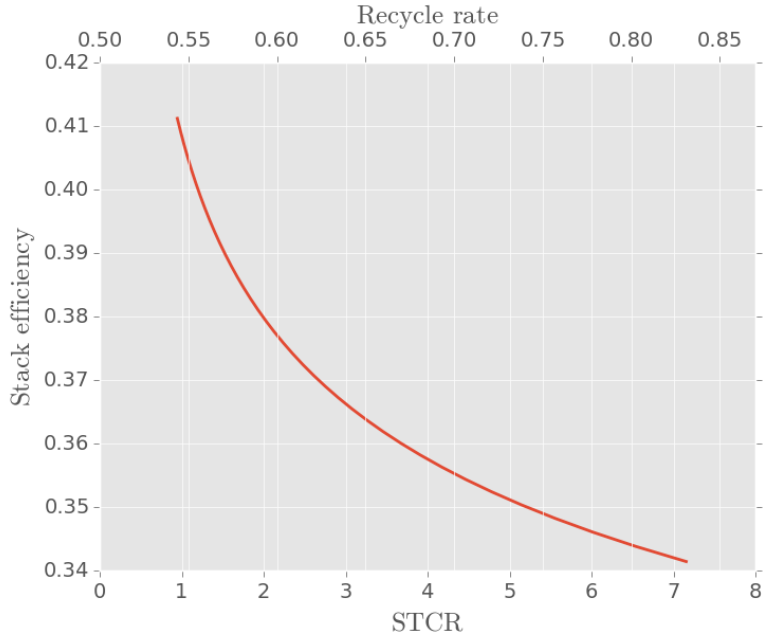

Figure 4.9: FC mode base-case scenario: Stack efficiency as a function of STCR.

the in-cell fuel utilization is kept constant as the STCR ratio is increased. It is important to mention, however, that when viewed from a system's perspective the

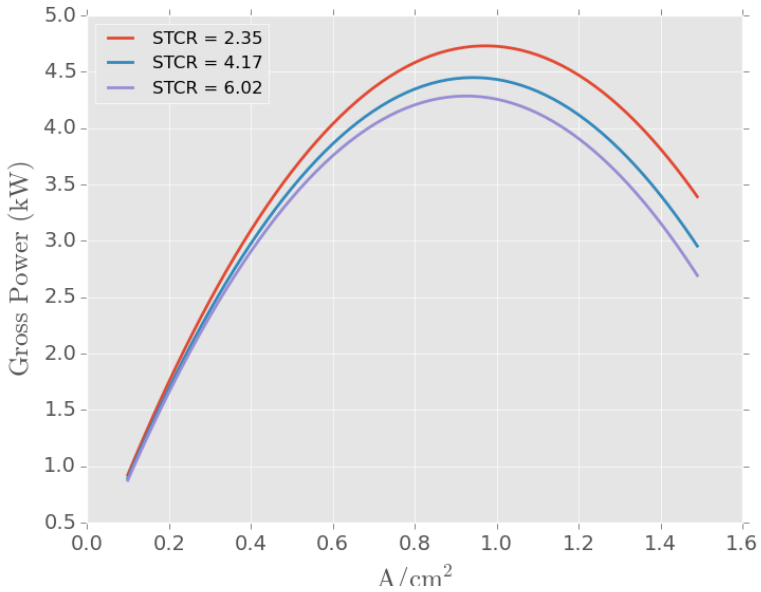

Figure 4.10: FC mode base-case scenario: Power at different operating points for different STCR ratios

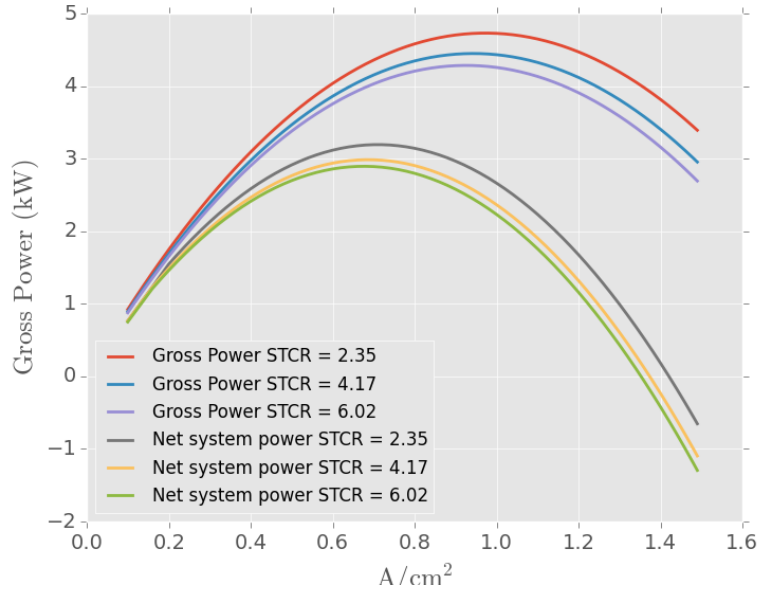

Figure 4.11: FC mode base-case scenario: Gross and Net System Power output at different operating points for different STCR ratios

increase in STCR ratio at fixed in-cell fuel utilizations ($U_{f,cell}$) leads to higher system fuel utilizations ($U_{f,sys}$), as more unreacted species are recycled back into the inlet of the cell. This, in turn, has a positive impact on the system efficiency, as the less input fuel is required to produce the same power. When analyzed from a net power perspective, however, Fig. 4.11 shows how increasing the STCR leads to lower powers for each operating point. This trend is accentuated at higher currents, where parasitic power consumptions plays a bigger role as explained in previous section.

4.2.1.2 Sensitivity to Fuel Utilization

As discussed in Section 4.1.2, fuel utilization is a critical parameter of the RSOC system and thus it is important to investigate how it impacts that stack and system performance. To do this, we use the assumptions for the base-case laid-out in Table 4.2 and vary the in-cell fuel utilization to values that are above and below the base-case assumption. Fig. 4.12 depicts the impact of fuel utilization on the stack's operating voltage and power generation. As seen in Fig. 4.12, operating the SOC

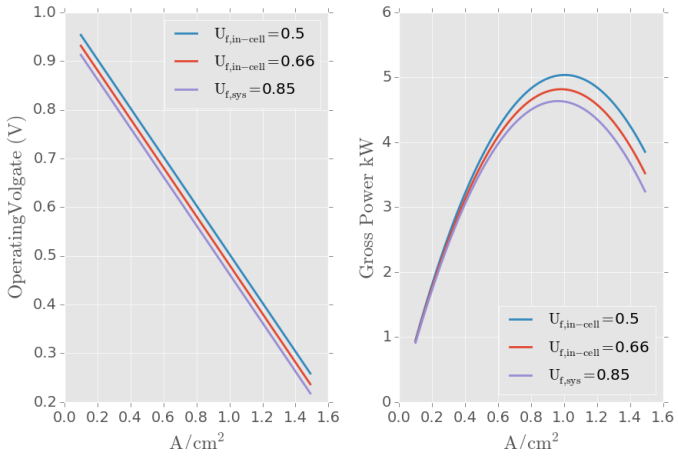

Figure 4.12: FC mode base-case scenario: Cell voltage and power for different in-cell fuel utilizations

with higher in-cell fuel utilization leads to lower operating voltages. As the $U_{f,in-cell}$

increases, more of the H_2 produced during the internal reforming is consumed by the SOC which in turn leads to a drop in EMF. Lower voltages, in turn, result in lower gross power densities for all currents. For the cases highlighted in Fig. 4.12, the difference in peak power arising from a decrease in U_f from 0.85 to 0.5 is roughly about 0.5 kW. Although these results would suggest that running at lower fuel utilizations is a better strategy, this results in low stack and system efficiencies, as less of the available fuel is converted into electricity (see Fig. 4.9). Put another way, if the system is operated with low $U_{f,in-cell}$, more methane is required to deliver a given amount of power, which negatively affects the economics of the system. Increasing the fuel utilization causes an increase in the heat generation of the stack, which requires additional air to flow through the cathode channel. As a consequence, the air blower parasitics increase, having an important impact on the overall system efficiency.

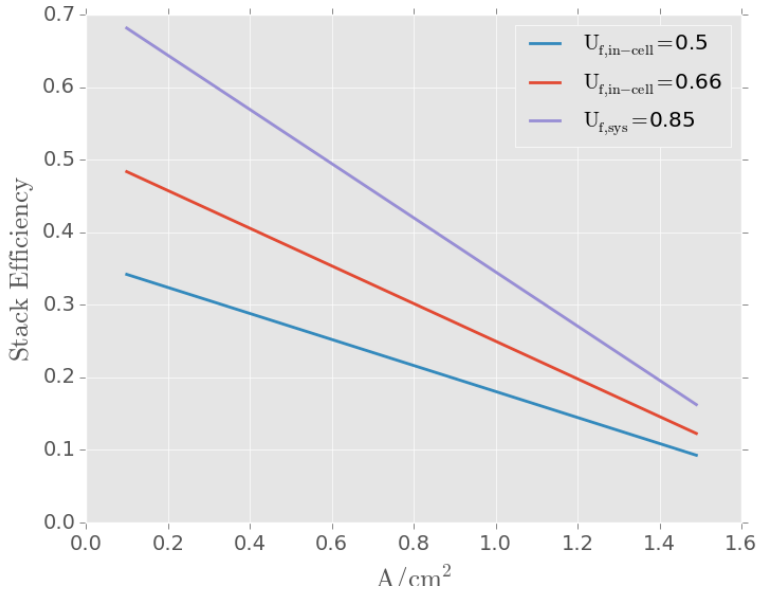

Figure 4.13: FC mode base-case scenario: stack efficiency for different in-cell fuel utilization rates.

4.2.2 Sensitivity to ASR

Lastly, the sensitivity of the stack's efficiency and power output to changes in Area Specific Resistance (ASR) is studied. As seen in equation (3.1), increases in ASR negatively affect the RSOC by lowering the voltage in FC mode (increasing it in EL mode) and thus converting more of fuel or electricity into resistive heating. For the purpose of the modeling presented in this thesis, the current-voltage relationship is assumed to be linear, and thus the ASR can be thought of as the slope in the i-V curve. Using the assumptions laid out Table 4.2, the stack's ASR was varied from 0.2-0.4 $\Omega \cdot cm^2$ and the stack's efficiency and gross power was evaluated across all currents. Fig. 4.14 shows the changes in the stack's gross power production as for the different ASR's. As expected, as the stack's ASR increases the gross power delivered by the stack decreases, with the trend becoming more pronounced at higher currents. This trend can be quite dramatic at high operating currents. For example,a change from $0.2\,\Omega\text{cm}^2$ to $0.4\,\Omega\text{cm}^2$ lowers the power produced by the stack at $1.0\,\text{A/cm}^2$ from 7.8 kW to 5.8 kW. This difference in gross power production is not only manifested in absolute terms, but also with respect to the current at which peak power occurs for each case. Fig. 4.14 clearly shows this trend, where the peak power shifts to lower currents as the ASR is increased. The increase in ASR will have an impact on the stack's efficiency as well as on the overall system efficiency. As seen in Fig. 4.15, as ASR is increased two important things happen: first, efficiency is lowered across all operating currents; and second the rate at which efficiency drops (e.g. the slope of the efficiency curve as a function of current density) is more pronounced for higher values of ASR. It is easy to see why it is desired to have RSOC with low resistances, as this can have an important impact on the system's overall profitability by increasing the amount of fuel/power generated per area of cell across all operating points. Due to the fact that the system modeled in this work relies on internal reforming to produce H_2 in fuel cell mode, some of the resistive heating that is generated by the stack is used

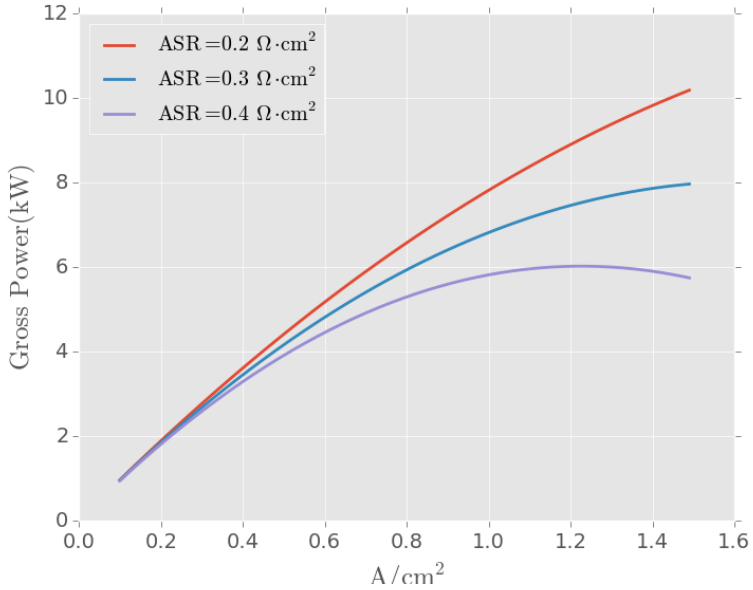

Figure 4.14: FC mode base-case scenario: gross power for different ASR values.

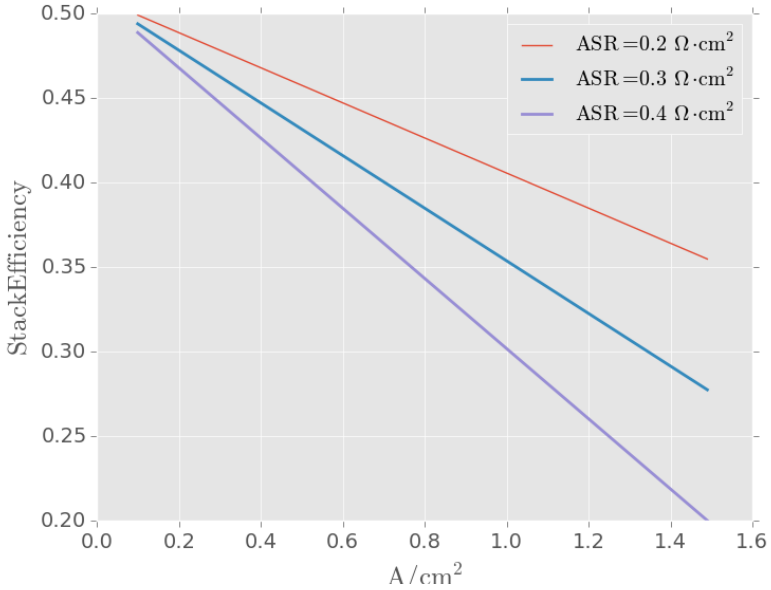

Figure 4.15: FC mode base-case scenario: stack efficiency for different ASR values.

to provide the necessary energy for the highly endothermic steam reforming reaction. This is an important element to consider, as it might mean that when operated at

very low currents, the stack might not be able to produce enough heat for the internal reforming reaction while maintaining the pre-defined temperature increase (ΔT_{cell}) across the cathode and anode channels. As a consequence, the system would require external heating for these cases which would lower the net system efficiency (which include parasitics) at low operating currents, which is the opposite behavior that occurs at the stack level, where efficiency always increases with decreasing current.

4.3 Electrolysis mode sensitivities

When operated in electrolysis mode, the system presented in Section 3.2 takes an electrical input and converts chemicals (CO_2 and H_2O) into CH_4. As in the case of fuel cell mode, it is important to understand the sensitivities that the system has to different stack-parameters and operating variables. To do this, a set of "base-case" assumptions for the parameters and operating variables in electrolysis mode is presented below. Unless otherwise stated, the sensitivity analysis is based on these values.

4.3.1 Base-case profile

As in the case of fuel cell mode, the operating current density is used as the main dial to control the output of the system. The main purpose of the electrolysis mode is to generate methane by reacting H_2 and CO_2. Although solid oxide cells are perfectly capable of doing co-electrolysis of H_2O and CO_2 to form H_2 and CO [31, 53, 59],in the base-case design defined in Section 3.2 the RSOC is only fed steam which is separated into H_2 and O_2. In that regard, the modeling of the stack is much simpler in electrolysis mode as there are no equilibrium reactions and the only conversion occurring is the electrochemical reduction of H_2O. Because the main goal of the electrolysis mode is to produce CH_4, it is useful to think of process as having to main elements: the electrochemical reduction of H_2O in the SOC, and the

Model Inputs	**Value**
Total Active Area	$1\,m^2$
ASR	$0.5\ \Omega cm^2$
current density	0.1 to 1.5 A/cm^2
Operating Pressure	1 bar
Anode Gas Recycle rate	0.10
System Steam Conversion	0.90
Inlet Fuel (steam) Composition	100% H_2O
Inlet Air Composition	79%N_2, 21%O_2
Nominal Cell Operating Temperature	1073 K
ΔT_{cell} anode channel	100 K
ΔT_{cell} cathode channel	100 K
Model Outputs	**Value**
H_2O feed rate	$0\,mol\,s^{-1}$ to $0.0855\,mol\,s^{-1}$
Air feed rate	mol/sec
Thermoneutral voltage	1.31 V
Inlet fuel Temperature	973 K
Stack electric load	5.7 kW to 19.6 kW
Stack voltage	1.14 V to 1.51 V
Parasitic electric load	kW
Stack efficiency	1.26 to 0.79
Net system efficiency	0.44 to 0.68
Methane generated	$0.007\,mol\,s^{-1}$ to $0.022\,mol\,s^{-1}$

Table 4.3: Electrolysis input and output summary

catalytic hydrogenation of CO_2 into CH_4 in the catalytic heat exchanger. As such, the sensitivity analysis will be divided into two categories: the impact of operating variables on the SOC and the impact on the catalytic hydrogenation reaction. This is somewhat different from the fuel cell mode, where the main operation (generation of electric power) happened within the solid oxide cell. Fig. 4.16 shows the relationship between current density, total stack electricity consumption (load) and the stack's voltage. The first thing to notice is that the power to current relationship is not does not feature a parabolic shape as it does in the fuel cell case. In the electrolysis case, increasing the operating current always requires an increase in power consumption, which is a direct consequence of the fact that when the polarity is reversed the

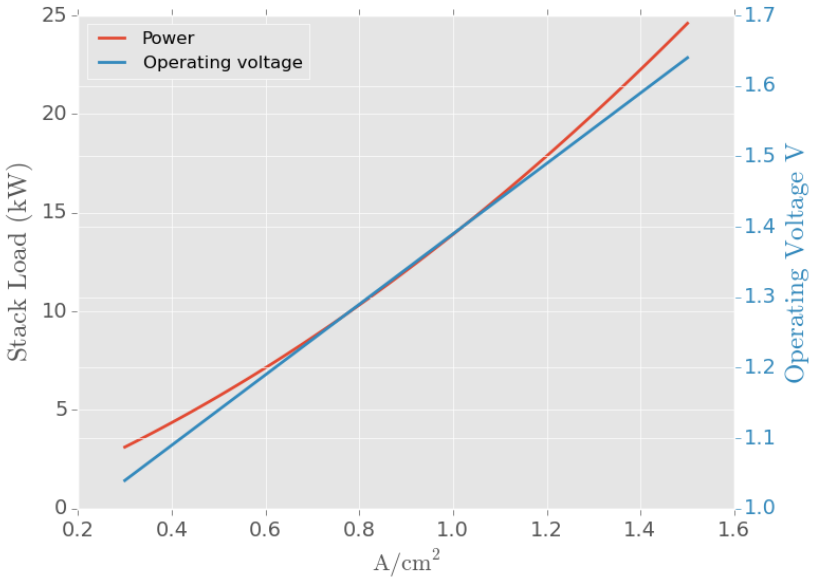

Figure 4.16: Electrolysis: stack load and voltage

voltage of the cell is always increasing (see equations (3.1) and (3.24)) thus the power required by the stack (which is simply $P = U \cdot i_{op}$) increases with increasing voltage cell. Another important feature of electrolysis mode worth highlighting is that the production of H_2 is linear with the current (see Fig. 4.17)and is not affected by the thermodynamic state of the stack, as it is defined by Faraday's law which depends on the operating current. Because the solid oxide cell is only splitting steam into hydrogen and oxygen, the efficiency of the stack will be equal to the ratio of the energy content in the hydrogen produced to the electricity input to the cell. Conventionally, this is usually written as :

$$\eta_{stack,EL} = \frac{\xi_{EL} \cdot LHV}{P_{stack}} \tag{4.6}$$

where ξ_{EL} is the molar extent of reaction of the electorchemical reduction of H_2O (reaction R3.16), $\xi_{EL} \cdot LHV$ is the energy content of the hydrogen generated by the stack [1] (based on the LHV of H_2), and P_{stack} is the total power load of the stack.

[1] ξ_{EL} is easily computed using equation (3.26)

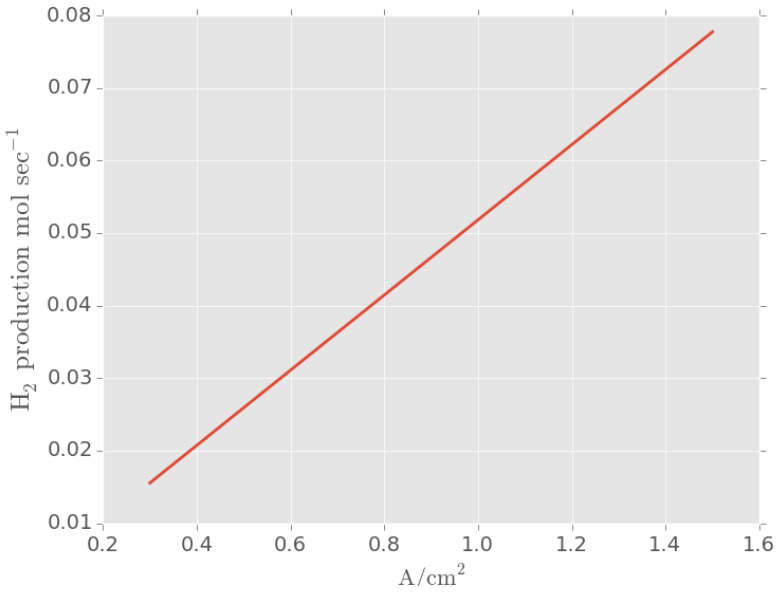

Figure 4.17: Electrolysis: H_2 generation

For the system presented in this dissertation, however, it is assumed that there is a fixed temperature change of 100 °C between the inlet and the outlet of the stack and therefore the enthalpy change associated with this temperature change must be considered. The efficiency of the stack then becomes[2]:

$$\eta_{stack,EL} = \frac{\sum \dot{N}_f^j \cdot h_f^j(T_{out}) - \sum \dot{N}_o^j \cdot h_o^j(T_{in}) + \xi_{EL} \cdot LHV}{P_{stack}} \tag{4.7}$$

Fig Fig. 4.18 shows the efficiency of the stack as a function of operating current density. It is worth noting that in Fig. 4.18 there are operating currents for which the efficiency $> 100\%$. As discussed in Section 2.1.3, in electrolysis mode it is possible to operate below the thermoneutral point which would lead to an endothermic operation. In this case, the efficiencies are $> 100\%$ because the definition in equation (4.6) does not take into account the heat that would have to be supplied in order to make up for the drop in stack temperature as a result of endothermic operation. If one

[2]In many cases, the efficiency of the stack is written as $\frac{U_{th}}{U_{op}}$. If one uses equation (3.1) and (3.24) and assumes ξ_{SRM} and $\xi_{WGS} = 0$ for electrolysis mode, then $\frac{U_{th}}{U_{op}} = \eta_{stack,EL}$

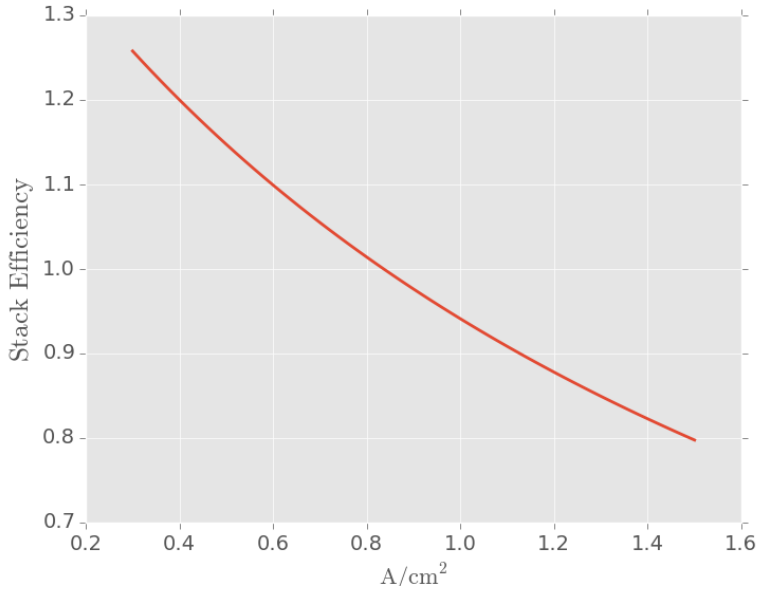

Figure 4.18: Electrolysis: stack efficiency

were to include this heating load, the stack efficiency would be below 100% for all values except for the current that corresponds to the thermoneutral voltage, where no external heating would be required and the efficiency would be equal to 100%.

Fig. 4.19 shows the heat generated or consumed by the stack as a function of operating current. In this figure, positive values represent heat consumption by the stack (e.g. endothermic mode) while negative values represent heat production by the stack (exothermic mode). As it can be seen, the curve exhibits a non-linear shape and therefore balancing the energy will have important impacts on the overall efficiency of the system, as it will increase the parasitic power consumption associated with each mode of operation. The parasitics in the exothermic case are much higher, as the power consumption of air blowers is a power law with respect to air volume (see section below for discussion on parasitics and system level efficiencies).

After H_2 is produced in the SOC, it needs to be reacted with CO_2 in order to make CH_4. As discussed in Section 3.4.6, the synthesis of methane occurs via the catalytic

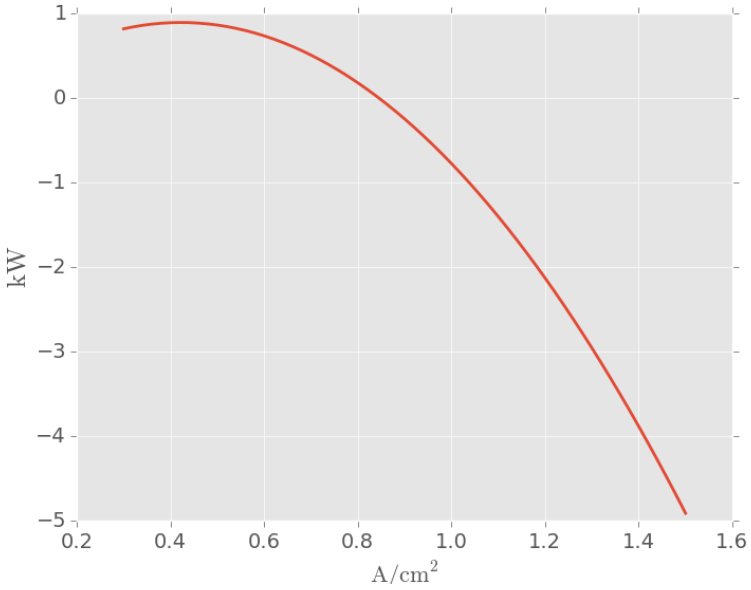

Figure 4.19: Electrolysis: stack heat requirements

hydrogenation of CO_2 on the surface of a heat exchanger coated with an active RU catalyst. Reaction R3.20 requires a 4 to 1 H_2:CO_2 ratio and since the reaction is highly exothermic, low temperatures are prefered. Thus, the exiting temperature and composition of the RSOC will have an important impact on the overall yield of CH_4. Fig. 4.20 shows the sensitivity of the catalytic hydrogenation to changes in reaction temperature for a stoichiometric reaction. As this figure shows, as the temperature increases, the equilibrium shifts to the left in reaction R3.20, favoring the steam reforming of methane thereby reducing the mole fraction of CH_4. On a conversion basis, Fig. 4.21 suggests that an increase in reactor temperature of 150 °C (from 250 to 400 °C) leads to a decrease in the per-pass yield of methane from 97% to 85%. Thus, heat management is crucial for maintaining high yields. From an energy perspective, the synthesis of CH_4 from H_2 and CO_2 implies a minimum energy penalty of 17%, as the ΔH_{rxn} for reaction R3.20 is -165 kJ mol^{-1}. Therefore, heat integration is an important feature of the system in order to achieve high overall yields.

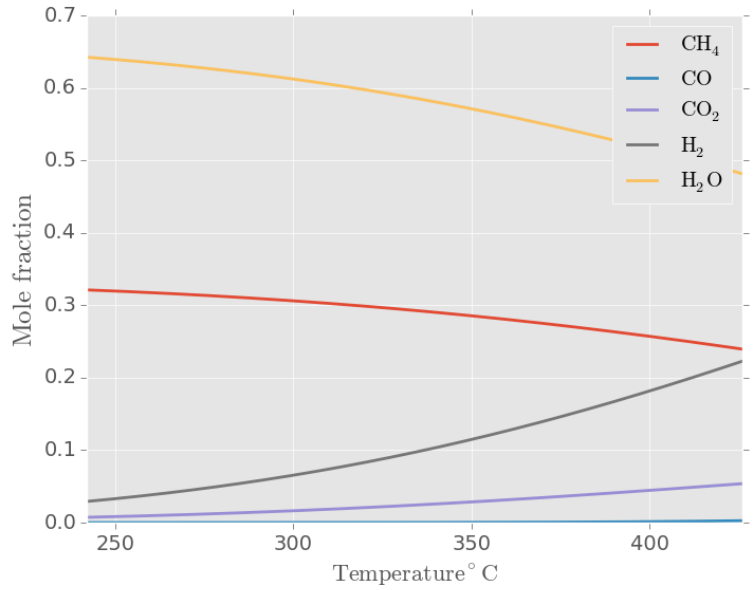

Figure 4.20: Methanator sensitivity to reaction temperature

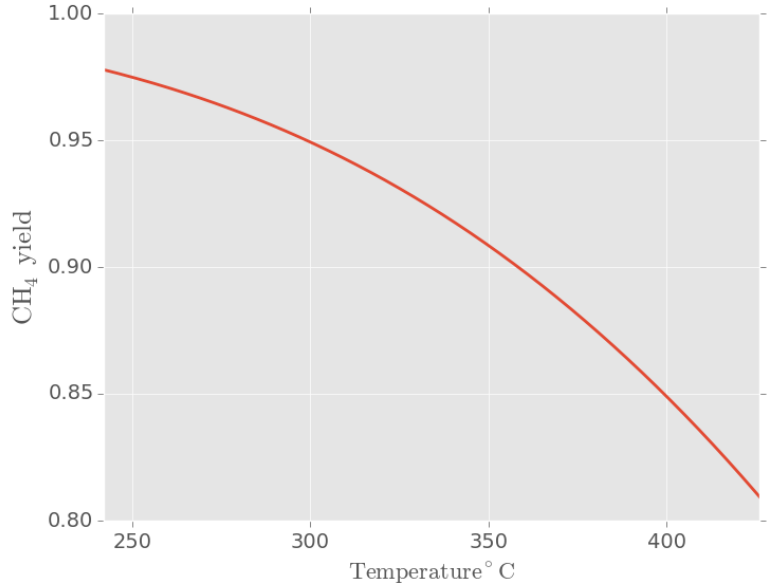

Figure 4.21: CH_4 yield as a function of reaction temperature

System Impacts When operating in electrolysis mode, the RSOC system involves several steps of heating, cooling, electrochemical conversion, and compression. For

this reason, it is important to understand how each unit operation contributes to the overall system efficiency. There are four main categories of energy loss and parasitic power consumption within the system:

(1) Evaporation of water into steam.

(2) CO_2, H_2 and H_2O conditioning before entering the SOC and/or the methanator.

(3) RSOC electric load and heating/cooling requirements.

(4) Turbomachinery work (blowers and pumps).

Thus, the net system efficiency can be written as:

$$\eta_{sys,net} = \frac{\dot{N}_{\mathrm{CH_4}} \cdot LHV}{P_{stack} + Q_{heaters} + Q_{evap} + W_{blower} + W_{comp}} \tag{4.8}$$

where $Q_{heaters}$ is the sum of all electric loads associated with the electric heaters (refer to Fig. 3.3 to see the complete list of heaters), Q_{evap} is the evaporator load, W_{blower} is the sum of the work of all blowers and fans, and W_{comp} is the work required by the methane compressor. As mentioned in Section 3.2.1.2, the model assumes that heat is integrated throughout the process in order to increase the overall efficiency. The main sources of heat are the exothermic methanation reaction and the exhaust of the RSOC which needs to be cooled before entering the methanator. Heat from the methanation reaction is used in the water evaporator, and the high temperature heat from the exhaust of the stack is used to pre-heat the inlet feeds and if necessary and available, can also be used in the evaporator. The net system efficiency for the base-case as a function of operating current density is shown in Fig. 4.22. As this figure shows, between 0.5 and $\sim 0.84\,\mathrm{A/cm^2}$, the overall efficiency shows an upward trend, reaching a maximum efficiency of 0.68 and then dropping to roughly 0.44 at the limit of $1.5\,\mathrm{A/cm^2}$. The shape of the overall efficiency curve can be explained by analyzing the heating requirements and system parasitics. When operating below the thermoneutral voltage, heat needs to be added to the stack in order to maintain

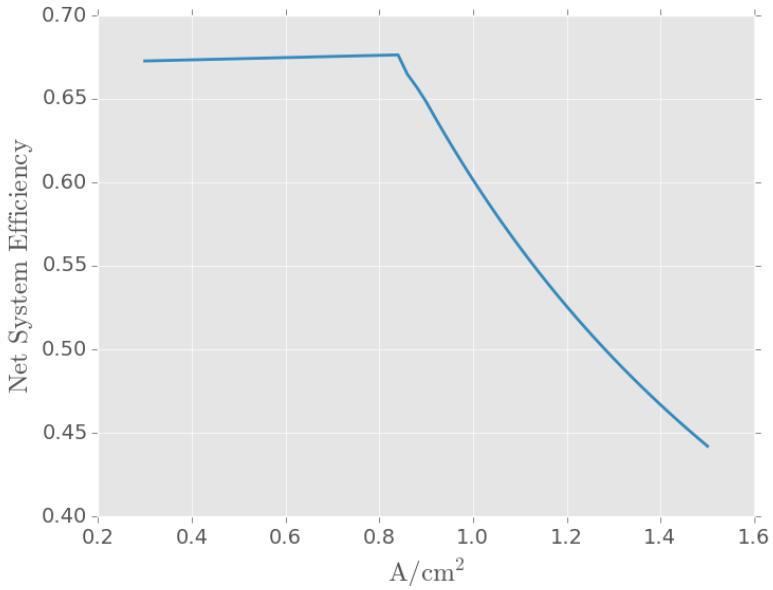

Figure 4.22: Electrolysis: Net system efficiency based on LHV

the desired constant operating temperature. This helps explain why the system efficiency curve increases as currents increase from 0.5 to 0.84 A/cm^2 (corresponding to endothermic operation). Fig. 4.23 shows a break-down of the system parasitics at different operating currents. As this figures shows, below the thermoneutral point, the largest contributor to system parasitics are heating loads. The total heating load is composed of different operations (e.g evaporation, CO_2 heating, etc.) that require different amounts of energy depending on the operating current. As Fig. 4.24 shows, below the thermoneutral point the main contributor to heating parasitics is the heating of the RSOC stack. As the current increases and the operation switches from endothermic to exothermic, both the RSOC heating and evaporator loads disappear and the total heating load consists of the heat required to pre-heat the CO_2 to the inlet temperature catalytic heat-exchanger conditions, the extra heat required to get the feed steam to the desired stack inlet temperature (Feed Extra Heater Load in Fig. 4.24), and the heat required to get the temperature of H_2 and H_2O to the inlet

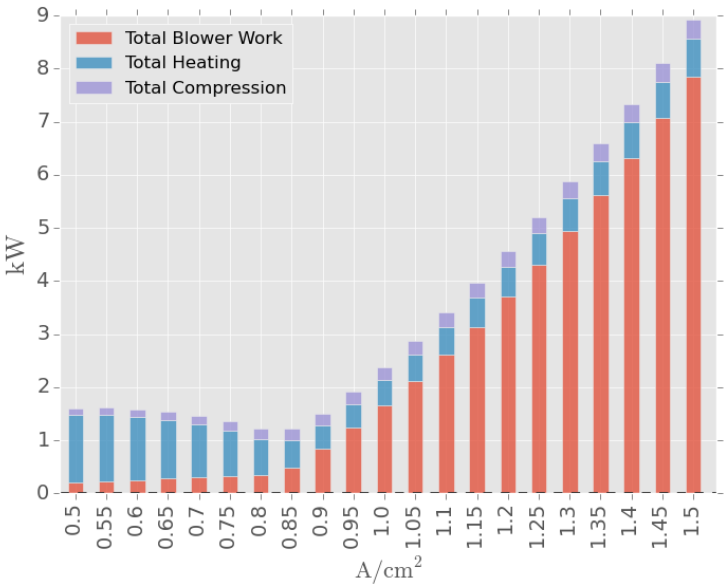

Figure 4.23: Electrolysis mode parasitics

temperature of the catalytic heat-exchanger (Methanation conditioning in Fig. 4.24). From the system diagram in Fig. 3.3, one would expect the outgoing gases from the cell to be able to provide all of the energy to pre-heat the steam coming in. However, this is not the case due to the fact that the temperature difference between inlet and outlet is only 100 °C and there is roughly a 500 °C temperature increase required. In the case of fuel cell operation, the exiting gases were able to pre-heat the inlet feed because the hot air from the cathode was mixed with the hot stream from the anode before entering the combustor, so even though the temperature difference across the cell was only 100 °C the flow rates in fuel cell mode are much higher than the ones seen in electrolysis mode, increasing the amount of energy available to transfer.

When the current of the stack increases and switches operating from endothermic to exothermic, the main driver of parasitic losses becomes the work associated with the air blowers, as Fig. 4.24 suggests. As the stack becomes more exothermic, the heat produced by the stack increases non-linearly thus increasingly larger volumes

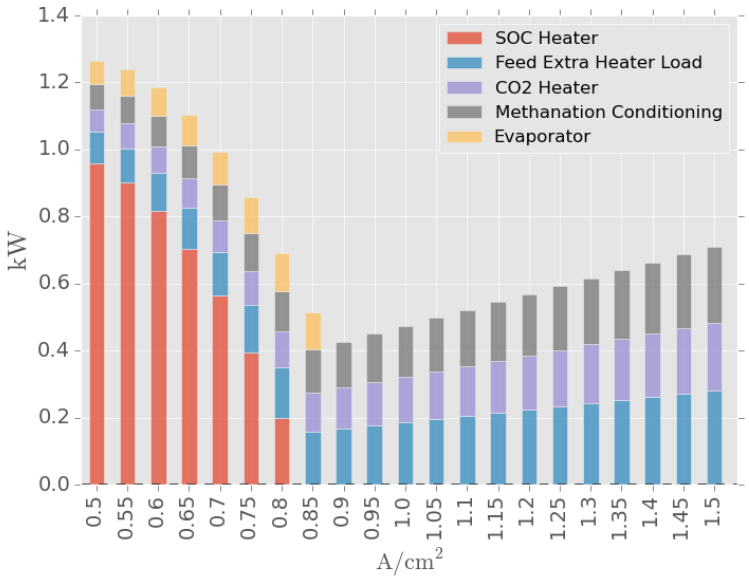

Figure 4.24: Electrolysis heating requirements breakdown

of air must be pushed through the oxygen electrode channel in order to keep the temperature across the stack within the allowable parameters. When analyzing the system efficiency, it is very important to remember that electrolysis of water is a thermondynamically unfavorable process that requires a substantial amount of work. Even at the high operating temperatures of the ROSC, the free energy involved in splitting steam into hydrogen and oxygen is roughly $190\,\mathrm{kJ\,mol^{-1}}$, which suggests that the dominating energy input into the system will be the electricity required by the stack. Indeed this is the case, as suggested by Fig. 4.25. In this figure, it can be seen that the total parasitics of the system never exceed 28% of the total power required by the system for the given range of currents. Thus, operating profitably in electrolysis mode will largely be driven by the cost of electricity. Chapter 5 provides an in-depth discussion of the influence of market prices on the mode of operation for the RSOC system.

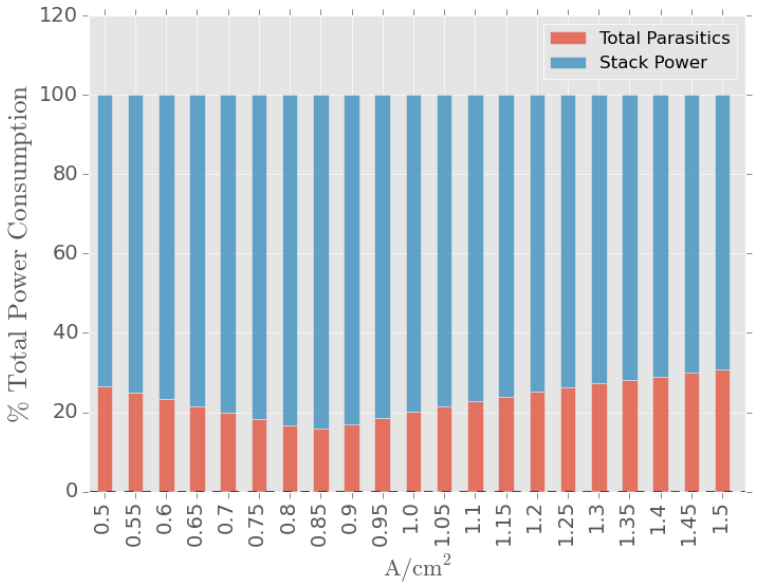

Figure 4.25: Electrolysis mode: parasitics vs. stack electricity load

4.3.2 Sensitivity to ASR

As in the case of fuel cell mode, it is important to understand the impact that variations in ASR will have on the efficiency of the stack and the system as a whole. The first thing to note is that hydrogen production increases linearly with the current and is not impacted by the thermodynamics of the stack (see equation (3.26)). Because of this and due to the fact that the exiting temperature of the stack is fixed, CH_4 production is not affected by changes in ASR. As such, variations in ASR impact the system by changing the voltage at which the stack is operating for a given current, as highlighted in Fig. 4.26. As the ASR is lowered, the operating voltage of the stack decreases impacting the stack's efficiency. Given that the thermoneutral voltage is fixed at 1.31 V, a lowering of the operating voltage results in a wider range of currents for which the stack is in endothermic mode. Furthermore, at low ASR's less of the input energy is lost as ohmic resistance which translates into a decrease in the power required to produce a specific amount of H_2. This is an important point, as

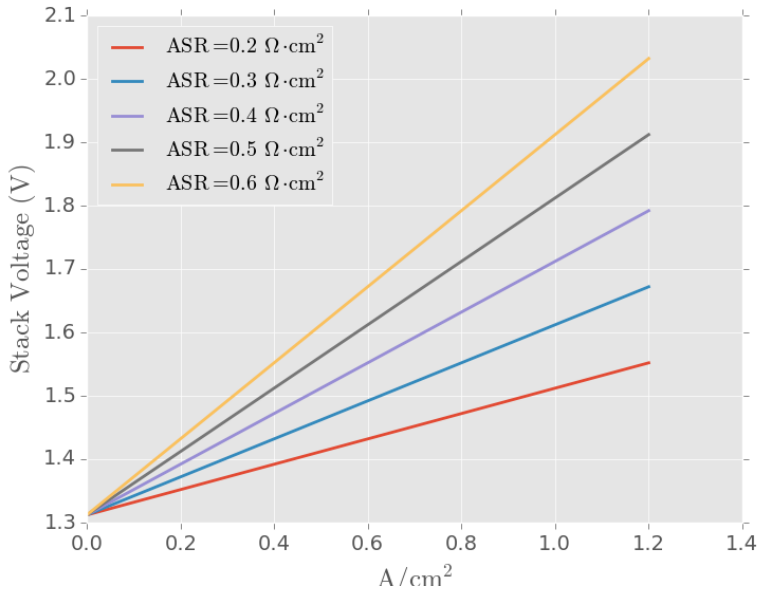

Figure 4.26: Electrolysis mode: voltage current relationship for different ASR's

it means that when viewed from the stack's perspective low ASR's result not only in higher efficiencies but also in lower rates of change in the efficiency as the current is increased as suggested by Fig. 4.27. In Fig. 4.27 one can easily appreciate that as ASR increases, the boundary between endothermic and exothermic operation (seen as a jump in the efficiency curve) moves to the left, suggesting that at high ASR's the stack will operate exothermically requiring active cooling and thus increasing the BoP parasitics. Fig. 4.28 shows the impact that variations in ASR has on the system as a whole. Increasing the ASR results in lowering the current at which the transition between endothermic and exothermic mode occurs, as well as a sharper and faster drop in overall efficiency at higher operating currents. As Fig. 4.28 suggests, at an current density of $1.1\,\mathrm{A/cm^2}$ and an ASR of $0.4\,\Omega\mathrm{cm^2}$, the system efficiency is around 68%, whereas a stack with an ASR of $0.6\,\Omega\mathrm{cm^2}$ operating with the same current exhibits an overall efficiency of $\sim 50\%$. The quick loss of overall efficiency is due to the fact that at higher ASR's the system requires more heat removal which

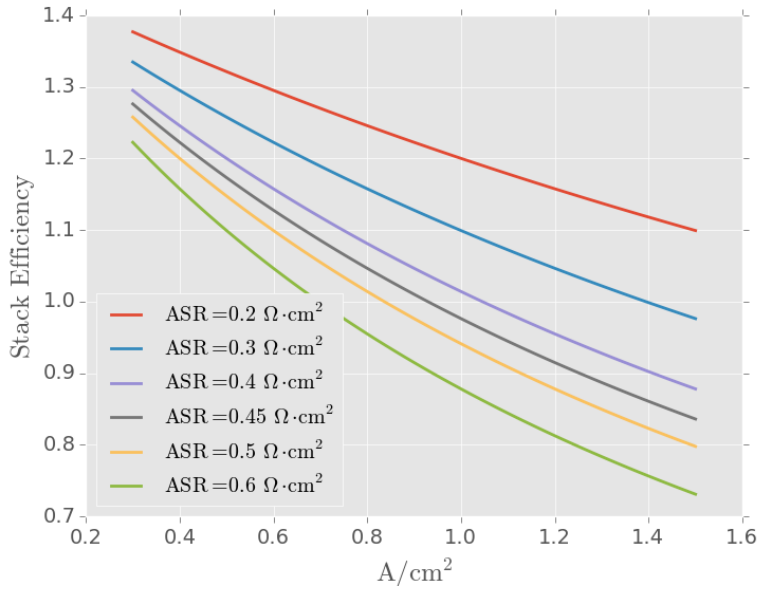

Figure 4.27: Electrolysis mode: stack efficiency at different ASR values.

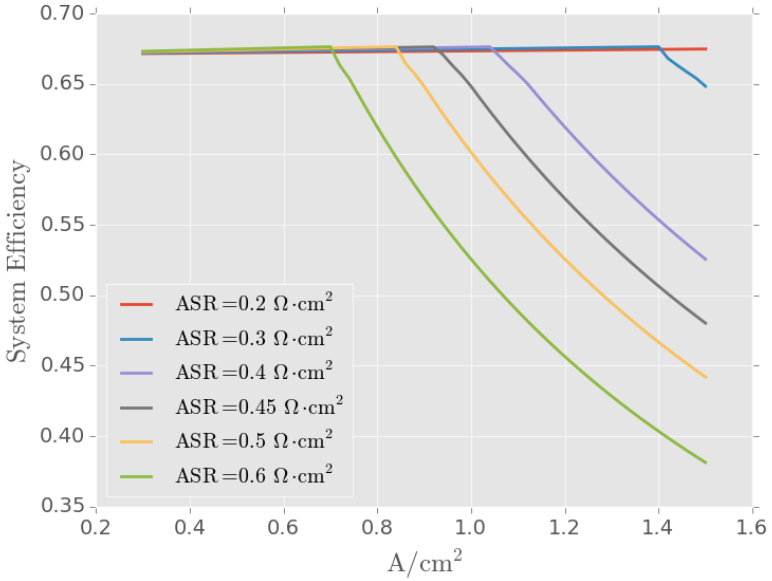

Figure 4.28: Electrolysis mode: system efficiency at different ASR values.

increases the parasitic power consumption of the air blowers. This will have a very important impact on the optimal operating strategy, as the degradation of the stack

is modeled as an increase in the system's ASR. As discussed in Chapter 5, increases in the stack's ASR as a result of degradation leads to a lowering of the capacity factor of the system, as larger spreads between electricity and fuel prices are required to operating when the system quickly looses efficiency. Fig. 4.29 depicts the changes in

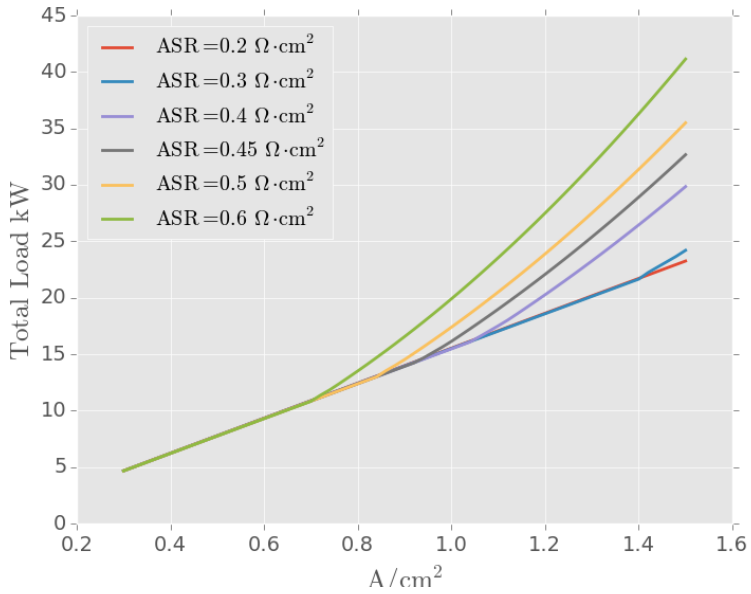

Figure 4.29: Electrolysis mode: Total system load for different ASR values.

total system load (e.g. electricity for stack + BoP) as a function of current density for a range of ASR values. As the ASR is increased, the total load rapidly increases once the system enters the exothermic operating regime.

4.4 Part-load operation

In the previous sections, the behavior of the RSOC system at different operating points and its sensitivity to operating parameters was presented. In this section, the impact of part-load operation on system efficiency and BoP over-sizing is discussed. The details and assumptions behind the modeling of part-load operation are described in Section 3.5.

4.4.1 Net system efficiency

Fig. 4.30 shows the net system efficiency at part-load operation in fuel cell mode using the assumptions in Table 4.2. The design point is chosen at $0.6\,\mathrm{A/cm^2}$ which corresponds to a net peak power output of 3.4 kW. Consistent with other findings in the literature [3, 87], the net efficiency of the system increases at part load operation. This is due to two main reasons: first, at lower currents there is a decrease in over-potentials within the cell, which boosts the electric efficiency of the cell. Secondly, according to equation (3.62) the system pressure drop scales with the ratio of the volumetric flowrate ($\dot{V}$) to the volumetric flowrate at the reference point ($\dot{V}_{design}$). Thus when operating at flowrates that are below the reference point, the system pressure drop is reduced thereby reducing the power consumption of the system blowers and pumps, which are the main drivers of parasitic loses.

Similarly, Fig. 4.31 shows the net system efficiency for part-load operation in electrolysis mode. For this particular case, the assumptions laid out in Table 4.2 were used and the design point is chosen to be at current density of $1.5\,\mathrm{A/cm^2}$, which corresponds to a maximum CH_4 production of $78\,\mathrm{mol/h/m^2}$. The net system efficiency displays a slight linear decrease below $0.9\,\mathrm{A/cm^2}$ (which corresponds to the operating points in which the stack operates endothermically), reaching a maximum at a point slightly above the current corresponding to the thermoneutral voltage, followed by a non-linear concave downwards decrease for all subsequent current densities. Just as in fuel cell operation, the parasitics associated with the blowers decrease with decreasing current density, however, when operating below the thermoneutral voltage the heating requirements of the stack are the main drivers of the total system parasitics (Fig. 4.23), thus the maximum system efficiency happens at a point slightly above the thermoneutral voltage. The decrease in net system efficiency becomes non-linear after the transition into exothermic operation for two main reasons: the heat generated by the stack increases non-linearly with increasing current density (Fig. 4.19),

which in turn means that the amount of air required to maintaining the temperature of the stack within the allowable parameters needs to increase in a non-linear fashion. Due to the fact that the system pressure drop is a power law to the volume of the flowing gases, the amount of work required by the blowers rapidly increases at higher flows which is reflected as a non-linear decrease in system efficiency.

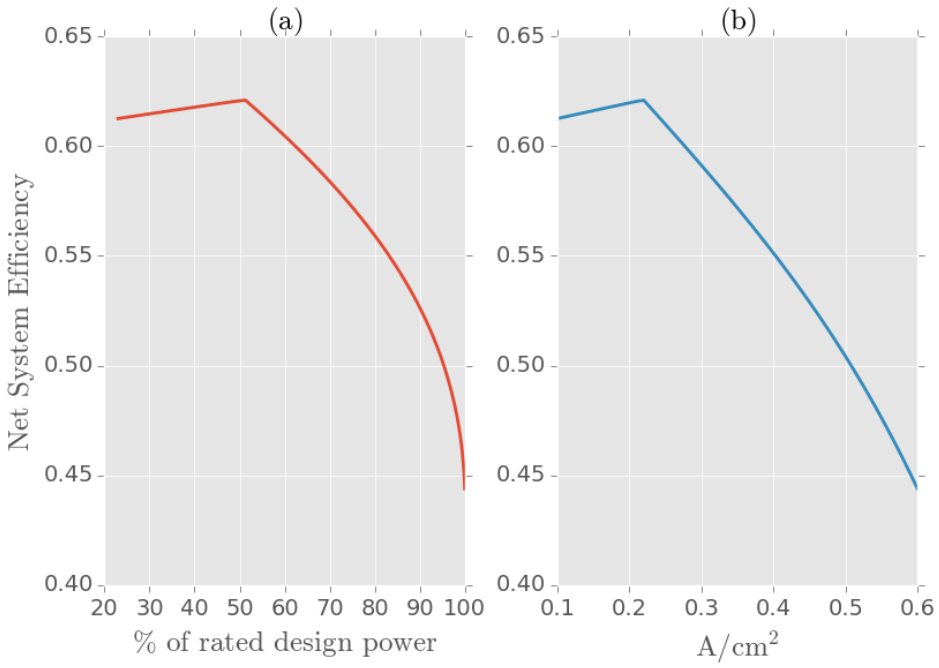

Figure 4.30: Part-Load FC operation: Net system efficiency fuel cell mode. (a): net system efficiency as a function of rated power. (b): net system efficiency as function of current density

4.4.2 BoP over-design

As described in Section 3.5, one of the key assumptions behind the part-load operation modeling is that the system is designed for the highest expected flowrates. As such, the BoP is expected to be oversized for every operating point except for the upper limit design point. Fig. 4.32 depicts the oversizing of the pre-heaters for fuel cell operation. The first graph in Fig. 4.32 shows the ratio of the required area to the

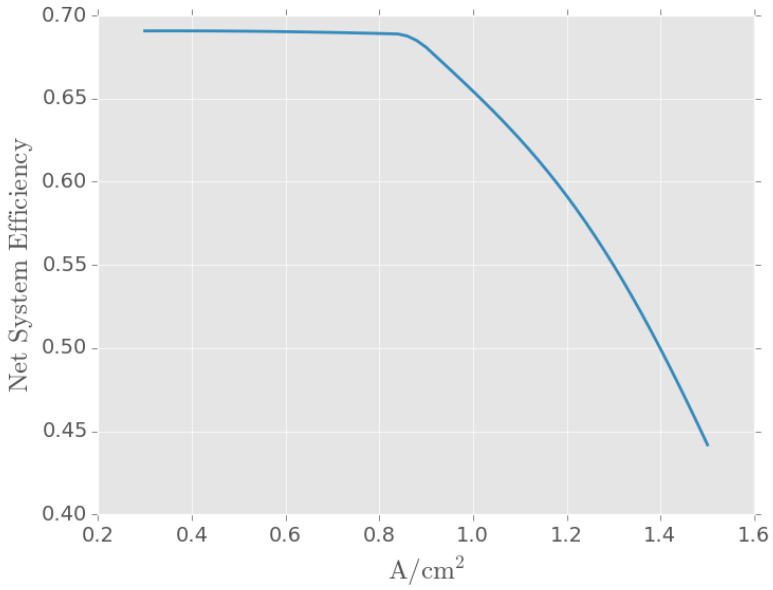

Figure 4.31: Part-Load electrolysis operation: Net system efficiency.

design area for the fuel pre-heater across different current densities. As expected, the ratio is the highest at the lowest current density and equal to 1 at the highest operating current density which is the operating design point. In the case of the fuel pre-heater, the oversizing is roughly a factor of 6 for the lowest current density. For the air pre-heaters, oversizing is much more dramatic and it is roughly a factor of 50 at the lowest current densities. Recall from section Section 4.2.1 that the amount of heat produced by the stack increases non-linearly as a function of current density, which in turn means that the size of the pre-heaters increases non-linearly as the operating current increases, causing the oversizing of the air pre-heaters to be extremely large. This will become a very important element when calculating total system costs, as increasing the systems capability to operate at higher currents has an important economic penalty (via the oversizing of the BoP). See Section 5.3.2.2 for a detailed discussion about this. Fig. 4.33 shows the oversizing for the fuel and air pre-heaters in electrolysis mode. Just as in the previous case, the air pre-heater is

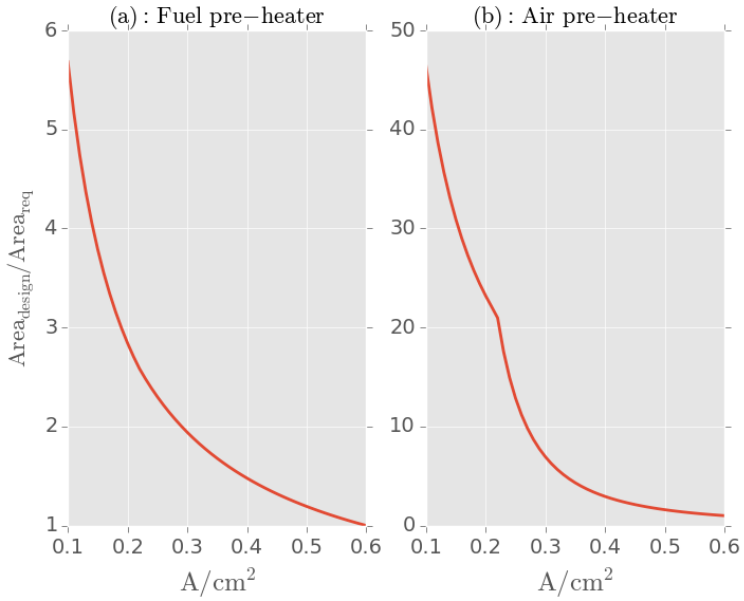

Figure 4.32: Fuel cell pre-heater oversizing. (a): Ratio of design area to required area for fuel pre-heater (b): Ratio of design area to required area for air pre-heater

much larger (and the oversizing is more extreme) than for the case of the feed (in this case H_2O). Below the exothermic operating mode, the RSOC does not require air to flow through and the "required" area is zero, making the ratio in Fig. 4.33:(b) infinity at currents below $0.9\,A/cm^2$. Lastly, it is worth mentioning that the pre-heaters can be shared between the two modes of operation, meaning there is no reason why there should be extra equipment for each mode of operation. This, however, means that pre-heaters will have to be designed for the point that results in the maximum flow rates independent of the mode of operation. In the case of the air pre-heater, it will have to be designed taking into account the electrolysis requirements as the maximum flow at $1.5\,A/cm^2$ is larger than that for the maximum point in fuel cell mode. This particular choice, will impact the system pressure drops and the parasitic loads.

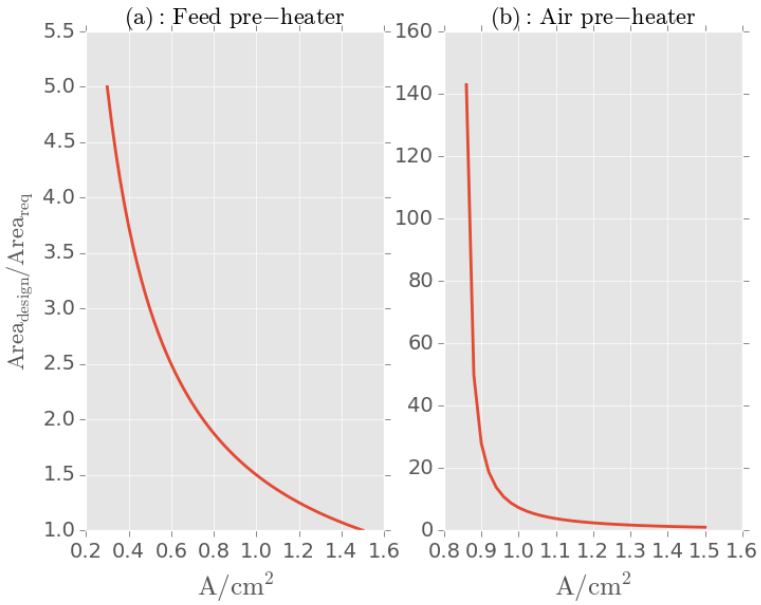

Figure 4.33: Electrolysis Pre-heater oversizing. (a): Ratio of design area to required area for feed pre-heater (b): Ratio of design area to required area for air pre-heater

Chapter 5

Optimization of RSOC operating strategy with market price time-series: the Danish case

In this chapter, the RSOC system described and tested in the previous chapters is used to run a series of temporal optimizations for finding the *optimal operating strategy* for a RSOC system that can buy or sell power in the Danish wholesale electricity and buy or sell fuel in the Danish gas market. We assume that the system is a marginal player within the grid whose decisions do not influence the market. The operating strategy is composed of two distinct variables: the mode of operation (fuel cell, electrolysis or idle); and the operating point (current density). Thus, the optimal strategy will be the operating mode and point for which the profits of the system are maximized for a set of fuel and electricity prices that vary at an hourly scale. While the *optimal operating strategy* would be more or less trivial for a system operating at fixed current and voltage, in Chapter 4 it was shown that the electric efficiency of the system in both directions varies as a function of current density, thus varying the operating point can be used as a strategy to maximize system profits as market prices fluctuate. As such, these optimizations will help explore three main questions:

(1) What is the economic value of running a SOC reversibly?

(2) What is gained from running the system at varying operating points (e.g. part-load operation)?

(3) What role could RSOC play in a grid that is largely dominated by variable renewable power?

The chapter is divided into four main sections: in the first section, a description of the Danish energy system and its electricity market structure is provided. In this section, a discussion of the transition to variable renewable power that the grid has experienced in the past decade and the impact that this had on wholesale electricity prices is also discussed. In the second section, the marginal market player optimization is presented and discussed. This section formalizes the general problem and describes the different optimization cases that are developed in order to answer three main questions described above. In the third section, results for all of the optimizations are presented and discussed. Particular emphasis is given to the sensitivity of the optimization to changes in stack parameters and operating variables (e.g. initial ASR and $U_{f,sys}$). Lastly, a discussion of the role that RSOC systems can play as variable renewable sources increase across different markets and grids is presented.

5.1 The Danish energy system

Denmark, with a population of roughly 5.5 million people, has one of the most modern energy systems in the world. As depicted in Fig. 5.1, in 2013, Denmark had a total gross energy consumption of 761 GJ, divided roughly as 37% oil (mainly used in transportation), 17% natural gas, 19% coal, 27% renewable (including waste) [23]. In the past decades, Denmark has managed to drastically reduce its energy intensity and cut carbon pollution intense while prospering economically. As shown in Fig. 5.2, by 2014 Denmark managed to reduced its gross energy consumption by about 7% relative to 1990, while increasing its GDP by a factor of 1.4. For this same period, Denmark's energy intensity decreased by 34% and its CO_2 emissions from energy consumption have gone from 61.3 to 42.1 million tons of CO_2, representing a 32% reduction relative to 1990 period[23]. In its "Energy Strategy 2050" [24], the Danish government set a series of ambitious energy policy milestones that have been driving the transformation of the Danish energy system. As part of this strategy,

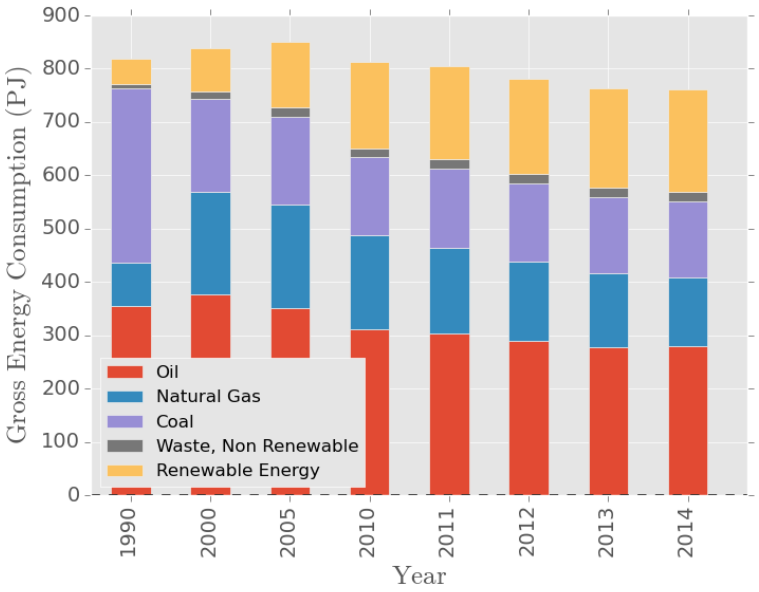

Figure 5.1: Gross Energy Consumption for Denmark [23]

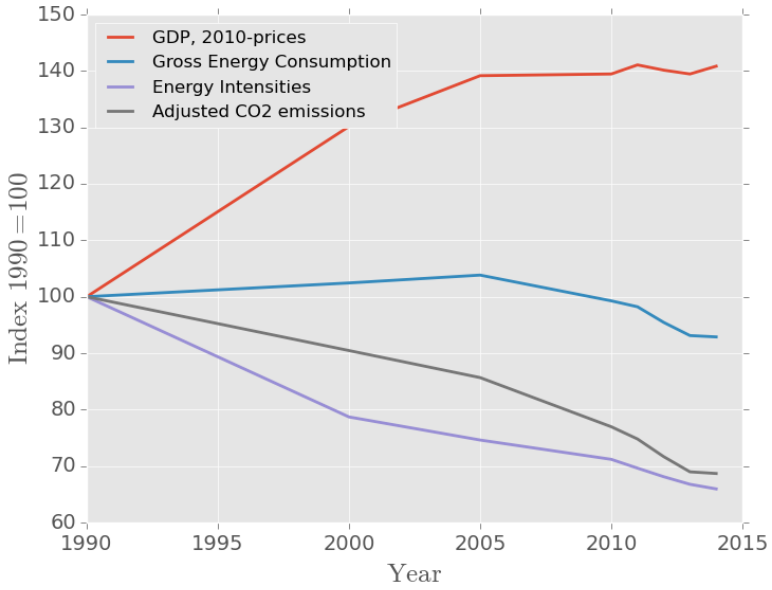

Figure 5.2: Gross Energy Consumption, GDP growth, Energy intensity and CO_2 emissions for Denmark 1990-2014 [23].

the government pledged the following: by 2020 half of the electricity consumption would be provided by wind; in 2035 all electricity and heat supply will come from

renewable sources; and by the year 2050 *all* energy supply (electricity, heat, industrial consumption and transportation) will be covered by renewable sources. As such, the Danish energy system is in the midst of a radical make over, favoring renewable energy over fossil fuels and transforming its once centralized base-load power system into a highly distributed highly intermittent one. The transformation of the Danish power sector began in the mid-1980's with the decision to incentivize the replacement of centralized power plants by a highly distributed network of local CHP plants and wind turbines. As highlighted in Fig. 5.3, the Danish power system has undergone a change that is impressive both in scope and speed. In 1990, the Danish system had 15 centralized power plants and virtually no distributed systems. By 2014, the Danish power system had transformed itself into a distributed network comprised of 20 centralized power stations, 640 local CHP plants and 5,175 wind turbines [101]. The vast network of CHP plants runs mostly on natural gas, biomass, or waste. CHP plants are a central piece of infrastructure for delivering heat throughout the country. In 2014, heat was consumed at a rate of $\sim$ 23 GW out of which 73% came from co-generated heat in both distributed and centralized CHP plans, while the other 27% was generated by dedicated heat producing plants.

Fig. 5.4 shows the evolution of electricity generation in the Danish grid. As this figure suggests, in less than 20 years, Denmark has gone form less than 5% of total electricity generation coming form renewables to roughly 45% in 2013. When taking a closer look as to what composes the 45% renewable power, it becomes clear that the production of renewable electricity has been largely driven by wind power. As Fig. 5.4 and Fig. 5.5 suggest, wind power has always represented the lion's share of the renewable power generated in Denmark. By 2013, wind was supplying 32% of the total electricity consumption of the country. Given Denmark's large agricultural sector and its vast network of local CHP plants, it's logical for wood and biomass to play an important role as renewable fuels for the generation of electricity. By 2013,

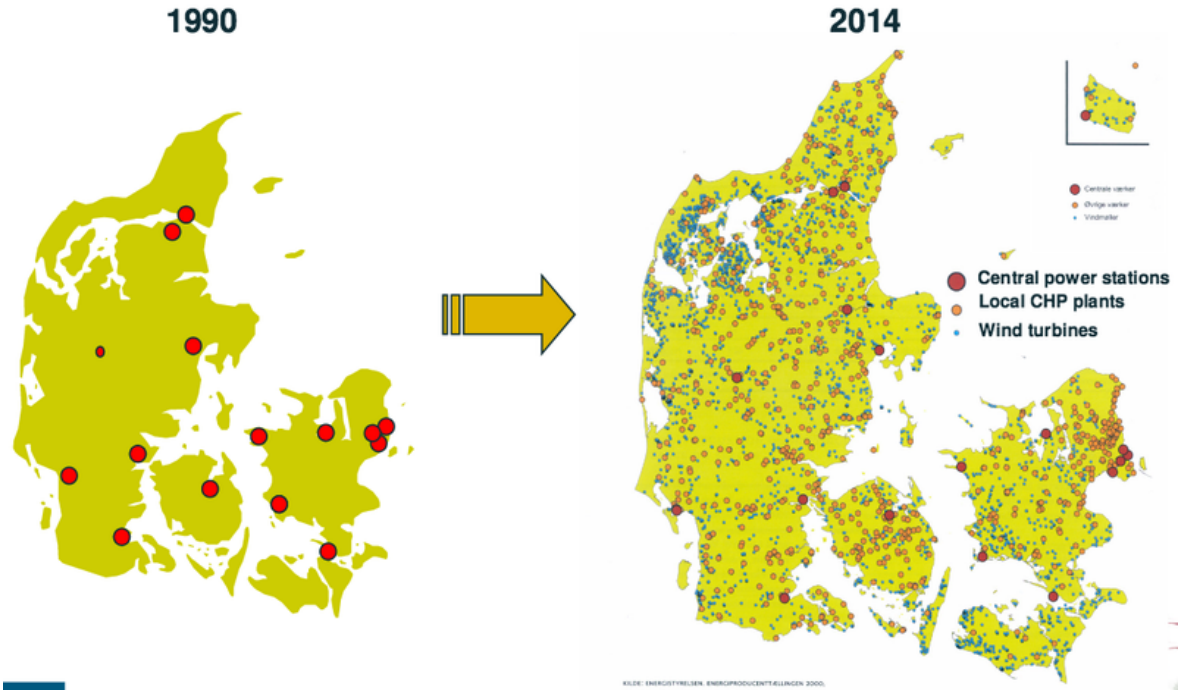

Figure 5.3: Evolution of power grid in Denmark [101]

wood and biomass represented about 18% of the total electricity supply.

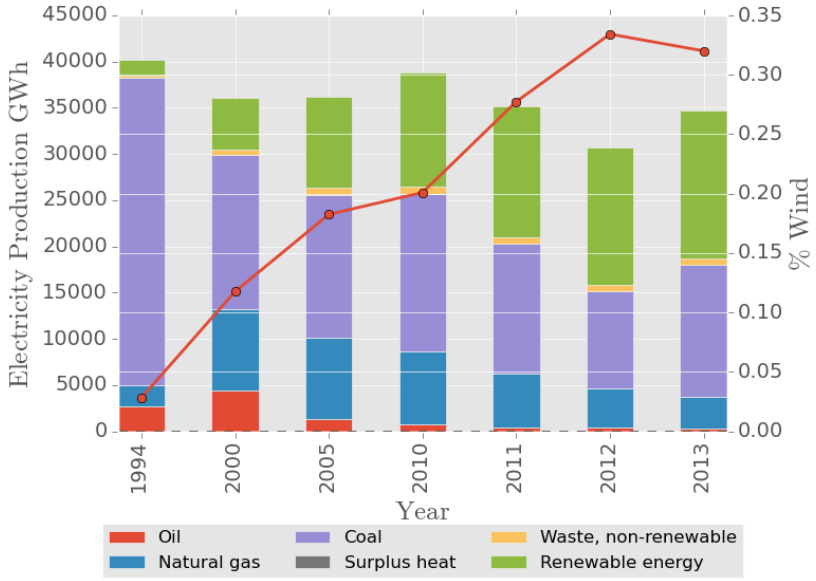

Figure 5.4: Electricity mix in Denmark [23]

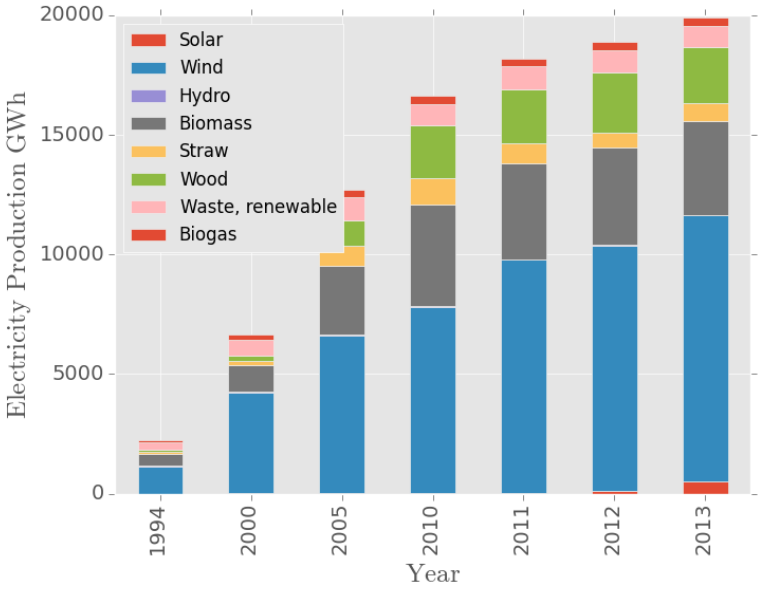

Figure 5.5: Renewable power production mix for Denmark [23]

5.1.1 Overview of the Danish Power system and its market structure

The Danish power system is a highly integrated and interconnected, characterized by its high penetration of wind power and its transparent market structure. At roughly 13.7 GW of installed capacity, the Danish power system is part of Nord Pool, the common Nordic electricity exchange which is comprised of three market places: "Elspot", a day ahead-market for electricity; "Elbas", an intra-day market where electricity can be traded up to one hour before the delivery hour; and "Eltermin" a Futures and Forward contracts market. The Danish power system is separated into two electricity systems: the Western Danish System (Jutland-Funen) which is synchronized to continental Europe, and the Eastern Danish System (Zealand) which is synchronized with the Nordic power system. The Eastern system is connected to the Nordic power system by alternating current via Sweden through four interconnections, two of them operating at 400 kV and two at 132 kV for a total import

capacity of 1300 MW and a total export capacity of 1700 MW. The Eastern system is also connected to continental Europe via a direct current interconnection of 600 MW [36]. The Western Danish System is connected to continental Europe (through Germany) via alternating current connections and to Sweden and Norway with a DC connection. The interconnection with Germany has an export and import capacity of 1780 MW and 1500 MW respectively, while the connection to Sweden has a total export/import capacity of 740/680 MW. The interconnection to Norway is composed of three DC interconnections with a maximum transmission capacity of 1000 MW. Lastly, the Eastern and Western grids are connected at one point, referred to as the Great Belt Power Link, a 400 kV DC connection with a transmission capacity of 600 MW. Fig. 5.6 depicts the different grids and its interconnections. Energinet.dk, an independent public enterprise owned by the Danish government, is the transmission system operator (TSO) that manages the grid. Apart from managing the power grid, Energinet.dk is also the system operator for the natural gas system.

5.1.1.1 The West Denmark electricity market

The West Denmark electricity market is divided into five distinct markets that operate at different time-scales and have different price structures: the primary reserves market; the automatic or secondary reserves market; the manual regulating power market; the intra-day market; and the day-ahead spot market [113]. In power markets, a real-time balance between supply and demand must be met in order to guarantee service to the end-users and the physical stability of the system. In the Danish system, primary, secondary and manual reserves are bundled into the "ancillary services" category [34].

Ancillary services Primary Reserves Market

The main purpose of the primary reserves market is to protect against frequency

Figure 5.6: Danish grid interconnections [36]

deviations that stem from small imbalances in supply and demand. Primary reserves require frequency stabilization of the system at a value close to 50 MHz. It operates in short time scales, with a maximum response time of 30 seconds, and are rarely used for more than 15 min [33]. For the Western Denmark market, Energinet.dk has set a requirement of ± 27 MW. Primary reserves are procured by Energienet.dk as upward regulation (used when frequency needs to be increased) and downward regulation power (in cases where the frequency needs to be decreased). Both types of regulating services are auctioned one day in advance and the 24 hour period is divided into 6 blocks. Sellers bid capacity and require a minimum of 300 kW in order to enter the auction. Bids from the auction are sorted by Energinet.dk by price and are selected from lowest to highest price until the TSO's requirements are met. Primary regulation

is paid out as a capacity payment equal to the price of the highest winning bid in the stack. As such, all winners have the obligation to make the agreed upon capacity available and to be able to respond within the short time frames required. There is no set formula for paying for supplied energy volumes (e.g. the actual amount of electricity provided), and these are set settled as ordinary imbalances [34]. Lastly, the TSO does not send an activation signal, but rather requires the winning units to trigger the upward/downward regulation based on their own measurements at the point of connection.

Secondary reserves market

The secondary reserves market are also used for frequency stabilization, but in this case they are only used in cases of major operational disturbances once primary reserves have kicked in. The main purpose of the secondary reserves is to replace the primary reserves after they have been activated and to restore any imbalances that might arise on the interconnections. In this sense, secondary reserve regulations are controlled by the status of the primary reserves and are triggered by a signal sent by the TSO requiring a specific output value which must be supplied within 15 minutes of receiving the signal. For this reason, secondary reserves are usually suppled by units that are already in operation or by fast-start units. Energinet.dk buys secondary reserves a month in advance and they are procured as upward and downward regulation reserves, where upward regulation is usually provided by a production unit and downward regulation by a consumption unit. The acceptance of bids is not only based on price, and the TSO takes into account the price of service, the place of delivery and the technical aspects of the production/consumption units. For the upward regulation service, energy volumes are settled based on the west Denmark spot price plus DKK 100/MWh. For downward regulation it is the spot market price minus 100/MWh, and a maximum price that does not exceed the regulating power price for downward regulation [34].

Manual regulating market

Manual reserves are yet another mechanism that the TSO can use to regulate the imbalances between supply and demand. Manual reserves derive their name from the fact that the upward and downward regulation reserve is activated manually by Energinet.dk's Control Center. The main objective of the manual reserves is to replace the primary or secondary reserves that have been activated and to ensure system balance in the case of major events that might cause outages at certain production points. Upward and downward reserves are procured on an hourly basis by the TSO via a daily auction that takes place one day in advance. The required start-up time has to be less than 15 min and full capacity is expected to be online within this time-frame[113]. When the auction opens, Energinet.dk specifies the reserve market requirement (MW) for the upcoming day and bidders submit hour-by-hour volumes and prices that they are willing to take. To participate in the regulating market, bidders must submit a minimum of 10 MW with a maximum allowable offer of 50 MW for each hour of the day. The TSO selects the bids for upward and downward according to price (from lowest to highest) until the pre-specified requirement is met and selected operators receive a payment equal to that of the highest winning bidder of upward/downward regulation. Energy volumes are settled according to either the spot price for electricity or the area's market price [37]. In this regard, one can think of operators that participate in the regulating market as having two sources of revenue: a (fixed) availability payment for upward/downward regulation independent of whether it is used or not, and a (variable) energy payment that is a function of how much energy was consumed/supplied during the regulation operation.

Intraday market (Elbas) Due to the high penetration of wind power in the Danish grid, matching supply and demand a day in advance can be a difficult task. In order to solve this problem, the Danish gird is part of the Scandinavian intra-day

power market (Elbas), which allows participants to trade upward and downward regulation 45 minutes before the operating hour. A minimum of 10 MW is required for participating in the intra-day market. Energinet.dk is responsible for sending bids to the Nordic Operation Information System (NOIS), which handles bids for Danish, Norwegian, Swedish and Finnish producers. The price of upward regulation at any given hour has a floor set by the electricity spot price (see below for details) and a ceiling of EUR 5000/MWh [37]. On the other hand, the maximum price for downward regulation at any give time is set by the spot price for the given hour. Bids are activated according to marginal price, thus the cheapest bidders go first and have a maximum response time of 15 min to reach full capacity. The intraday and manual reserves markets differ in two important ways: first, for manual reserves, power is traded a day in advance whilst on the intraday system power is traded on an hourly basis; second, because the manual reserves require a given amount of power to be available, an "availability" fee is paid whether the upward or downward regulation is used or not, which, for obvious reasons, is not the case for the intra-day market.

Day-ahead spot Market (Elspot) Elspot is the day-ahead spot market place for the Nordpool Market which represents about 70% of the total electricity consumed in Nordic countries [35]. The day-ahead market functions via an auction, where aggregated supply and expected demand curves set the price for all bidding areas. Pricing in the day-ahead market depends on the market equilibrium (balance between purchase and sale for the whole area) and on transmission bottlenecks. Orders (supply and purchase) can be done for single hours, as block orders (specified volume for at least three consecutive hours) or as "flexible orders" which allow users to set the energy volume, time interval and an order price limit. The latter type of bid allows energy intense industries to sell power to the market by deliberately scaling back or shutting down industrial processes [97]. Prices in the day-ahead market are

determined by two different mechanisms. If there are no bottlenecks in the system (e.g., the electricity can flow freely through the interconnections), the clearing price is simply the "system price" which is determined by the intersection of the aggregate supply and demand curves for bids in the market. That is, the system price represents an market without congestions where location of a particular bid within the system (e.g. being in Norway vs Sweden) is not a factor for determining the final clearing price. In the case of grid congestions, the system is divided into several different price areas. Bids are aggregated by areas and a new price that reflects transmission limitations, the "area price", is calculated.

5.1.1.2 The importance of wind in the Danish power system

As stated before, the Danish power sector is undergoing an important transformation and today it is the country with the most wind power as a fraction of its total generation. Thus, before we delve into simulating the interaction of reversible solid oxide cell systems with the electricity market, it is important to make a few observations about the importance of wind in the Danish market, and how it can affect wholesale market prices and volatility at different timescales. Wind generation in Denmark follows a seasonal cycle, where production peaks during the winter months and is its the lowest during the summer. Fig. 5.7 shows the hourly production of wind power in Western Denmark for the period 2009-2014 (blue curve) and a seasonal rolling average (purple curve)[1]. The figure highlights two important features: the first is the seasonality of wind generation, which can be clearly seen from the smoothed curve, and the second is the year-on-year increase in wind generation that the Danish system has experienced. At large scales, the amount of wind available in the system will have an impact on prices as the marginal cost of wind tends to be very close to zero. In a study of the Eastern Denmark grid, Mauritzen reports that wind power has a

[1]The rolling average is computed using a window of 2,016 hrs which roughly corresponds to a 3 month period

statistically significant effect on the volatility of electricity prices, where wind tends to *reduce* intraday price volatility, while at the same time *increasing* price volatility over larger windows [90]. Woo et. al did a regression analysis on the ERCOT system at a 15 min resolution and found that rising wind generation tends to reduce the level of spot prices, it is also likely to enlarge the spot-price variance [128]. Similarly, Ketterer reports that in the case of the German grid, increasing wind availability tends to suppress spot-prices while increasing their volatility [77].

Fig. 5.8 shows a time-series for the day-ahead spot prices for the Western Denmark area. There are three observations are worth mentioning from this plot: first, prices can vary considerably from hour to hour; second, the figure shows an unusual up-tick on the 7$^{\text{th}}$ of June 2013 where prices reached 2000 Eur/MWh during four hours of the day; and the last is that during many hours of the year, the spot price of electricity seems to dip below zero. In order to clarify points one and three, Fig. 5.9 shows a

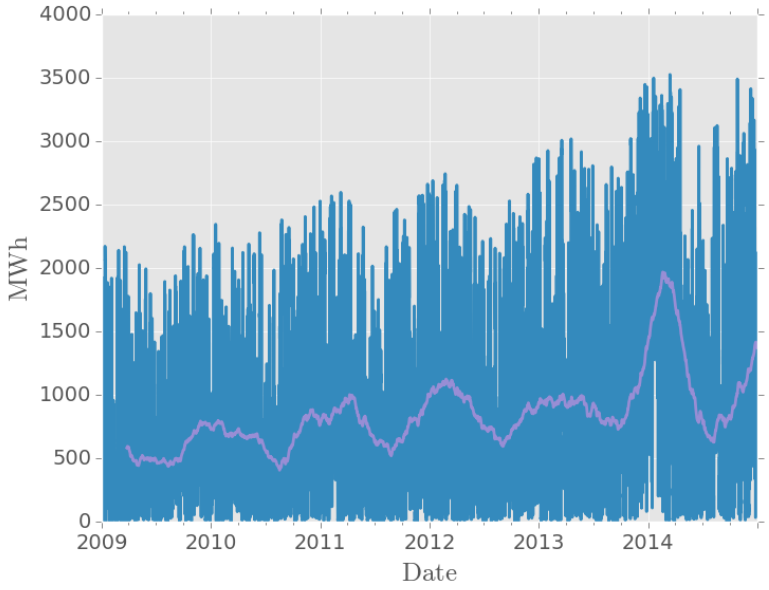

Figure 5.7: Wind power generation Western Denmark (2009-2014)

time-series for the same period but with the 2013 spike filtered out. It is clear from

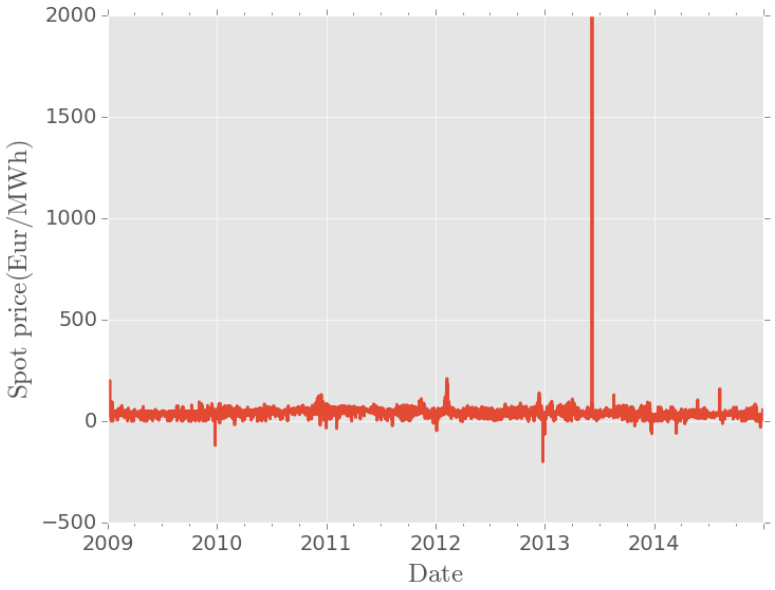

Figure 5.8: Western Denmark day-ahead spot prices (2009-2014)

this chart that the prices exhibit considerable variability and it is not uncommon for prices to dip below zero. As discussed in Section 5.1.1.1, the prices for the day-ahead market in Western Denmark are set by a competitive bidding process that matches expected supply and demand. In this process, producers bid a price based on their marginal generation costs. Because wind power has a marginal cost of zero, large availability of wind in periods of low demand can have an important influence on the price of electricity. Although Western Denmark is well connected to other countries that have the ability to absorb its production when demand is not there, particularly Norway with its vast system of hydro-power plants, this is not always the case and it is not uncommon for prices to be suppressed by wind availability.

The optimization studies presented in the subsequent sections of this chapter uses the price of electricity and the price of fuel as the main inputs in order to determine the optimum operating strategies. Thus, the volatility of these prices will have an important impact on the mode of operation (e.g. electrolysis) and the operating point

Figure 5.9: Western Denmark day-ahead spot prices with spikes filtered out (2009-2014)

(current density). In financial markets, volatility is usually the degree of fluctuations of prices over time and it is quantified as the standard deviation of the return [114]. When studying electricity markets, the norm is to use the logarithmic volatility, which is simply the standard deviation of the log-arithmetic return, as the measure of price fluctuations. For a given period Δt, the logarithmic return of an instrument with price at time t $p(t)$ is defined as:

$$R_{\Delta t}(t) = \ln\left(1 + \frac{p(t+\Delta t) - p(t)}{p(t)}\right) \tag{5.1}$$

Fig. 5.10 shows the daily average price volatilities of electricity in Western Denmark (DK1) and natural gas in the Nordpool market. As it can be seen, the volatilities of electricity prices are much larger than the ones for natural gas, thus fluctuations in the prices of electricity will in large part drive the decision for the optimum operating mode and operating point of the RSOC system. The fact that electricity prices show higher volatility than that of natural gas is not unique to Denmark, but rather an

underlying feature of these commodities. Generally speaking, volatility of natural gas is in the 3-5% range, while volatility of the Nordic market is in the 16-20% range[114].

Fig. 5.11 shows the relationship between the fraction of the total electric demand

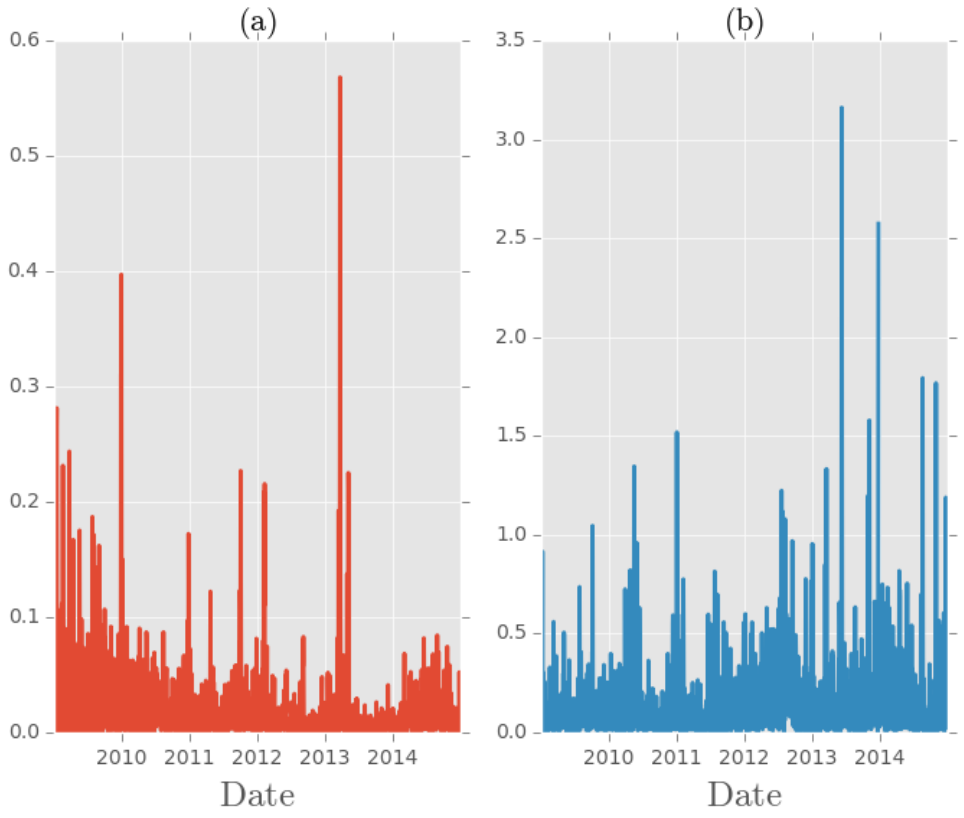

Figure 5.10: (a): average daily logarithmic volatility for natural gas. (b): average daily log volatility for DK1 electricity

in western Denmark being supplied by wind power and the hourly spot price in the Elspot market. As suggested by the graph and its linear fit, prices tend to decrease as a larger fraction of the total demand is supplied by wind. The figure also suggests that as the fraction of wind increases, the prices exhibit less scatter. Another thing worth noting is that during 5% of the time, the fraction of the total consumption coming from wind exceeds 100%. This means that at these points in time, there is mismatch between supply and demand that needs to be managed. In many cases

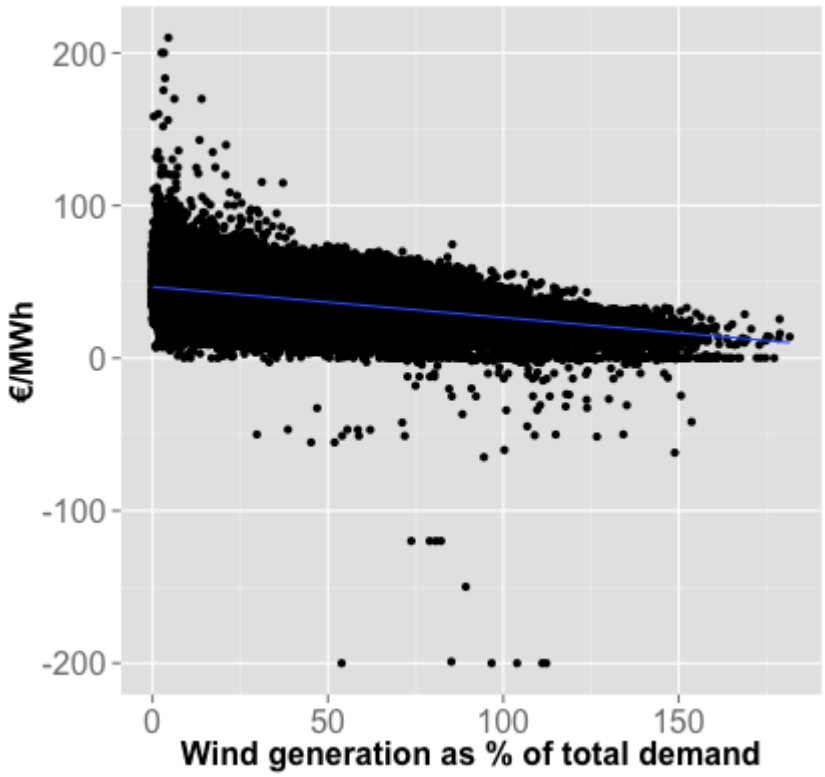

Figure 5.11: Day-ahead hourly spot market price vs. wind fraction of total demand for the year 2009-2014.

this means exporting power to Norway, Sweden or Germany, and if this is not possible then production curtailment will be required. As expected, when the total wind exceeds the total demand, prices tend to be low and in many cases they converge to zero and/or become negative. A negative price means that the generator will *pay* the off-taker to consume the electricity. Negative spot prices have been occurring more frequently in Western Denmark as the penetration of wind has drastically increased in the past few years. As Fig. 5.12 shows, negative price occurrences went from less than 10 times in 2009 to more than 45 in 2014. Although this still represents less than 1% of the time, there is a clear increasing trend as the share of wind in the system increases. Fig. 5.13 price hist shows the distribution of negative prices as a function of the fraction of total demand being served by wind power. The curve shows a slight

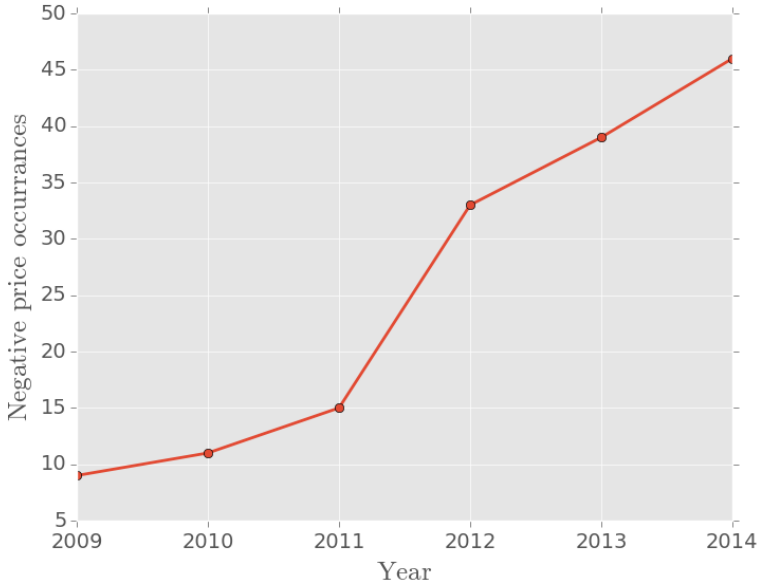

Figure 5.12: Yearly frequency of negative prices in Western Denmark

positive skewness with most of the negative prices occurring when the fraction of wind is between 100-130%. Lastly, Fig. 5.14 shows the distribution of negative prices for each day of the week. Again, because negative prices tend to occur when demand is low and wind production is high, it is no surprise that Sunday is the day of the week in which negative prices occur more frequently.

5.2 Optimum operating strategy of a RSOC in the Danish system

As discussed throughout this chapter, the Danish electricity system is part of a broad highly deregulated power market. Because of their high share of wind power, prices in the Danish system can vary dramatically at an hourly, daily and seasonal scale. In this section, a series of optimization routines used to maximize the profits that a RSOC system can make in the Danish grid by varying the mode of operation (fuel cell, electrolysis, idle) and the operating point (e.g. current) in response to market

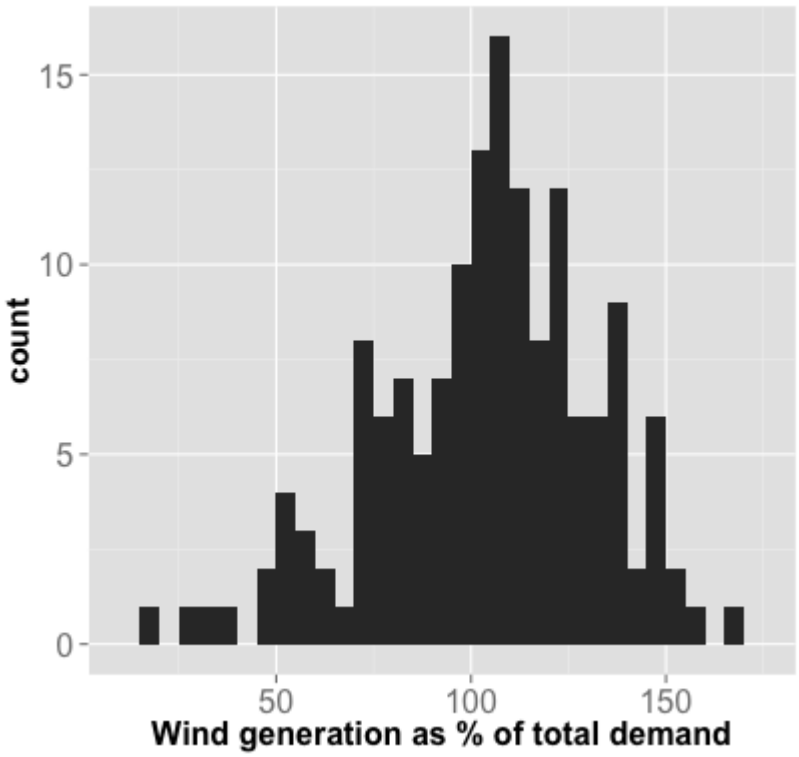

Figure 5.13: Negative price distribution vs. wind percentage of total demand for the year 2009-2014.

prices are developed. Contrary to other studies of that use RSOC technology for arbitrage operations in the Danish grid [73], the "energy hubs" that we have defined in Section 3.2 are open at both ends meaning that any fuels generated by the system are sold within that time-period and none are stored for future use. Because our system has the ability to take and/or inject fuel at any point in time into the grid, we can think of the "energy hub" that is open at both ends as a storage device with infinite storage capacity (e.g. the natural gas grid). This is a subtle, yet crucial point. By opening the system at both ends, there is no speculation about future prices and thus the optimization is set up such that the decision to operate is a function of existing price signals. Contrary to conventional energy storage optimizations, where the future prices must be known or estimated, the system profits of the energy hub

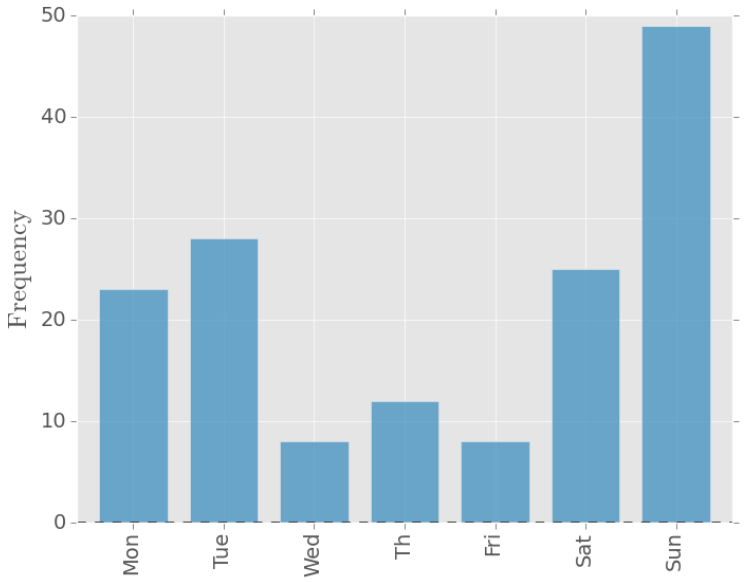

Figure 5.14: Negative price frequency in DK1 for each day of the week.

can be maximized with no information about the future. Furthermore, because the system uses commercially available CH_4 when running in fuel cell mode, the use of the proposed RSOC system is somewhat different from traditional energy arbitrage cases. In the case of batteries, pumped hydro, and flow batteries, the total energy sold cannot exceed the total energy stored. In our case, this constraint is lifted as the available fuel is not bound by a physical or chemical reservoir, but rather by the instantaneous price of natural gas quoted in the open market.

Unless stated otherwise, the following assumptions are used in order to construct the temporal optimization for finding the optimum operating strategy:

1. We are a small price taker in the market and our decision to operate does not influence market prices.

2. The decision of operating mode and operating point is made with perfect price information (e.g. the prices are known before the decision is made).

3. We assume that the transient response of the RSOC system is instantaneous (e.g. no time loss when flipping between operating modes and points).

4. There is no constraint on the amount of CO_2 available in electrolysis mode.

5.2.1 Data

For this analysis, we use the day-ahead wholesale electricity prices for Western Denmark for the years 2009-2014 available through Energinets website. For the price of fuel, we use the day ahead prices for natural gas quoted in the Norpool market for the same time period as the electricity time-series. The price of natural gas is given once a day resolution, while the wholesale electricity prices have an hourly resolution. In order to harmonize the datasets, we assume that the hourly price of natural gas is equal to the daily clearing price, thus for a single day the data is comprised of 24 distinct price pairs. Fig. 5.15 and Fig. 5.16 show the electricity and natural gas datasets for the years 2009 and 2014 plotted on an hourly basis and aggregated by week[2]. There are two things worth highlighting about these graphs: first, the average spread between natural gas and electricity is much larger for the weeks in 2009; second, electricity prices can exhibit dramatic price variations, whereas natural gas has less day-to-day volatility.

5.2.2 Problem formulation

The RSOC system has three mutually exclusive modes of operation and sees two distinct market signals at each time step:

1. Electricity is bought from the grid at time t for a price $p_e(t)$ and it's used to synthesize natural gas that is sold for a price $p_{NG}(t)$ hydrogenation of CO_2 (electrolysis mode).

[2]As explained above in Section 5.1.1.2, there is an important difference in total wind generation between 2009 and 2014, thus these two years represent the years with the smallest and largest share of wind in the Danish grid

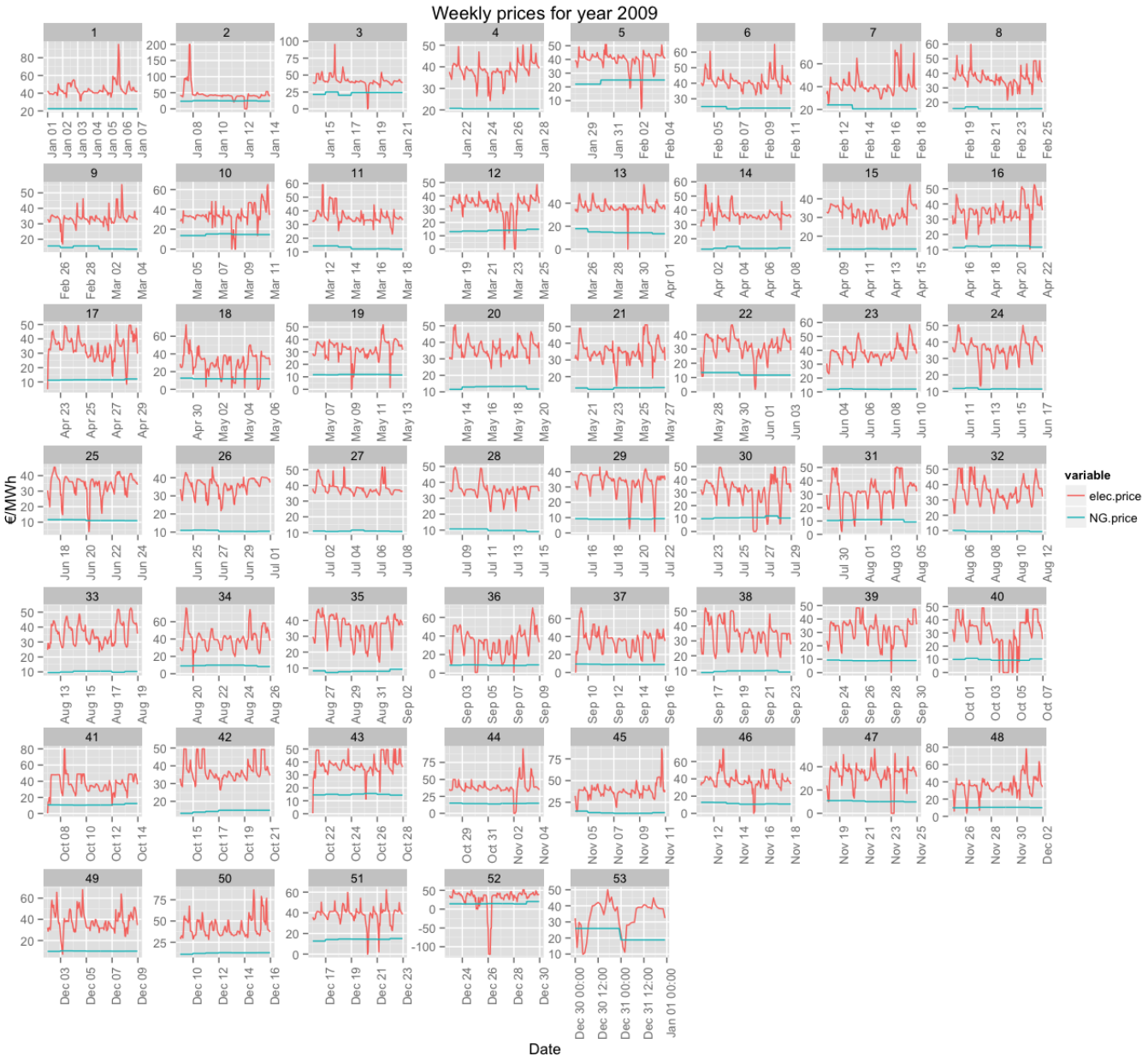

Figure 5.15: Western Denmark electricity and natural gas prices for each week of the year 2014

2. Natural gas is bought from the grid at time t for a price $p_{NG}(t)$ and used to generate electricity which is sold at a price $p_e(t)$ (Fuel cell mode).

3. System sits idle (Idle mode).

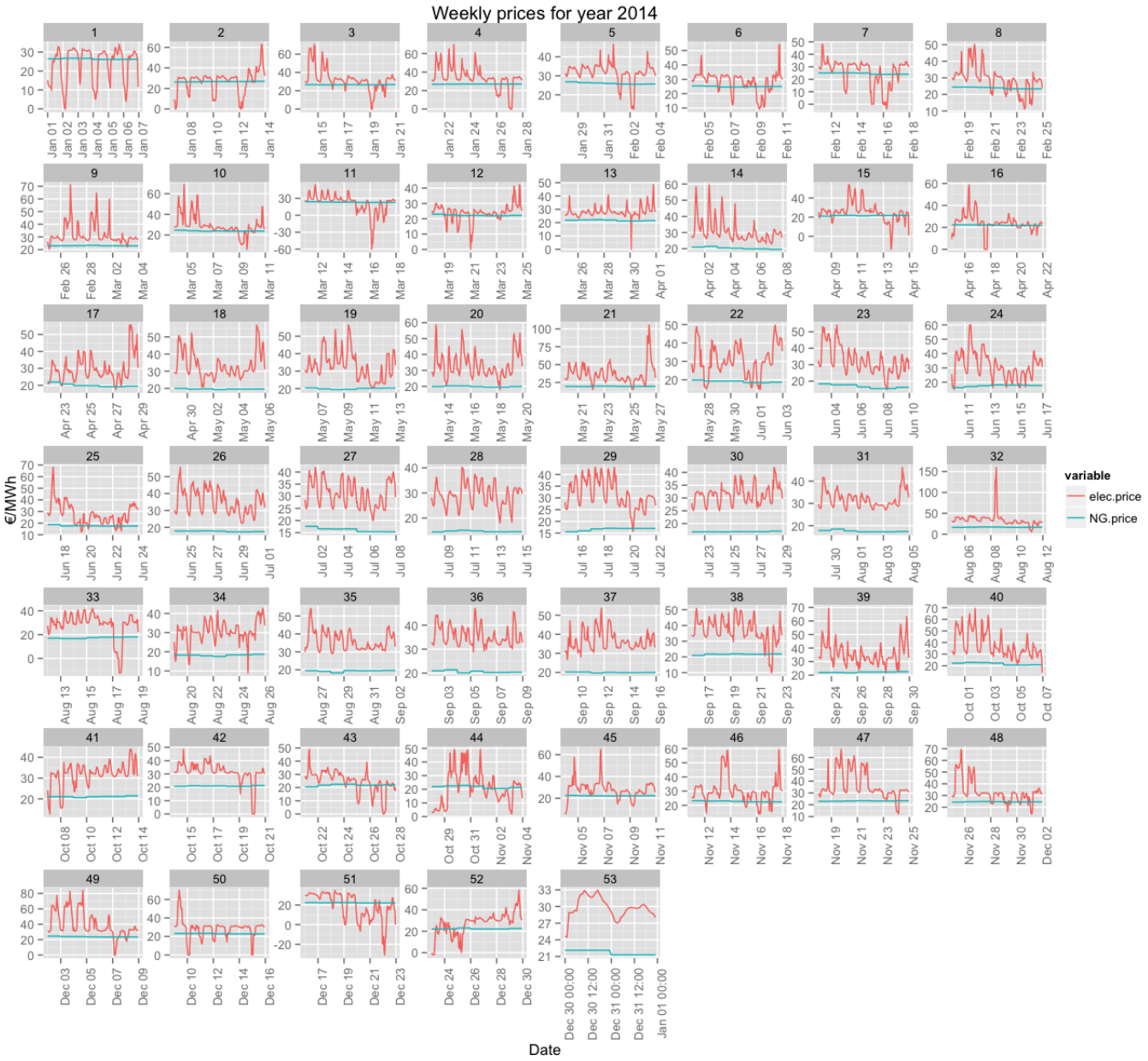

Figure 5.16: Western Denmark electricity and natural gas prices for each week of the year 2014

Thus, at each interval t and for a set of prices $p_e(t)$ and $p_{NG}(t)$, we are interested in finding the optimal operating current, i, that maximizes profits over a given time interval. It is important to emphasize that the optimum operating mode and point at each timestep is *independent* of the capital cost of the system, as this is treated as a

sunk cost at the beginning of the project. The investment cost will have an impact on the overall profitability of the system (discussed in Section 5.3.2.2) but the optimal operation is solely based on the system's marginal costs (e.g. fuel and electricity). Thus, the objective function for the optimization can be written as:

$$\max \sum_{t=1}^{N} \pi(t,i) \tag{5.2}$$

where $\pi(t,i)$ is the profit at time t, i is the operating current and N is the number of hours in each interval (days, weeks, etc.). It is important to mention that because our system receives an instantaneous sell price for the energy product that it generates (whether fuel or electricity) and it does not hold on the generated fuel to be used at a later time, the maximum profit for any time interval N will be equal to the sum of the maximum profits at every single time-step, which simplifies the computational time required for finding the optimum strategy:

$$\max \sum_{t=1}^{N} \pi(t,i) = \sum_{t=1}^{N} \max \pi(t,i) \tag{5.3}$$

The profit function $\pi(t,i)$ can be simply thought of as the difference between operating revenues and costs at hour t. Thus:

$$\pi(t,i) = rev(t,i) - cost(t,i) \tag{5.4}$$

It is important to mention that the initial investment costs associated with the RSOC are not taken into account when deciding what the operating strategy should be. Investment costs are treated as sunk costs that occur at $t = 0$ and therefore do not affect the decision to operate in the future. Thus, all costs are taken to be marginal operating costs.

Due to the fact that our system can earn a profit by selling fuel or electricity, the revenue portion of the profit equation depends on the mode of operation, which is determined by the sign of the operating current;$i < 0$ for fuel cell, $i >$

0 for electrolysis, and $i = 0$ for idle:

$$rev(t,i) = \begin{cases} p_e(t)E_T(i) & \text{if } i > 0 \\ p_{NG}(t)F_{gen}(i) & \text{if } i < 0 \\ 0 & \text{if } i = 0 \end{cases} \tag{5.5}$$

where $p_e(t)$ and $p_{NG}(t)$ are the price of electricity and natural gas at time t, $E_T(i)$ is the total electricity generated by the system when operated as a fuel cell at current i and $F_{gen}(i)$ is the total amount of methane generated by the system when operated in electrolysis mode and at current i. Similarly, the cost component of the profit is also a function of operating mode and operating point:

$$cost(t,i) = \begin{cases} p_{NG}(t)F_{cons}(i) & \text{if } i > 0 \\ p_e(t)E_{cons}(i) & \text{if } i < 0 \\ 0 & \text{if } i = 0 \end{cases} \tag{5.6}$$

where $F_{cons}(i)$ is the amount of fuel consumed in fuel cell mode operating at current i and $E_{cons}(i)$ is the total electric consumption of the system when operating in electrolysis mode at current i. Thus the $\pi(t,i)$ takes the following form:

$$\pi(t,i) = \begin{cases} p_e(t)E_T(i) - p_{NG}(t)F_{cons}(i) & \text{if } i > 0 \\ p_{NG}(t)F_{gen}(i) - p_e(t)E_{cons}(i) & \text{if } i < 0 \\ 0 & \text{if } i = 0 \end{cases} \tag{5.7}$$

In order to maintain the results of the optimization within the bounds of physical reality, it is important to constrain the operating current density:

$$-1.5 \leq i \leq 1.0 \tag{5.8}$$

It can be seen that by changing the constraints in (5.8), one can easily force the optimization to only operate under a particular mode. For example, if we only want

to consider the system in fuel cell mode then we would change the operating current constraint to $0 \leq i \leq 1.0$. Similarly, we can as easily define an electrolysis only system by changing the constraint to currents that are $-1.5 \leq i \leq 0$.

At each time interval t, the optimization calls on the computational model described in Chapter 3 to calculate $E_T(i), F_{gen}(i), F_{cons}(i),$ and,$E_{cons}(i)$ for any given current and stack and system level assumptions. This particular feature, the ability for the optimization routine to call on a complex system model, is one of the unique aspects of this work and an important contribution of this thesis.

5.3 Optimization results

Using day-ahead electricity and natural gas prices for Western Denmark for the years 2009-2014, the optimization presented in Section 5.2.2 is solved at an hourly resolution. The objective function is maximized numerically using the Nelder-Mead simplex algorithm available via the optimization module in Python's SciPy library. The Nelder-Mead algorithm is a robust method for non-linear optimizations although it is very slow compared to other algorithms. The optimization was attempted using much faster techniques such as the sequential least squares programming (SLSQP) algorithm or the L-BFGS algorithm, however due to the non-smooth nature of the objective function, these algorithms failed to converge.

For the purpose of the results presented herein, unless it is otherwise stated Table 5.1 lists the assumptions used in the RSOC computational model. The "energy hub" has a SOC stack with an effective area of $100\,\mathrm{m}^2$, which in fuel cell mode corresponds to 317 kW of peak power production and 774 kWh of CH_4 consumed (LHV) ($0.6\,\mathrm{A/cm}^2$, 0.62V) and in electrolysis mode has a maximum stack power load of 2410 kW and 1152 kWh of CH_4 (LHV) generated ($-1.5\,\mathrm{A/cm}^2$, 1.64 V).

As described in Chapter 4, the system can be quite sensitive to the value of some of the parameters listed in Table 5.1. The interaction of the RSOC system with

Parameter	Value
Area	$100\,\mathrm{m}^2$
$U_{f,sys}$	0.85
ASR_o	$0.5\ \Omega\mathrm{cm}^2$
λ_{SC}	0.90
Recycle rate (FC)	0.668
Steam-to-carbon	2.0
T_{op}	$750\,^{\circ}\mathrm{C}$
ΔT_{cell}	100 K
Inlet air composition	0.21 O_2, 0.79N_2
CO_2 price	\$30/ton
Constraints	$-1.5\mathrm{A/cm}^2 \leq i \leq 0.6\mathrm{A/cm}^2$
Degradation	0%/1000 hrs (*no degradation*)

Table 5.1: Model assumptions for optimization runs

market signals adds a new dimension of complexity to the problem, and therefore it is important to understand the implications of designing a system with a given set of parameters and operating it under certain assumptions. To do this, we create a series of "case studies" under which we vary the underlying assumptions presented in Table 5.1 in order to assess the impact that it has on the solution of the optimum operating strategy and system profits for the optimization problem presented in Section 5.2.2.

Table 5.2 presents a list of all the cases that are evaluated. There are five parameters that are varied across these cases: the price dataset, the initial ASR (ASR_0), the degradation rate, the BoP size (oversizing), and the operational limits (current limits). The cases in Table 5.2 are coded using a simple nomenclature: the first element of the name contains the type of operation (FC - fuel cell; Rev - reversible) and the second element is the sensitivity test being performed (BC - base case, PS - price sensitivity, ASR - Initial ASR, Deg - degradation rate). So, a simulation where only fuel cell operation at a fixed current is permitted is coded as FC-curr, whereas a reversible case that varies the initial ASR is coded as Rev-ASR_i.

Case	Varying parameter	Value
Rev-BC	None	NA
FC-curr1	Fixed current	0.3 A/cm^2
FC-curr2	Fixed current	0.4 A/cm^2
FC-curr3	Fixed current	0.5 A/cm^2
Rev-ASR$_1$	ASR$_0$	0.2 Ωcm^2
Rev-ASR$_2$	ASR$_0$	0.3 Ωcm^2
Rev-ASR$_3$	ASR$_0$	0.4 Ωcm^2
Rev-ASR$_4$	ASR$_0$ & current limit	0.2 Ωcm^2, (1.8A/cm^2, $-$3.5A/cm^2)
Rev-ASR$_5$	ASR$_0$ & current limit	0.3 Ωcm^2, (1.25A/cm^2, $-$2.45A/cm^2)
Rev-ASR$_6$	ASR$_0$ & current limit	0.4 Ωcm^2, (0.95A/cm^2, $-$1.85A/cm^2)
Rev-deg1	Deg rate	0.1%/1,000 hr
Rev-deg2	Deg rate & BoP size	0.1%/1,000 hr, Area
Rev-PS1	Prices, SNG price	DK2050, low SNG
Rev-PS2	Prices, SNG price	DK2050, high SNG
Rev-PS3-ASR	Prices, ASR$_0$	0.2 Ωcm^2, DK2050
Rev-PS4-ASR	Prices, ASR$_0$	0.3 Ωcm^2, DK2050
Rev-PS5-ASR	Prices, ASR$_0$	0.4 Ωcm^2, DK2050
Rev-PS6-ASR	Prices, ASR$_0$ & current limit	0.2 Ωcm^2, DK2050, (1.8A/cm^2, $-$3.5A/cm^2)
Rev-PS7-ASR	Prices, ASR$_0$ & current limit	0.3 Ωcm^2, DK2050, (1.25A/cm^2, $-$2.45A/cm^2)
Rev-PS8-ASR	Prices, ASR$_0$ & current limit	0.4 Ωcm^2, DK2050,(0.95A/cm^2, $-$1.85A/cm^2)

Table 5.2: Cases for optimum operating strategy

5.3.1 Base case (Rev-BC): system profile results

As described in previous chapters, the behavior of the RSOC system is highly sensitive to the assumptions and system parameters chosen. In order to understand the results of the optimization across the 2009-2014 time-frame, it is important to set up a baseline where all parameters are well defined and understood. We have chosen scenario Rev-BC (see Table 5.2) as the "base-case" scenario that we will use to understand the system behavior and the economic consequences of the optimization exercise. Scenario (Rev-BC) is an hour-to-hour optimization based on the assumptions laid out in (Table 5.1) and the problem formulation defined in Section 5.2.2. In the previous sections, we discussed how the price of electricity has great volatility in the Danish grid, how it varies across seasons, and how it has been changing as the

fraction of wind has increased in the past years. Because the optimization determines the operating mode and the operating point of the RSOC based on the electricity and fuel prices, in order to highlight the system behavior at different times within the timeframe analyzed, we have chosen a few representative weeks across seasons and years (see Figs. 5.17 to 5.20). Each one of these figures contains five panels in which the first has a time-series of the fuel and electricity prices, the second contains a plot of the current density of the RSOC, the third panel plots the voltage, the fourth panel shows the ASR of the system at each hour, and the fifth panel shows the system instantaneous profits which are being maximized by the optimizer.

Fig. 5.17 shows system profile for the first week of 2009. The first thing that we can see is that for this week, the price of electricity is always above the price of fuel which means that the system will only operate as a fuel cell or in idle mode. The price time-series also suggests that prices of electricity are on average 3-4$\times$ the price of fuel and in some cases can be much more than that. For these periods, the system should operate at relatively high current densities in order to favor high power densities over efficiency. The sign and value of the current density in the second panel tells us the operating mode of the system. When the current density is <0 the system is in electrolysis mode, when it is >0 it is in fuel cell mode and when it is at 0 it is idling. As seen from the second panel, there are only a few instances in which the system idles (8 out of 168) and the rest of the time it is operating in fuel cell mode. During the hours in which the difference in prices between fuel and electricity is very high (e.g. 7th of January), the optimization resolves to high current densities sacrificing system efficiency in favor of delivering more electricity at times of high prices. This behavior is one of the unique aspects of this work, as it shows the value that can be gained by defining the optimum operating point in terms of exogenous market prices rather than in terms of endogenous system parameters. This becomes clear when looking at the hourly profits series, where we can see that the profits for January

7th are much higher than for any other day of the week. As a matter of fact, the weekly profits for this series is $742 out of which $417, roughly 56%, come from the operation of that particular day.

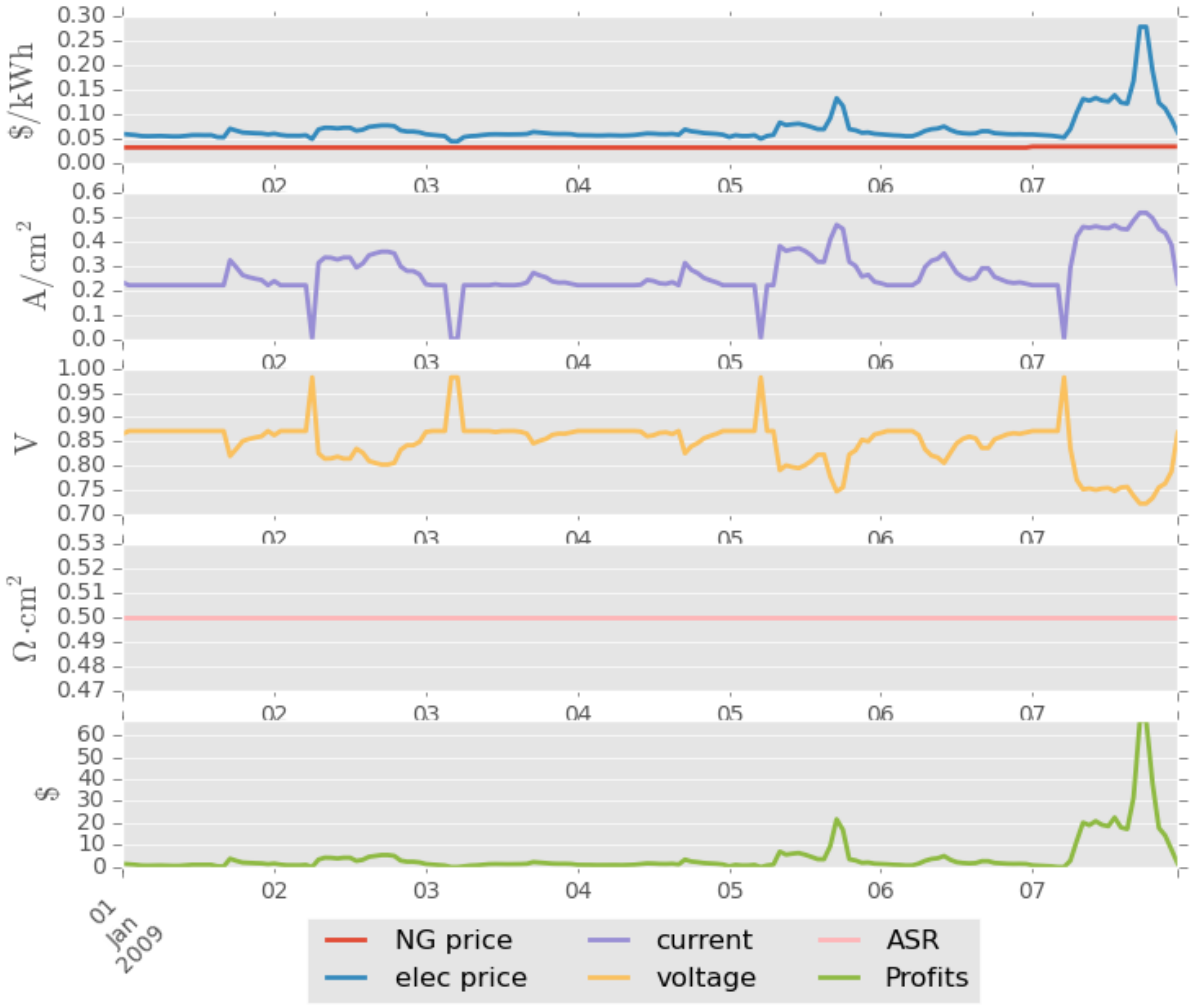

Figure 5.17: System profile Jan 1st - Jan 7th 2009.

Fig. 5.18 shows a time-series for the week of September 8-14 of 2011. This is an interesting week as it highlights the inherent value that can come from operating reversibly when prices swing. As shown by the price series panel, there are many instances in which the price of electricity dips below the price of natural gas which

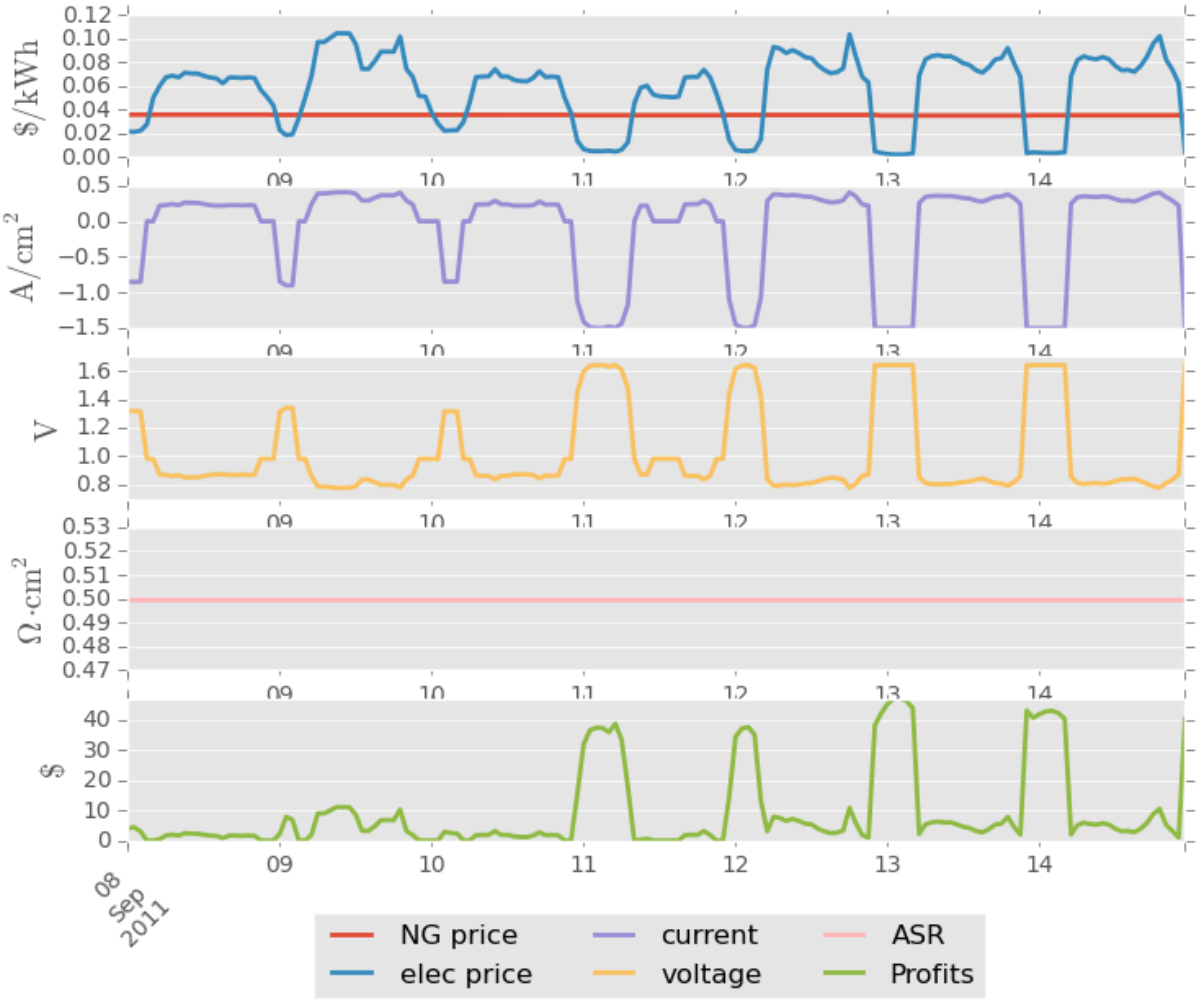

Figure 5.18: System profile Sep 8th - 14th 2011.

opens the possibility for operating in electrolysis mode. For this particular week, the system spends 23% of its time in electrolysis mode, 14% of the time in idle mode, and 63% of the time in fuel cell mode. One interesting aspect of this particular week is that not only do the prices fluctuate constantly and dip below the price of natural gas, but the magnitude of the swings is pretty large which means that fuel cell operation will occur at relatively high current densities. Lastly, it is worth highlighting certain aspects of the profit time-series. From looking at the last panel of the figure, it

becomes clear that operating in electrolysis mode is more profitable than operating in fuel cell mode. The main reason behind this is that the operating current densities of the electrolysis mode tend to be much higher than those of the fuel cell, even though it means operating at low efficiencies. For this particular week, during certain hours of the day the price structure is so favorable to electrolysis that the system operates at the limit of $-1.5\,\mathrm{A/cm^2}$ even though that means operating at net system efficiencies of about 45%. As a matter of fact, of the $1572 generated during the September 8-14 period, 73% of them are generated during electrolysis mode, which highlights the value that reversibility can have in periods of low electricity prices.

Fig. 5.19, which represents a series for the 23rd-29th of April of 2013, highlights a week of the year in which the optimum operating strategy is to idle most of the time. Even though prices fluctuate and the price of electricity tends to be above the price of fuel, the spread between them is too small to trigger fuel cell operation. For this particular period, the system idles 86% of the time. The remaining 14% is broken down into 11% fuel cell mode and 3% electrolysis. Even though the profits generated by this week are extremely low, just as in the case described in Fig. 5.18, the lion's share of the profits are generated while operating in electrolysis mode (see bottom panel of Fig. 5.19).

Lastly, figure Fig. 5.20 shows a time-series for the 15th-24th of December 2014. The first thing that we notice from this series is that the system never operates in fuel cell mode, and spends 31% of the time in electrolysis mode and 69% idling. When inspecting the price time-series it can be see that the price of electricity for these dates tends to be quite low, with an average price of just $0.02/kWh. As a matter of fact about 8% of the time the price tends to be negative, which helps explain the large profits at a few points in time and the high current densities at which it is operating. Due to the existence of negative prices, the profits made during this week are $2480 which is quite high compared to other weeks.

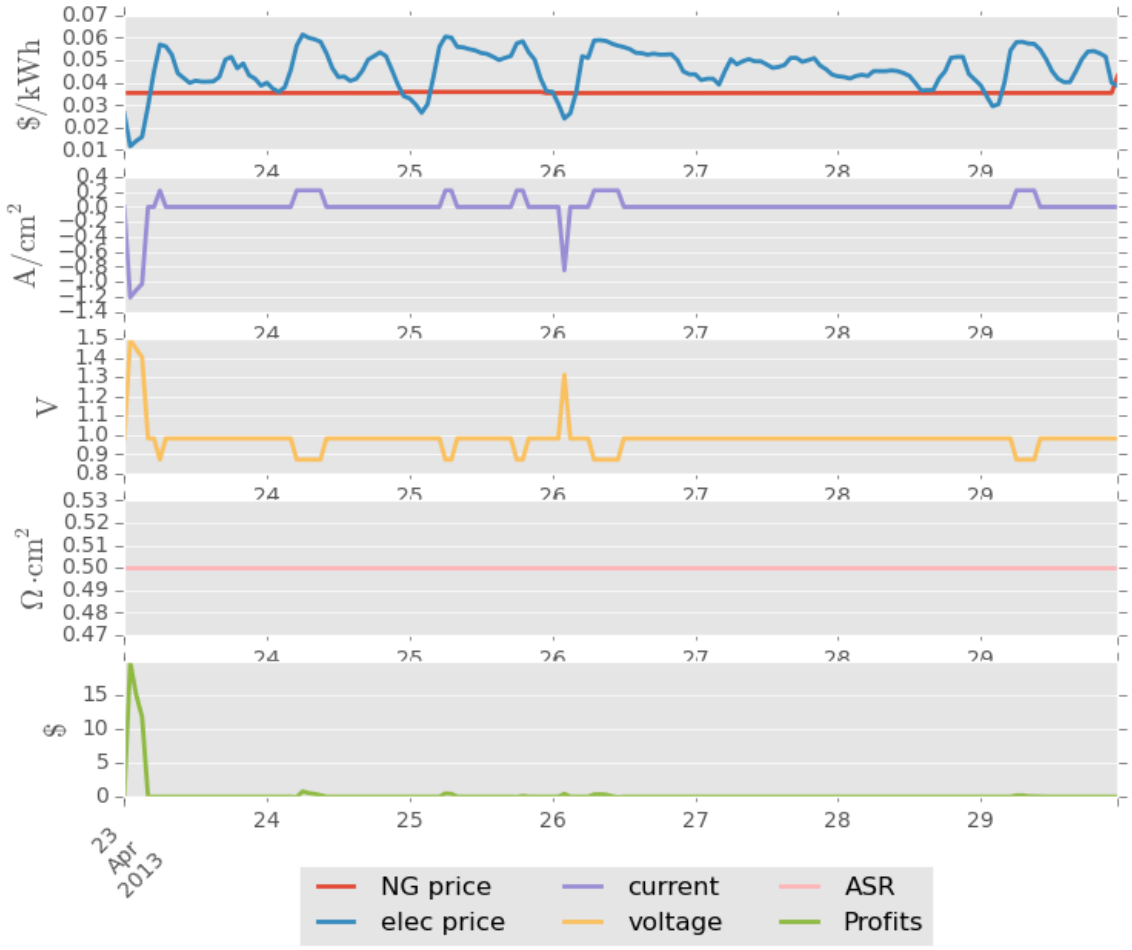

Figure 5.19: System profile April 23-29 2013.

It is important to mention that for the base case presented above, the RSOC system did not exhibit any degradation throughout its lifetime and thus its aging did not affect its efficiency and did not influence the BoP requirements.The impact that degradation has on the optimum operating strategy and the overall system costs is developed in Section 5.3.5.

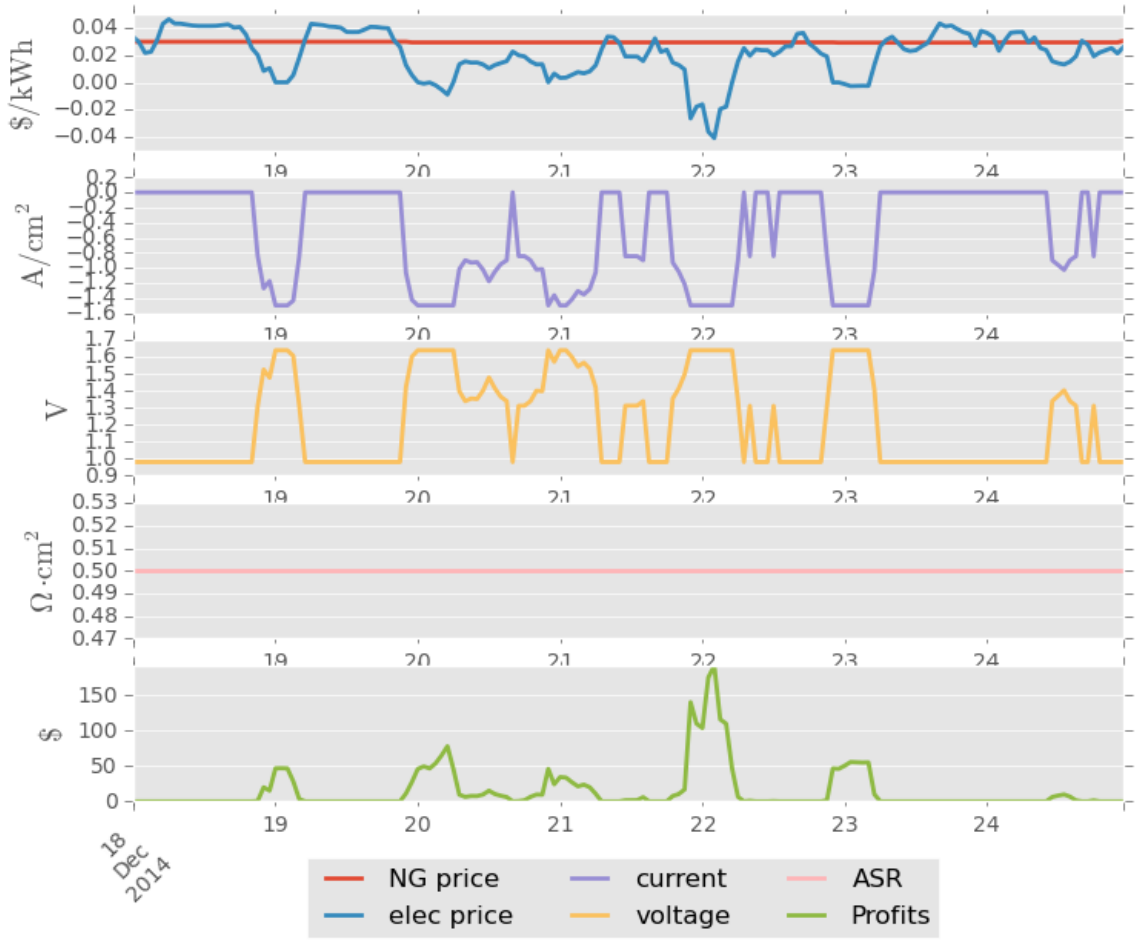

Figure 5.20: System profile Dec 18-24 2014

5.3.2 Base case (Rev-BC): yearly analysis

In Section 5.3.1, the results for four different weeks from the optimization of the RSOC system were presented in order to show how the system responded to different price structures across time. In this section, results of the optimization for the period 2009-2014 are presented on a yearly basis. Rather than highlighting results of individual weeks, the main focus of this section is to aggregate the hour-to-hour results and present the optimization results from an overall perspective. Fig. 5.21 shows the % of time that the RSOC spends on each mode for the 6 years of operation. As the

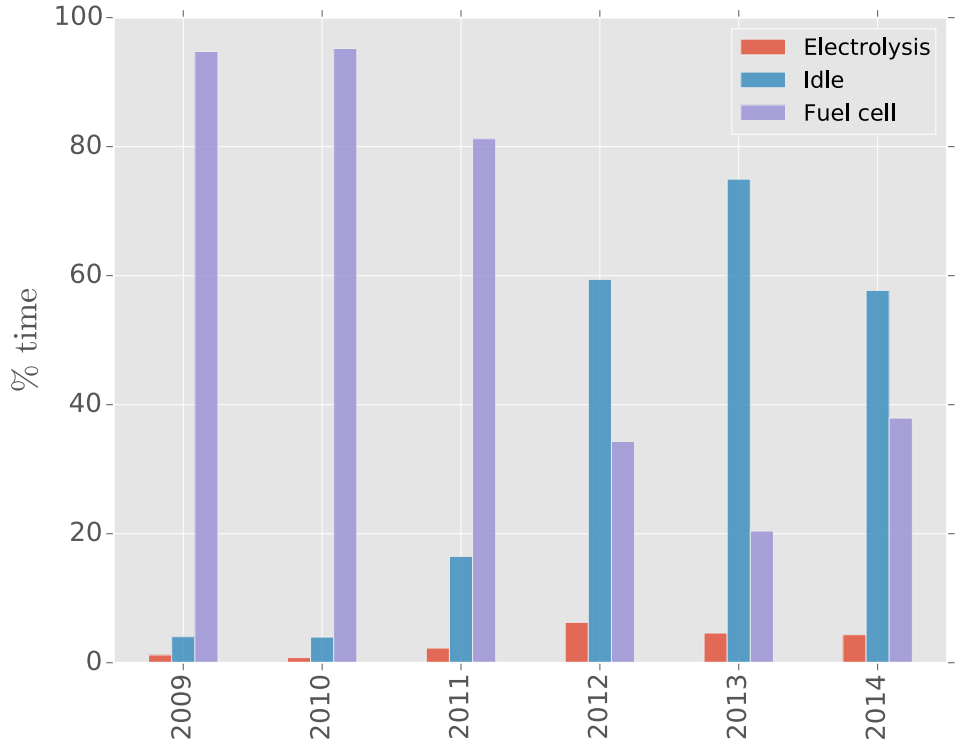

Figure 5.21: Mode of operation per year

figure suggests, during the first three years of the series the system spends most of its time in fuel cell mode. Starting in 2012, the system spends more than 50% of the time idling and 2013 represents the year for which it idles the most. As described in previous sections, the system idles when it can't make a profit by operating as either a fuel cell or an electrolyzer. Thus, if the system is idling most of the time it is because the electricity and fuel price structure does not offer a big enough spread to operate at the highest possible efficiency (lowest aggregate output). On aggregate, electrolysis operation occurs 3.25% of the time, idle 36%, and fuel cell 60.75% of the time. Fig. 5.22 shows the yearly profits of the RSOC system per year. The first thing to notice is that yearly system profits drop year on year. This is to be expected, as Fig. 5.21 suggested that the system spends more time idling in the later years. Nonetheless, the change in profitability is quite dramatic. For the six years of

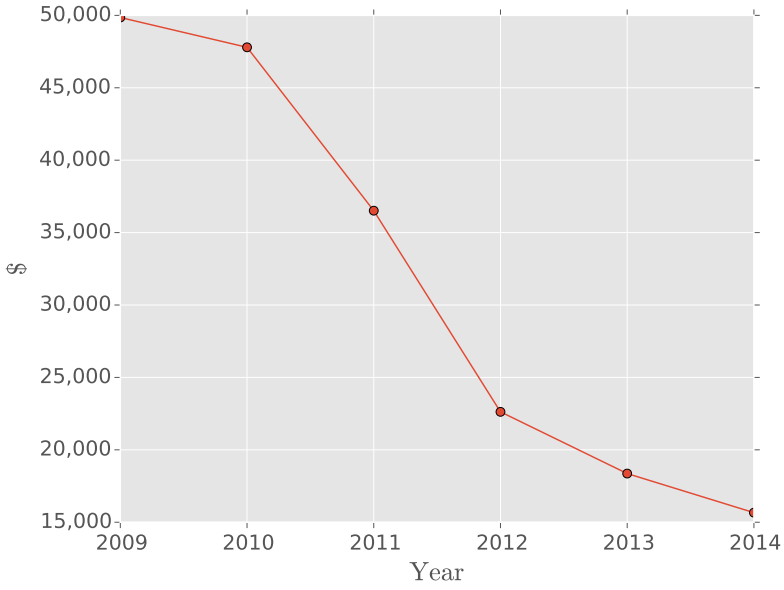

Figure 5.22: 2009-2014 base-case optimization yearly profits.

operation, the cumulative profitability is $190,805 and the % contribution for each year is shown in figure Fig. 5.23. As suggested by this figure, roughly 50% comes from the first two years of operation. In contrast, the last two years of operation represent about 20% of the total profits. It is important to highlight that for the basecase, no degradation of the cell is assumed thus the system does not become inherently more inefficient with time. When degradation is considered (see section Section 5.3.5 blow), a critical question when analyzing the financial return of the system (e.g. once the investment costs are included) is whether it would pay to replace the cell at some point during the study period in order to maximize the NPV of the system. Put another way, absent catastrophic failures that inflict irreversible damage, how should the lifetime of the RSOC stack be evaluated.

Figure 5.24 shows the capacity factor for each year of operation. Given that the system can operate both as a fuel cell and an electrolyzer, in this the capacity factor is obtained by summing all the hours in which the system operates either as a fuel

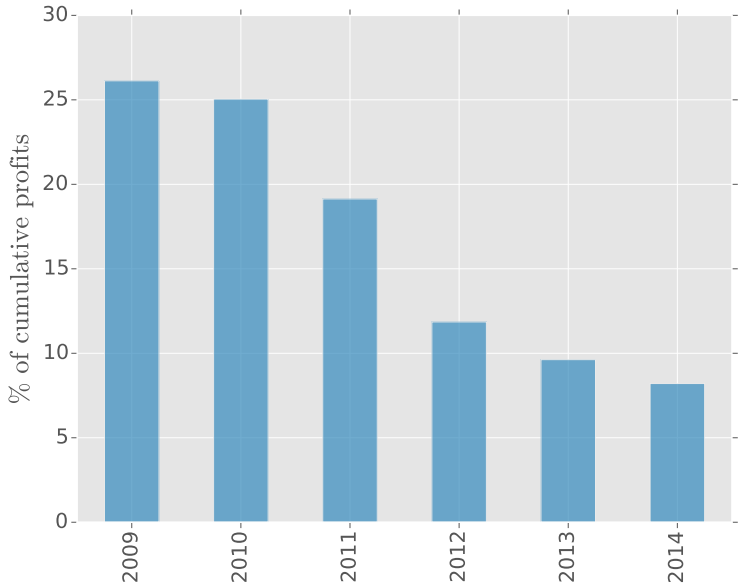

Figure 5.23: Percent contribution of each year to 6 year cumulative profits

cell or as an electrolyzer and dividing it by the number of hours in the year. As it can be seen, the first three years of operation has relatively high capacity factors, while the last three have particularly low capacity factors. It is important to keep in mind that the capacity factor itself does not tell you anything about the profitability of the operation, but just gives you an idea of what percentage of the year the system is running. Assuming the system is running, the profitability will be determined by the particular price structure of electricity and natural gas, the cost of CO_2, as well as other system parameters such as the ASR and the degradation rate. The contribution of each mode of operation to the yearly profits is shown in Fig. 5.25. The results laid out in this chart are quite surprising. Recall from Fig. 5.21 that at in the early years, fuel cell operation is more common than electrolysis mode which never occurs more than 8% of the time. Yet, Fig. 5.25 suggests that the contribution of electrolysis to the total profits becomes a critical component of the yearly profits. In 2014, electrolysis mode represents 65% of the total profits even though it only operates 5% of the time.

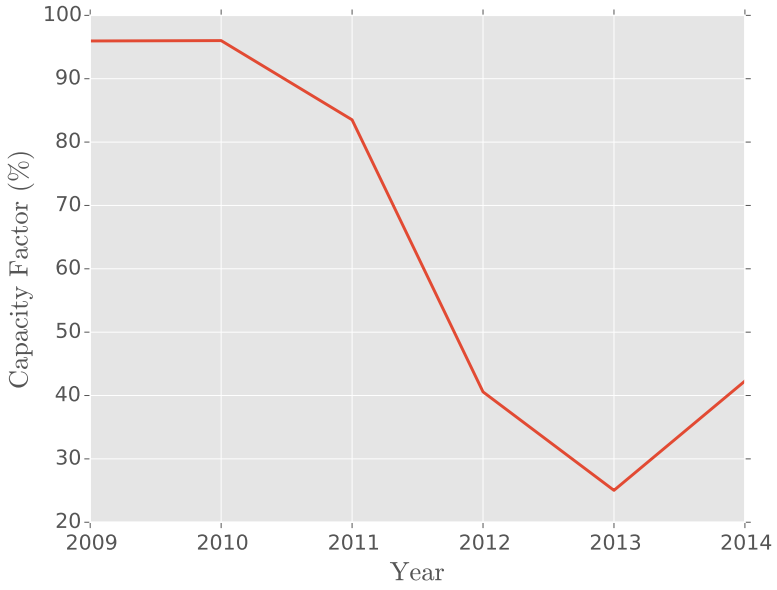

Figure 5.24: Yearly capacity factors for the Rev-Base simulation

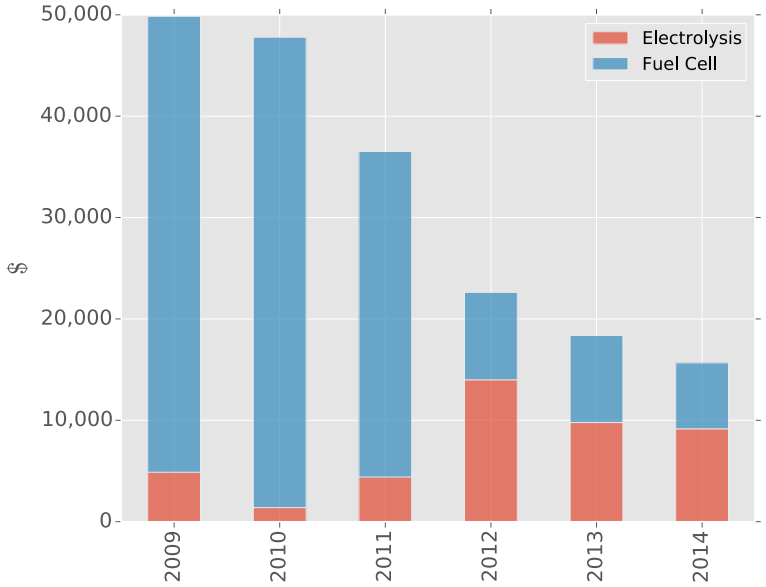

Figure 5.25: Contribution of each mode of operation to yearly profits

5.3.2.1 The contribution of negative prices

In the previous section it was shown that as the fraction of wind has increased in the Danish electricity grid, the contribution of electrolysis mode to overall system profits has increased (see Fig. 5.25). At the same time, inSection 5.1.1.2 it was shown that negative electricity prices have been occurring with more frequency as the fraction of wind has increased throughout the years. Thus it seems appropriate to analyze what the contribution of negative prices is to the yearly profits. The first thing to recall is that even though their frequency has been increasing with time, they are still relatively rare events occurring less than 1% of the time. One would be tempted to think that their contribution to overall system profits would be marginal at best. This, however, is not the case. Fig. 5.26 shows the contribution of negative and non-negative prices to electrolysis profits for each year in the time-series. The figure is quite revealing and surprising. It suggests that for the years analyzed in the time-series , the rare moments in which negative prices occur represent 44% ($25314) of all the profits generated during electrolysis mode, even though they only represent 7% of the hours spent in electrolysis mode. Furthermore, the ($25314) represent roughly 12% of the total system profits, even though negative prices occur less than 1% of the time. This result is quite astonishing and sheds some light into the value that can be derived from exploiting low frequency events such as negative electricity prices.

5.3.2.2 Full plant cost analysis: base-case (Rev-BC)

The results presented in the previous sections highlight the operational profits that the RSOC system attains for the years 2009-2014 given a wide variety of assumptions such as initial ASR, degradation rate, and the price of CO_2. It is important to highlight that these results only give us a glimpse of the plant profits, as the investment costs are treated as sunk costs and therefore do not influence the optimal operating strategy. That is, the decision of how and when to operate is purely based on marginal costs

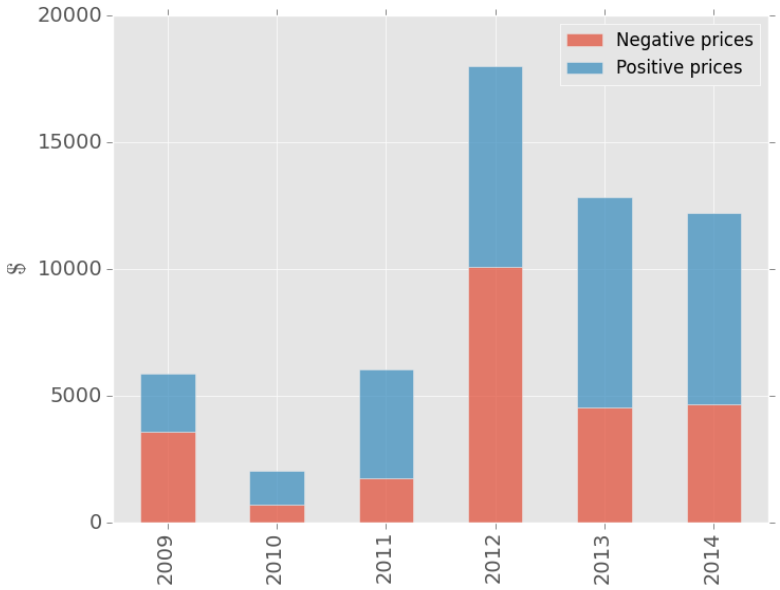

Figure 5.26: Contribution of positive and negative electricity prices to total electrolysis profits

(e.g. fuel and electricity). However, in order to get the full picture regarding the system's profitability from an investment point of view, CAPEX costs associated with the RSOC system and the impact that different strategies have on the BoP and its associated investment cost must be considered. In this section we analyze the results presented above in conjunction with the total plant cost (TPC).

Calculating the TPC is not a straight forward task and it inevitably involves large uncertainties. In order to come up with the TPC for each of the scenarios described above, we employ the cost model discussed in Section 3.6. As expected, each of the components will have to be sized according to the assumptions for the specific simulation/scenario that is being investigated. For illustrative purposes, all the component costs for the base-case RSOC simulation (Rev-BC) as well as the sizing variables and their corresponding values are shown in Table 5.3. It is important to highlight that even though the methanation catalyst tends to have a lifetime of $\sim 25,000$hrs [47], due to the fact that the system spends so little time in electrolysis

mode under the base scenario (< 3% of the time), we assume that the lifetime of the catalyst is extended by a factor of 3, giving it a lifetime of 10 yrs. The same idea is applied to the monolith structures, which typically have shorter lifetimes. Again, we assume a lifetime of 10 years due to the little usage that they have under this scenario.

Given that the RSOC has a much shorter lifetime than other components ($\sim$ factor of 4 difference), stacks will have to be replaced throughout the lifetime of the plant. Thus, even though the HeX network represents a higher portion of the initial investment, the fact that the components have such different lifetimes makes the comparison somewhat misleading. In order to solve this problem, each component in the system is annualized as explained in Section 3.6. This, in effect, allows for a "true" contribution of each component to the TPC to be performed.

Fig. 5.27 shows the breakdown of the annualized TPC aggregated by component type. For the base case, the annualized TPC is \$153,551 or \$1,543/m^2. The first thing one notices is that the the equipment used for managing and exchanging heat (HeX's, evaporators and condensers) represent roughly 50% of the TPC. The heat exchange equipment (air and fuel pre-heaters) constitute 23.8% of the TPC, while the evaporator represents 19.8%. At the same time, we see that the RSOC cost (including assembly) is 14.3% and once we include the installation and piping and the inverter the cost associated with the electrochemical section of the plant is roughly 35% of the total cost of the plant. The methanation section itself is less than 4.8%.

A closer look at the cost breakdown in Fig. 5.27 suggests a series of paradoxical results. First, it indicates that the equipment used for evaporating water is more expensive than the technology used to for splitting water into H_2 and O_2 (RSOC). It also suggests that the system used for transferring and recycling heat (heat exchangers) is also more expensive than the electrochemical stack. At a first glance this might look like a computational mistake, however these paradoxical and counterintuitive

Component	Sizing variable	Lifetime (yrs)	Cost ($)	Annualized Cost ($)
Fuel preheater	2 m^2	20	20,650	1,949
Fuel pump	1.47 kW	20	36,170.0	3,414
Air preheater	144.6 m^2	20	216,948.	20,478
Steam preheater	29.7 m^2	20	136,955	12,928
Methane compressor	37.14 kW	20	55,630	5,251
Feed pre-conditioner	2 m^2	20	11,526	1,088
SOC	100 m^2	6	100,000	20,979
Balance of Stack	100 m^2	6	1,214	254
Stack Assembly	100 m^2	6	3,146	660
Air blower	1,976.4 $ft^3 min^{-1}$	2.5	3,065	1,379
Air blower (Methanator)	1,490.4 $ft^3 min^{-1}$	2.5	2,588	1,164
Air blower (EL)	6,079.536 $ft^3 min^{-1}$	2.5	6,016	2,706.42
Catalytic Combustor	1.44 $kg\,s^{-1}$	2.5	430.0	193.0
Inverter	2410 kW	20	196,303	18,529
Evaporator	0.55407 ton hr^{-1}	20	321,458	30,343
Electric heater (feed)	28.04 kW	20	12,175	1,149
Methane electric heater	23 kW	20	10,186	962
Electric heater CO2	20.18 kW	20	9,055	855
Monoliths	0.92 m^3	10	1,241	855
Monoliths housing	2.77 m^3	20	14,605	1,378
Catalyst	11,296 g	10	41,593	5,922
Water condenser	0.29484 ton hr^{-1}	20	77,867	7,350
Insturmentation and control	2410 kW	20	82,223	176.75
Piping and valves	2410 kW	20	75,382	7,116
Annualized TPC:	**$153,551**			

Table 5.3: Component costs and TPC for base-case scenario. All values in $2009 dollars. Interest rate set at 7%

results are likely due to the fact that the costing heuristics used for calculating the TPC have been developed for very large scale chemical processes, where unit scale is the main driver for reducing costs. As a consequence, when these techniques are applied to much smaller systems they can result in counterintuitive numbers. The methane based RSOC system presented herein is very small compared to traditional power and or chemical infrastructure, which helps explain why the cost of some of these components might seem expensive when compared to the solid oxide stack. For reference, in fuel cell mode the system generates roughly 317 kW of electric power

which is 1,577 times smaller than the typical (500 MW) coal fired power plant. At such differences of scale, it is not surprising that some of the equipment costs become very expensive when compared to components which do not rely on unit scale for cost reductions, as is the case of the RSOC[3]. Thus, it is important to treat these numbers conservatively and to acknowledge that even though they represent best engineering practices, they could easily change if the components were designed and mass-manufactured for small scale applications. Indeed, as work by Dahlgren et. al [21] suggests, in certain cases the mass-manufacturing of small-scale components can lead to larger cost reductions than those attained through traditional economies of unit scale. Although the study of cost reduction via mass-manufacturing is outside the scope of this work, it is important to keep in mind that lower system costs could be achieved when using different scaling and development paradigms.

As explained before, the cost of each component is annualized using an annuity formula eq. (3.68) and the total plant cost on an annualized basis (TPC_{yr}) is simply the sum of all annualized system components. Thus, the total annual profit for the RSOC system at year n, $\Pi(n)$, is computed by subtracting the annual operational profits (π_n)from the annualized total plant cost:

$$\pi_n = \sum_{t=8766(n-1)}^{8766n} \pi(t,i) \tag{5.9}$$

$$\Pi(n) = \pi_n - \text{TPC}_{yr} \tag{5.10}$$

It then follows that for an investment to break even, $\pi_n = \text{TPC}_{yr}$. Using the values reported in Table 5.3 and the results from the base-case simulation, the annual operational profits, the annualized total plant costs and the total annual profits are plotted in Fig. 5.28.

As seen in Fig. 5.28 there is a big discrepancy between the profits that the system makes and the annuity that must be paid for the investment. For the base case

[3]see Section 3.6.1 for a discussion on cost reduction for the SOC stack

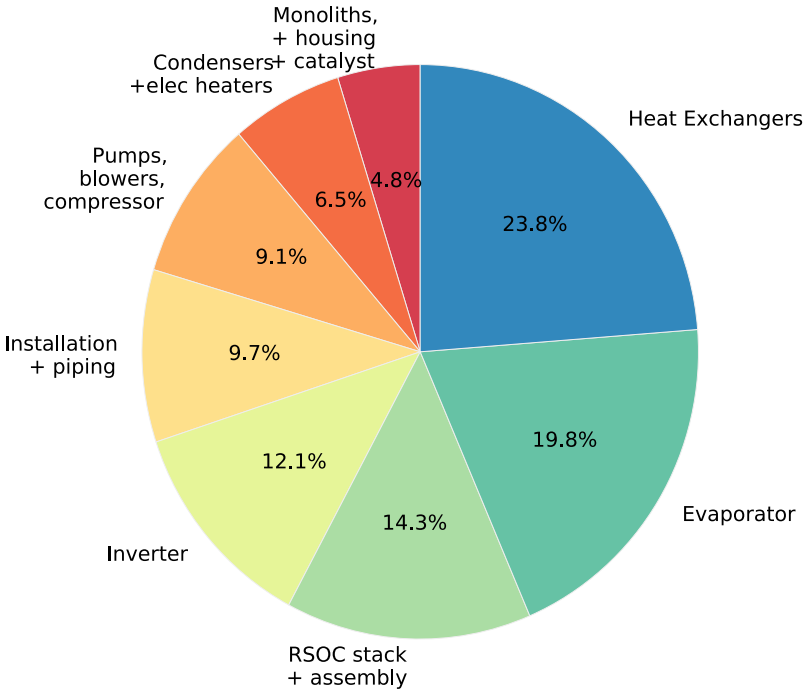

Figure 5.27: Break-down of TPC for Rev-BC simulation. Annualized TPC: $154,113

(Rev-BC), there is no year in which the system can break-even. As a matter of fact, during the highest grossing year (2009) the system is only able to make a profit that represents $\sim$ 30% of the investment annuity. As discussed in the previous section, the system profits diminish year-on-year thus the total plant profits become more negative, while the annuity stays constant. That is, the cash generated by the system decreases while investment costs stay constant.

The main driver of this behaviour is not the low capacity factors that the system exhibits in the later years, after all the first two years have capacity factors $> 90\%$ and the system is still unable to break even, but rather the electricity and natural gas prices in the Danish system for the years analyzed. Generally speaking, the prices of

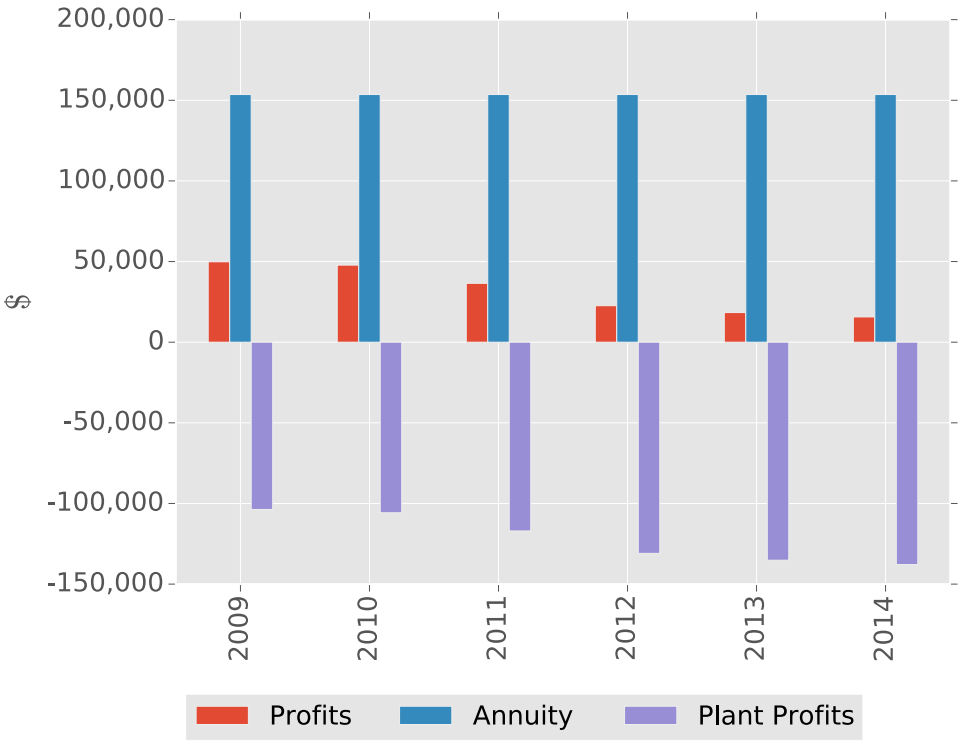

Figure 5.28: Yearly operating profits, annualized CAPEX and plant profits for Rev-BC simulation.

electricity are too low (relative to gas) for fuel cell operation to be attractive, and are too expensive for making synthetic natural gas. This has important consequences, as it suggests that under the given set of CAPEX costs and the existing price structure, a distributed RSOC system that makes fuels and/or electricity and sells it in the energy only spot markets *is not economically feasible*.

As mentioned in 5.1.1.1, in the Danish Electricity Market Primary, Secondary and Manual Reserves are bundled into Ancillary Services which can provide an extra source of revenue for generating units in the electricity market. Due to the lag associated with the thermal response of Solid Oxide Cells, RSOC are not well suited for Primary Reserves that provide frequency control services which require response times of less than 30 seconds. In the Danish Electricity Market, Secondary and Man-

ual Reserves require response times of 15 min, which can be achieved by SOCs [3, 95]. Because of the nature of RSOC systems, rapid system response will largely be limited by the thermal inertia of the system and the interactions between BoP components and the RSOC stack. In Denmark, Manual Reserves are procured on an hourly basis by the TSO via a daily auction that takes place one day in advance in which bidders submit hour-by-hour volumes and prices for upward and downward regulation and each winner receives two payments: the equilibrium price resulting from the auction for the regulating MWs won plus a payment for the energy generated/consumed, which is settled at the hourly spot price.

For the time period studied and under the base-case assumptions, RSOC are not profitable investments when they only participate in the electricity and fuel spot markets. Although the inclusion of regulating service revenues is outside the scope of this dissertation, given the economics of RSOC systems under the current market structures in the Danish markets, offering upward/downward regulation can become an important revenue generator that will surely help the overall economics of the system. Therefore, the economic analysis presented in the previous sections can be thought of as a very conservative case in which no capacity payments are procured in the market, and therefore it does not consider all the value that RSOC can provide to the electricity network. Indeed, given that RSOC can easily consume energy by switching to electrolysis mode, or provide dispatchable power by running in fuel cell mode, this infrastructure is ideally suited for providing upward/downward regulation for the Danish market. It is important to highlight the value that his can have, as increasing the penetration of variable renewable energy in the system will inevitably depress the wholesale price of electricity which will make it harder for the system to recover its costs when its only source of revenue is the day-ahead electricity market. As the energy system evolves over time to one in which variable renewable electricity is the main source of power, flexible systems that can provide dispatchable power

and/or a sink for excess electricity will be of great value. In this sense, RSOC are very well suited for providing useful services to the network of the future.

If the existing investment costs are too high and the spot market prices too low, could changes in the underlying assumptions make the system attractive from an investment perspective when only revenues from the spot fuel and energy markets are considered? In the next sections, a series of simulations where the underlying assumptions and/or strategies are modified in order to assess what could make the system more attractive from an investment point of view. Before delving into this analysis, a brief discussion on the "value" of reversibility is offered by comparing the "optimum" plant profits that were discussed in this section with the cases in which the system is operated at fixed points and modes.

5.3.3 Fuel cell only operation

In order to assess the value that operating a stack reversibly and at multiple points can have, it is important to compare against a baseline for fuel cell only operation. This case can then be used to compare against the results from the previous section (Section 5.3.2) in order to have a better picture of the economic gains that can be achieved by the optimum operating strategy that has been described before.

Using the assumptions described in Table 5.1 a fuel cell only simulation at fixed voltage and current is performed using the electricity and fuel prices for the years 2009-2014 (same as the Rev-BC simulation). Because the system has different efficiencies and power outputs at different operating points, Figure 5.29 shows the results for simulations at 0.3, 0.4 and 0.5 A/cm^2, which corresponds to voltages of 0.83, 0.78 and 0.73 V respectively. As seen from this graph, operating at 0.3 A/cm^2 results in the highest operational profits ($\sim \$110,000$) given the fuel and electricity prices for the time-series analyzed. Thus, this current density is chosen as the operating point. It can be seen that the \$110,000 represents roughly 57% of the operational profits

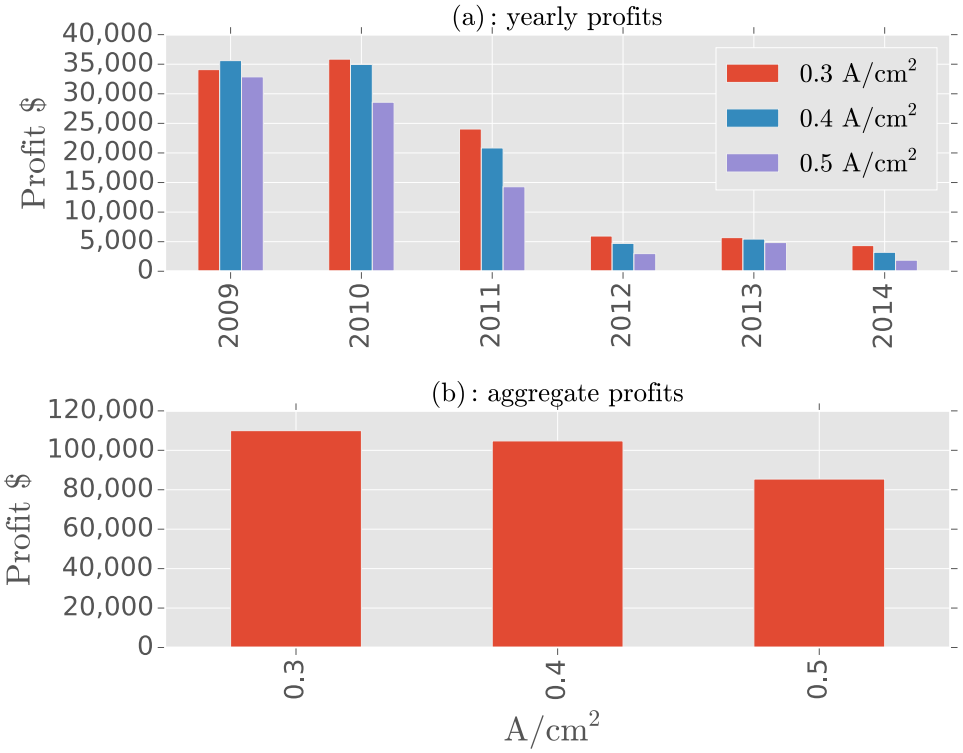

Figure 5.29: Fuel cell only: (a): yearly profits for different operating currents; (b): aggregate profits for different operating currents

of the reversible system with variable operation ($\sim \$190,805$). However, due to the fact that the fuel cell only case does not require the electrolysis ancillary equipment (methanator monliths, compressor, heaters), the TPC will vary from the RSOC system. Thus, in order to do a proper comparison, the TPC for the fuel cell only case must be computed.

Figure 5.30 shows the breakdown of the annualized TPC for the fuel cell operating at 0.3 A/cm^2. For the case of the fuel cell only operation, it can easily be seen that the system has two main cost drivers: the cost of the stack and its peripherals and the cost of the pre-heaters (heat exchangers). The former represents $\sim$ 46% of the TPC, while the heat exchanger system (feed and air pre-heaters) account for 36.2% of the TPC. Together, these two categories represent about 80% of the TPC.

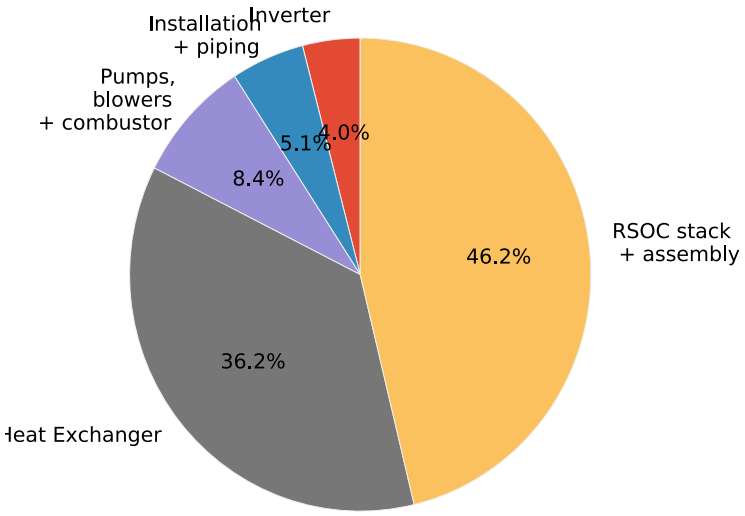

Figure 5.30: Breakdown of TPC for fuel cell only mode. Annualized TPC:$47,501

Using the method described in previous sections, the annualized cost of the plant is \$47,501 or \$475/m^2. It is worth comparing the annualized TPC for the fuel cell only case against that of the RSOC system (153, 551), which suggests that the investment cost for the fuel cell only case is about 3 times less than that of the fully reversible system. For the 6 years analyzed, Fig. 5.31 shows the yearly operating profits, annualized TPC and the plant profits for the fuel cell only system.

As with the reversible system, the fuel cell only case is unable to generate a profit on any of the years it operates. Although the current fuel and electricity price structure in the Danish markets favor the operation in fuel cell mode over electrolysis (see Section 5.3.2), the spread between the electricity and gas prices is very narrow and therefore not much money can be made. Although the system is unable to make a positive profit on any of the years, the cumulative losses for the 6 year time series are -\$175,000 while for the reversible base case discussed in the previous section the

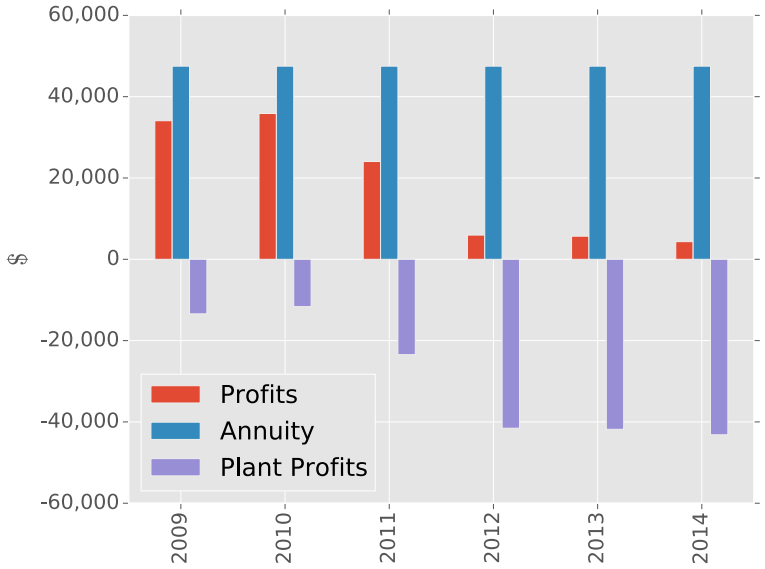

Figure 5.31: Yearly operating profits, annualized CAPEX and plant profits for fuel cell only optimization.

cumulative losses amount to -$730,000. This suggests that given the current electricity and fuel prices in the Danish markets, the ability to operate reversibly is not very attractive. This, of course, can change if technology sees major cost reductions, the system is further optimized to boost yields and efficiency, and/or if the underlying market structure changes.

5.3.4 Sensitivity to ASR (Rev-ASR)

As discussed in Section 4.2.2 and Section 4.2.2 variations in ASR lead to changes in the cell's efficiency and its total power output (fuel cell mode) and total load (electrolysis mode) for a given operating point. As such, it is important to understand how the results of the price optimization change with varying ASR. Using the assumptions presented in Table 5.1 4 simulations, with initial ASR of 2, 3, 4 and 5 Ωcm^2 are carried out. In all simulations, the operating current is limited to -1.5 A/cm^2 for electrolysis mode and 0.6 A/cm^2 for fuel cell mode. A discussion on the impact of

modifying this constraint is provided in Section 5.3.4.2

Figure 5.32 shows the yearly operating profits for each one of the simulations. As

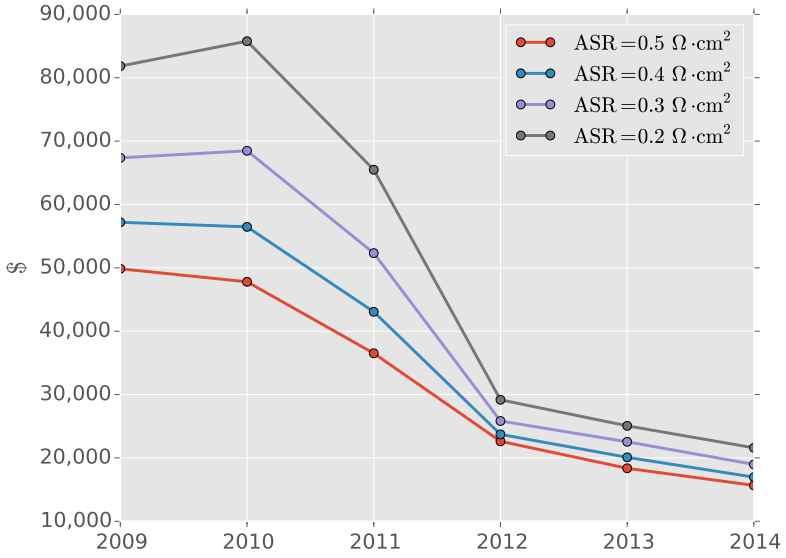

Figure 5.32: ASR sensitivity: yearly operational profits for different initial ASR assumptions

expected, the lower the initial ASR the higher the yearly profits tend to be. This is particularly true for the first three years (2009-2011). For example, the difference between the operational profits in 2009 between the simulation with initial ASR of 0.2 Ωcm^2 and the one with ASR of 0.5 Ωcm^2 is $\sim \$32,000$, which is roughly the same amount that the system with ASR of 0.5 Ωcm^2 makes for the years 2013 and 2014 combined. For the later years, the difference between the lowest and highest ASR simulations are smaller (both in magnitude and as a percentage), which is mainly due to the fact that during these years the system idles for the majority of the time (see Fig. 5.24). The other thing worth noting from Fig. 5.32 is that as the ASR is lowered, the cumulative profits of the year 2010 increase faster than those of 2009, thus for ASR values that are less than or equal to 3, 2010 becomes the year that generates the highest operational profits.

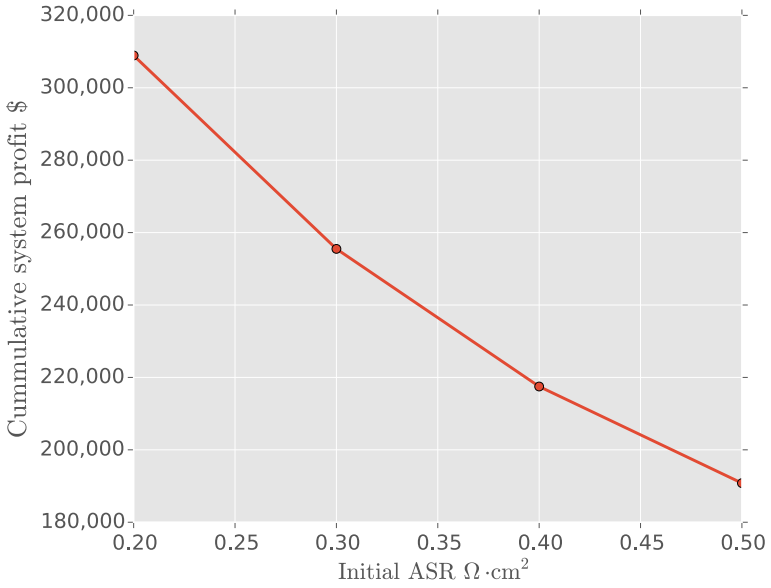

Figure 5.33: ASR sensitivity: Cumulative yearly operational profits for different initial ASR values

Fig. 5.33 shows the cumulative operating profits for the whole time-series for each simulation ASR. As it can be seen from this plot, the cumulative profits vary dramatically across different initial ASR values. The differences between the lowest initial ASR (0.2 Ωcm^2) and the highest (0.5 Ωcm^2) represents an increase of 60% in cumulative profits, which is quite striking. The economic gains from having stacks with lower ASR go beyond the increased operational profits, as the cost of the BoP will also vary considerably. The impact of initial ASR on the system's CAPEX and the total plant profits is discussed in the section below.

5.3.4.1 Full plant cost analysis (Rev-ASR)

As discussed in previous section, in order to assess the profitability of an investment in a system such as the one described herein it is important to consider the total investment costs associated with the capital expenditures. In Chapter 4 it was shown that changes in ASR have an impact on the heat generated by the system, and

Equipment Category	**ASR 0.5** (%)	**ASR 0.4** (%)	**ASR 0.3** (%)	**ASR 0.2** (%)
Heat Exchangers	23.76	22.59	20.56	15.045
Pumps, blowers, compressor	9.07	6.71	6.87	7.45
Monoliths + catalyst	4.80	5.16	5.45	6.0
Evaporator	19.79	21.3	22.51	24.8
Installation + piping	9.70	9.81	9.5	9.49
RSOC + assembly	14.28	15.36	16.24	17.88
Condenser + heaters	6.51	7.01	7.41	8.16
Inverter	12.08	12.06	11.46	11.2
TPC	**$153,551**	**$142,552**	**$134,869**	**$122,501**

Table 5.4: Contribution of each equipment category and TPC at different ASR

therefore it will have consequences with respect to the sizing of the equipment in the BoP. Because the temperature of the stack is maintained constant by sweeping excess air through the oxygen electrode, as less heat is generated by the stack the air pre-heaters will decrease in size for a given design point. For the base case analysis, it was shown that one of the key drivers of the TPC is the cost of the heat exchangers (see Fig. 5.27), thus if less sweep air is required for smaller inital ASR's, then this can have an important impact on the investment cost of the system.

Table 5.4 shows the cost % for each of the major equipment categories for the four different initial ASR simulations. As it can be seen from this figure, as the initial ASR is lowered, the contribution of the heat exchange network becomes less important. For the base case, which corresponds to the highest initial ASR, the heat exchangers represent 23% of the annualized TPC. In contrast, when the ASR is lowered to $0.2\Omega\text{cm}^2$, the contribution of the heat exchangers to the TPC is reduced to 14%. As a consequence, the the SOC and the evaporator become much more important and for the low ASR case they represent 16% and 23%, respectively, of the annualized TPC. From Table 5.4 we can see that, as described above, the reduction in ASR results in a decrease in the size of plant components which reduces the TPC. Under the base case assumption (ASR = $0.5\Omega\text{cm}^2$) the annualized TPC $\sim 153,551$

and for the smallest ASR this drops to $\sim 122,501$, which represents a 20% reduction.

A full picture can be appreciated in Fig. 5.34, which shows the operating profits, annuities and plant profits for all ASR simulations. From this figure we can appreciate

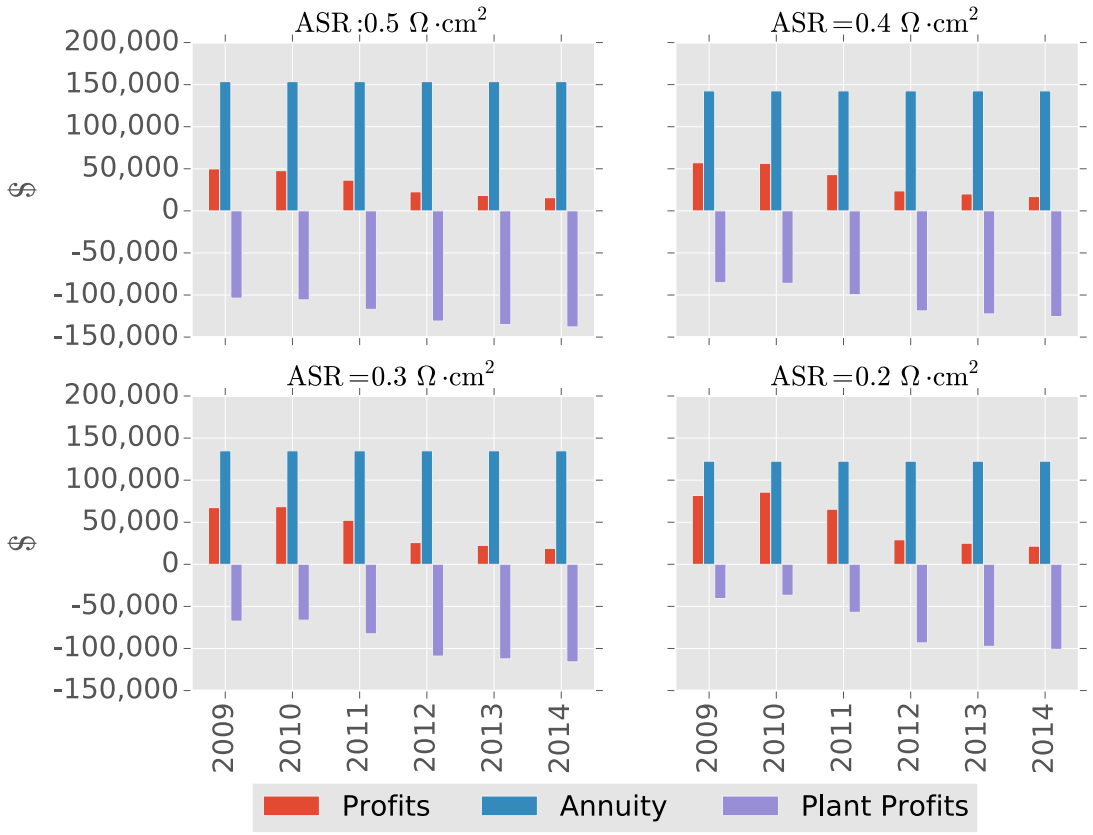

Figure 5.34: ASR sensitivity: Operating profits, annuities and plant profits for different initial ASR.

that the lowering of the ASR has an impact on the operational profits (red bar) apart from the impact that it has on the TPC annuity. Recall from Chapter 4 that as the ASR is lowered the efficiency increases across all operating currents, which in turn means that for a given fuel and electricity price at time t operating a lower ASR will result in the ability to operate at higher currents, generating more electricity or fuel for a fixed electricity/fuel price pair. In other words, lowering the ASR means more output (and thus higher profits) for any given t in which the system operates

while also lowering the BoP investment costs due to less handling of heat and air. Figure 5.35 shows the power output and operational profits for the first week of 2009

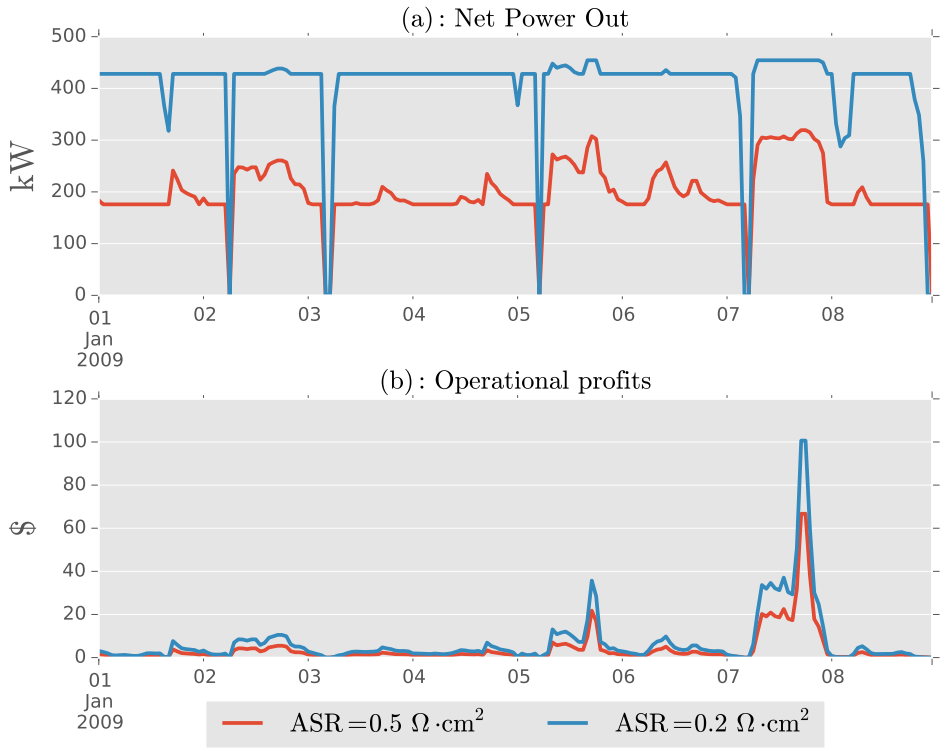

Figure 5.35: Net power out and operational profits for first week of January 2009 for different initial ASR.

for the highest and lowest initial ASR simulations. As it can be seen, the power generated by the system follows the same trends except for the fact that at 0.2 Ωcm^2, the output is much higher which in turn increases the operational profits. For very favorable moments in time, the ability to operate at higher outputs can make an enormous difference in the total operational profits . For example on January 7th, the peak profits go from $\sim$ \$66/hr to $\sim$ \$100/hr. This difference, accumulated over the lifetime of the device can make a big difference as seen in total yearly profits depicted in Fig. 5.34. Finally, Fig. 5.36 shows the cumulative plant profits for the whole time-series for different initial ASR values. As it can be seen, under the current

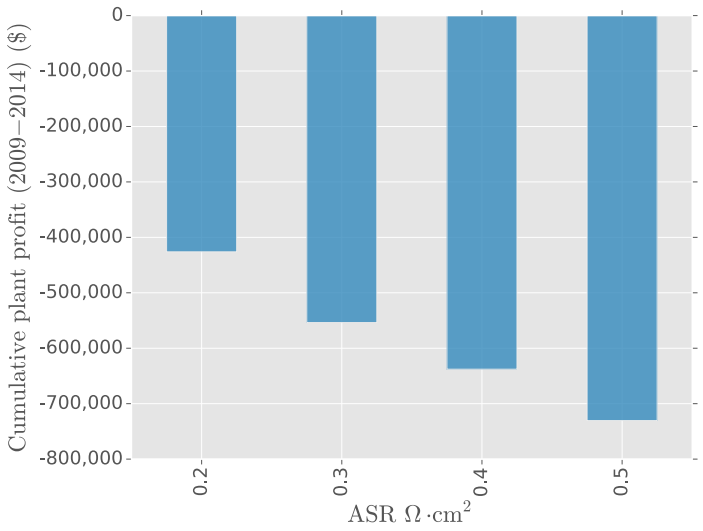

Figure 5.36: Cumulative total plant profits for different initial ASR values.

conditions market conditions and cost assumptions, lowering the ASR does not lead to a profitable system. Nonetheless, lowering the initial ASR to 0.2Ωcm^2 cuts the loss by about 40%, suggesting that improvements in ASR should be a focus of research in order to make these systems more competitive and attractive in the future.

5.3.4.2 Variations on operational limits

In the previous section a discussion about the impact of lowering the initial ASR on total plant profitability was presented. It was shown that reductions in ASR can lead to substantial improvement in the plant economics, as the BoP costs are reduced when the ASR is decreased. The reason why a reducing the initial ASR leads to a reduction in the cost of the BoP is due to the fact that as the ASR is lowered, less energy is lost to resistive heating which leads to shrinkage in the size of the heat exchangers and air blowers that are used throughout the system. This reduction rests on the fact that the simulation is bound at -1.5 A/cm^2 in electrolysis mode and 0.6 A/cm^2 in fuel cell mode, which correspond to voltages of 1.63 V and 0.68

Scenario (ASR Ωcm^2)	**FC limit A/cm^2**	**EL limit A/cm^2**
0.5	0.6	-1.5
0.4	0.95	-1.85
0.3	1.25	-2.45
0.2	1.8	-3.5

Table 5.5: Fuel cell and electrolysis operational bounds for different ASR

V respectively. These values, in turn, correspond to the "safe" operating limits of the SOC that minimize irreversible cell degradation. In recent studies, it has been shown that overpotential, and not current density, is the key parameter that leads to long-term irreversible degradation of the Ni based electrodes in SOC [60]. Recall from Section 2.1.2 that the operating voltage is a function of current density and ASR ($U_{op} = OCV - i * \text{ASR}$), therefore lowering the ASR of the stack while maintaining the current density constant will lead to increases in operating voltage for stacks operated in fuel cell mode and decreases in operating voltage for stacks operated in electrolysis mode. Thus, as the ASR is lowered the current density limits can be modified as long as the voltages at the limits stay within the pre-defined safe zones (0.68V/1.63 V for fuel cell/electrolysis mode).

As the ASR is lowered, the current densities in which the system can operate can be increased which will be benefitial to the system as the amount of H_2 produced/consumed by the stack is proportional to the total current. For a system of fixed active area, lowering the ASR and increasing the operating bounds will lead to potentially more power/fuel being produced for a particular electricity/fuel price pair. In order to assess the impact that this modification has on the system's economics, the simulations described in the previous section were ran again, this time modifying the optimization constraints to reflect the new operational limits that correspond to each new ASR. Table 5.5 lists these new limits. Figure 5.37 compares the base-case operating limits with the new limits listed in Table 5.5 for the years 2009-204. As

suggested by the figure, increasing the operating limit leads to an increase in operating profits at each ASR, and the gains become larger as the ASR is lowered. For the 0.4 Ωcm^2 case, the operational profits for the 6 years increase by \$24,428 which represents an change of 12.3% with respect to the baseline case. For the 0.3 Ωcm^2 case, the gains represent a total of \$69,127 which correspond to a 27% increase. Lastly, for an ASR of 0.2 Ωcm^2 changing the operational limits results in an increase of \$170,280, which amounts to a 55% increase with respect to the baseline.

At a first glance it seems like changing the operational limits greatly boosts the economics of the system, however the numbers only reflect part of the story as increasing the operational current density will lead to increasing the BoP component sizes.Thus, the new TPC for each simulation must be taken into account in order to fully appreciate the impact that modifying the operating limits has on the economics of the system. In the previous section, it was shown how a reduction of BoP size with decreasing ASR boosted the economics of the system. However, in the case of increasing the operational limits of the stack, a reduction of ASR does not lead to a reduction in the size of the BoP. On the contrary, the TPC increases with decreasing ASR as shown in Table 5.6.

A/cm^2	**Annualized TPC base(\$)**	**Annualized TPC (\$) new limits(\$)**
0.2	122,501	262,705
0.3	134,869	201,455
0.4	142,522	169,538

Table 5.6: Annualized TPC comparison:base operating limits & new operating limits

Recall from Section 4.2.1 that the heat production in the stack increases non-linearly with current density, while the production/consumption of H_2 is linear in the current. Thus, the size of the BoP (mainly driven by size of heat exchangers and air blowers) will increase faster than the output, and under the given market prices this leads to a very non-economic system. Figure 5.38 compares the total

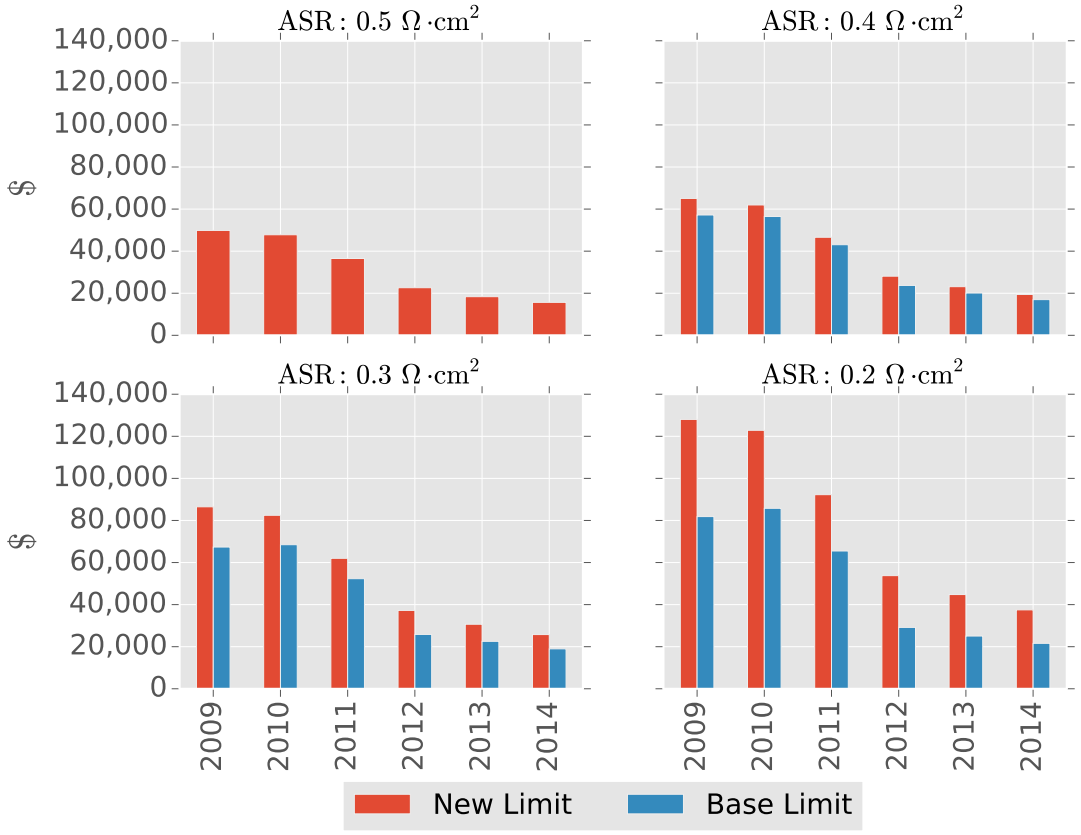

Figure 5.37: Comparison of operating profits for changes in operating limits for different ASR values

plant profits (e.g. operational profits minus annualized TPC) for both the base-case limits (-1.5A/cm^2–1.5A/cm^2) and the new limits reported in Table 5.5.

The results highlighted in Fig. 5.38 suggest that under the current market conditions, lowering the cost of the BoP, and not increasing the output capacity, leads to a more economic system. This result is not surprising, as the low capacity factors discussed in previous sections requires the CAPEX to be low for the system to be economical, as the extreme events (such as electricity prices converging to zero and dipping into negative territory) are not enough to make up for the high CAPEX associated with such a system. Thus, given the existing fuel and electricity prices the reduction of CAPEX costs is identified as the key element for making these sys-

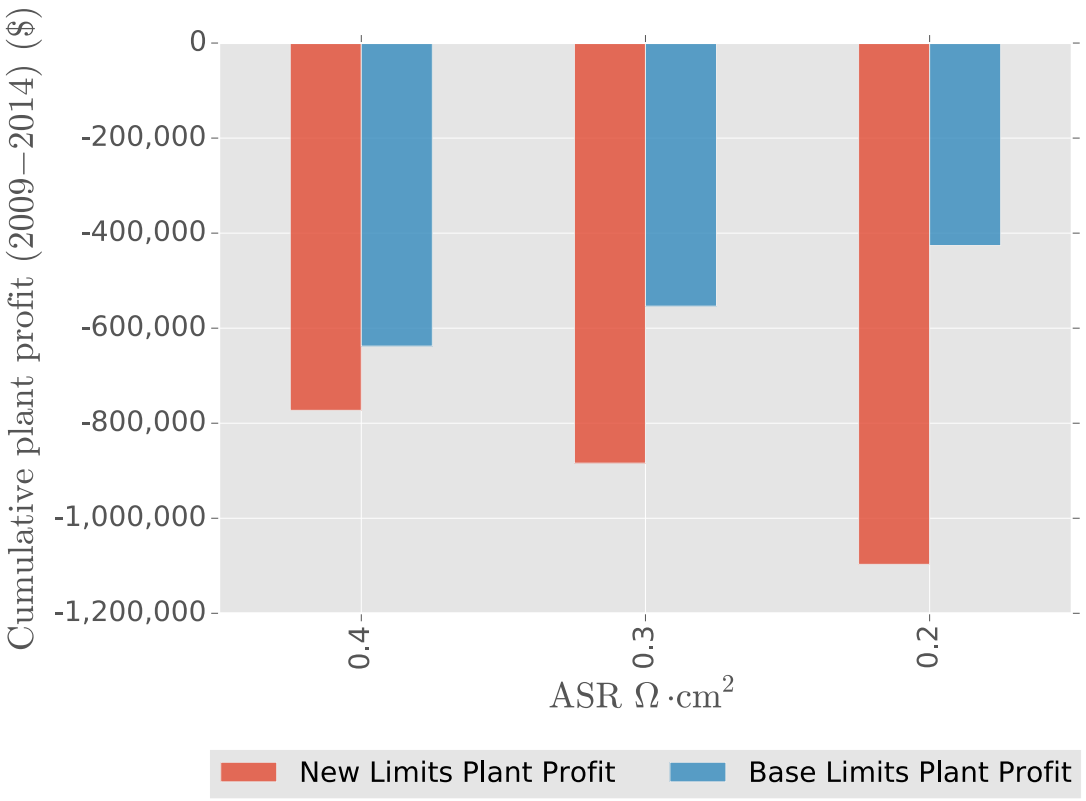

Figure 5.38: Comparison of total plant profits for changes in operating limits for different ASR values

tems more economically attractive. These reductions, in turn, can be achieved by technological improvements (e.g. lowering ASR), cost reductions from scaling and manufacturing, as well as optimizing the operating parameters in a particular design.

It is important to stress that the results presented in this section do not take into account any of the gains that might be achieved by the higher efficiencies that are expected from future SOC designs. For example, future designs that may allow for CH_4 reforming without the need to dilute CH_4 with H_2O to avoid carbon deposition will greatly boast the overall efficiency of the system. Likewise, future cell designs that may operate at lower temperatures ($\sim 600°C$) and high pressures and low ASRs are expected to boost the overall efficiency of the system by allowing for in-situ

Simulation	TPC ($) Base	TPC ($) Breakeven	% Change
ASR : $0.5\Omega \cdot cm^2$	154,113	31,800	-79%
ASR : $0.4\Omega \cdot cm^2$	142,522	36,248	-75%
ASR : $0.3\Omega \cdot cm^2$	134,869	42,583	-68%
ASR : $0.2\Omega \cdot cm^2$	122,501	51,486	-58%

Table 5.7: TPC Breakeven requirements

CH_4 formation in the cell channels, resulting in the overall reaction becoming less exothermic and allowing for lower operating voltages [125].

5.3.4.3 TPC required for breaking even

In the previous section, the impacts that initial ASR has on the economics of the RSOC system have been discussed. One of the key findings of these simulations is the importance and impact that system costs, in particular BoP costs, have on the profitability of the system. As such, it is important to recall that the TPC used in these analyses is based on the model and assumptions presented in section X. Although these assumptions represent a conservative case with the best available data, it is important to highlight that CAPEX cost reduction are path dependent processes which can have quick unforeseen cost declines. For this reason, it is a useful exercise to compute what the required TPC would have to be in order for the system to break-even in the Danish electricity and fuel markets for the years 2009-2014. This estimate can be easily calculated by assuming that the in order for the system to break-even, the annualized TPC would have to be equal to the average annual operating profits. For each of the different cases analyzed in the previous sections, the average annual operating profits can be computed by adding the cumulative profits and diving them by the number of years. Table 5.7 shows the CAPEX costs that would be required to break-even for simulations with different initial ASRs for the years 2009-2014. As highlighted in the previous section, as the initial ASR is lowered, the BoP costs decrease due to the shrinking of the heat exchangers and blowers required

for operating the system. At the same time, operating profits increase with decreasing ASR as less energy is lost to resistive heating. As such, the TPC required for breaking even increases with decreasing initial ASR, which means that at lower ASRs, the cost improvements of the system with respect to the original TPC calculation would have to be less dramatic. As shown in Table 5.7, at an ASR of 0.5 Ωcm^2, costs would have to decrease by about 79% in order for the system to break-even, whereas for the 0.2 Ωcm^2 case the system would have to be 58% cheaper to achieve break-even point. That is, for a system with an initial ASR or $0.2\Omega cm^2$ it would require a reduction of 2x for it to break-even, even under the unfavorable conditions that currently exist in the Danish electricity market. As it has been seen throughout multiple industries and sectors, cost reductions of a factor 2 can be achieved in a relatively short time, particularly if there are agreed upon standards and the costliest components can be mass-produced.

5.3.5 Impact of degradation rate: (Rev-Deg)

Long-term stability of the RSOC is one of the key concerns of this technology, thus degradation is an important parameter to study. As discussed in Section 3.3.3, stack degradation is modeled as an increase in the system's ASR, so from an operational and economic point of view degradation impacts the system in two distinct ways: it changes the relationship between power consumption/generation and heat production, thereby changing the parasitic loads and equipment requirements; and it shortens the life of the cell, which in turn has a direct impact on the TPC. Indeed, these two dimensions are intricately connected and one affects the other. As such, modeling the impact of degradation can be a tricky task, and requires some assumptions in order to simplify the problem. In order to understand the impact that degradation has on this RSOC system, a series of simulations that assumed a constant degradation were performed. The main purpose of the simulations was to understand how degradation

affected the operating strategy and the BoP component sizing and investment. In order to simplify the problem, the following assumptions were made:

1. Degradation is assumed to occur at a fixed rate of 1%/1,000 hrs.
2. The stack degradation is a function of the lifetime of the device and is independent of mode of operation or on the particular operating point (e.g. current density or voltage).
3. The lifetime of the device is fixed at 6 years.

Recall from Section 4.2.2 and Section 4.3.2 that increasing the ASR of a system will lead to more heat being generated by the stack per unit of power generated (fuel cell mode) or mole of H_2 produced (electrolysis mode). Therefore for a given operating point, as the stack ages the air requirements will increase in order to maintain the temperature gradient for the stack within the allowable range. From an operational point of view there are two approaches one can take for dealing with a degrading system: one can oversize the BoP (particularly air heaters and blowers) such that the initial operating ranges are maintained as the system ages; or one reduce the operating limits (current densities) as the system degrades so that the heat produced by an aging stack never exceeds the amount of heat produced by the stack at the initial design (initial ASR). Put differently, with the oversizing strategy a penalty in CAPEX is assumed in exchange for maintaining high outputs throughout the lifetime of the device, whereas with the heat limiting strategy, a penalty on the potential output at the operating limits is assumed in exchange for lower investment costs.

In order to assess the impact that these two strategies have on the system economics, two simulations were performed using the base-case assumptions Table 5.1 and a degradation of 1%/1,000 hrs. In the first simulation (termed "BoP oversizing"), the BoP is over-sized such that the operating ranges stay constant throughout the lifetime of the device. In the second simulation ("No oversize"), the size of the BoP

is the same as in the base case with no degradation, but the operating ranges are reduced as the stack ages so that the heat generated by the degrading stack never exceeds that of the heat generated at the operating limits for the initial ASR (0.5 Ωcm^2). For completeness, these two strategies are compared with the no degradation case (base-case). Figure 5.39 shows the yearly operational profits for the BoP over-

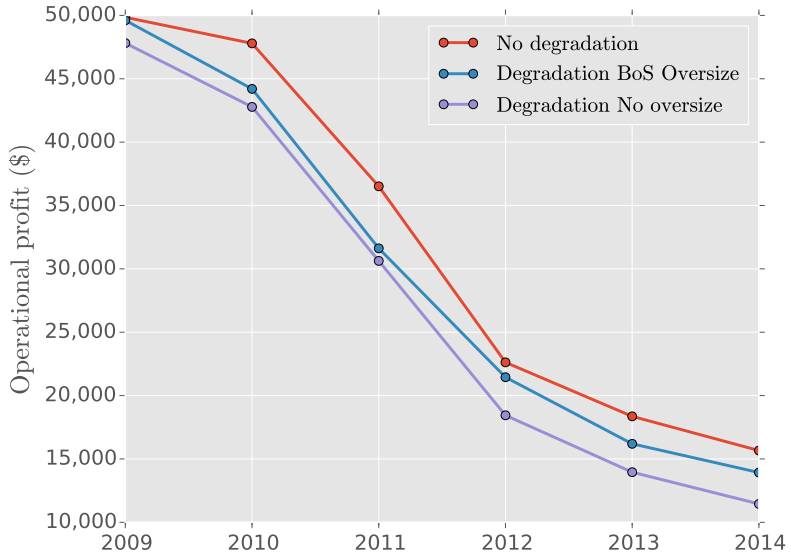

Figure 5.39: Yearly operating profits for no degradation, degradation with BoP oversize, and degradation wit no oversize

sizing simulation, the no oversizing simulation, and the no degradation simulation. As expected, the no degradation simulation has the highest profits, followed by the BoP oversize case, followed by the no oversizing case. Figure 5.40 shows the six year cumulative profits for each strategy. As shown by this graph, the no degradation case has total operating profits of $190,805, the over-design strategy has cumulative operating profits of $177,004, and the no over-design strategy has total operating profits of $165,071. Thus, there is a 7% increase in operational profits by oversizing the BoP. However, the oversizing strategy will have an important impact on the CAPEX, as the size of the air pre-heater increases by a factor 2.27, going from 145 m^2 for the

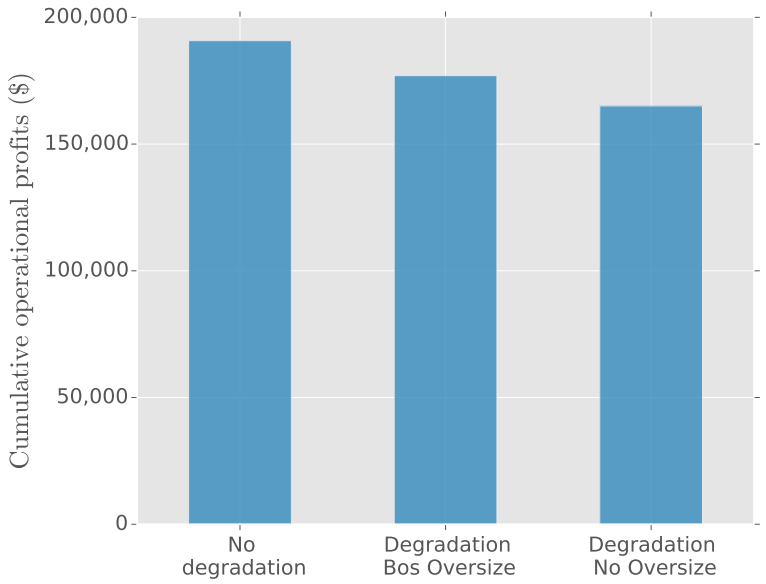

Figure 5.40: Cumulative operating profits for no degradation, degradation with BoP oversize, and degradation wit no oversize

Case	Area Air Pre-heater m^2	$\dot{V}_{air}$ FC $\left(\frac{m^3}{sec}\right)$	$\dot{V}_{air}$ EL $\left(\frac{m^3}{sec}\right)$	Annualized TPC ($)
No oversize	145	1.22	3.75	153,551
Oversize	330	1.95	8.2	167,602

Table 5.8: Area of air pre-heaters, air flow rates and annualized TPC for different degradation strategies.

base case and no oversizing case to $330\,m^2$ for the oversized case. Section 5.3.5 lists the difference in air pre-heater sizes, the volumetric flow rates of air at the design points[4] and the impact that these differences have on the annualized TPC. As the table suggests, the oversizing of the BoP leads to an increase of $\sim \$14,000$/yr, which

[4]The design points are taken as the maximum operating current for each simulation at the maximum ASR that the system experiences throughout its lifetime. For the oversizing case, this is -1.5 A/cm^2 for electrolysis mode and 0.6 A/cm^2 for fuel cell mode at an ASR of 0.7628 Ωcm^2 ($ASR_0 * (1 + .01/1000 * 8760 * 6)$). In the case of no oversizing, since the limits decrease with time such that no oversizing is required, the design point is simply -1.5 A/cm^2 for electrolysis mode and 0.6 A/cm^2 for fuel cell mode at an ASR of 0.5 Ωcm^2

represents an increase of 9.15%. Given that the *cumulative* operational profits increase 7% by oversizing the BoP, this seems to be a losing strategy as the cost of the equipment increases faster than the gains associated with being able to keep the outputs high. The cumulative effect of this is illustrated in Fig. 5.41, which shows the cumulative plant profits for the six year time series. As expected, none of the

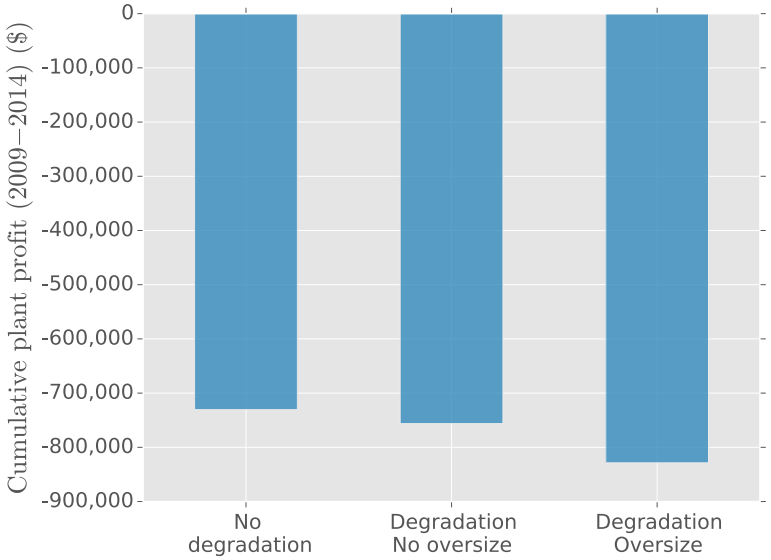

Figure 5.41: Cumulative total plant profits for no degradation, degradation with no oversize, and degradation with BoP oversize

systems are profitable for the timeseries analyzed and the oversized BoP strategy yields the worst results. It is worth noting, that there is a bigger difference between the oversized strategy and the no oversizing strategy, than between the degradation and the non degradation case. Although this is a surprising outcome, it is somewhat misleading as the profits generated by the system towards the later years (when the cumulative effects of the aging stack are the largest) are small compared to the profits made during the first two years. Therefore although it seems that degradation does not have a big impact this is a consequence of the particular timeseries analyzed, rather than an intrinsic feature of the system.

The results presented in this section suggest that at high initial ASR, low degradation rates (1%/1,000 hrs) and for the particular timeseries analyzed, oversizing the BoP in order to maintain output throughout the lifetime of the device is not a financially sound strategy. In this case, lowering the output as the device ages in exchange for lower CAPEX costs is a better strategy.

5.3.6 Simpler chemistries to lower CAPEX

Although analyzing different chemistries for the RSOC system is outside the scope of this work, it is important to highlight that simpler chemistries could lead to simpler configurations for the RSOC system. This, in turn, could mean lower capital costs, which would make the system more attractive from an investment point of view.

The cost analysis presented throughout this chapter suggests that under the current market structures, methane based RSOC systems that only participate in electricity and fuel spot markets in Denmark cannot recover their costs. As it has been shown throughout this section, the high CAPEX associated with the system (mainly driven by the BoP) as well as the current prices for fuel and electricity in the Danish markets, are the main elements behind the unfavorable economics of the system. It is important to highlight that these calculations relate to a specific technological choice (methane based RSOC system) and a series of underlying assumptions.

As it was discussed in Chapter 3, an important driver for the complexity of the RSOC system stems from the units required to catalytically hydrogenate CO_2 into CH_4 downstream of the RSOC. Thus, if a different fuel is chosen as the product of the electrolysis operation and for the operation in fuel cell mode, the CAPEX and overall system economics will surely change. The simplest possible design would be to have H_2:H_2O chemistry, where pure H_2 would be used as the feedstock fuel in fuel cell mode, and H_2 would be generated in electrolysis mode by electrolyzing steam rather than synthesizing CH_4 from H_2 and CO_2. This would simplify the systems design, as

all the infrastructure required for heating, cooling, compressing and reacting the gases downstream of the RSOC would not be required, as the product of the stack would be a mixture of H_2 and H_2O, which can be easily separated via the condensation of liquid water. This design choice, in turn, would have lower capital and operating costs.

A quick glance at the system component costs in Table 5.3 gives a hint of the savings that could be achieved by simpler designs. If one removes the methane air blower, the CO_2 heater, the monoliths and their housing, the catalyst, the water separator and the methane heater, the CAPEX for the RSOC would automatically decrease by roughly 13%. This rough calculation only highlights the reductions in CAPEX that could be achieved by the removal of the components that are required for the methanation downstream of the SOC, however there could be other important gains both in the CAPEX and in the operation of the system that stem from the simpler H2:H2O chemistry. For the simple H_2:H_2O case, the system could have higher conversion efficiencies and power densities. For example, if the system is operated in fuel cell mode with pure H2 as a fuel, there would be no need to dilute the feed with steam in order to avoid coking (as is the case with CH_4), which would result in higher operating voltages for a given current, leading to higher efficiencies and power densities. At the same time, this would change the energy balance around the stack, which would benefit the CAPEX of the system by decreasing some of the BoP components and allowing for improved heat integration across the whole system.

Thus, the simple approximation of a 13% reduction in CAPEX should be treated as a rough estimate of cost reductions that could be achieved by simpler designs, bearing in mind that the savings are probably be much higher. To fully understand what these could be, a proper analysis and optimization would have to be performed to understand the sensitivities of the system to different operating variables and design choices, as well as to get a better feel for the trade-offs associated with this

different design.

5.3.7 Value of reversibility

Throughout this chapter, it has been shown that under current market prices for electricity and natural gas, the RSOC based "energy-hubs" are not attractive from an investment perspective. This is largely due to the fact that the ingredients are just not right: prices of electricity are too high to results in economically attractive SNG production, while at the same time being too low to make electricity in fuel cell mode. Thus, it is hard to make a case for RSOC given current conditions. Nonetheless, RSOC systems still provide unique capabilities by marrying renewable electricity with high energy dense fuel production, and therefore it is valuable to explore scenarios in which reversibility can provide a unique value.

As explained at the beginning of this chapter (Section 5.1), Denmark has enacted ambitious decarbonization goals that will reshape its energy system in the coming decades. As part of these policies, the Danish government has set a target of having a fossil fuel free energy sector (including heat and transport) by the year 2050. This will require big investments in wind, solar and biomass, as well as in technologies that can deliver high energy dense fuels for some sectors such as heating and transportation. In order to better understand what such a system might look like, the Danish Energy Agency (DEA) has developed models that are consistent with the targets set forth for the years 2020, 2035, and 2050 [24] in which they forecast energy demand, supply by type of technology, as well as electricity and fuel prices. These scenarios carry a large degree of uncertainty and should be used to describe a set of possibilities given a series of constraints, and thus should not treated as accurate forecasts. Because wind power is expected to provide a large fraction of the electricity in the 2035 and 2050 scenarios, whole-sale electricity prices are expected to be significantly lower [5]. Thus, the 2035

[5] see Section 5.1.1.2 for a discussion on the impact of wind in whole-sale electricity markets

and 2050 scenarios can be used to get a better feel for the value that RSOC might provide within systems of very high or 100% renewable penetration. As a matter of fact, the DEA considers synthetic natural gas (made from biomass) as one of the key technologies for heating, transportation, and some peak electricity requirements. In this section, the 2050 fuel and electricity prices developed by the DEA are used as inputs into the RSOC computational model which is used to compute hourly electricity and fuel production, operational profits, and total system profitability.

5.3.8 2050 scenario

Electricity data for the 2050 scenario is not available at an hourly resolution in the Energiescenarier document published by the DEA [22]. Nonetheless, the consulting company Ea Energy Analyses on petition from the Danish Comission on Climate Change policy published a study of the production of SNG using solid oxide electrolysis in which a yearly electricity price times series for the years 2020, 2035 and 2050 is provided [29]. This timeseries is used for the purpose of modeling the RSOC system in the year 2050.

As mentioned in previous sections, the price of natural gas is one of the key drivers for determining the mode of operation of the system and its overall profitability. Thus, choosing a SNG price for 2050 is an important step and assumption. To illustrate the sensitivity of the results to the SNG price, two 2050 are performed: a "high SNG" case, and a "low SNG" case, where the prices of SNG are 140 DKK/GJ and 91 DKK/GJ, respectively. Fig. 5.42 shows the hourly electricity prices for the 2050 scenario (sorted from lowest to highest) as well as the two SNG prices that are used in the simulation. All prices are in 2010 USD. The time-series has an average electricity price of 7.05 ¢/kWh, with a standard deviation of 5.8 ¢/kWh, showing a lot of variance in the price. The lower quartile (25%) is at price of 1.6 ¢/kWh, the second quartile (50%) at 6.4 ¢/kWh, while the top quartile (75%) sits at 11.39 ¢/kWh. Thus, the

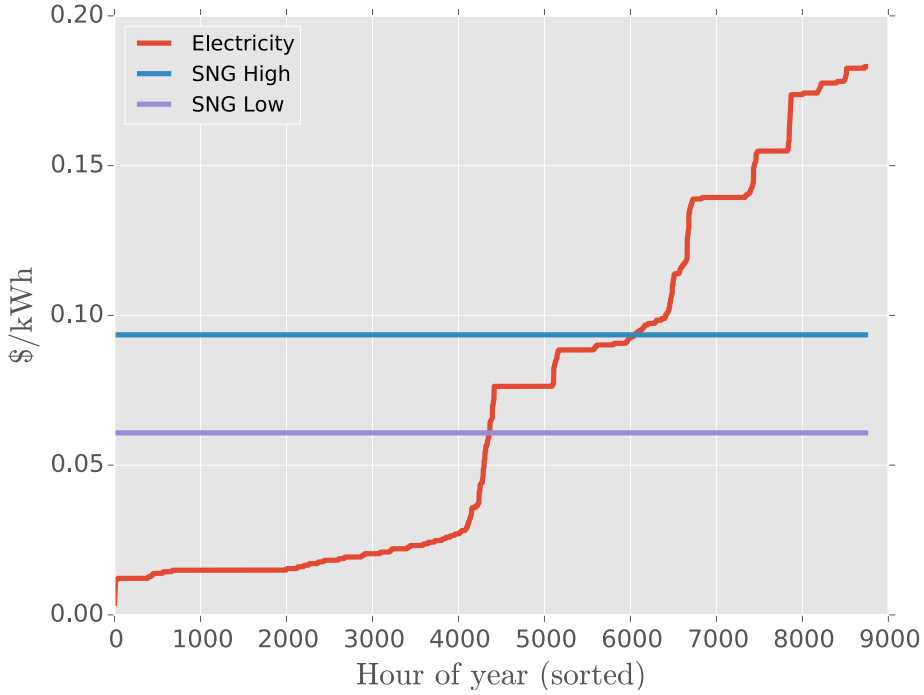

Figure 5.42: Electricity and SNG prices for 2050 scenario. Prices in 2010 USD.

distribution of prices tends to occur at the high and low extremes. For example, 4,000 hours of the year (45% of the time) the price of electricity is below 2.5 ¢/kWh, while the top 10% of prices are at 16.9 ¢/kWh and above. This distribution of prices is not surprising, as the 2050 scenario is based on a 100% renewable grid with high penetration of wind, which as previously discussed would tend to reduce whole-sale spot prices while increasing its volatility. In order to determine the optimum operating mode and point, it is necessary to run the optimization discussed in previous sections, but by visually inspecting this plot it can be seen that for the high SNG case, the price of electricity is lower than the price of gas for roughly 70% of the time, while for the low SNG case it is roughly 50% time. This suggests that electrolysis mode will be favored more in the high SNG case than in the low SNG case.

Using the assumptions described in Table 5.1 two hourly optimizations, one for the low SNG and one for the high SNG price, are performed in order to determine the

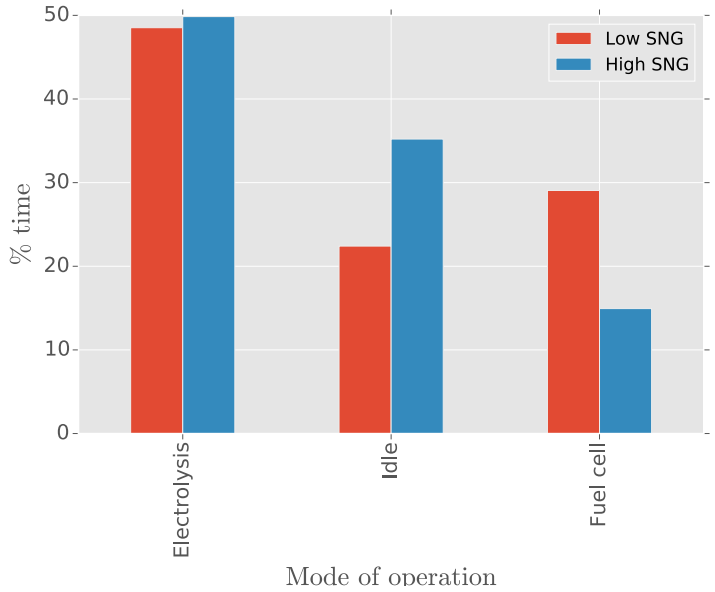

Figure 5.43: Operation by mode for 2050 scenario at low and high SNG prices

optimal operating strategy for the 2050 time-series. The results of these optimizations are shown in Figs. 5.43 and 5.44.

Figure 5.43 shows the % of the time that the system spends on each mode. The first thing to notice is that in the low SNG case, the system idles roughly 20% of the time while in the high SNG case the idling time is roughly 35%. As a consequence the low SNG case operates in fuel cell mode about twice as much as in the high SNG case (roughly 30 vs 15% of the time). This is a stark contrast to all the previous cases that use the 2009-2014 time-series, where the main mode of operation was either fuel cell or idle and in which electrolysis mode was used $< 5\%$ of the time. Thus, reversibility plays different roles depending on the underlying price structure. This becomes even clearer when analyzing Fig. 5.44, where the operating profits for each mode are displayed as well as the percent contribution of each mode to the total yearly operating profits. As the graph shows, the yearly operating profits for the low SNG case are $\sim \$135,000$ and $\sim \$285,000$ for the high SNG case. In the low SNG case the

fuel cell operation contributes about 21% of the profits while in the high SNG case fuel cell mode it contributes less than 2%. This finding suggests two things: first that given the price structure of 2050, electrolysis is the profit driver for the RSOC system; and second, that if the price of gas is too high and electricity prices are very depressed (the high SNG case), reversibility does not offer much value as the ability to operate in fuel cell mode becomes irrelevant for the system's economics [6]. On the other hand reversibility can offer substantial value (21% of profits) if the price of gas is low and there are sufficient instances of high electricity prices (the low SNG case) such that selling power becomes an attractive proposition. The operational profits are only part

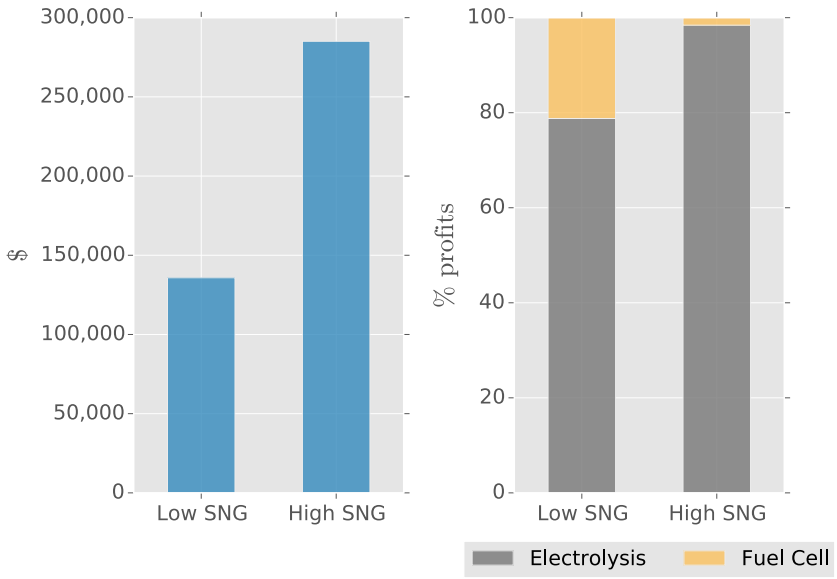

Figure 5.44: 2050 operational profits for Low and High SNG cases; % profit contribution of each mode for low and high SNG cases

of the story, so the annualized TPC must be considered in order to get a sense of how these scenarios compare to the ones that have been discussed in previous sections.

[6] It is worth mentioning that although fuel cell mode might not provide much value to the system economics, one can imagine cases in which this ability becomes important for stabilizing the grid at particular points in time. In this case, this service would have to be priced through a different mechanism which would ultimately end up showing in the system economics.

Fig. 5.45 shows the operating profits, the annualized TPC and the total plant profits for the high and low SNG cases. The annualized TPC is the same as the base-case described in previous sections with the exception that the one used in the 2050 scenarios is scaled to 2010 dollars, thus the TPC is slightly higher. Fig. 5.45 suggests

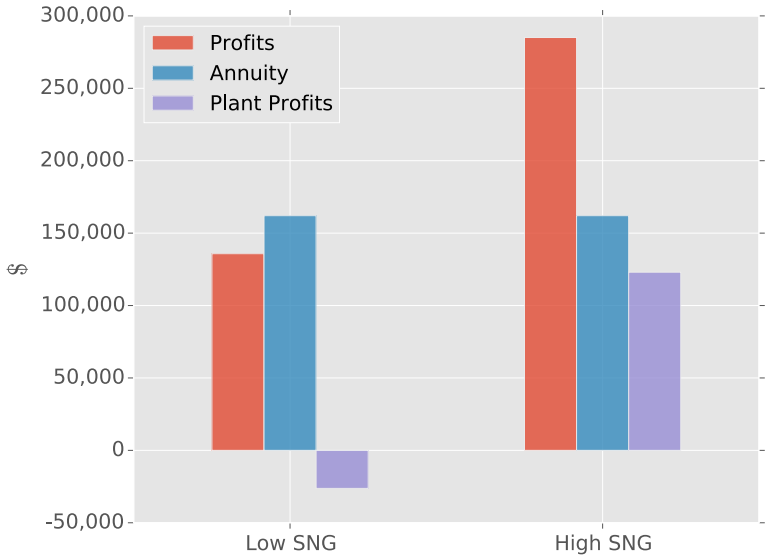

Figure 5.45: 2050 operational profits for Low and High SNG cases; % profit contribution of each mode for low and high SNG cases

that in the low SNG case, the system exhibits a total loss of $\sim \$26,255$/yr. In the high SNG case, the system shows a total plant profit of $\$123,014$ which corresponds to an Return on Investment of 75%. Given the inherent uncertainty associated with the underlying prices of these scenarios, these results should not be taken as definitive answers. Nonetheless, it is worth highlighting a few observations. In the low SNG case, even though the optimization points towards a net yearly loss it is less than 20% of the annuity, which is a very encouraging result as the CAPEX calculations have an inherit error in the order of $\pm$ 30% which suggests that the results are within the margin of error. On top of this, the TPC calculated assumes current technology and prices, and one would expect that technical innovation over a 35 year period

would help bring down the cost of the SOC stack and the BoP components, as well as improving on key cell parameters such as ASR and overall lifetime. As such, the TPC used for this calculation can be considered somewhat conservative. Furthermore, the low SNG helps highlight the value that can be derived from reversible operation as the profits generated in fuel cell mode are roughly $28,517 which is similar to the net loss, suggesting that the ability to operate reversibly (20% of the time in fuel cell mode in this case) might be a key factor for making the system profitable in markets that have relatively low fuel prices and highly scattered and depressed electricity price.

On the other hand the high SNG scenario points towards a very profitable operation given the 2050 assumptions. But as Fig. 5.44 suggests, under these assumptions reversibility does not offer any value as fuel cell mode contributes to less than 2% of the operational profits. This is a very important finding, as it suggests that in highly liberalized markets with 100% renewable power and high gas prices, electrolysis is where the future (and value) of SOC system lies. Reversibility is not really important, and the focus then becomes in designing the cheapest SOC power-to-gas facilities. This, in a way, is not surprising as electrolysis in this particular market is providing a very useful service: it is taking a relatively cheap input (electricity) and converting it to an extremely valuable product (SNG) with a relative high efficiency. The fact that the SNG is used in sectors that are intrinsically hard to decarbonize and where few alternatives exist (such as transport and industry) is reflected in the high price of SNG vs renewable power.

The results from the two 2050 optimizations suggest that RSOC systems are likely profitable in an energy system that develops into something resembling the 2050 vision developed by the Danish government. Given the expected distribution of spot electricity prices, electrolysis will become the main profit driver of these systems. Therefore, if one thinks of the infrastructure as mainly being power-to-gas systems,

then the value of reversibility (e.g. the ability to sell power in moments in which electricity prices are high) largely depends on the value and price of SNG. In some cases, reversibility might end up being a key economic enablers, and in others it might not be worth the effort.

5.3.8.1 Sensitivity to ASR in low SNG scenario

As shown in Section 5.3.4, variations on the system's ASR have an impact on the capital cost and profits of the system. Therefore, it is worth investigating what these impacts would be for the 2050 scenario. In the previous section, it was shown that for an ASR of 0.5 Ωcm^2 (the base case assumption) the 2050 scenario under the low SNG price is very close to profitability, making this an interesting case to study. To do this, the optimization for the 2050 scenario (low SNG case) was re-computed using three different initial ASR values: 0.2, 0.3 and 0.4 Ωcm^2. For all other parameters and assumptions, including the current density limits, the base case assumptions described in Table 5.1 were used. That is, the only difference between the system used in the 2050 scenario described in Section 5.3.8 and the one presented in this section is a change in the system's initial ASR. Figure 5.46 summarizes the operational profits, the annuities, and the total plant profits for each case.

Figure 5.46 highlights some important findings. As expected, the operational profits increase as the ASR is lowered due to the fact that the system has higher efficiencies for a given operating point as the ASR is lowered (refer to Section 4.3.2 for an in depth discussion about this). As the figure suggests, the operational profits go from \$135,800 for an ASR of 0.5 Ωcm^2 to \$189,500 for the 0.2 case, which implies an increase of 39.5%. With respect to the annuity (e.g. the annualized TPC), this value decreases as the ASR is lowered for each case and at 0.2 Ωcm^2 it reaches \$129,284.0 which implies a 20% reduction with respect to the base case value (\$162,053). Putting together the annuities and the operational profits, an interesting picture emerges. As

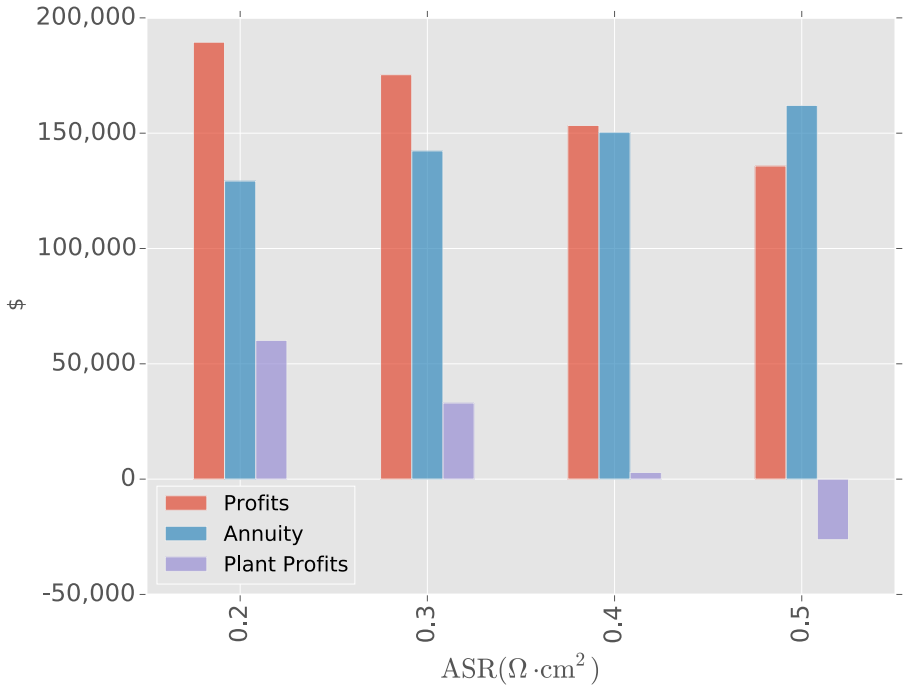

Figure 5.46: 2050 low SNG price scenario sensitivity to ASR

suggested by Fig. 5.46, lowering the ASR to 0.4 Ωcm^2 implies profitability, albeit a very small one ($\sim$ \$2,912). This trend increases as the ASR is lowered. As a matter of fact, for the lower limit (0.2 Ωcm^2) the total plant profits are \$60,165 which implies a return of 46%. It is worth noting that in the previous section the system under the high SNG case showed total plant profits of \$123,014 for the base case scenario, therefore lowering the ASR to 0.2 Ωcm^2 represents total plant profits that are roughly 50% of the plant profits seen in the optimistic high SNG scenario. Put differently, one can achieve very optimistic results for the 2050 dataset even under low SNG prices by improving (lowering) the system's ASR. This results highlights the importance of this parameter and, once again, points towards ASR as a key element to improve as the technology progresses.

5.3.8.2 Sensitivity to operating limits in low SNG scenario

In Section 5.3.4.2, the impact of changing the current density limits as the ASR was lowered was studied. As detailed in this section, as the ASR is lowered the current density limits can be modified as long as the voltages at the upper and lower bounds stay within the pre-defined safe zones (0.68V/1.63 V for fuel cell/electrolysis mode). Increasing the operating current density limits might be attractive because they imply a wider range of fuel/electricity production capabilities, which can increase the operational profits if operated above the previous limits. However, increasing the operating limits implies an increase in the BoP components as higher current densities imply larger volume of gases and larger areas of heat exchange. Thus, it is not clear whether or not increasing the operating limits is a winning strategy. As a matter of fact, in Section 5.3.4.2 it was shown that for the 2009-2014 timeseries, the increase in the TPC associated with increasing the operating limits was larger than the gains in operating profits and thus the strategy did not make much sense.Indeed, it was the combination of increasing profits while at the same time lowering the TPC that resulted in positive results for the lowering of the ASR studied in the previous section.

In order to assess whether this strategy makes sense under the 2050 scenario, the optimizations for the 2050 low SNG case were re-conducted using the new operating current density limits described in Table 5.5 for ASR values of 0.2, 0.3, and 0.4 Ωcm^2. The results of these optimizations are shown in fig Fig. 5.47.

The first thing to notice from Fig. 5.47 is that the operating profits substantially increase as the ASR is lowered and the operational limits are increased. At the 0.2 Ωcm^2 limit the difference is quite dramatic, going from $\sim \$190,000$ to $\sim \$382,000$. This is largely due to the fact that the capacity factor for the 2050 scenario is quite high ($\sim 80\%$) thus the system can take advantage of the higher fuel/power production abilities. Not only this, but as shown in Section 5.3.8, the system spends more than half the time in electrolysis mode which exhibits larger power densities (and thus

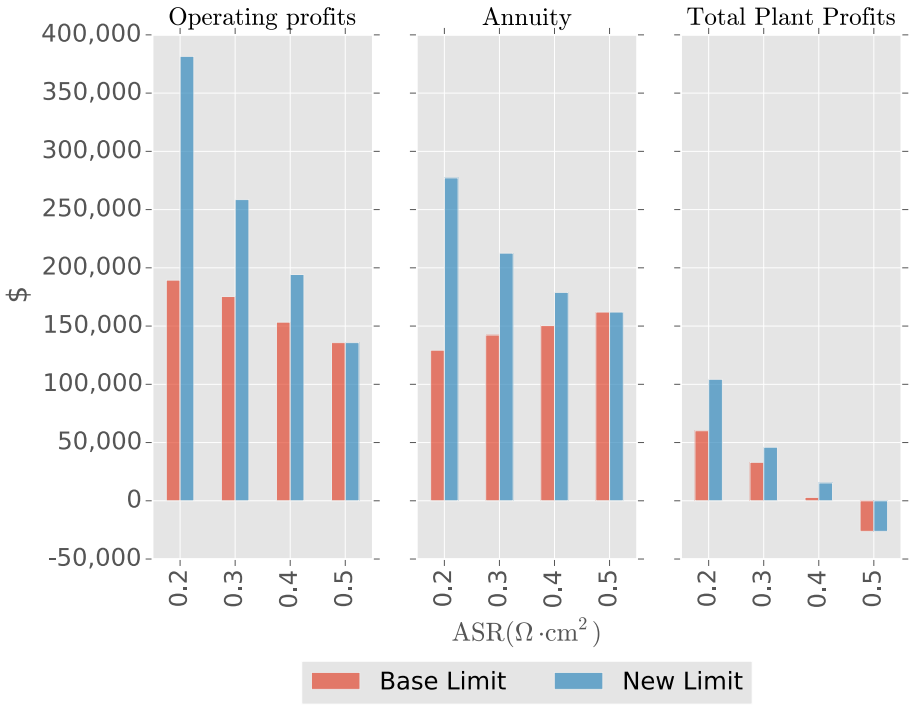

Figure 5.47: Operating profits, annuity and total plant profits for 2050 low SNG price case at different ASR and operating current density limits

potential profits) than the fuel cell mode. With respect to the annuity, as expected the figure shows that under the new operating limit assumptions as the ASR is lowered the annuity increases. As previously discussed, this is an expected behaviour as the BoP needs to be scaled up in order to handle larger gas volumes for higher limits. It is important to notice that as the ASR is lowered, the percent difference between the base case and the new limit Annuity becomes larger and larger. For example, the percent difference between the two cases for the 0.4 Ωcm^2 case was 18.93%, where for the 0.2 Ωcm^2 case it is roughly 115%. Therefore, if the strategy is to pay-off, the increase in operational profits needs to outweigh the rapid increase in TPC.

For the three cases evaluated, it can clearly be seen that the gains in operating profits outweigh the costs of the new annuity, and thus increasing the operating limits increases the total plant profits across all ASR values. The main reason behind this

is, again, the high capacity factors seen for the 2050 dataset and the fact that the system spends a lot of time in electrolysis mode compared to fuel cell mode. Put differently, the investment in BoP required to operate at higher currents is paid for by the fact that the system does not idle much and the prices of electricity are very low for many instances during the year (see Fig. 5.42), thus electrolysis operation becomes a profitable endeavor. This is an important change from the 2009-2014 dataset, where an increase in operating limits did not make financial sense as the system tended to idle a lot and spent $< 5\%$ of the time in electrolysis mode.

	ROI (%) Base Limit	**ROI (%) New Limit**
0.2 Ωcm^2	46.5	37.6
0.3 Ωcm^2	23.2	21.6
0.4 Ωcm^2	1.9	8.6
0.5 Ωcm^2	-16.2	-16.2

Table 5.9: Return on Investment of base and new operating limits for the 2050 low SNG cases.

The fact that the new operating limits yield higher operational profits does not necessarily mean that they are better investments, as the capital tied up as the system size increases is increased. Thus, it is worthwhile to compute the Return on Investment, simply defined as the Total Plant Profits dived by the Annuity, for each case in order to better assess the situation. Table 5.9 shows the return for each ASR case under the base and new limit simulations. As this table suggests, only for the 0.4 Ωcm^2 case does the increase in operational limits lead to an increase in ROI. For all other cases, the best strategy is to keep the base case limits. In other words, even though increasing the operating limits does yield larger profits, for all cases except for an ASR of 0.4 Ωcm^2, they are smaller relative to the investment required to build and operate the plant. It is noteworthy, however, that the "optimum" design limit could lie somewhere between the base and the new limit, which means that for each ASR an optimization to find the best operating limit may be required. This particular work

is outside the scope of this dissertation, however it is important to mention it so that future modeling efforts can be steered towards interesting and fruitful endeavors. In this spirit, the following chapter lays out some of the areas of research where the work presented throughout this dissertation could be expanded and ideas for improving it.

Chapter 6

Future work

The future of RSOC based systems and "energy hubs" like the one described in this thesis will likely transition from the laboratory into pilot and full scale implementations over the next decades. Given that these systems are extremely novel, there is still much work to be done on both the theoretical and experimental side of things in the years to come. In this regard, RSOC systems are a fertile ground for research, development, and commercialization. This chapter intends to describe some areas of research where the work presented in this dissertation can easily be extended in order to answer questions that might prove to be critical for the future of this technology. In this sense, the discussion presented below is not intended as an exhaustive inventory of all possible areas of research, but rather as a list of relevant questions and areas of research that are natural extensions of the work presented herein.

6.1 Variations on system design

The RSOC system presented in this thesis is a CH_4 based system in which the stack is operating at atmospheric pressure and that electrolyzes only steam in electrolysis mode. The primary reason for choosing this design was threefold: first, given that we were interested in using electricity prices for the spot market in Western Denmark, methane as a fuel made perfect sense since Denmark has a ubiquitous natural gas grid and is part of a larger Scandinavian natural gas market for which price data going back to 2009 was available. Second, RSOC are novel pieces of technology and thus simulating a relatively simple stack operation (atmospheric pressure and steam

electrolysis) was favored over more complex setups (e.g. co-electrolysis, pressurized operation) in order to offer insights of what a system that is based on current technology might look like; third, because the purpose of the work was to make a case for distributed infrastructure, simplification of the BoP was an initial design parameter. Of course, these decisions carry some trade-offs and do not necessarily yield the most efficient or intelligent design. Therefore, exploring variations on the system design represent relatively low hanging fruit that might offer important new insights.

6.1.1 Co-electrolyis and pressurized systems

When operating in electrolysis mode, the system presented in this dissertation electrolyzes steam to generate H_2 and O_2. However, SOCs have the ability to electrolyze steam and CO_2 simultaneously. Indeed, this capability is one of the defining features and characteristics of SOCs, and therefore it should be evaluated in the context of the system presented herein. Co-electrolysis is particularly relevant for cases in which the fuel being synthesized requires syngas (e.g. methanol, DME, FT liquids), rather than CO_2 and H_2. For these cases, co-electrolysis leads to a reduction in the complexity of the BoP as it removes the necessity of a shift reactor in order to have the H_2/CO ratio required for a particular synthesis.

Operating SOCs at high pressures offers some interesting benefits, such as lowering of ASR at a fixed temperature, decreasing concentration overpotential by increasing gas diffusion, and in cases where fuel synthesis downstream of the stack requires high pressures (methanol, FT liquids, DME) it can yield improvements in system efficiency as compressing water and CO_2 is energetically cheaper than syngas. Thus, running type of simulations presented in the preceding chapters but with pressurized stacks should be studied. Apart from these benefits, if high pressure can be combined with lowering the operating temperature of the stack, some new and very interesting systems can be designed. For example, if the temperature of the stack can be lowered

to $\sim 680\,^{\circ}\mathrm{C}$ and the pressure increased to ~ 20 bar it is possible to design RSOC systems in which methanation is promoted inside the cell channels [9, 127], which in turn could mean simplification of the BoP, very high round-trip efficiencies for closed systems (Wendel et al. report r.t.e $> 70\%$) and potentially improved stat-up times. The work developed by Jensen et al. [73] is based on such a system at a very large scale (250 MW) and their work includes an economic assessment. However, this study assumes constant fuel and electricity prices and is a closed system focused exclusively on electricity storage and price arbitrage. Thus, variable operation with an open system operating under these conditions (high pressure low temperature) is an obvious next step within this line of research which has the potential of delivering important insights that may be used to push the technology forward.

6.2 Heat integration

As thoroughly discussed in Section 4.3, heat integration is a key element of the RSOC system, particularly when it is operating in electrolysis mode. Although the system intended to integrate heat in a sensible manner, heat integration was not a particular objective of the work in this thesis and therefore it warrants deeper exploration in the future. A detailed pinch analysis for RSOC systems with variable operation is an important next steps. This could be particularly relevant not only from an operation point of view, but also from a CAPEX perspective as heat exchangers were the most expensive equipment in the RSOC system (see Section 5.3 for a detailed discussion). Thus, any work that might yield improvements in system efficiency and the size of the heat exchange network will have important impacts on the system's economics.

6.3 Economic optimization and stack degradation

Degradation of the SOC is a question of the utmost importance. Modeling degradation is particularly difficult, as the many of the micro processes are still hotly debated

and the degradation that might be measured for a particular cell at a given set of conditions does not necessarily translate to a stack degradation, as the stacking, wiring, and integration of the cells into stacks influences the system's performance. In the case of SOCs that switch back and forth between modes, reversibility has the potential to *reduce* the overall degradation of the stack, as the work by Graves et al. [54] shows. This is a key finding that has important consequences for the future modeling of such systems. The framework used to model degradation in this dissertation was very simplistic, as it was only trying to capture the effects that an increase in ASR (as a consequence of a time dependent degradation function) would have on the operating strategy and the size of the BoP. However, if degradation changes as a function of reversing the operation, then the particular operating strategy *and* history will influence the lifetime of the stack and the economics of the system. This is particular hard problem, as it not only involves a time dependency but also a dependence on the particular history of the device. That is, it's not only important to keep track of the systems history in terms of hours of operation, but also on the number of particular switching cycles it has gone through (reversibility) and the particular current/voltages it has operated in. For example, operating a total of 10 hours at the over-voltage limits might have a very different impact on the lifetime of the device then operating for 10 hours at lower over-voltages and with two mode switches. Obviously such modeling is somewhat arbitrary (as the particular mechanisms of the degradation are still unknown or very hard to model from a fundamental point of view) and it will largely depend on the degradation function, but it is an interesting and important area of research as this type of situation, where the system is switching back and forth and operating at the limits, will become more common in markets with high penetration of intermittent energy sources.

6.4 Scaling down BoP components

One of the most attractive elements of RSOC systems is the fact that they are intrinsically small, and therefore lend themselves for building distributed infrastructure. Although the actual RSOC has no problem being small, many of the BoP component economics depend on scaling in size (e.g. making compressors, blowers, heat exchangers bigger) rather than in a small unit mass-manufactured paradigm. This is a challenge for building small distributed systems, as the standard textbook economics favor larger installations because many of these components become prohibitively expensive at small scales. Thus, the miniaturization of many of the BoP components is a critical area of research that has applications beyond the distributed RSOC systems. The main cost driver for the BoP were found to be the heat exchangers. This, in large part, is due to the fact that the empirical relationships used for costing the equipment are power laws that decrease with increasing unit size. Thus, at small scales these are quite expensive. Thus, research in miniaturization is required in order for these systems to be more economic. A good example of small-scale mass-manufactured cheap heat exchangers is found in a car's radiator, whose main purpose is to transfer heat away from the engine at rates in the tens of kW's. Car radiators, as anyone that has owned a car can attest, are cheap goods that can be bought for \$500-\$1,000 ($\sim \$20 - \$50$/kW), which is one or two orders of magnitude lower than what traditional engineering empirical laws dictates for industrial heat exchangers.

6.5 Ancillary services and other markets

As discussed in Chapter 5, RSOC have the ability to offer a wide variety of grid services that can be very valuable both from a revenue generating and an electricity system point of view. In particular, RSOC are well poised to provide Manual Reserves and Secondary reserves that require response times of $\sim$ 15 minutes. The transient operation of each RSOC system will ultimately depend on the particular design, as

the response time will depend not only on the stack itself but on the response rates of the BoP components. Due to the fact that the analysis presented herein did not consider any non electricity or fuel spot market profits, an obvious next step would be to explore the how the economics of the system change when it sells ancillary services to the grid.

Lastly, a rich area of research is to apply the model and methods described throughout this thesis to see how the economics change in different markets around the world. Due to the regional nature of power and gas markets, each market will vary in its price formation fundamentals and will be driven by different factors. For this reason, it is worth exploring the value that the RSOC systems can provide across different markets, and to investigate the importance that energy only vs. energy and ancillary services strategies might have in each distinct market and region.

Chapter 7

Conclusion

The work presented in this dissertation has, to a great level of detail, explored the technical and economic dimensions of a methane based RSOC system. These so called "energy hubs", are systems that have the ability to generate electricity from a fuel (methane, hydrogen, methanol) or generate fuel from electricity in an efficient and bidirectional fashion. Because stacks are inherently small, these systems can be designed to operate at many scales by scaling in numbers (e.g. number of stacks) rather than in unit size. Thus, RSOC systems can allow for high energy density fuels to be synthesized from electricity in a distributed fashion, thereby bridging the distributed generation infrastructure with the historically massively large and centralized infrastructure for making fuels. If CO_2 can be recycled from the atmosphere (using industrial and/or natural processes), then the synthesized fuels are carbon neutral and can be used to displace fossil fuels while exploiting the existing infrastructure. This feature, the ability to make carbon neutral fuels, will become particularly important for decarbonizing certain applications within the transportation sector which require high energy density fuels such as aviation, marine transport and heavy duty trucking. Due to their bidirectionality, RSOC have the ability to use high energy density fuels for energy storage applications, which is an attractive feature as existing infrastructure such as the natural gas grid can be used as the storage reservoir.

In order to study the viability and value of RSOC based systems, a computational model was built to simulate a methane based RSOC system operating under a wide variety assumptions. The system was then used to simulate the interaction of the

RSOC with spot electricity and fuel markets in Denmark. The main findings and contributions of this dissertation are the following:

- A 0-D computational model to simulate a methane based RSOC system with internal reforming was built using open source software (python). Due to the flexibility of the design and the fact that it is based on open source tools, the model can be easily built upon and improved by the community interested in this area of research. The model can be used both for system level and/or stack level analysis. The ability to easily modify the stack and system parameters is one of its core design principles. Chapter 3 contains an in depth description of the model and its philosophy.

- Sensitivities to different assumptions and parameters were tested in order to understand the key drivers of the system (see Chapter 4). When operating in fuel cell mode, it was found that at the system level the RSOC will be greatly affected by the parasitic power consumption of the BoP and all ancillary equipment associated with the conversion of DC into AC. For the base case assumptions described in Table 4.2, the system was found to have a maximum system efficiency of 59.5%. Because the system uses anode gas recycling to provide the necessary steam for the internal reforming reaction, the system was also found to be quite sensitive to the recycle rate and steam to carbon ratio utilized.

- In electrolysis mode, the systems exhibits a maximum efficiency of 68% at a voltage near the thermoneutral point. When operated below the thermoneutral voltage (1.312 V), the main parasitics are heating requirements for the stack (endothermic mode) and heating for steam generation. When operated above the thermoneutral voltage, the stack operates in exothermic mode and thus the heating requirements become less important and the parasitic load associ-

ated with the air blowers (used for moving the air required to cool the stack) dominate. Because the load of the blowers is a power law with respect to the volumetric flowrate of the gas, overall efficiency drops quickly as more air is required. Variations in ASR impact the system by changing the voltage at which the stack is operating for a given current. The maximum efficiency is fixed at 68%, but as ASR is decreased the current at which the peak efficiency occurs is higher. This, in turn, implies that at lower ASRs the system will operate on average at higher efficiencies for a given range of currents.

- The computational model introduced in Chapter 3 is able to simulate part-load operation, allowing for the system to operate at different points (e.g. current densities), which is a crucial feature for integration with intermittent renewable sources and spot electricity markets. Operating in part-load, however, implies over-designing the BoP components such as heat exchangers, blowers, and evaporators. Just like other systems reported in the literature, the net efficiency of the system increases at part load operation.

- In Chapter 5 a series of temporal optimizations for finding the optimal operating strategy for a RSOC system that can buy/sell power/fuel in the Danish wholesale electricity and gas markets were developed. Hourly data for fuel and electricity prices for the years 2009-2014 were used, and the optimum operating strategy consisted in finding the mode of operation (fuel cell, electrolysis, idle) and the operating current density at which the operating profits (revenues - variable costs) were maximized for each hour of the time-series.

- For the 2009-2014 timeseries and using the base-case assumptions (750 °C, $0.5\Omega\text{cm}^2$, 85% U_f), fuel cell mode is the dominant active mode. Electrolysis only occurs 3% of the time, however, it represents $\sim 29.5\%$ of the total profits. Thus, the ability to operate in electrolysis mode is a key element of the system.

- Electricity price volatility due to an increased penetration of wind is shown to be a critical profit driver of the RSOC system. The swings in electricity prices and the increasing frequency of negative prices, make electrolysis mode a very profitable operation. As the previous bullet point highlights, even though electrolysis does not occur frequently throughout the timeseries, it becomes very important for the system's profits. As such, price volatility should incentivize deployment of these systems, which should help reduce their costs via learning and cummulative production.

- The total plant costs (CAPEX) were computed using the framework developed in Section 3.6, and the investment costs were converted into a fixed annuities, such that the break-even point for the system would be the point in which the sum of the operating profits for a given year equals the calculated TPC annuity. For a system comprised of $100m^2$ of active area under the base-case assumptions, the annualized TPC was calculated to be \$153,551 (2009 dls). For the 2009-2014 timeseries, the RSOC is not found to be a profitable investment.

- Sensitivity to ASR was tested for the temporal optimizations. Lowering of the ASR was found to have an important impact on the operational profits, with the difference between the lowest initial ASR (0.2 Ωcm^2) and the highest (0.5 Ωcm^2) representing an increase of 60% in cumulative profits. The lowering of the ASR also has a big impact on the TPC, as the BoP becomes smaller due to the fact that less air is required to cool the stack over a wider range of currents. The impact on the TPC is mainly driven by smaller heat exchangers in the system. The difference in annualized TPC between a system with initial ASR of 0.5 Ωcm^2 and one with 0.2 Ωcm^2 is roughly 20%. It is concluded that lowering the ASR of the system represents an important area of research and development that could potentially have a big impact on the commercialization

of RSOC systems.

- The sensitivity of the system to the stack's degradation rate was also tested. In order to simplify the problem, a degradation of 1% ASR/1,000 hrs that is linear with time and only depends on the lifetime of the device (rather than its particular history) is assumed. The lifetime of the stack is kept constant and the impact of degradation on the operational profits and TPC is tested under two different strategies: one in which the BoP is oversized so that the operating limits stay constant, and one in which the BoP is not oversized but the operating limits decrease as the stack ages. The two strategies are compared to the base case with no degradation. For the 2009-2014 timeseries, the system does not yield a positive investment and given the particular changes within the prices in western DK (where the system idles most of the time during the later years), oversizing the BoP is the strategy with the worst financial return. Thus, it is concluded that for the assumptions and structure of prices analyzed, it is better to sacrifice output in return for lower CAPEX costs.

- A projected price time-series for the Danish energy system in 2050 (which is assumed to be 100% fossil fuel free on all energy flows) was used to evaluate the role that RSOC systems could play under these scenarios. Two prices of synthetic natural gas (SNG), 140 DKK/GJ ("high price") and 91 DKK/GJ ("low price"), were used as the price signals for the fuel in the system. The temporal optimizations suggest that for a market that exhibits electricity prices similar to those of the 2050 projection (low average prices, high variance), methane based RSOCs are very profitable for the high SNG price (ROI $\sim$ 75%). For the high SNG case, electrolysis mode occurs about 50% of the time, fuel cell mode about 15% of the time and the system idles roughly 35% of the time. Even though electrolysis mode occurs only 50% of the time, it represents more than 95% of

the system profits. Therefore electrolysis mode is the critical profit driver in this scenario. In this case, the value of reversibility does not rest on the profits derived from fuel cell mode, but rather from the services that such flexibility might provide for things like grid balancing requirements and load-following.

- For the low SNG simulation, the system exhibits less idling (22% of time), and fuel cell mode occurs about 28% of the time. In this case, however, fuel cell mode represent 21% of the operating profits, making it a much more relevant operation for the system profits. For this scenario, the total plant profits exhibit a yearly loss that is about 20% shy of the annualized TPC. Given that the method for calculating the TPC has an inherent error $\pm 30\%$, these results are encouraging and suggest that the systems can be profitable in the future, particularly if one assumes that technology will improve over the next decades and that CAPEX costs will go down. When the ASR is lowered (to 0.4, 0.3 or 0.2 Ωcm^2), the total plant profits become positive which imply a potentially attractive investment. Lastly, sensitivity to operating limits is tested. Except for the case in which the ASR is lowered to 0.4 Ωcm^2 and the operating limits are increased (0.95A/cm^2 in fuel cell mode and -1.85A/cm^2 in electrolysis mode), increasing the operating limits does not yield a higher return on investment. This is mainly due to the fact that the gains associated with the increased limits are lower than the investment required to increase the size of the BoP.

In conclusion, the work presented in this dissertation has provided a detailed technical and economic study of a methane based RSOC system, and concludes that such systems are feasible from a technical perspective and offer a potential path for bridging the electricity systems with the fuel synthesis infrastructure in a bi-directional and efficient manner. When tested against the Danish spot electricity markets, the system cannot cover its investment costs even when it is operated in a variable fashion in

order to optimize the potential profits at every hour. However, the carbon constraints imposed by climate change and the high variability in electricity prices associated with markets with high penetration of variable renewable power, point towards a path in which RSOC not only become an attractive investment, but are key enablers of a zero carbon energy system.

Bibliography

[1] Easa I. Al-musleh, Dharik S. Mallapragada, and Rakesh Agrawal. "Continuous power supply from a baseload renewable power plant." In: *Applied Energy* 122 (2014), pp. 83–93. ISSN: 03062619.

[2] Kevin J Albrecht. "Physically based dynamic modeling of planar anode supported SOFC." PhD thesis.

[3] Kevin J Albrecht and Robert J Braun. "Dynamic modeling of SOFC Co-Generation systems for light commerical applications." In: *Proceedings of the ASME 2014 12th International Conference on Fuel Cell Science, Engineering and Technology FUELCELL2014*. 2014, pp. 1–10.

[4] M R Allen et al. *IPCC Fifth Assessment Synthesis Report-Climate Change 2014 Synthesis Report*. 2014.

[5] L Barelli, G Bidini, and A Ottaviano. "Hydromethane generation through SOE (solid oxide electrolyser): Advantages of H2OCO2 co-electrolysis." In: *Energy* 90, Part 1 (2015), pp. 1180–1191. ISSN: 03605442.

[6] Calvin H Bartholomew and Robert J. Farrauto. *Fundamentals of Industrial Catalytic Processes*. 2nd ed. John Wiley & Sons, Inc., 2011, p. 992. ISBN: 9781118209738.

[7] Calvin H Bartholomew and Robert J Farrauto. "Hydrogen Production and Synthesis Gas Reactions." In: *Fundamentals of Industrial Catalytic Processes*. John Wiley & Sons, Inc., 2005, pp. 339–486. ISBN: 9780471730071.

[8] W. L. Becker et al. "Production of Fischer-Tropsch liquid fuels from high temperature solid oxide co-electrolysis units." In: *Energy* 47.1 (2012), pp. 99–115. ISSN: 03605442.

[9] David M. Bierschenk, James R. Wilson, and Scott a. Barnett. "High efficiency electrical energy storage using a methaneoxygen solid oxide cell." In: *Energy & Environmental Science* 4 (2011), p. 944. ISSN: 1754-5692.

[10] G. Botta et al. “Thermodynamic Analysis of Coupling aSOEC in Co-Electrolysis Mode with the Dimethyl Ether Synthesis.” In: *Fuel Cells* 0 (2015), n/a–n/a. ISSN: 16156846.

[11] R.J. Braun, S.A. Klein, and D.T. Reindl. “Evaluation of system configurations for solid oxide fuel cell-based micro-combined heat and power generators in residential applications.” In: *Journal of Power Sources* 158.2 (2006), pp. 1290–1305. ISSN: 03787753.

[12] Robert J. Braun. “Optimal Design and Operation of Solid Oxide Fuel Cell Systems for Small-scale Stationary Applications.” PhD thesis. University of Wisconsin-Madison, 2002.

[13] Annabelle Brisse, Josef Schefold, and Mohsine Zahid. “High temperature water electrolysis in solid oxide cells.” In: *International Journal of Hydrogen Energy* 33.20 (2008), pp. 5375–5382. ISSN: 03603199.

[14] Maciej Chaczykowski. “Transient flow in natural gas pipeline - The effect of pipeline thermal model.” In: *Applied Mathematical Modelling* 34.4 (2010), pp. 1051–1067. ISSN: 0307904X.

[15] S H Chan, H K Ho, and Y Tian. “Multi-level modeling of SOFC gas turbine hybrid system.” In: 28 (2003), pp. 889–900.

[16] Xinbing Chen et al. “Syngas production by high temperature steam/CO ₂ coelectrolysis using solid oxide electrolysis cells.” In: *Faraday Discuss.* 182 (2015), pp. 341–351. ISSN: 1359-6640.

[17] Arnab Choudhury, H. Chandra, and A. Arora. “Application of solid oxide fuel cell technology for power generation - A review.” In: *Renewable and Sustainable Energy Reviews* 20 (2013), pp. 430–442. ISSN: 13640321.

[18] C Colpan, I Dincer, and F Hamdullahpur. “Thermodynamic modeling of direct internal reforming solid oxide fuel cells operating with syngas.” In: *International Journal of Hydrogen Energy* 32.7 (2007), pp. 787–795. ISSN: 03603199.

[19] P. Costamagna, L. Magistri, and a.F. Massardo. “Design and part-load performance of a hybrid system based on a solid oxide fuel cell reactor and a micro gas turbine.” In: *Journal of Power Sources* 96.2 (2001), pp. 352–368. ISSN: 03787753.

[20] Eric Dahlgren. “Rescaling Capital : The Potential of Small-Scale and Mass-Produced Physical Capital in the Energy and Materials Processing Industries.” PhD thesis. Columbia University, 2013.

[21] Eric Dahlgren et al. “Small Modular Infrastructure.” In: *The Engineering Economist* 58.4 (2013), pp. 231–264. ISSN: 0013-791X.

[22] Danish Energy Agency. “”Energiscenarier frem mod 2020, 2035 og 2050”.” In: (2014), pp. 1–2.

[23] Danish Energy Agency. *Energy in denmark 2014*. Tech. rep. Copenhagen: Danish Ministry of Energy, Utilities and Climate, 2016, p. 24.

[24] Danish Energy Agency. *Energy scenarios for 2020, 2035 and 2050*. Tech. rep. Copenhagen K: Energistyrelsen, 2013.

[25] Myriam De Saint Jean, Pierre Baurens, and Chakib Bouallou. “Economic assessment of a power-to-substitute- natural-gas process including high-temperature steam electrolysis.” In: *International Journal of Hydrogen Energy* 40.20 (2015), pp. 6487 –6500. ISSN: 0360-3199.

[26] Myriam De Saint Jean, Pierre Baurens, and Chakib Bouallou. “Parametric study of an efficient renewable power-to-substitute-natural-gas process including high-temperature steam electrolysis.” In: *International Journal of Hydrogen Energy* 39.30 (2014), pp. 17024–17039. ISSN: 03603199.

[27] J Dean, Robert J Braun, and D Munoz. *Analysis of Hybrid Hydrogen Systems Final Report Analysis of Hybrid Hydrogen Systems Final Report*. Tech. rep. January. 2010.

[28] Melis S. Duyar et al. “Kinetics of CO2 methanation over Ru/Al2O3 and implications for renewable energy storage applications.” In: *Journal of CO2 Utilization* 12 (2015), pp. 27–33. ISSN: 22129820.

[29] Ea Energianalyse et al. *Biogas-SOEC Electrochemical upgrading of biogas to pipeline quality by means of SOEC electrolysis Project no. 10677*. Tech. rep. Harold Topse, 2012.

[30] Soren Lyng Ebbehoj. “Integration of CO2 air capture and solid oxide electrolysis for methane production.” PhD thesis. Denmark Technical University, 2015, p. 283. ISBN: 9788792986320.

[31] Sune Dalgaard Ebbesen, Christopher Graves, and Mogens Mogensen. “Production of Synthetic Fuels by Co-Electrolysis of Steam and Carbon Dioxide.” In: *International Journal of Green Energy* 6.6 (2009), pp. 646–660. ISSN: 1543-5075.

[32] Sune Dalgaard Ebbesen et al. "High temperature electrolysis in alkaline cells, solid proton conducting cells, and solid oxide cells." In: *Chemical reviews* 114.21 (2014), pp. 10697–734. ISSN: 1520-6890.

[33] Claus Krog Ekman and Søren Højgaard Jensen. "Prospects for large scale electricity storage in Denmark." In: *Energy Conversion and Management* 51.6 (2010), pp. 1140–1147. ISSN: 01968904.

[34] Energinet.dk. *Ancillary services to be delivered in Denmark Tender conditions*. 2012.

[35] Energinet.dk. *Day ahead market*. 2013.

[36] Energinet.dk. *Electricity interconnections*. 2015.

[37] Energinet.dk. *Regulation C2 : The balancing market and balance settlement*. 2008.

[38] Hanaa Er-rbib and Chakib Bouallou. "Modeling and simulation of CO methanation process for renewable electricity storage." In: *Energy* 75 (2014), pp. 81–88. ISSN: 03605442.

[39] Robert J. Farrauto et al. "Precious Metal Catalysts Supported on Ceramic and Metal Monolithic Structures for the Hydrogen Economy." In: *Catalysis Reviews* 49.October 2011 (2007), pp. 141–196. ISSN: 0161-4940.

[40] Qingxi Fu et al. "Syngas production via high-temperature steam/CO2 co-electrolysis: an economic assessment." In: *Energy & Environmental Science* 3.10 (2010), p. 1382. ISSN: 1754-5692.

[41] Jiajian Gao et al. "A thermodynamic analysis of methanation reactions of carbon oxides for the production of synthetic natural gas." In: *RSC Advances* 2.6 (2012), pp. 2358–2368. ISSN: 2046-2069.

[42] Jiajian Gao et al. "Recent advances in methanation catalysts for the production of synthetic natural gas." In: *RSC Adv.* 5.29 (2015), pp. 22759–22776. ISSN: 2046-2069.

[43] Kristin Gerdes, William Morgan Summers, and John Wimer. *Cost Estimation Methodology for NETL Assessments of Power Plant Performance DOE/NETL-2011/1455*. Tech. rep. National Energy Technology Lab, D.O.E, 2011, p. 26.

[44] Kristin Gerdes et al. *Integrated Gasification Fuel Cell Performance and Cost Assessment*. Tech. rep. National Energy Technology Laboratory, 2009.

[45] Hossein Ghezel-ayagh. "Solid Oxide Fuel Cell Program at FuelCell Energy, Inc." In: *10th Annual SECA Workshop* (2009).

[46] Emanuele Giglio et al. "Synthetic natural gas via integrated high-temperature electrolysis and methanation: Part II-Economic analysis." In: *Journal of Energy Storage* 2 (2015), pp. 64–79. ISSN: 2352152X.

[47] Emanuele Giglio et al. "Synthetic natural gas via integrated high-temperature electrolysis and methanation: Part IEnergy performance." In: *Journal of Energy Storage* 1 (2015), pp. 22–37. ISSN: 2352152X.

[48] Alain Goeppert et al. "Air as the renewable carbon source of the future: an overview of CO2 capture from the atmosphere." In: *Energy & Environmental Science* 5.7 (2012), p. 7833. ISSN: 1754-5692.

[49] Sergio Yesid Gomez and Dachamir Hotza. "Current developments in reversible solid oxide fuel cells." In: *Renewable and Sustainable Energy Reviews* 61 (2016), pp. 155–174. ISSN: 18790690.

[50] Sriram Gopalan et al. "Analysis of self-sustaining recuperative solid oxide electrolysis systems." In: *Journal of Power Sources* 185.2 (2008), pp. 1328–1333. ISSN: 03787753.

[51] Raymond J. Gorte, Seungdoo Park, and John M. Vohs. "Direct oxidation of hydrocarbons in a solid-oxide fuel cell." In: *Nature* 404.6775 (2000), pp. 265–267. ISSN: 00280836.

[52] Christopher Ronald Graves. "Recycling CO2 into Sustainable Hydrocarbon Fuels: Electrolysis of CO2 and H2O." PhD thesis. 2010. ISBN: 978-1-124-54322-2.

[53] Christopher Graves, Sune Dalgaard Ebbesen, and Mogens Mogensen. "Co-electrolysis of CO2 and H2O in solid oxide cells: Performance and durability." In: *Solid State Ionics* 192.1 (2011), pp. 398–403. ISSN: 01672738.

[54] Christopher Graves et al. "Eliminating degradation in solid oxide electrochemical cells by reversible operation." In: *Nature Materials* 14.February (2014), pp. 239–244. ISSN: 1476-1122.

[55] Christopher Graves et al. "Sustainable hydrocarbon fuels by recycling CO2 and H2O with renewable or nuclear energy." In: *Renewable and Sustainable Energy Reviews* 15.1 (2011), pp. 1–23. ISSN: 13640321.

[56] J. Guan et al. *High Performance Flexible Reversible Solid Oxide Fuel Cell*. Tech. rep. October 2004. 2007.

[57] S. Ahmad Hajimolana et al. “Mathematical modeling of solid oxide fuel cells: A review.” In: *Renewable and Sustainable Energy Reviews* 15.4 (2011), pp. 1893–1917. ISSN: 13640321.

[58] J Hanna et al. “Fundamentals of electro- and thermochemistry in the anode of solid-oxide fuel cells with hydrocarbon and syngas fuels.” In: *Progress in Energy and Combustion Science* 40 (2014), pp. 74–111. ISSN: 0360-1285.

[59] John B Hansen, Niels Christiansen, and Jens Ulrik Nielsen. “Production of Sustainable Fuels by Means of Solid Oxide Electrolysis.” In: *ECS Transactions* 35.1 (2011), pp. 2941–2948. ISSN: 19386737.

[60] A Hauch et al. “Sulfur Poisoning of SOFC Anodes: Effect of Overpotential on Long-Term Degradation.” In: *Journal of The Electrochemical Society* 161.6 (2014), F734–F743. ISSN: 0013-4651.

[61] Hongpeng He and Josephine M. Hill. “Carbon deposition on Ni/YSZ composites exposed to humidified methane.” In: *Applied Catalysis A: General* 317.2 (2007), pp. 284–292. ISSN: 0926860X.

[62] J. Stephen Herring et al. “Progress in high-temperature electrolysis for hydrogen production using planar SOFC technology.” In: *International Journal of Hydrogen Energy* 32.4 (2007), pp. 440–450. ISSN: 03603199.

[63] A. Hornes et al. “Catalytic properties of monometallic copper and bimetallic copper-nickel systems combined with ceria and Ce-X (X = Gd, Tb) mixed oxides applicable as SOFC anodes for direct oxidation of methane.” In: *Journal of Power Sources* 169.1 (2007), pp. 9–16. ISSN: 03787753.

[64] A. Hornes et al. “Structural, catalytic/redox and electrical characterization of systems combining Cu-Fe with CeO2 or Ce1-xMxO 2-?? (M = Gd or Tb) for direct methane oxidation.” In: *Journal of Power Sources* 196.9 (2011), pp. 4218–4225. ISSN: 03787753.

[65] Aitor Hornes et al. “Electrochemical performance of a solid oxide fuel cell with an anode based on Cu-Ni/CeO2 for methane direct oxidation.” In: *Journal of Power Sources* 249 (2014), pp. 520–526. ISSN: 03787753.

[66] Infomine Inc. *InfoMine*. 2016.

[67] International Energy Agency. *Key World Energy Statistics 2015*. Tech. rep. Paris, France: International Energy Agency, 2015, p. 82.

[68] International Energy Agency. *World Energy Outlook*. Ed. by International Energy Agency. Paris, France: IEA Publications, 2015, p. 726. ISBN: 9789264208056.

[69] Tomoyuki Inui et al. “Methanation of CO2 and CO on supported nickel-based composite catalysts.” In: *J. Chem. Soc.{,} Faraday Trans. 1* 75.0 (1979), pp. 787–802.

[70] V M Janardhanan and O Deutschmann. “Modeling of solid-oxide fuel cells.” In: *Zeitschrift fur Physikalische Chemie* 221.4 (2007), pp. 443–479. ISSN: 0942-9352.

[71] C. Janke et al. “Catalytic and adsorption studies for the hydrogenation of CO2 to methane.” In: *Applied Catalysis B: Environmental* 152-153.1 (2014), pp. 184–191. ISSN: 09263373.

[72] J.H Jensen, J.M Poulsen, and N.U Andersen. “From Coal To Clean Energy.” In: *Nitrogen+Syngas* April (2011), pp. 1–5.

[73] S. H. Jensen et al. “Large-scale electricity storage utilizing reversible solid oxide cells combined with underground storage of CO ₂ and CH ₄.” In: *Energy Environ. Sci.* (2015). ISSN: 1754-5692.

[74] Søren Højgaard Jensen et al. “Hydrogen and synthetic fuel production using pressurized solid oxide electrolysis cells.” In: *International Journal of Hydrogen Energy* 35.18 (2010), pp. 9544–9549. ISSN: 03603199.

[75] Karen Wonsyld et al. “Operational Robustness Studies of Solid Oxide Electrolysis Stacks.” In: *Journal of Energy and Power Engineering* 9.2 (2015), pp. 128–140. ISSN: 19348975.

[76] P. Kazempoor and R. J. Braun. “Hydrogen and synthetic fuel production using high temperature solid oxide electrolysis cells (SOECs).” In: *International Journal of Hydrogen Energy* 40.9 (2015), pp. 3599–3612.

[77] Janina C Ketterer. “The impact of wind power generation on the electricity price in Germany.” In: *Energy Economics* 44 (2014), pp. 270–280. ISSN: 0140-9883.

[78] Ruth Knibbe et al. “Solid Oxide Electrolysis Cells: Degradation at High Current Densities.” In: *Journal of The Electrochemical Society* 157.8 (2010), B1209. ISSN: 00134651.

[79] Jan Kopyscinski, Tilman J. Schildhauer, and Serge M A Biollaz. “Production of synthetic natural gas (SNG) from coal and dry biomass - A technology review from 1950 to 2009.” In: *Fuel* 89.8 (2010), pp. 1763–1783. ISSN: 00162361.

[80] Jakub Kupecki. "Off-design analysis of a micro-CHP unit with solid oxide fuel cells." In: *International Journal of Hydrogen Energy* 40.35 (2015), pp. 12009–12022. ISSN: 0360-3199.

[81] Rainer Kungas, John M. Vohs, and Raymond J. Gorte. "Effect of the Ionic Conductivity of the Electrolyte in Composite SOFC Cathodes." In: *Journal of The Electrochemical Society* 158.6 (2011), B743. ISSN: 00134651.

[82] Klaus S. Lackner. "Capture of carbon dioxide from ambient air." In: *The European Physical Journal Special Topics* 176.1 (2009), pp. 93–106. ISSN: 1951-6355.

[83] Klaus S. Lackner et al. "The urgency of the development of CO2 capture from ambient air." In: *Proceedings of the National Academy of Sciences of the United States of America* 109.33 (2012), pp. 13156–62. ISSN: 1091-6490.

[84] M. A. Laguna-Bercero. "Recent advances in high temperature electrolysis using solid oxide fuel cells: A review." In: *Journal of Power Sources* 203 (2012), pp. 4–16. ISSN: 03787753.

[85] N. Laosiripojana and S. Assabumrungrat. "Catalytic steam reforming of methane, methanol, and ethanol over Ni/YSZ: The possible use of these fuels in internal reforming SOFC." In: *Journal of Power Sources* 163 (2007), pp. 943–951. ISSN: 03787753.

[86] Grégoire Léonard, Davide Giulini, and Diego Villarreal-Singer. "Design and Evaluation of a High-Density Energy Storage Route with CO 2 Re-Use , Water Electrolysis and Methanol Synthesis." In: *Proceedings of the 26th European Symposium on Computer Aided Process Engineering ESCAPE 26*. Ed. by Kravanja Zdravko and Milos Bogataj. Vol. 2. Portoroz, Slovenia: Elsevier B.V, 2016, pp. 0–5. ISBN: 9780444634283.

[87] Yang Li, Yiwu Weng, and Shilie Weng. "Part-load, startup, and shutdown strategies of a solid oxide fuel cell-gas turbine hybrid system." In: *Frontiers in Energy* 5.2 (2011), pp. 181–194. ISSN: 20951701.

[88] P.J Linstrom and W.G. Mallard, eds. *NIST Chemistry WebBook, NIST Standard Reference Database Number 69,* Gaithersburg MD: National Institutes of Standards and Technology.

[89] Yoshio Matsuzaki and Isamu Yasuda. "Electrochemical Oxidation of H2 and CO in a H2-H2O-CO-CO2System at the Interface of a Ni-YSZ Cermet Electrode and YSZ Electrolyte." In: *Journal of The Electrochemical Society* 147.5 (2000), p. 1630. ISSN: 00134651.

[90] Johannes Mauritzen. "What happens when it's Windy in Denmark? An Empirical Analysis of Wind Power on Price Volatility in the Nordic Electricity Market." In: *An Empirical Analysis of Wind Power on Price Volatility in the Nordic Electricity Market (December 28, 2010). NHH Dept. of Finance & Management Science Discussion Paper* 2010/18 (2010).

[91] Jaroslaw Milewski, Andrzej Miller, and Jacek Salacinski. "Off-design analysis of SOFC hybrid system." In: *International Journal of Hydrogen Energy* 32.6 (2007), pp. 687–698. ISSN: 03603199.

[92] G. Alex Mills and Fred W. Steffgen. "Catalytic Methanation." In: *Catalysis Reviews* 8.1 (1974), pp. 159–210. ISSN: 0161-4940.

[93] Q Nguyen Minh and Mogens Mogensen. "Reversible Solid Oxide Fuel Cell Technology for Green Fuel and Power Production." In: *The Electrochemical Society* (2013), pp. 55–62.

[94] A. F Nakajo. "The Effects of Dynamic Dispatch on the Degradation and Lifetime of Solid Oxide Fuel Cell Systems." In: *ECS Transactions* 35.1 (2011), pp. 285–296. ISSN: 1098-6596. arXiv: `arXiv:1011.1669v3`.

[95] Kimihiro Nanaeda et al. "Dynamic modeling and evaluation of solid oxide fuel cell combined heat and power system operating strategies." In: *Journal of Power Sources* 195.10 (2010), pp. 3176–3185. ISSN: 03787753.

[96] Richard Newby and Dale Keairns. *Analysis of Natural Gas Fuel Cell Plant - Revision 1 DOE/NETL-2013/1593*. Tech. rep. US Department of Energy, 2013.

[97] Nordpool. *Flexible Order*. 2015.

[98] J. E. O'Brien et al. "High-temperature electrolysis for large-scale hydrogen and syngas production from nuclear energy - summary of system simulation and economic analyses." In: *International Journal of Hydrogen Energy* 35.10 (2010), pp. 4808–4819. ISSN: 03603199.

[99] George a Olah, Alain Goeppert, and G K Surya Prakash. "Chemical recycling of carbon dioxide to methanol and dimethyl ether: from greenhouse gas to renewable, environmentally carbon neutral fuels and synthetic hydrocarbons." In: *The Journal of organic chemistry* 74.2 (2009), pp. 487–98. ISSN: 1520-6904.

[100] George a Olah, G K Surya Prakash, and Alain Goeppert. "Anthropogenic chemical carbon cycle for a sustainable future." In: *Journal of the American Chemical Society* 133.33 (2011), pp. 12881–98. ISSN: 1520-5126.

[101] Henning Parbo. "Distributed generation trends and regulation: The Danish Experience." In: *EPRG Workshop on Distributed Generation and Smart Connections*. Cambridge, 2014.

[102] Roland Peters et al. "Analysis of solid oxide fuel cell system concepts with anode recycling." In: *International Journal of Hydrogen Energy* 38.16 (2013), pp. 6809–6820. ISSN: 03603199.

[103] Floriane Petipas, Annabelle Brisse, and Chakib Bouallou. "Model-based behaviour of a high temperature electrolyser system operated at various loads." In: *Journal of Power Sources* 239 (2013), pp. 584–595. ISSN: 03787753.

[104] *Porous Cordierite Honey comb Monolith*. 2016.

[105] Ernst Riensche, Ulrich Stimming, and Guido Unverzagt. "Optimization of a 200 kW SOFC cogeneration power plant Part II: variation of the flowsheet." In: *Journal of Power Sources* 73 (1998), pp. 251–256. ISSN: 03787753.

[106] R. Rivera-Tinoco et al. "Investigation of power-to-methanol processes coupling electrolytic hydrogen production and catalytic CO2 reduction." In: *International Journal of Hydrogen Energy* 41.8 (2016), pp. 4546–4559. ISSN: 03603199.

[107] N. M. Sammes, Y. Du, and R. Bove. "Design and fabrication of a 100 W anode supported micro-tubular SOFC stack." In: *Journal of Power Sources* 145.2 (2005), pp. 428–434. ISSN: 03787753.

[108] Javier Sanz-Bermejo et al. "Part load operation of a solid oxide electrolysis system for integration with renewable energy sources." In: *International Journal of Hydrogen Energy* 40.26 (2015), pp. 8291–8303. ISSN: 03603199.

[109] Warren D Seider et al. *Product and process design principles : synthesis, analysis, and evaluation*. John Wiley & Sons, 2008, 2008, p. 736.

[110] Roger A. Sheldon. "Utilisation of biomass for sustainable fuels and chemicals: Molecules, methods and metrics." In: *Catalysis Today* 167.1 (2011), pp. 3–13. ISSN: 09205861.

[111] S. C. Singhal. "Solid oxide fuel cells for stationary, mobile, and military applications." In: *Solid State Ionics* 152-153 (2002), pp. 405–410. ISSN: 01672738.

[112] Vaclav Smil. *Prime Movers of Globalization*. 1st. Cambridge, Massachusetts: The MIT Press, 2010, p. 261. ISBN: 978-0-262-01443-4.

[113] Peter Sorknæs et al. "Market integration of wind power in electricity system balancing." In: *Energy Strategy Reviews* 1.3 (2013), pp. 174–180. ISSN: 2211467X.

[114] A Sorokin et al. *Handbook of Networks in Power Systems I*. Energy Systems. Springer Berlin Heidelberg, 2012. ISBN: 9783642231933.

[115] A. Boudghene Stambouli and E. Traversa. "Solid oxide fuel cells (SOFCs): A review of an environmentally clean and efficient source of energy." In: *Renewable and Sustainable Energy Reviews* 6.5 (2002), pp. 433–455. ISSN: 13640321.

[116] Xiufu Sun et al. "Thermodynamic analysis of synthetic hydrocarbon fuel production in pressurized solid oxide electrolysis cells." In: *International Journal of Hydrogen Energy* 37.22 (2012), pp. 17101–17110. ISSN: 03603199.

[117] J Thijssen. *The Impact of Scale-Up and Production Volume on SOFC Manufacturing Cost*. Tech. rep. 2007, pp. 1–84.

[118] R Turton et al. *Analysis, Synthesis and Design of Chemical Processes*. Prentice Hall International Series in the Physical and Chemical Engineering Sciences. Pearson Education, 2008. ISBN: 9780132459181.

[119] Shailesh D Vora. "Fuel Cell Program Overview Office of Fossil Energy." In: *15th Annual SECA Workshop*. Pittsburgh, PA, 2014.

[120] K. Wang et al. "A Review on solid oxide fuel cell models." In: *International Journal of Hydrogen Energy* 36.12 (2011), pp. 7212–7228. ISSN: 03603199.

[121] Wei Wang and Jinlong Gong. "Methanation of carbon dioxide: An overview." In: *Frontiers of Chemical Engineering in China* 5.1 (2011), pp. 2–10. ISSN: 16737369.

[122] Wei Wang et al. "Progress in solid oxide fuel cells with nickel-based anodes operating on methane and related fuels." In: *Chemical Reviews* 113.10 (2013), pp. 8104–8151. ISSN: 00092665.

[123] Andre Webber et al. "Oxidation of H 2 , CO and methane in SOFCs with Ni / YSZ-cermet anodes." In: *Solid State Ionics* 153 (2002), pp. 543–550. ISSN: 01672738.

[124] MR Weimar et al. *Cost Study for Manufacturing of Solid Oxide Fuel Cell Power Systems*. Tech. rep. September. Pacific Northwest National Laboratory, US D.O.E., 2013.

[125] Christopher H Wendel. "Design and Analysis of Reversible Solid Oxide Cell Systems for Electrical Energy Storage." PhD thesis. Colorado Shcool of Mines, 2015.

[126] Christopher H. Wendel, Pejman Kazempoor, and Robert J. Braun. "A thermodynamic approach for selecting operating conditions in the design of reversible solid oxide cell energy systems." In: *Journal of Power Sources* 301 (2016), pp. 93–104. ISSN: 03787753.

[127] Christopher H. Wendel et al. "Modeling and experimental performance of an intermediate temperature reversible solid oxide cell for high-efficiency, distributed-scale electrical energy storage." In: *Journal of Power Sources* 283 (2015), pp. 329–342. ISSN: 03787753.

[128] C K Woo et al. "The impact of wind generation on the electricity spot-market price level and variance: The Texas experience." In: *Energy Policy* 39.7 (2011), pp. 3939–3944. ISSN: 0301-4215.

[129] Kyle Yakal-kremski et al. "Effect of Current Switching on LSM-YSZ Composite Electrode Durability." In: *ECS Transactions* 41.33 (2012), pp. 129–136.

[130] Keiji Yamahara et al. "Ionic conductivity of stabilized zirconia networks in composite SOFC electrodes." In: *Solid State Ionics* 176.15-16 (2005), pp. 1359–1364. ISSN: 01672738.

[131] Sangseok Yu et al. "Development of a catalytic combustor for a stationary fuel cell power generation system." In: *Renewable Energy* 35.5 (2010), pp. 1083–1090. ISSN: 09601481.

[132] R Zahradnik and R A Glenn. "Direct methanation of coal." In: *Fuel* 50.1 (1969), pp. 77–90. ISSN: 0016-2361.

[133] Jifeng Zhang and Jean Yamanis. *Techno-Economic Feasibility of Highly Efficient Cost-Effective Thermoelectric-SOFC Hybrid Power Generation Systems: Final Technical Report*. Tech. rep. United Technologies Research Center, 2007, pp. 1–75.

[134] Xiongwen Zhang et al. "A review of integration strategies for solid oxide fuel cells." In: *Journal of Power Sources* 195.3 (2010), pp. 685–702. ISSN: 03787753.